NUMERICAL AND EXPERIMENTAL INVESTIGATION OF THE PERFORMANCE OF AN EVAPORATIVELY-COOLED CONDENSER

JAHANGEER S/O K. ABDUL HALIM

NATIONAL UNIVERSITY OF SINGAPORE

2012

NUMERICAL AND EXPERIMENTAL INVESTIGATION OF THE PERFORMANCE OF AN EVAPORATIVELY-COOLED CONDENSER

Founded 1905

JAHANGEER S/O K. ABDUL HALIM

(*MSc, M.Eng Mech.*)

A THESIS SUBMITTED

FOR THE DEGREE OF DOCTOR OF PHILOSOPHY

DEPARTMENT OF MECHANICAL ENGINEERING

NATIONAL UNIVERSITY OF SINGAPORE

2012

ACKNOWLEDGEMENTS

The author dedicates this work to God and to His true representatives for their blessings and causeless descending mercy.

The author would like to express his profound thanks and gratitude to his project supervisors Professor A. A. O Tay and Dr Md. Raisul Islam for giving an opportunity to work under them as well as for their impeccable guidance, advice and patience throughout the project. In particular, their timely recommendations and suggestions have been invaluable for the successful completion of this research work.

The author also would like to thank his colleagues for their true friendship and valuable help that they extended throughout the entire period of the project. The author is grateful to all the technical staffs in the thermal division, who have given him valuable help whenever required. Of these, Mr.Yeo Khee Ho, Mr. Chew Yew Lin and Mr.Tan Tiong Thiam deserve the author's deepest appreciation and gratitude.

Finally, the author would like to express his gratitude and thanks to his parents, wife and children, siblings, for their patience and support throughout this work.

The author would also like to acknowledge the financial support for this project provided by the National University of Singapore.

TABLE OF CONTENTS

APPENDICES

SUMMARY

To eliminate the complexity involved in the form of cooling towers and pumping system and for convenience, most small and medium type vapour compression air-conditioning systems are fitted with air-cooled condensers. This is despite their poor efficiency compared to the water cooled condensers. Air-cooled condensers in the vapour compression refrigeration system generally have a higher condensation temperature resulting in a correspondingly higher pressure and temperature lift between the evaporator and condenser. Coefficient of Performance (COP) of air-conditioner systems is inversely proportional to this temperature lift. For the reduction of the temperature lift in the condenser, faster heat rejection methods need to be explored. Evaporative cooling of the air-cooled condensers with fine water spray is identified as one of the faster heat rejection techniques for this category of condensers. This work addresses the research need for the detailed study of the evaporatively-cooled condensers, both theoretically and experimentally, with a view to improve the performance of the air-conditioners.

A review of the published literature on the evaporative cooling related research revealed that not much work has been done on the detailed theoretical analysis, numerical modeling and experimental investigation on the evaporative cooling of condensers of the air-conditioners described above. There are very few experimental studies involving the evaporatively-cooled condensers used in the small and medium scale air-conditioners. However, the cited literature suggests that there is a great potential for the improvement in energy efficiency through the incorporation of the evaporatively-cooled condensers in such air-conditioners. As for the theoretical treatment of the evaporatively-cooled condensers, no detailed theoretical or numerical formulation has appeared in the published literature. Some of the studies on the falling

film evaporation on horizontal and vertical tubes for non-air-conditioning application cannot be readily applied for the evaporatively-cooled condensers as they do not consider the cross-flow of air or the condensing refrigerant in the tubes. Therefore, for the accurate establishment of the performance improvement of evaporatively-cooled condensers, further detailed studies, both theoretical and experimental are required.

In the present study, an attempt was made to develop a detailed model for a small tube element of the evaporatively-cooled condensers for analysis of the heat and mass transfer characteristics. This was performed through determination of the relevant heat transfer coefficients as well as the mass of water evaporated from the water film-air interface. To achieve this, a detailed theoretical model was first developed for a small element of a bare condenser tube in which the conservation equations of mass, momentum and energy were solved simultaneously. The detailed model developed for the small element was subsequently extended both for the full serpentine bare and finned-tube evaporatively-cooled condensers. The full serpentine finned model included a two dimensional wet fin model to determine the wet fin efficiency and heat transfer with the evaporative cooling.

By introducing assumptions and using the heat transfer coefficients extracted from the detailed model, a simplified model was developed for practising engineers to design and develop evaporatively-cooled condensers. In the simplified model, the entire serpentine tube system was assumed to be equivalent to a vertical conduit with the condensing refrigerant flowing through the conduit and the falling water film on both sides of the conduit. Also, in the simplified model, the refrigerant mass flow rate was assumed as constant whereas, the mass flow rate of water varies as it traverses down the vertical conduit. The simplified model was numerically solved with the help of the 4^{th} order Runge-Kutte numerical scheme for the determination of the refrigerant

and water properties leading to the determination of design parameters for evaporatively-cooled condensers.

The performance of the evaporatively-cooled condenser in terms of the required tube length for a constant heat rejection rate in the condenser was determined with and without fins using both the detailed model and simplified model and they were found to be in good agreement.

The effect of the main design variables of evaporatively-cooled condensers were investigated using the simplified model. The main design variables considered for the investigation included water mass flow rate, refrigerant mass flow rate and inlet temperature, air inlet temperature and relative humidity. The parametric study revealed that the average water evaporation rate from the condenser tube surface increases with increasing refrigerant inlet temperature and mass flow rate, decreasing ambient temperature and relative humidity, and decreasing film Reynolds number (mass flow rate of water). It was also observed that higher water evaporation rate from the condenser tube surface caused the condenser tube dimension to reduce.

An experimental program was undertaken to evaluate the performance of a 5.8 kW single split air-conditioner with and without the evaporative cooling incorporated. The test rig was designed and fabricated following closely a real air-conditioner in a residential setup and comprehensively instrumented to measure as many operating variables as possible. Two condensers, with and without fins, were used and they were housed in a duct with glass enclosures for visualization and ensuring of the water spray over the condenser tube surface. Tests were carried out for a series of operating conditions for the cases of with and without evaporative cooling for both the condensers.

Coefficient of Performance (COP) of the air-conditioner was determined and compared for all the four condenser configurations with different input parameters. Evaporatively-cooled condensers with the fins performed much better compared to the other configuration of the condensers. The performance of the bare-tube evaporatively-cooled condenser was also observed to be better than air-cooled condenser and has potential for practical implementation.

With the potential of incorporating the investigated evaporatively-cooled condensers in the small and medium sized air-conditioners for both residential and commercial applications, the derived benefits as well as the challenges that may arise in their implementation were also addressed in this study. They were summarized with a brief account in terms of the benefits derived in the Singapore context; technical challenges such as the fouling and corrosion of the condenser tubes are concerned. A simple economic analysis was also carried out to determine the payback period of an evaporatively-cooled air-conditioner and the payback period was found to be attractive enough for the implementation of the evaporatively-cooled condensers in air-conditioners.

LIST OF TABLES

LIST OF FIGURES

NOMENCLATURE

A_f	fin area (m^2)
C	constant in equation 3.33
COP	Coefficient of Performance
C_e	coefficient in equation 3.52
C_{pw}	specific heat capacity of water (kJ kg^{-1} K^{-1})
C_{pr}	specific heat capacity of refrigerant (kJ kg^{-1} K^{-1})
dT_r	increment in refrigerant temperature (K)
dT_w	increment in water temperature (K)
dX	increment in refrigerant quality (dimensionless)
D_i	inside diameter of tube (m)
D_o	outside diameter of tube (m)
E_e	coefficient in equation 3.52
h	enthalpy, (J kg^{-1})
h	combined heat transfer coefficient (Wm^{-2} K^{-1})
h_1	enthalpy at the inlet of compressor (kJ kg^{-1})
h_2	enthalpy at the exit of compressor (kJ kg^{-1})
h_3	enthalpy at the exit of condenser (kJ kg^{-1})
h_4	enthalpy at the inlet of evaporator (kJ kg^{-1})
h_a	convective heat transfer coefficient of air (Wm^{-2} K^{-1})
h_r	convective heat transfer coefficient of refrigerant (Wm^{-2} K^{-1})
h_d	mass transfer coefficient (Wm^{-2} K^{-1})
h_{fg}	latent heat of evaporation (kJ kg^{-1})
h_g	enthalpy of refrigerant vapour (kJ kg^{-1})
h_f	enthalpy of refrigerant liquid (kJ kg^{-1})
h_i	film-tube interface heat transfer coefficient (Wm^{-2} K^{-1})
h_o	film-air interface heat transfer coefficient (Wm^{-2} K^{-1})

k	thermal conductivity (W m^{-1} K^{-1})
k	tube segment number
L	tube length (m)
L_e	Lewis number
M_r	mass flow rate of refrigerant (kg s^{-1})
M_w	mass flow rate of water (kg s^{-1})
m_a	air mass flow rate (Kg s^{-1})
m_v	mass flow rate of water evaporated (Kg s^{-1})
n	constant in equation 3.33
N	number of tubes
N_f	number of fin
Nu_i	bulk water-to-wall Nusselt number
Nu_o	bulk water-to-interface Nusselt number
P_e	coefficient in equation 3.52
P_1	compressor suction pressure (Pa)
P_2	compressor discharge pressure (Pa)
q	heat flux (W m^{-2})
Q_a	heat transfer rate to ambient air (W)
Q_f	heat transfer rate to fin (W)
Pr	Prandtl number (dimensionless)
Re	Reynold's number (dimensionless)
R	tube radius (m)
R_f	fouling resistance (m^2 KW^{-1})
R_{if}	interface thermal resistance (m^2 KW^{-1})
t	time (s)
T_a	ambient air temperature (^{0}C)
T_b	fin base temperature (^{0}C)
T_f	fin temperature (^{0}C)
T_r	refrigerant temperature (^{0}C)

T_w	water temperature (^{0}C)
u	velocity along water film flow (m s^{-1})
U	overall heat transfer coefficient (Wm^{-2} K^{-1})
v	velocity normal to water film flow (m s^{-1})
V	velocity of air (m s^{-1})
V_f	volume flow rate of air (m^3 min^{-1})
W	length of the tube segment (m)
W_{comp}	compressor work input (W)
W_e	coefficient in equation 3.52
X	refrigerant quality

Greek letters

α	thermal diffusivity (m^2 s^{-1})
ε	effectiveness
Γ	mass flow rate of water per unit tube length (kg m^{-1} s^{-1})
τ	shear stress (N m^{-2})
θ_i	water entry angle (degree)
θ_o	water exit angle (degree)
η	Efficiency, condenser performance index
μ	kinematic viscosity (kg m^{-1}s^{-1})
ω	humidity ratio of air kg of water/kg dry air)
ρ	density (kg m^{-3})
δ_w	water film thickness (m)
δ_f	fin thickness (m)
δ_s	scale thickness (m)

Subscripts

1-phase	single phase
2-phase	two phase

a	air
av	average
b	bulk, base
cl	clean conditions
ec	evaporative condenser
ev	evaporator
f	fin, fluid
fl	fouled conditions
i	inlet, inside, initial
if	interface
l	liquid
m	moist
max	maximum
o	outlet, outside
p	plate
r	refrigerant
r-w	refrigerant to water
sub	subcooled
sup	superheated
t	tube
v	vapour
wall	wall
w	water

Chapter 1
INTRODUCTION

Air-conditioning has become an integral part of day to day life around the globe as far as human comfort is concerned. In tropical countries like Singapore, application of air conditioning is turning out to be a necessity rather than a luxury as previously perceived. Worldwide, a significant percentage of the total energy consumption, approximately 30%, is used (Tiwari, 2007) for air-conditioning applications. Considering the uncertainty in the oil supply and escalating price of oil in the recent past coupled with the depletion of fossil fuel, energy efficiency and energy conservation are important topics for research. Furthermore, as the air-conditioners become more energy efficient, their contributions to the green house gas emission will be significantly reduced. While considering energy efficiency of air-conditioning systems, researchers and engineers used to focus only on the energy efficiency improvement of large central air-conditioning plants. However, taking into account the ever increasing oil prices and dwindling supply of fossil fuel around the globe, energy efficiency research and development should be extended to the much larger number of smaller unitary and self-contained air-conditioning systems as well. Looking at developed countries like Singapore, almost all dwellings are installed with split and window air-conditioners. Hence a small amount of energy saving from such air-conditioning systems will contribute to very large energy savings at the national level.

Air-conditioning systems are designed to control the internal environment with respect to temperature, humidity, air movement and air freshness to a level in which most human beings will feel comfortable. This is based on a combination of dry bulb

(T_{db}) and Relative Humidity (RH) of the conditioned air as the design parameters. Currently, almost all the air-conditioning systems around the world work on the vapour compression cycle with a moderate Coefficient of Performance (COP). The COP of an air conditioning system can be improved quite significantly through more efficient heat exchange between the system and the surroundings. This will also make the air conditioning system more environmentally friendly. The two main heat exchanging devices in air-conditioners working on the vapour compression cycle are the evaporator and the condenser. Hence, it is very important to explore ways of improving the efficiency of these heat exchangers such that the entire system becomes efficient, economical and environmentally friendly.

1.1 Vapour Compression Refrigeration Cycle

A schematic diagram of a vapour compression refrigeration cycle and the four main components: evaporator, compressor, condenser and expansion valve are shown in Figure 1.1 and the ideal cycle is depicted on a p-h diagram in Figure 1.2. The processes the working fluid (refrigerant) undergoes in this cycle, include evaporation (low temperature heat absorption), compression (work input), condensation (heat rejection) and expansion. The desired cooling effect obtained at the evaporator is a result of the evaporation of the low boiling point refrigerant absorbing heat from the space to be cooled. The absorbed heat in the evaporator makes the refrigerant vapour slightly superheated. The compressor transforms this slightly superheated refrigerant vapour to high pressure and high temperature vapour, which subsequently enters the air- or water-cooled condenser and rejects both sensible and latent heat in the condenser tubes. Through the above heat rejection occurring in the condenser,

superheated refrigerant vapour is condensed and in most of the cases, exits as a sub-cooled liquid from the condenser.

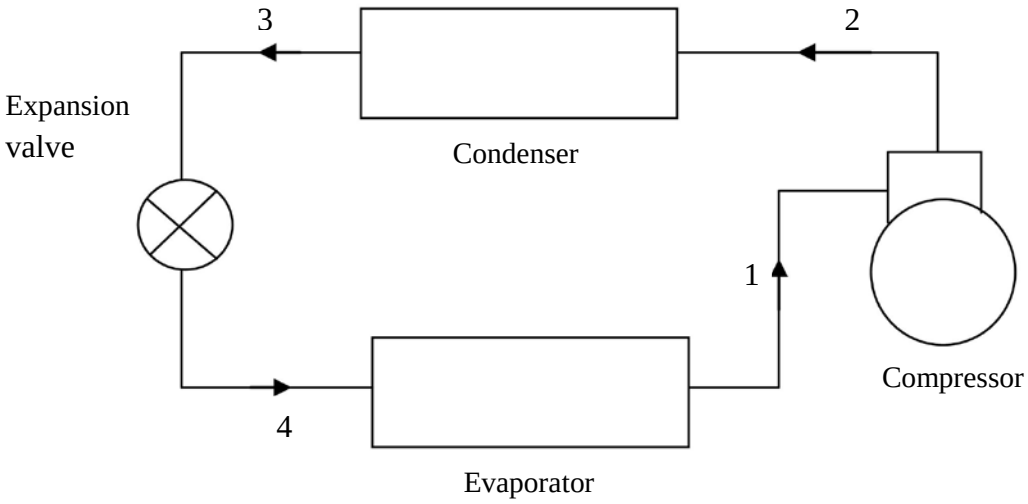

Figure 1.1 *Schematic diagram of a vapour compression refrigeration cycle*

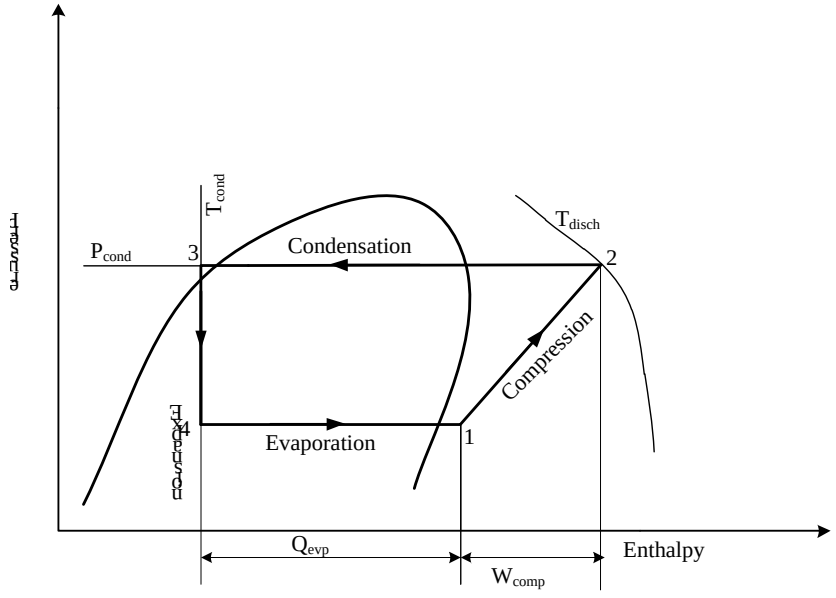

Figure 1.2 *Vapour compression refrigeration cycle on P-h chart*

The liquid refrigerant at high pressure and moderate temperature at the condenser outlet is expanded with the help of a thermostatic expansion valve and re-enters the evaporator at low temperature, low pressure and low quality; and the cycle is repeated.

1.2 Role of the Condenser in the Vapour Compression Cycle

The condenser in the cycle is used to reject both the heat of compression and the heat absorbed by the evaporator. To do this, the condenser's refrigerant temperature must be higher than that of the fluid which cools the condenser (ambient air in the case of an air-cooled condenser). A temperature profile, shown in Figure 1.3, can be used to demonstrate the behavior of a typical condenser. As can be seen from the figure, the state of the refrigerant entering the condenser is superheated. At a short distance from the condenser inlet, the refrigerant is cooled to the saturation point (de-superheating). Condensation follows as the refrigerant changes phase from vapour to liquid. The temperature is decreased slightly as a result of the pressure decrease. Beyond the point where the entire vapor is condensed, the refrigerant is sub-cooled until it emerges from the condenser. Generally, the condensers are manufactured in counter flow or cross-flow arrangements so that a higher heat exchanger performance is achieved.

Any kind of pressure drop in the condenser is undesirable as far as the performance of the air conditioning system is concerned. This is due to the fact that as the state of the refrigerant in the condenser is saturated (pressure and temperature dependant), there is a corresponding refrigerant temperature drop as the pressure is decreased. This causes a reduction in the temperature difference between the

refrigerant and the cooling fluid and, hence a reduced heat rejection from the condenser.

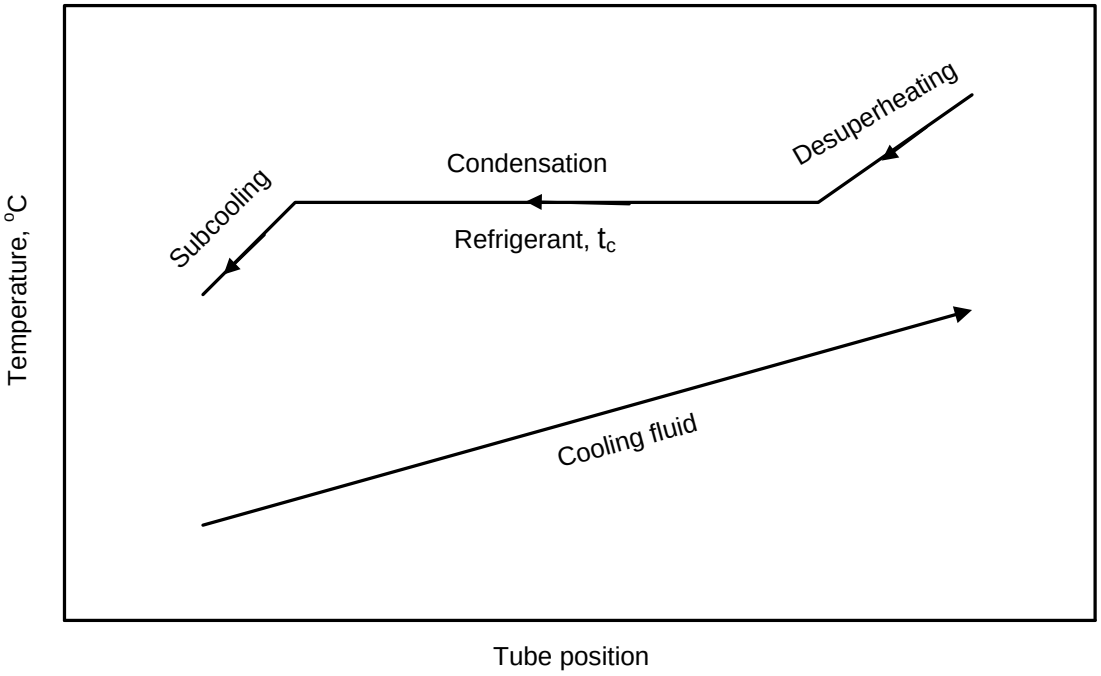

Figure 1.3 *Refrigerant state in the condenser*

1.3 Significance of the Present Study

Vapour compression air-conditioning systems working in tropical climatic conditions usually have a relatively high compressor pressure-lift. The lowering of the condensing temperature will help reduce this lift, thereby reducing the power required by the compressor. The inclusion of water sprays or droplets in air-cooled condensers is a possible option for improving the performance of the condenser and reducing the pressure lift of compressor. Such cooling of the condenser using spray of water or other suitable cooling agents is generally known as evaporative cooling.

Currently, small to medium-sized air-conditioners are fitted with air-cooled condensers, which have an inferior heat transfer performance compared to water cooled condensers. However, replacing of the air-cooled condensers with water-

cooled condensers is not economical for small to medium-sized air-conditioners due to the complexities involved with the presence of cooling towers and pumping systems. However, as indicated by some researchers in their work, potential for the implementation of evaporative cooling techniques with fine sprays of water is very high. The water used for the spraying can be recycled water in the form of evaporator condensate or disposed water from washing machines, etc. used in almost every house, which is otherwise wasted by draining out. Though previous research work has been cited on such evaporative spray cooling, a detailed numerical and experimental investigation of various important parameters which would directly or indirectly affect the performance of the air-conditioning system needs to be considered.

1.4 Possible Effect of Evaporatively-Cooled Condenser on Performance of Air-conditioning System

Figure 1.4 shows the modified p-h diagram in which are indicated with the reduced pressure lift and temperature resulting from the incorporation of evaporative cooling on a condenser tube bundle shown in Figure 1.5. As water is sprayed on the condenser tube bundle at a pre-determined flow rate, a thin water film is formed on the tube surface. This thin water film is evaporated by absorbing heat from the condenser tube surface. The evaporation rate of the thin water film could be increased through simultaneous blowing of ambient air across the condenser tubes. The higher value of latent heat taken from the condenser tube surface because of the faster evaporation rate of the thin water film causes the refrigerant vapour to dissipate the heat at a faster rate and condense as shown in Figure 1.6. This in turn reduces the condensing pressure and temperature of the refrigerant vapour in the condenser tube.

For given cooling load and ambient air conditions, this reduction in condensation pressure causes a reduction in pressure lift between the evaporator and condenser. This reduction in the pressure lift could reduce the compressor power input significantly.

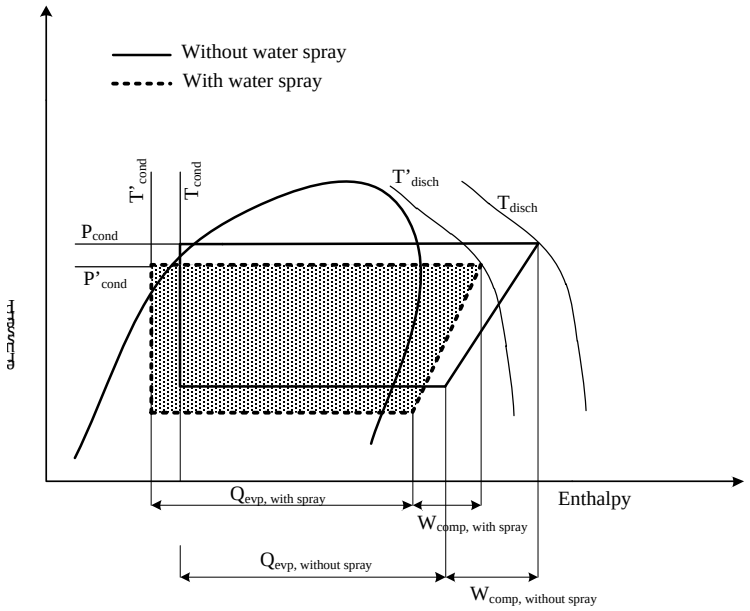

Figure 1.4 *P-h representation of the vapour compression cycle with and without water spray*

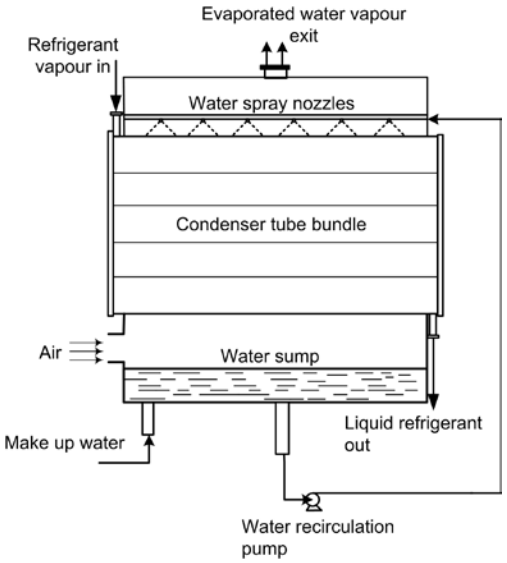

Figure 1.5 *Condenser tube bundle with evaporative-cooling*

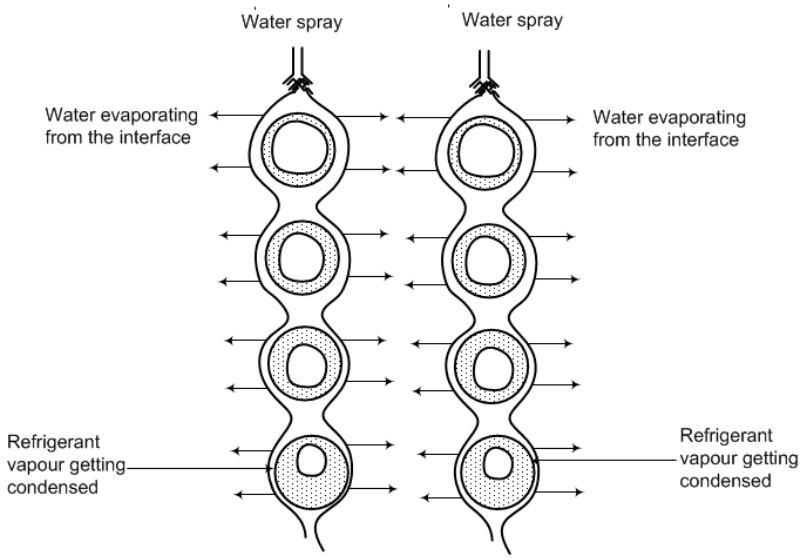

Figure 1.6 *Cross-section of a condenser tube bank with the water spray*

1.5 Objectives of the Present Study

The present study was motivated from the aforementioned observations with regard to the performance of condensers and their impact on the Coefficient of Performance (COP) of vapour compression air-conditioning systems. The main objectives of the study are:

1. Development of a detailed theoretical model to study the heat and mass transfer characteristics of unfinned (bare) and finned serpentine tubes of evaporatively-cooled condensers of air-conditioners under different operating conditions.

2. Development of a simplified model to assist practising engineers in designing evaporatively-cooled condensers.

3. Experimental study of the performance of air-conditioners with evaporatively-cooled condensers.

4. Experimental verification of the accuracy of the detailed and simplified models.

1.6 Layout of the Thesis

After an introduction to the study, a survey of the published literature on past work on spraying of water on horizontal or vertical tubes and vapour compression air conditioning systems is presented in Chapter 2.

In Chapter 3 of the thesis, detailed numerical models for a small tube element as well as for a small segment of bare serpentine tube are developed to investigate the heat and mass transfer characteristics and the overall performance of the evaporatively-cooled condenser tubes. Chapter 3 also contains the results and discussion of a numerical parametric study performed on the small segment as well as the full serpentine tube evaporatively-cooled condenser. In Chapter 4, a numerical model for finned-tube evaporatively-cooled condenser as well as the results of a numerical parametric study performed using the model is presented. The details of the experimental investigation covering the design and construction of the test rig, the instrumentation and the details of the tests carried out are presented in Chapter 5. The comparison of the experimental and numerical results under different operating conditions is described in chapters 6. In Chapter 7, a simplified model, its validation using the detailed model, and experiments as well as a detailed numerical study is described.

Chapter 8 describes the potential technical challenges like fouling and corrosion in the evaporatively-cooled condenser. Chapter 8 also gives an account of the economical and environmental benefits derived from the air-conditioners fitted with the evaporatively-cooled condensers. .

Finally, Chapter 9 presents conclusions drawn from the research work and the recommendations for future investigations.

Chapter 2
LITERATURE REVIEW

The Coefficient of Performance (COP) of air conditioning systems can be improved by reducing the pressure lift between the evaporator and the condenser. Incorporation of evaporatively-cooled condenser in air-conditioners is one of the possible ways to achieve this reduction in pressure lift between the two heat exchangers. However, to achieve the pressure lift reduction using evaporative cooling, it is important to understand the heat and mass transfer processes in the evaporatively-cooled condenser. Experimental and theoretical findings of past researchers from published literature, which directly or indirectly relate to the present work are reviewed through a detailed literature review. The review is mainly focused on the evaporatively-cooled condenser of air conditioning systems, heat and mass transfer characteristics in evaporative cooling, falling film studies on horizontal tubes and finally, falling film studies on vertical plates.

2.1 Evaporatively-cooled Condenser of Air-Conditioning Systems

Leidenfrost et al. (1980) performed a second law analysis through a numerical study of four kinds of condensers namely; air-cooled condenser, air-cooled condenser with pre-cooled air, water cooled condenser and evaporative-cooled condenser. The air cooled condenser was optimized with respect to surface area and power consumption. The condensing temperature from this optimization was used for the determination of second law efficiency. This efficiency provided a reference for comparison of performance of the other systems chosen. Overall, the intention of the study was to investigate the expenditure of additional power to change the state of

surroundings to a lower value and hence a lower condensing temperature could be beneficial to the overall performance of the refrigeration process and its power consumption. Leidenfrost et al. concluded that evaporative cooled condenser was the most efficient followed by water cooled condenser, due to the high transfer coefficient of water. The air-cooled condenser with pre-cooled air has the lowest efficiency at 80 % relative humidity and it is only beneficial if the RH is 65% or below. Their results also suggested that by wetting the condenser tubes could be used either for reducing the condensing temperature or reducing the larger heat exchanger area (order of 10^4 m^2) or reduction of both through an optimization process. Furthermore, it was observed that evaporative condenser increases the overall efficiency of the power plant increase by 1% for every ^{o}C of lowered condensing temperature. The result of the study also emphasized the wetting of the heat exchange surface whenever hot and humid climatic conditions are encountered. They also reported that from working fluid temperature in the tube, tube length can be optimized and tube wall temperature could tell about selection of material and material thickness required.

Prasad et al. (1983) studied evaporative cooling using dehumidified air. They used a bed of silica gel for dehumidification of air and compared its performance with calcium chloride, and copper sulphate. The reasons cited on the use of the bed of silica gel was the dip in performance by the evaporative cooling system in regions of relative high humidity. Hence, they recommended the use of sorbents to dehumidify the air. In their experimental set up, Prasad et al. incorporated the silica gel positioned in front of the fan blower with the evaporative system.

Retrofitting of an existing 5-ton air conditioning system with a two-phase natural circulation heat recovery loop and an evaporative-cooled condenser in a humid climate was investigated and reported by Mathur (1990). The results showed that the system performance of the air-conditioning system increased by 84.4% and results in a diversified peak reduction of 6.78 kW as a result of the retrofit.

Wang et al. (1998) reported heat and mass transfer characteristics of fin-and-tube heat exchangers with and without hydrophilic coating. The heat exchangers tested in the study of Wang et al. consisted of three different louvre fin patterns and their corresponding plain fin counterpart. They observed that for completely-dry test conditions, the enhancement level for the enhanced fin pattern decreases with increase of fin pitch. They also reported that for dehumidifying test conditions, the effect of hydrophilic coating on the sensible heat transfer coefficients was negligible and there were no detectable changes of the sensible heat transfer coefficient with change of inlet relative humidity. They also concluded that the pressure drops for the hydrophilic coated surfaces were sensitive to the inlet relative humidity.

An incorporated evaporative condenser comprising a system of fins, basin of water condensates, circuit pump and system of drop cloud via spraying was developed by Vrachopoulos et al. (2005). Their concluding remarks state that the incorporated evaporative condenser improves the coefficient of performance of provisions up to 211% by decreasing the temperature lift of the system. They suggested from their findings that the life span of the cooling unit brought energy savings of up to 58% resulting from the significant reduction in the temperature lift.

A study on direct evaporative cooling to improve the energy efficiency of air-cooled condensers was carried out by Yu (2005). In this study, Yu has strategically

chosen various operating conditions and staging of condenser fans. The evaporative coolers were installed in front of air-cooled condensers to pre-cool the outdoor air before admitting it into the condenser. Yu had reported that a drop of 2.1 to 6.2 ^{o}C in condenser temperature, which corresponds to a 1.4 to 14.4 % in chiller power and a 1.3 to 4.6 % in refrigeration effect, was observed. He had also predicted the potential saving of more chiller power if the outdoor air were dry enough with a significant difference between its dry and wet bulb temperatures. According to Yu, further investigation was required in evaluating the variation in the dryness of outdoor air under local weather conditions for the proper use of direct evaporative coolers.

Hajidavalloo (2006) reported his research findings on the application of evaporative cooling in the small size refrigeration system for regions of very hot weather conditions. In the study, a real air conditioner was used to test the innovation by putting two cooling pads in both sides of the air conditioner and injecting water on them in order to cool down the air before it is passed over the condenser. The experimental results showed that the thermodynamic characteristics of the new system are considerably improved. He reported that the power consumption was decreased by about 16% and the coefficient of performance increased by about 55%.

Youbi-Idrissi et al. (2006) indentified some key parameters in the incorporation of the evaporative cooling system in a simple refrigeration system. The key parameters are; spray flow rate, wetted area, and collecting ratio. Youbi Idrissi et al. observed that beyond a certain flow rate, spraying water will not enhance the heat transfer rate of the condenser, which he called the spray ‘flow rate threshold’.

Bilal and Zubair (2006) investigated evaporative fluid coolers and evaporative condensers to investigate the effect of fouling and scaling on their performance. They

developed simple theoretical models for evaporative cooler and condenser, which are integrated with the fouling model presented in their earlier work, using the experimental data on tube fouling. An asymptotic fouling model, similar to the one developed for cooling towers, in conjunction with the numerical model of the counter flow evaporative cooler and condenser have been used to study the risk-based performance characteristics of evaporative coolers and condensers, including the effect of fouling on the performance index. They compared the predictions from the models with the published experimental and numerical results. It was demonstrated that there was over 50% decrease in effectiveness for both the evaporative cooler and condenser. Furthermore, it was found that there was about 5% increase in the process fluid outlet temperature for the given fouling model. This also demonstrated the generality of the fouling model in that it not only applies to evaluating the performance of cooling towers but also of evaporative coolers and condensers. Also, a parametric study was performed to evaluate the effect of elevation and mass flow rate ratio on typical performance parameters such as effectiveness for rating calculations while surface area for design calculations.

El-Baky et al. (2007) in their studies investigated heat-pipe heat exchangers. The heat-pipe heat exchangers are used in heat recovery applications to cool the incoming fresh air in air conditioning applications. Their research findings suggested that the temperature changes of fresh and return air were increased with the increase of inlet temperature of fresh air. The effectiveness and heat transfer for both evaporator and condenser sections were also increased by about 48%, when the inlet fresh air temperature was increased to 40 ^{o}C. They reported that the effect of mass flow rate ratio on effectiveness was positive for the evaporator side and negative for

the condenser side. The enthalpy ratio between the heat recovery and conventional air mixing was increased to about 85% with increasing fresh air inlet temperature.

2.2 Heat and Mass Transfer Characteristics in Evaporative-cooling

Sprays of water and ethylene glycol were used for liquid droplet spray to produce a fine mist and to investigate the technical feasibility of air-cooled compact heat exchangers for more effective heat rejection system by Yang et al. (1974). The heat and mass transfer studies were between a condensing vapour or hot fluid system and ambient air. They experimentally investigated the effects of water and ethylene glycol spray on the heat transfer and friction loss performance of three automotive radiator cores. The radiator cores used were plain finned, louvered and perforated types. Yang et al. reported that the frictional losses were not affected by the sprays, while the overall heat transfer coefficient by 40%. They also reported that the overall heat transfer coefficient improvement deteriorates as the air-side Reynolds number was increased. Yang et al. attributed this to the breakup of thin liquid films formed on the fin surfaces. Another observation made was that augmentation of air-side convective heat transfer by liquid spray is mainly due to the formation of liquid film on the heat transfer surface despite the different temperature at which the two sprayed fluid evaporates; i.e. the contribution of evaporation is rather negligible.

William and Weirum (1981) studied analytically and experimentally liquid spray cooling of a heated surface. They developed a conduction controlled analytical model of droplet evaporation and later validated with experimental measurements at atmospheric pressure. Three distinct operational modes of spray cooling were identified as: (i) Drywall state, in which the surface vapourizes all the impinging

spray (ii) Spray film cooling, in which the spray forms a thin liquid film on the surface and (iii) finally the Leidenfrost state, in which the impinging droplets are deflected from the surface by a thin vapour film formed on impact. Their research primarily concerned with the dry wall state and the transition from it to the flooded state (spray film cooling). Two main variables measured from the experiments of their studies were surface temperature and the heat flux through the metal wall upon which the water droplets are impinging. As the mass flux of droplets on to the surface is proportional to the heat flux, the flow rate was not measured from the experiments. Their research findings include the following:

1. Over the range of heat flux considered (50 – 300 kW/m^2), the spray cooling mechanism appears to be that of conduction controlled heat transfer through the droplet with the operation only at the droplet surface.

2. The effect of decreasing the surrounding pressure is quite marked; decreased wettability leads to reduced flooding coefficient, h while the Leidenfrost state temperature increases resulting in the heat transfer remaining essentially constant

3. Spray cooling at atmospheric pressure appears to behave the same way as ordinary pool boiling.

4. But, for cooling at vacuum conditions, the mechanism seems to be one of conduction through the liquid film with no nucleate boiling within the film.

Experimental and numerical determination of mass transfer coefficient for simultaneous air and water flow was performed by Rana et al. (1985). They defined

and considered a new term called “evaporative effectiveness”, which he defined as the ratio of energy dissipation in evaporative to simple water cooling. The variation of evaporative effectiveness is investigated and found to range from 0.85 to 1.78. Rana et al. used the Lewis relation for an air-water mixture for the theoretical calculation of the mass transfer coefficient. This study had come up with three correlations; two for the mass transfer coefficient and one for the evaporative effectiveness.

Nakayama et al. (1988) experimentally investigated the heat transfer from tube banks to air/water mist flow. They used three types of tubes to form the banks namely; smooth tube, microfinned tube and finned tube. The dimensions of the two kinds of micro-finned tube used were: 1 mm high, pitch 0.7 mm and 5mm high and 2.5 mm pitch. Nakayama et al. conducted their experiments by spraying of fine water spray in the air and onto the horizontal tubes, arranged in a bank deep in the vertical direction and relatively short in the direction of air stream. For uniform wetting of the tube surface, the tubes’ surface was provided with micro-fins and porous structures. Nakayama et al. concluded his research finding as follows:

1. Average heat transfer coefficients of the tube bank could be raised markedly by the water injection without penalty of increased flow resistance.

2. The experimental data had shown 300-500% of heat transfer enhancement.

3. The heat transfer coefficient on individual tubes depends to a considerable extent on the temperature potential ΔT. This suggests the importance of evaporation of water (mass transfer) from the wetted part of the tube’s surface in enhancement of heat transfer.

4. Further corroboration of the importance of evaporation is given by the observed effectiveness of microstructures provided on the heat transfer surface.

Chan et al. (2003) in their work on an air-cooled finned heat exchanger with a thin water film, a two dimensional model for the heat and mass transfer in a finned channel was modeled adopting a porous medium approach. Based on this model, the characteristics of the heat and mass transfer were investigated in a plate-fin heat exchanger with the interstitial surface fully covered by thin water film. Assuming Lewis number as unity and the water vapour saturation curve as linear, Chan et al. obtained an exact solution to the energy and vapour concentration equations. Chan et al.'s findings can be summarized as follows:

1. When the interstitial surface is covered with thin water film, the temperature difference between the channel wall and the air becomes smaller due to the water evaporation from the fin surface and consequently, the cooling effect improves considerably compared with that in sensible cooler without water evaporation

2. The maximum cooling enhancement is by a factor η, which is associated with the ratio between the latent heat of water evaporation and the sensible heat of the air

3. It was also observed that, in a typical finned heat exchanger incorporating evaporative cooling, the cooling enhancement is usually less than the maximum attainable and depends on the ratio of the thermal conductance between the fin and the air to the conductive conductance through the fin.

4. As the ratio of the thermal conductance between the fin and the air to the conductive conductance through the fin mostly depends on the fin thickness, the cooling enhancement also depends on this parameter. When the fin is not sufficiently thick, the cooling enhancement by the evaporative cooling decreases resulting in the reduced fin efficiency. Therefore the fin thickness in the evaporative cooler should be increased compared with that in the sensible cooler to take full advantage of the evaporative cooling.

Hsu et al. (1989) analyzed wet surface heat exchangers to find the best configuration for optimum performance. In their analysis, three laboratory models and a commercial prototype were used to cool a stream of air to a temperature lower than the inlet wet-bulb temperature by the evaporation of water. The three laboratory models and prototype used were: a unidirectional, a counterflow, a counterflow closed loop configuration and a cross-flow closed loop commercial unit, respectively. Shyr Tzer Hsu et al. reported in their research findings, that the inlet dew-point temperature can be approached with moderate flow and simple geometries of the heat exchangers.

A simple numerical model of a water spray humidifier was developed by Kachhwaha et al. (1990). In this analysis, a set of one dimensional, ordinary differential equations based on conservation of energy and mass was developed and solved numerically to model the stream wise behaviour of hot flue gas and water drops in a humidification process for sulphur emission control. Similar simulation of hollow cone spray and air interaction was formulated by number of other researchers. An integral analysis was proposed by Yeung et al. (1986) for the case of negligible mass transfer and incompressible gas phase.Yeung et al. (1982) in their work also

presented a similarity analysis of gas liquid spray systems, conical and flat spray, based on a simplified set of governing equations.

Masters (1991) provided a summary on the design and empirical analyses on the equipments involving heat and mass transfer. The analysis of any system involving combined heat and mass transfer phenomenon involves solving of mass, momentum and energy conservation equations for the concerned phases. According to Masters, this coupled phenomenon is very complex because of the factors like turbulence and non-linear variation resulting from properties.

Tsay (1994) carried out a numerical analysis to study heat and mass transfer characteristics in a counter-flow wet surface heat exchanger. He solved the coupled conservation equations for hot fluid, liquid film and moisture stream. The heat transfer rates in the wet surface of the heat exchanger were compared with that obtained from dry surface. In addition, he investigated the effects of latent heat transfer associated with liquid film vaporization on the thermal performance of the heat exchanger. In his results, Tsay highlighted that the energy transport across the liquid film is mostly absorbed by the film vaporizing process and only 10 % of the energy is used for the moist air stream heating up. He also reported that the mass loss of liquid due to evaporation is negligibly small.

A methodology to calculate the effectiveness of a wet surface crossflow plate heat exchanger was found in the work of Stoitchkov et al. (1997). They developed a method with the incorporation of a correction for the effectiveness method of Maclaine-cross et al. (1981). The method of Maclaine-cross et al. was improved through a different approach in determining the mean surface temperature and

deriving a new equation for calculating the ratio of total to sensible heat taking into account the barometric pressure. Stoitchkov et al. in their concluding remarks claimed that the correction together with the estimation of mean surface temperature gives a reliable and fast procedure for real performance prediction of wet surface heat exchangers by analogy to that of dry surface heat exchangers.

The effect of the water sprays commonly used to cool freshly drawn glass fibres was investigated through a numerical model study by Sweetland et al. (1999). They used Karman-Pohlhausen treatment for the velocity and thermal boundary layers accounting for an entrained water spray. The various parameters investigated by Mathew et al. included sauter mean diameter, spray density and spray placement along the glass fibres. Mathew et al. reported that the spray cooling acts to thin thermal boundary layers surrounding the fibres and to raise the convective heat removal from the fibres. They also observed from their results that the effectiveness of the spray cooling can be increased by improving the atomization quality of the spray. Another point highlighted in the study was that the vertical placement of the spray nozzles within the fibre bundle is a less critical parameter.

2.3 Falling-film Studies on Horizontal Tubes

A number of published studies on numerical and experimental investigation on the falling film evaporation/absorption on horizontal tubes have been cited.

Fletcher et al. (1974) presented experimental data for evaporation of thin water film on an electrically heated horizontal tube. They reported their findings on heat transfer coefficients with variation of liquid mass flow rate, heat flux and the saturation temperature of liquid for water and brine. Fletcher et al. also reported

highest value for circumferential heat transfer coefficient at the top of the tube. They also observed nucleate boiling for lower saturation temperatures and higher heat fluxes. In their experiments on a single horizontal tube, the saturation temperature of water sprayed on the tube ranged from 65 to 130 ^{o}C.

Solan and Zfati (1974) conducted experimental investigation of the falling water film on a heated horizontal tube bundles (tube diameter of 38 mm) with constant wall temperature. They have developed a parabolic equation for film velocity and a cubic polynomial function for temperature distribution on film. Evaluated parameters by Solan and Zfati included circumferential film thickness and local convective heat transfer coefficients. They started the computation at the top of the tube with a viscous boundary layer as a two-dimensional jet impinging on a flat surface. Their analytical results for laminar flow model showed good agreement with the measured average convective heat transfer data for film Reynolds number up to 600.

Moalem and Sideman (1976) investigated the characteristics of the various parameters affecting the film side and overall heat-transfer coefficients in a horizontal evaporator-condenser. They considered a laminar flow for practically interesting range of operating conditions. Their investigation included study on the controlling effect of the evaporation side film on the heat and mass transfer rates. They compared their results with available experimental data and shown that the laminar theory yields transfer coefficients which are some 50 per cent of the experimental ones. However, when the effect of ripples was taken into account, the calculated convective heat

transfer coefficient values matched with the measured values with an accuracy of about 10-30 per cent.

Rogers (1977) reported evaporation and boiling from horizontal tubes for non-air-conditioning applications. He developed a theoretical model for isothermal conditions of the horizontal tube and investigated laminar falling film flow on the horizontal tube. Rogers adopted an analytical approach to understand the film flow behavior with special attention given to the interruption of falling films. Roger treated the laminar falling film flow over the tube as a developing and a developed flow regions. He used an integral method for solving of the momentum and energy equations.

Lorenz and Yung (1979) in their study proposed a simple model for combined evaporation and boiling from a horizontal tube. The main consideration in their model was higher convective heat transfer coefficient in the thermally developing region of a horizontal tube and lower convective heat transfer coefficients in the thermally developed region of the lower tubes in a tube bundle. This trend reported by them is analogous to the convection problem involving single-phase flow in tubes having higher heat transfer coefficients at the tube inlet than the farther downstream of the tube. They determined the average convective heat transfer coefficient for the tube bank from the arithmetic average of the heat transfer coefficients of all the individual tubes in the tube bank.

A theoretical model for numerically solving the coupled heat and mass transfer processes was developed by Choudhary et al (1981). The simultaneous heat and mass transfer studied by them included the absorption of vapour into laminar thin

liquid film flowing over cooled horizontal tubes. They developed a single tube model for constant temperature of the tube wall. They incorporated the change in solution flow rate and film thickness due to the absorption of vapour. They used Nusselt's condensation theory and the longitudinal and transverse velocities were determined from Nusselt's fully developed velocity profile and continuity equation, respectively. They also performed a co-ordinate transformation technique to convert the irregular physical domain into a regular computational domain so that the required boundary conditions can be applied for accurate numerical simulation.

Parken and Fletcher (1982) conducted experimental studies on thin water film over 25.4 mm and 50.8 mm diameter smooth horizontal brass tubes. They made use of the same test facility as that used by Fletcher et al. The only difference in the experimental test facility used by Parken et al. was in the water spraying method. The water was fed from a slit positioned at 3mm above centred on the test tube. Carefully deposited water on the tube surface resulted in a laminar film flow with film Reynolds number ranging from 1500 to 6000. They conducted a laminar analysis consisting of two methods, an integral approach using a cubic polynomial velocity and a finite difference technique with a stagnation boundary layer profile for the determination of the film thickness and the evaporation heat transfer coefficient. Their analytical results were found to be in good agreement with the measured data.

Chyu and Bergles (1987) studied heat transfer for saturated falling-film evaporation on a horizontal smooth tube through analysis and experimentation to investigate the effects of film flow rate, liquid feed height, and wall superheat. They have developed two models for the prediction of evaporative heat transfer of a

saturated falling film on a horizontal tube. Both their models were based on three pre-defined heat transfer regions: namely, the jet impingement region, the thermal developing region, and the fully developed region. According to them, the difference between the two models is only in the fully developed region. A conduction solution based on Nusselt's film condensation analysis was used in model-1, whereas, model-2 uses the Chun and Seban (1972) correlation for developed film evaporation. Their predictions using the model-2 were in good agreement with the experimental data and the Owens (1978) prediction when the liquid feed is in a sheet. The convective heat transfer coefficient predicted by model-1 was lower than other predictions and experimental data at low Reynolds number. They cited the possible reason as the simplified conduction solution for the fully developed region underestimates the heat transfer.

Sarma et al. (1992) reported an analytical study of falling film evaporation on a horizontal tube with the constant heat flux condition assumed at the tube wall.

Liu et al. (2002) carried out numerical and experimental investigations on the evaporation heat transfer from horizontal tube bundle evaporators. They considered both laminar and turbulent flow models for their investigation and the models were developed for numerical simulation for the determination of the convective heat transfer coefficient for a falling water film on a horizontal heated tube. Experimental results of Liu et al. agreed well with the numerical results obtained from the turbulent model. They also reported their finding on the effect of the tube diameter on the heat transfer as insignificant for the low and moderate Reynolds number ranges. According to Liu et al., the tube positions and tube spacing within the bundle do not affect the heat transfer rate significantly and suggested that their effect can be neglected for

actual evaporators. They also formulated a dimensionless heat transfer equation based on the turbulence model presented, which could predict evaporation heat transfer characteristics of falling water film over a wide range.

Armbruster and Mitrovic (1995) investigated falling film flow over smooth horizontal tubes. For sub-cooled water with a counter-current air flow, they observed an increase in the convective heat transfer coefficient with air velocity. They also reported that this effect was more dominant at low partial vapor pressure, and was insignificant at high relative humidity. The effects of air velocity and relative humidity were small at high heat fluxes. According to them, the air temperature is not having a significant effect on the convective heat transfer coefficients. They observed from their experimental results for water on an adiabatic surface the effects of air velocity and relative humidity on the temperature of the liquid to be very small.

Kocamustafaogullari and Chen (1988) investigated the flow along a vertical tube bank of horizontal evaporators. They analysed the convective heat transfer coefficients of the tubes from top to bottom. Their theoretical model included a hydrodynamic model with the incorporation of a thin liquid film falling between the tubes. They have approximated the flow as a uniform velocity impinging jet on the top of the horizontal tube. For the determination of the velocity profile near the impinging point, the stagnation point boundary layer theory was applied. Their parametric study included finding out the effect of variable flow rate, saturation temperature, tube spacing on the local average convective heat transfer coefficient. They observed a gradual decrease of convective heat transfer coefficient from the topmost tube until a fully developed region was achieved.

2.4 Falling Film Studies on Vertical Plate

Chun and Seban (1971) reported investigation on falling film evaporation on vertical tube both for laminar and turbulent flow regimes In the laminar flow regime, the principal mode of heat transfer is through conduction which is in line with the assumption made by Nusselt in his classic theory on falling film condensation. They also established experimentally the effect of ripples on the convective heat transfer coefficient values. Upon observing an increased value of heat transfer in their experiments, further investigation on this confirmed the reason behind the trend as the presence of ripples. They also presented some empirical equations for predicting laminar and turbulent flow heat transfer coefficients in falling films on vertical tubes without nucleate boiling. Chun and Seban also suggested Weber Number (W_e), a dimensionless number, for predicting the transition from laminar to turbulent flow in falling film on vertical tube. They set the transition value from laminar to turbulent flow on vertical tube as $W_e = 1$.

Chen et al. (1976) investigated the falling film evaporation on two vertical tubes; one a plain tube and the other one a Wolverine turbo B tube. They determined the convective heat transfer coefficients for the tubes with falling film of R-11. Chen et al. measured the average convective heat transfer coefficient values for their test section of the 1.8 m tube. They observed that the falling film heat transfer characteristics of the Turbo-B tube were similar to its pool boiling characteristics. They also concluded that the benefits of the enhanced surface of the tube in suppressing the dry patch formation in comparison to the plain tube. This allows the tubes to be used for higher heat flux application without the film completely dried out.

Yan (1994) investigated the effect of film vaporization on turbulent mixed convective heat and mass transfer in a vertical channel through a detailed numerical study. Their main focus of attention was in investigating the role of the latent heat transfer associated with the film vaporization in the combined heat and mass transfer of the air-water system in a downward flow. Yan concluded that heat transfer along the gas-liquid interface is dominated by latent heat transfer and they have also proven that the assumption of an extremely thin film thickness by Lin et al. (1980) is inappropriate, particularly with a large liquid mass flow rate. They also reported that the opposing buoyancy forces causes an enhancement in heat and mass transfer compared with that from forced convection.

Heat and mass transfer characteristics for a falling liquid film evaporating into a gas stream were investigated by Tsay and Lin (1995).They considered liquid water film falls along a vertical plate subjected to a uniform heat flux and in the numerical analysis the respective governing equations for the liquid film and gas stream were solved together.

He et al. (1998) developed a turbulent model and reported results for combined heat and mass transfer in a uniformly heated vertical tube with water film cooling.

Miller and Keyhani (2001) experimentally investigated the mechanism of heat and mass transfer in a falling film on an experimental vertical tube absorber. They experimentally measured the temperature profile along the length of the vertical absorber tube using thermo-graphic phosphors. They also developed correlations for the coupled heat and mass transfer processes and validated with the experimental data. The predicted and measured data were found to be in good agreement.

Assad and Lampinen (2002) developed a laminar falling film liquid evaporation model for a constant temperature vertical plate. In their study, they treated the flow as a counter-current one. Their laminar falling film model has also considered the cases with and without the interfacial shear stress. They reported that the interfacial shear stress has a negative effect on the evaporator performance only for counter-current flow. Assad and Lampinen concluded that increase in distance between the plates increases the cooling rate and decreases the pressure drop of vapour. However, the evaporator operates at maximum volumetric cooling rate when the distance between the plates is about 3.5 to 4 mm. Moreover the lower the liquid mass flow the higher the cooling rate and volumetric cooling rate. According to them, their model is a good tool for the prediction of the vertical evaporator performance.

Uche et al. (2002) experimentally investigated falling and rising film evaporation on a vertical plate for desalination of sea water. For the prediction of the convective heat transfer coefficient, they analysed and adopted several correlations suited to the design of the evaporators. The six correlations selected by Uche et al. were: Nusselt (1916) analysis for laminar films: Correlation proposed by Kutateladze (1979) for wavy falling films causing enhanced heat transfer. Correlation proposed by Labuntsov (1957) for turbulent falling films, Chun and Seban's (1971) correlation for vertical heated tubes at atmospheric and vacuum pressures. Sandall et al.'s (1988) correlation for turbulent falling films and correlation proposed by Alhusseini, Tuzla and Chen (1998) that takes into account the effects on the Prandtl number in the heat transfer coefficients in the laminar region. They compared their calculated values of convective heat transfer coefficient with those measured in a real plant for saturation temperatures of 5, 7.5 and 10 ^{o}C. While comparing the above results, they observed

that the trends were same as experimental values; however, the agreement was not good.

Islam et al. (2003) investigated the performance of absorbers through falling film absorption study. They developed a detailed model to characterise the heat and mass transfer of the thin falling solution film on the vertical absorber plate. They determined the convective heat and mass transfer coefficients and used them as the input in the simplified model developed for the design and performance evaluation of the absorbers. Islam et al. compared their numerical predictions with the published experimental results of Miller and they were found to be in good agreement.

2.5 Summary

A review of the published literature on the various aspects affecting the performance of evaporatively-cooled condenser relevant to the present topic was carried out. It is concluded from the related literature available that more research effort in the form of detailed modeling and numerical simulation is necessary for the evaporatively-cooled condenser, which is an important component of a vapour compression air-conditioning system. Notably, there was hardly any literature dealing with a complete study on evaporatively-cooled condensers with the necessary modeling for the three distinct regions in the condenser. Some of the models found in the reviewed literature were not comprehensive enough to precisely predict the heat and mass transfer phenomena occurring at the condenser tube surface as most models had assumed the condenser tube and water film temperatures to be equal. This necessitates further investigation with the development of detailed mathematical

models for obtaining the temperature distribution of the thin water film flowing over the condenser surface.

Incorporation of an evaporative cooling system in an air-cooled condenser can help to achieve better energy efficiency of small and medium-size air-conditioners, which are in widespread use in Singapore and the region. In a tropical set-up, the performance of the air-conditioners drops significantly because of the extreme ambient conditions. It is also understood from the literature review that there was not a single study related to the implementation of evaporative cooling in a tropical set-up, where high ambient temperature and relative humidity are prevalent. This fact observed from the literature review adds more impetus in proceeding with the current investigation on evaporatively-cooled condenser of air conditioners in the tropics. A detailed numerical study complemented with validating experiments on the evaporatively-cooled condenser would shed light on potential energy saving at the national and regional levels.

Most of the experimental investigations cited in the literature dealt with how to incorporate the evaporative cooling system in normal air-cooled air-conditioners without a comprehensive supporting numerical tool to predict their performance. Other literature cited in the review included those on the coupled heat and mass transfer on a horizontal single tube bank as well as vertical tubes for non-air conditioning applications like desalination etc. It is understood from the literature review that further studies are required on coupled heat and mass transfer from either horizontal or vertical tube surface of any configuration with simultaneous blowing of hot and humid air across the tubes in a cross-flow fashion. However, the investigations cited in the review helped to understand the underlying principles of the

coupled heat and mass transfer associated with falling film studies, which would enable the development of detailed theoretical models for the prediction of simultaneous heat and mass transfer from evaporatively-cooled condensers.

From the published literature, it is clear that several issues related to feasibility of incorporating different designs of evaporative cooling techniques in an air-cooled vapour compression air-conditioning system need further investigation with the help of a detailed numerical and experimental study. This situation is the motivating factor behind the present work.

Chapter 3
DETAILED MODEL FOR EVAPORATIVELY-COOLED CONDENSERS

In the present study, an attempt is made to develop a unified approach to the modeling of heat and mass transfer processes in an evaporatively-cooled condenser of an air-conditioner. In a normal air-cooled air-conditioner, the superheated high pressure refrigerant vapour emerging from the compressor enters the condenser and traverses along the serpentine tubes and is condensed to a sub-cooled state by cross-flow air cooling. In this present study, besides this, a fine water spray is introduced at the topmost tube and the water drips down to the tubes vertically below. Development of a detailed mathematical model for the full serpentine condenser tubes with the dripping water spray is complex. In the first step, a detailed model is developed for an element of bare serpentine tube of an evaporatively-cooled condenser. The detailed model developed is used to investigate the heat and mass transfer characteristics of the falling film for the tube element. The detailed model for the tube element is then integrated over the full length of the bare serpentine tube to obtain the performance of an evaporatively-cooled serpentine bare-tube condenser.

3.1 Physical Arrangement of the Condenser

The bare serpentine tube evaporatively-cooled condenser considered here is shown in Figure 3.1. The refrigerant vapour enters the condenser tubes from a header or distributor and while traversing along the tube, it gets condensed with the rejection of the heat to the cooling medium, air. In the present study, as shown in Figure 3.1, in addition to the cross-flow of the air, water is sprayed on to the condenser tubes, giving

an improved heat transfer due to the two-phase heat transfer resulting from the evaporation of the water from the hot condenser tubes. For the detailed model development, a small cross-sectional element of length W as shaded in Figure 3.1 is considered. Details of the tube element with the falling water film and the air-interface considered are shown in Figure 3.2. The detailed model for the tube element will be extended for a small segment of the bare-tube and subsequently integrated for the entire serpentine tube with the tube bends neglected. In the system simulation with the detailed model developed, the wall temperature of any horizontal tube is not constant in the longitudinal direction. But, for a specific small element of the tube, the wall temperature along the perimeter of the tube can be assumed to be constant.

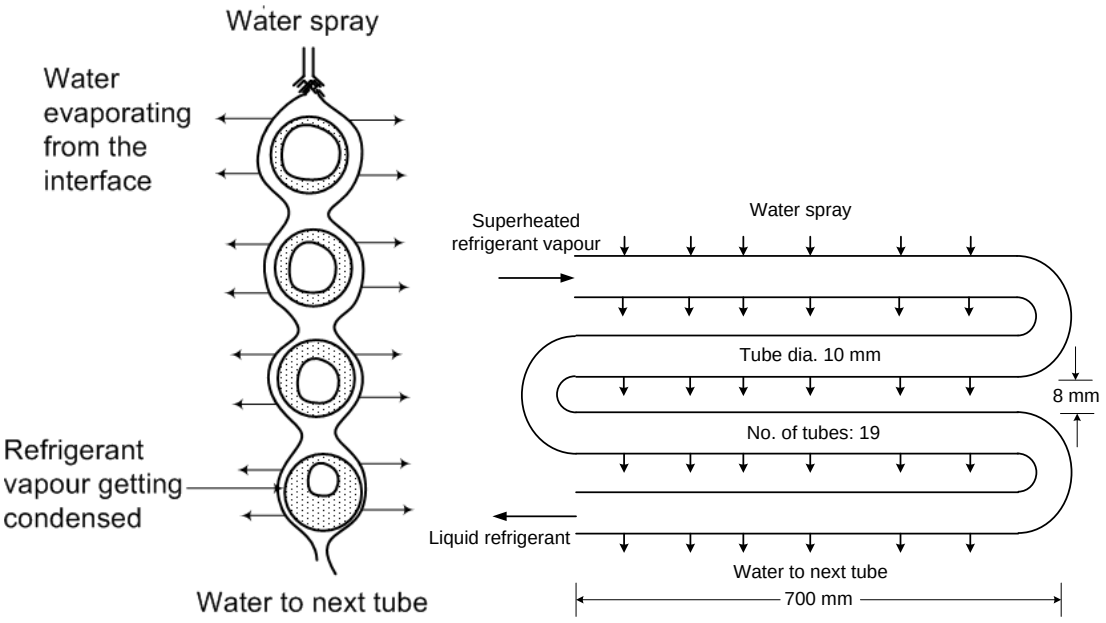

Figure 3.1 *Condenser tube bank with evaporative-cooling*

3.2 Detailed Model for Tube Element of length W of Condenser Tube

The schematic of the physical model for which the detailed theoretical model is developed from the conservation of mass, momentum and energy equations is

shown in Figures. The refrigerant vapour from the compressor enters the condenser tube bank and flows in a direction counter to that of a thin water film flowing vertically downwards along the periphery of the tube surface. The falling film formed by the water spray at a flow rate per unit length of tube of 2Γ kg/m s, splits into two streams along the periphery left and right side of the tube and forms an interface surface with the surrounding air, resulting in an exchange of heat and mass of evaporated vapour from the water film. The difference in vapour pressure between the water film and the surrounding air causes the mass transfer from the water film interface to the air. The required heat for this evaporation process of the falling water film is obtained from the tube surface resulting in greater heat transfer from the refrigerant vapour and subsequent lowering down of the refrigerant condensing temperature and pressure. The interface between the tube surface and the water film will henceforth be called the film-tube interface.

3.2.1 Assumptions in the development of the model

The round tube falling film configuration shown in Figure 3.2 will have a thicker film near the entrance and exit regions of the tube because of the asymptotic nature of the film thickness variation with angular position. Due to this asymptotic nature of the film thickness variation, in this numerical study, computation starts and stops at a sufficient distance away from the inlet and the outlet of the physical domain, respectively. The water film flow entry and exit angles (θ_i and θ_o, respectively) are determined following the sensitivity analysis method presented by Papia (2006), and accordingly, the values of the water film flow entry and exit angles are both taken as 9^o.

The following assumptions are made in the development of the models presented in the following sections of this chapter.

i) The system operates under steady state conditions

ii) Pressure drop in the falling film is negligible

iii) Heat transfer by conduction in the direction of falling water film flow is negligible

iv) There is vapour pressure equilibrium between the air and the liquid water at the interface

v) The shear force exerted by the vapour on the liquid is negligible.

vi) The flow is laminar and no wavy flow exists throughout the surface.

vii) Negligible inter-tubular evaporation viii) Newtonian falling film fluid

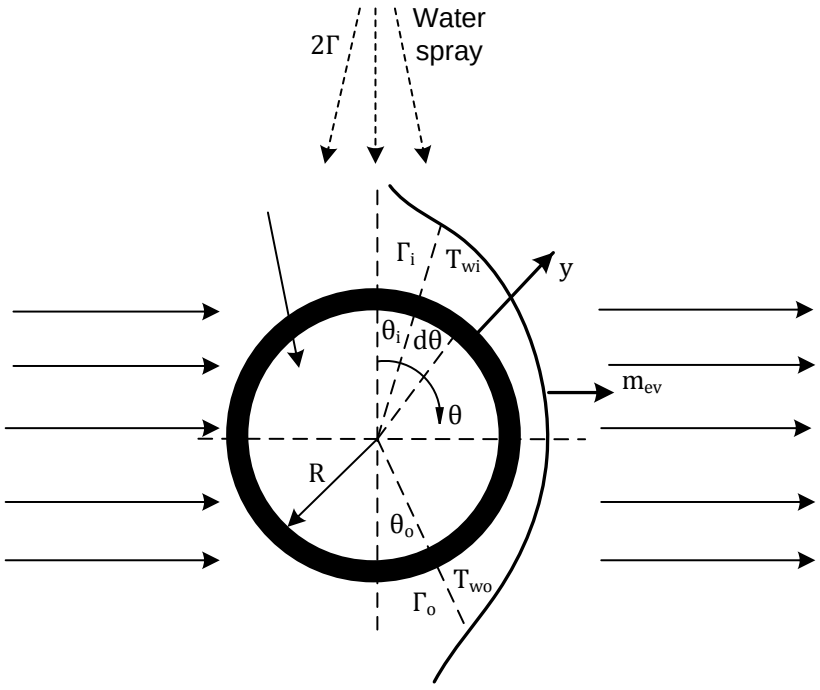

Figure 3.2 *Falling film on a small round tube segment of length W*

3.2.2 Governing equations

A small fluid element (Figure 3.2) of the falling film with various forces acting on it is shown in Figure 3.3

3.2.2.1 The continuity equation

For steady state conditions, a mass balance on a small element of the falling water film as shown in Figure 3.3 gives:

$$\rho_w uWdy + \rho_w vWRd\theta = \rho_w uWdy + \frac{\partial}{R\partial\theta}(\rho_w uWdy)Rd\theta + \rho_w vWRd\theta + \frac{\partial}{\partial y}(\rho_w vWRd\theta)dy \tag{3.1}$$

Simplification of the equation (3.1) yields the continuity equation as:

$$\frac{\partial u}{R\partial\theta} + \frac{\partial v}{\partial y} = 0 \tag{3.2}$$

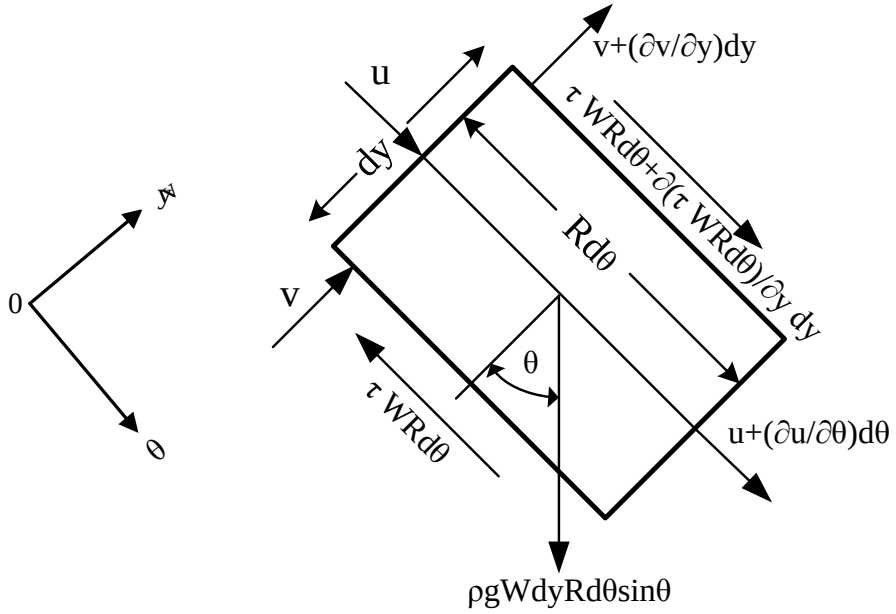

Figure 3.3 *Fluid element of falling film over the tube segment of length W*

3.2.2.2 The momentum equation

As the major forces on the fluid element act along the θ-direction only, the momentum along the θ-direction is considered and derived as follows:

Newton's second law is applied to the fluid element shown in Figure 3.3.

Newton's second law states that rate of change of momentum in the fluid element is equal to the net sum of forces acting on the fluid element.

For a control volume, the various momentum and force components are listed as follows:

Net rate of change of momentum along the θ - direction = $-\frac{\partial}{R\partial\theta}\left(\rho_w u^2 W\right)dyRd\theta$ (3.3)

Net shear force = $-\frac{\partial\tau}{\partial y}WRd\theta dy$ (3.4)

Gravity force acting on the fluid = $\rho_w gWdyRd\theta\sin\theta$ (3.5)

Equations (3.3), (3.4) and (3.5) are used to substitute in the Newton's second law as:

$$-\frac{\partial}{R\partial\theta}\left(\rho_w u^2 W\right)dyRd\theta = -\frac{\partial\tau}{\partial y}WRd\theta dy + \rho_w gWdyRd\theta\sin\theta \quad (3.6)$$

The momentum flux $\frac{\partial}{\partial\theta}\left(\rho_w u^2\right)$ can be assumed to be negligible due to the dominance of viscous force over the inertia force and the resulting equation is the momentum equation for the falling film process on the tube element considered:

$$-\frac{\partial\tau}{\partial y} + \rho_w g\sin\theta = 0 \quad (3.7)$$

3.2.2.3 The energy equation

To obtain the energy equation, an energy balance is performed for the fluid element shown in Figure 3.3, neglecting the heat conducted in the flow direction, as the temperature gradient along the liquid layer can be shown to be small compared to that across the layer.

With reference to Figure 3.3, the various thermal energy components entering and leaving the fluid element are listed as follows:

Nett heat conducted along the y-axis = $-k_w W \frac{\partial^2 T_w}{\partial y^2} Rd\theta dy$ (3.8)

Nett heat convected along the y-axis = $-\rho_w W C_p \frac{\partial}{\partial y}(vT_w) Rd\theta dy$ (3.9)

Along the θ-axis as shown in the diagram, the mode of heat transfer is only through convection; and

the nett heat convected along the θ-axis = $-\rho_w W C_p \frac{\partial}{R\partial\theta}(uT_w) dy Rd\theta$ (3.10)

In the absence of heat generation within the element, the nett heat transfer must be equal to zero, that is:

$$-k_w W \frac{\partial^2 T_w}{\partial y^2} Rd\theta dy = -\rho_w W C_p \frac{\partial}{R\partial\theta}(uT_w) Rd\theta dy - \rho_w W C_p \frac{\partial}{\partial y}(vT_w) Rd\theta dy \quad (3.11)$$

Simplification of equation (3.11) gives the final form of the energy equation as:

$$\frac{\partial}{R\partial\theta}(uT_w) + \frac{\partial}{\partial y}(vT_w) = \alpha \frac{\partial^2 T_w}{\partial y^2} \quad (3.12)$$

The applicable boundary conditions are as follows:

At the entrance section of the water film, i.e. at $\theta = \theta_i$, $0 \le y \le \delta$ the following are assumed:

i) T_w = water inlet temperature = $T_{w,in}$

ii) $\Gamma =$ water flow rate per unit length of tube = Γ_0

At the tube surface, i.e. at y = 0, $\theta_i \le \theta \le \theta_o$ the following are assumed:

u = velocity of water film in the θ-direction = 0 (3.13)

v = velocity of water film in the y-direction = 0

$T_w = T_{wall}$

At the water-air interface, i.e. at y = δ, $\theta_i \le \theta \le \theta_o$,

$$\frac{du}{dy} = 0 \quad \text{and } \tau = 0 \tag{3.14}$$

The rate of water evaporation per unit surface area, $m_{ev} = \frac{h_a}{C_{pm}}\left(\omega_{w,if} - \omega_a\right)_\delta$ (3.15)

$$-k_w\left(\frac{\partial T_w}{\partial y}\right)_{y=\delta} = m_{ev}h_{fg,w} + h_a\left(T_{w,if} - T_a\right) \tag{3.16}$$

The temperature of water at the water-air interface,

$$T_{w,if} = f\left(\omega_{if}\right) \tag{3.17}$$

The flow velocity along the water film flow (θ-component) can be obtained from the momentum equation (3.7), the boundary conditions and the shear stress equation,

$$\tau = -\mu \frac{du}{dy}. \tag{3.18}$$

Integration of equation (3.7) yields:

$$\tau = \rho_w g \sin\theta \, y + B_1 \tag{3.19}$$

Using the boundary condition equation (3.14),

$$B_1 = -\rho_w g \sin\theta \, \delta \tag{3.20}$$

$$\therefore \ \tau = \rho_w g \sin\theta \left(y - \delta\right) \tag{3.21}$$

Substituting equation (3.18) in to equation (3.21) gives:

$$\frac{\partial u}{\partial y} = \frac{\rho_w g \sin\theta}{\mu}\left(\delta - y\right) \tag{3.22}$$

Integrating equation (3.22) and applying the boundary condition equation (3.13) yields:

$$u = \frac{\rho_w g \sin\theta}{\mu}\left(\delta y - \frac{y^2}{2}\right) \tag{3.23}$$

Using continuity equation (3.2) and the boundary conditions listed above, the y-component of the velocity can be obtained as:

$$v = -\frac{\rho_w g y^2}{2\mu R}\left(\sin\theta \frac{d\delta}{d\theta} + \delta\cos\theta - \frac{y}{3}\cos\theta\right) \tag{3.24}$$

The film thickness, δ_w appearing in the velocity expressions above is determined by adopting the method of Bird et al. (1981) and the expression is:

$$\delta_w = \left(\frac{3\Gamma\mu}{\rho_w^{\,2} g \sin\theta} \right)^{1/3} \tag{3.25}$$

The film Reynolds number, Re_f, is defined as follows:

$$\mathrm{Re}_f = \frac{4\Gamma}{\mu} \tag{3.26}$$

For evaporation involving water and air, Lewis Number, L_e =1 (Incropera, 2007) and h_d is defined as: $h_d = \dfrac{h_a}{C_{pm}}$, $\therefore$ the rate of water evaporated at the water-air interface per unit area can be determined from the expression:

$$m_{ev} = \frac{h_a}{C_{pm}} (\omega_{w,if} - \omega_a) \text{, where, } \omega = f(P_v) \tag{3.27}$$

The convective heat transfer coefficient for the case of cross flow of air across condenser tube banks is (Incropera et al. 2007) given by:

$$h_a = \frac{k_a C_1 C_2 \,\mathrm{Re}^n}{D} \tag{3.28}$$

The constants C_1, C_2 and n are functions of the tube pitch to diameter ratio.

The vapour pressure at the interface and the interfacial temperature (Perry, 2008) are related as follows:

$$P_{v,if} = \exp\left(23.19 - \frac{3830}{(T_{w,if} - 44.83)} \right) \tag{3.29}$$

The heat transfer from the interface of water film to air in the superheated region of the condenser for a small elemental area *dA* can be written as:

$$dQ_{\text{sup}} = -k_w (dA) \left. \frac{dT_w}{dy} \right|_{y=\delta} \tag{3.30}$$

Heat lost by refrigerant in the super heated region of the condenser is given by:

$$dQ_{\text{sup}} = -M_r C_{pr,\text{sup}} dT_r = (dA) h_{r,\text{sup}} \left(T_{r,av} - T_{wall} \right) \tag{3.31}$$

Similarly, the heat transfer from the superheated refrigerant vapour to the water film at the condenser tube wall can be written as: $dQ_{\text{sup}} = (dA) k_w \left. \frac{dT_w}{dy} \right|_{y=0}$ (3.32)

Heat lost by refrigerant in the sub-cooled region of the condenser is given by:

$$dQ_{sub} = -M_r C_{pr,sub} dT_r = h_{r,sub} (dA) \left(T_{wall} - T_{r,av} \right) \tag{3.33}$$

The heat transfer coefficients associated with the falling water film around the tube periphery in this model are: the heat transfer coefficient from the film to interface (h_o) and the heat transfer coefficient from the film to wall (h_i).

The expression for these heat transfer coefficients are established through the following energy balances:

$$h_o \left(T_{w,b} - T_{w,if} \right) = -k_w \left. \frac{dT_w}{dy} \right|_{y=\delta} = m_{ev} h_{fg,w} + h_a \left(T_{w,if} - T_a \right) \tag{3.34}$$

For the superheated region of the condenser;

$$h_i\left(T_{wall}-T_{w,b}\right)=-k_w\left.\frac{dT_w}{dy}\right|_{y=0}=h_{r,\sup}\left(T_{r,av}-T_{wall}\right) \tag{3.35}$$

where, $T_{w,b}$ is the mixed-mean bulk film temperature.

For the sub-cooled region of the condenser;

$$h_i\left(T_{wall}-T_{w,b}\right)=-k_w\left.\frac{dT_w}{dy}\right|_{y=0}=h_{r,sub}\left(T_{r,av}-T_{wall}\right) \tag{3.36}$$

For the two-phase region of the condenser;

$$h_i\left(dA\right)\left(T_{wall}-T_{w,b}\right)=-k_w\left(dA\right)\left.\frac{dT_w}{dy}\right|_{y=0}=M_r h_{fg,r}dX \tag{3.37}$$

3.2.3 Numerical Solution Technique

3.2.3.1 Physical and computational domain

The physical domain in the detailed model is a horizontal tube; water film enters at the top of the condenser tube and flows around the circumference of the tube. The water film thickness is changed as it traverses around the tube because of the evaporation of the water from the hot tube surface and flow over the circumference of the tube. Therefore, the geometry of the film is irregular and the discretized computational domain will be non-uniform. Consequently, a one-to-one co-ordinate transformation of the physical domain into a rectangular computational domain with appropriate transformation relations is carried out.

The physical to computational domain transformation in this model is from (θ, y) physical domain coordinates to (ξ,η) computational domain co-ordinates as

shown in Figures 3.4 and 3.5, with the co-ordinates and grids clearly shown. The transformation relations are as follows (Choudhury et al., 1995):

$$\xi = \frac{\theta}{\pi} \qquad \eta = \frac{y}{\delta} \tag{3.38}$$

3.2.3.2 Equations with co-ordinate transformation

Using the above transformation relations, the energy equations, along with the other parametric relations in the computational domain(ξ, η), required for the solution of the energy equation, are obtained and listed below:

The film thickness given in equation (3.25) in the transformed computational domain can then be written as (Bird et al., 1960): $\delta_w = \left(\frac{3\Gamma\mu}{\rho_w^{\,2} g \sin \pi\xi} \right)^{1/3}$ (3.39)

The transformed velocity component in the θ direction can be expressed as:

$$u = \frac{\rho_w g \delta^2 \sin\theta}{2\mu} \left(2\eta - \eta^2 \right) \tag{3.40}$$

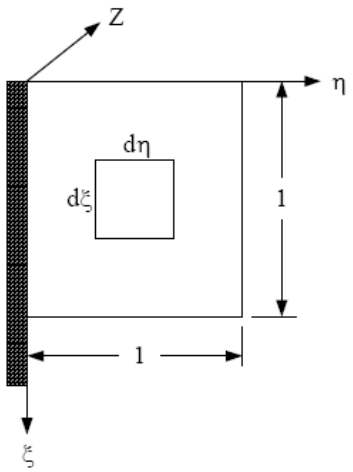

Figure 3.4 *Computational domain for the falling film on a single round tube*

The transformed velocity component in the y direction can be written as:

$$v = \frac{\rho_w g \delta^2 \eta^2 \cos\theta}{6\mu R}\left[\left(\frac{3\Gamma\mu}{\rho^2 g \sin(\pi\xi)}\right)^{1/3} - \delta(3-\eta)\right] \tag{3.41}$$

The transformed energy equation in the computational domain can be expressed as:

$$\frac{1}{\pi R}\frac{\partial}{\partial\xi}(uT_w) + \frac{1}{\delta}\frac{\partial}{\partial\eta}(vT_w) - \left(\frac{\Gamma\mu}{9\rho_w{}^2 g \sin(\pi\xi)}\right)^{1/3}\frac{1}{\delta R\tan(\pi\xi)}\left(uT_w - \frac{\partial}{\partial\eta}(\eta u T_w)\right) = \frac{\alpha}{\delta^2}\frac{\partial}{\partial\eta}\left(\frac{\partial T_w}{\partial\eta}\right) \tag{3.42}$$

The detailed derivation of equation (3.42) is given in Appendix A.

The heat transfer coefficients in the transformed co-ordinates are expressed as:

$$h_o(T_{w,b} - T_{w,if}) = -k_w \left.\frac{dT_w}{d\eta}\right|_{\eta=1} = m_{ev} h_{fg,w} + h_a(T_{w,if} - T_a) \tag{3.43}$$

For the superheated region of the condenser;

$$h_i(T_{wall} - T_{w,b}) = -k_w \left.\frac{dT_w}{d\eta}\right|_{\eta=0} = h_{r,\sup}(T_{r,av} - T_{wall}) \tag{3.44}$$

For the sub-cooled region of the condenser;

$$h_i(T_{wall} - T_{w,b}) = -k_w \left.\frac{dT_w}{d\eta}\right|_{\eta=0} = h_{r,sub}(T_{r,av} - T_{wall}) \tag{3.45}$$

For the two-phase region of the condenser;

$$h_i(T_{wall} - T_{w,b}) = -k_w \left.\frac{dT_w}{d\eta}\right|_{\eta=0} = M_r h_{fg,r} dX \tag{3.46}$$

3.2.3.3 The solution procedure

The numerical computational grid structure in the transformed co-ordinate system is shown in Figure 3.5. The grids in the ξ and η directions are divided into 'm' and 'n' equal divisions, respectively. If the number of divisions in the two transformed directions is not equal, the grid intervals in the two directions can be expressed as:

$$\Delta\eta = \frac{1}{n} \quad \text{and} \quad \Delta\xi = \frac{1}{m-1/2} \tag{3.47}$$

The values of m and n used in the present simulation are 20 and 40, respectively.

All the parametric equations required to solve the energy equation along with the energy equation are discretised. The central difference and upwind schemes are used for discretisation of the energy equation. The discretisation is carried out using finite difference techniques following the methods of Patankar (1981).

The discretised form of the film flow rate around the tube surface per unit length of tube surface is obtained as:

$$\Gamma_{(i,j)} = \frac{\delta^3{}_{(i,j)}\rho_w{}^2 g \sin\theta}{3\mu} \tag{3.48}$$

The discretised form of the velocity components, u and v are given by:

$$u_{(i,j)} = \frac{\rho_w g \delta^2{}_{(i,j)} \sin\theta}{2\mu}\left(2i\Delta\eta - (i\Delta\eta)^2\right) \tag{3.49}$$

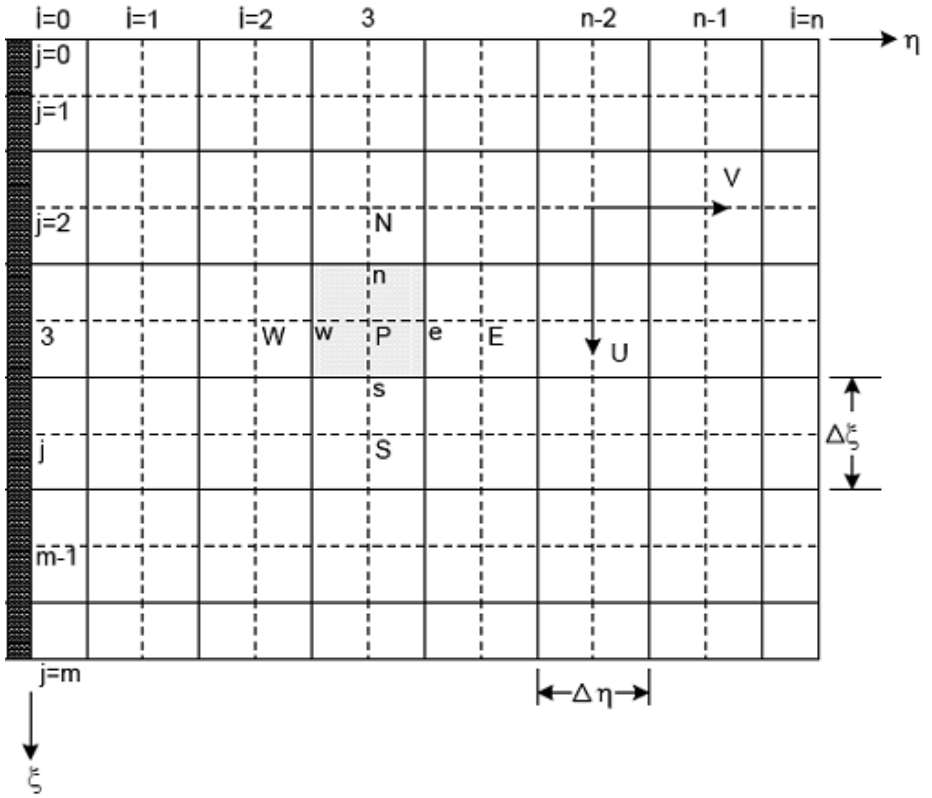

Figure 3.5 *Grid structure for the numerical computation of the detailed model*

$$v_{(i,j)} = \frac{-\rho_w g (i\Delta\eta)^2 \delta_{(i,j)}{}^2 \cos\theta}{6\mu R} \cdot \left(\frac{3\Gamma_{(i,j)}\mu}{\rho_w{}^2 g \sin\theta} \right)^{1/3} - \delta_{(i,j)}\left(3-(i\Delta\eta)\right) \tag{3.50}$$

The discretised form of mass of the water vapour evaporated from the film-air interface can be expressed as:

$$m_{ev(j)} = \frac{h_a}{C_{pm}}(\omega_{w,if(j)} - \omega_a) \tag{3.51}$$

Finally, the discretised form of the energy equation in the transformed co-ordinates is written as:

$$W_e T_{w(i-1,j)} + P_e T_{w(i,j)} + E_e T_{w(i+1,j)} = C_e \tag{3.52}$$

For brevity, the coefficients W_e, P_e, E_e and C_e, in the above discretised energy equation are described in appendix A.

A FORTRAN computer code is written to solve the discretised equations in the computational domain shown in Figure 3.5.

1) As stated in the beginning of this chapter, for a specific small element of the tube, the wall temperature along the perimeter of the tube can be assumed to be constant.

2) The inlet falling water film temperature is assumed to be known at the start of the computation and the interface temperature is taken as the inlet falling water film temperature.

3) The water properties are determined from the inlet temperature.

4) For a given film thickness and the fluid properties in Step 3, the water flow rate per unit length and the velocity components are determined from the equations (3.48), (3.49) and (3.50), respectively.

5) The mass of the water vapour evaporated from the interface is determined using the equation (3.51).

6) The tri-diagonal matrix obtained from the energy equation for the grid points of the computational domain in Figure 3.5 are solved for the temperature at various grid points in the η direction for a particular ξ.

7) From an energy balance for the fluid element at the tube interface, the temperature at the interface is determined in comparison with the assumed interface temperature through iteration.

8) Upon the determination of the interface temperature in Step 7, the temperature along the grid points are found in the η direction for the particular ξ value.

9) The computation is repeated for the next ξ value following Steps 3 to 8 until the desired tube periphery is covered in the ξ direction.

The computational procedure for the detailed model is depicted in the flow diagram as shown in Figure 3.6.

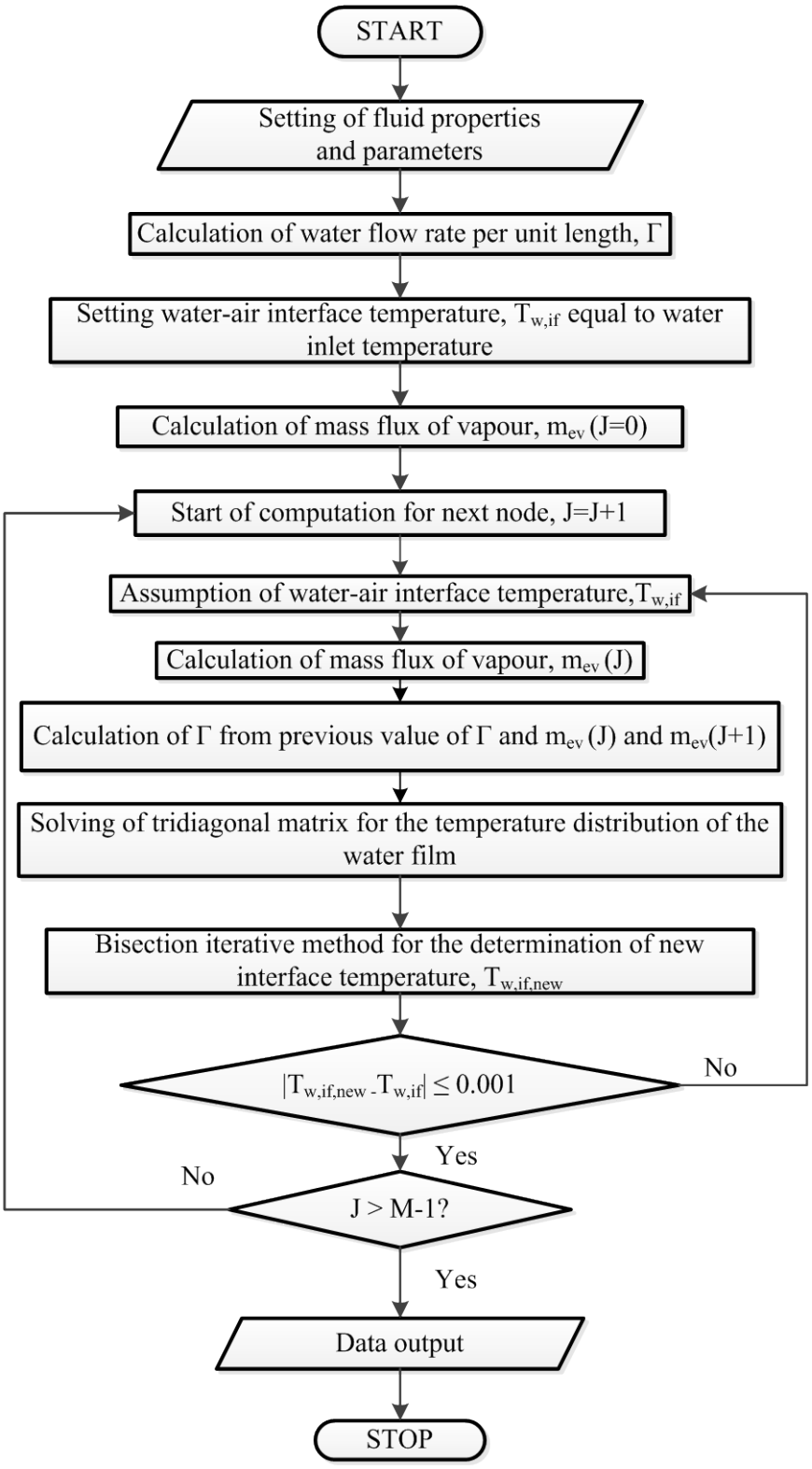

Figure 3.6 *Flow diagram for calculation of the thin film water temperature distribution using the detailed model for a tube element of length W*

3.3 Horizontal Bare Condenser Tubes with the Falling Film

The refrigerant and water flow path in the serpentine tube of the evaporatively-cooled condenser is depicted in Figure 3.7. The serpentine tube is divided into a number of equal segments, the length of each segment is ΔL. The variables i, j, k in Figure 3.7 represent tube number, segment number for each of the tube and total segment number, respectively. The super-heated refrigerant vapour enters from left into the odd numbered tubes and from right into the even numbered tubes. Hence, the segment number j, for individual tube is counted from left to right for odd numbered tubes and from right to left for even numbered tubes. Water mass flow rate per unit length of the tube, 2Γ kg/m s, falls on the top tube and is split into two paths on either side of the tube with a flow rate of Γ kg/m s each as shown in the figure. The water flow rate per unit tube length 2Γ for the tube segments below, which is less the quantity of water evaporated from the tube surface $m_{ev,}$ are indicated with relevant suffix i and j as shown in the Figure 3.7. In the present study, the inter-tubular evaporation is neglected.

The detailed model developed for the tube element of the condenser tube described in the preceding section will be integrated over a small segment ΔL of the bare serpentine tubes of the evaporatively-cooled condenser for the determination of its heat and mass transfer characteristics and hence, its performance. For this, the serpentine tube is divided into three sections based on the state of the refrigerant, namely superheated, two-phase and sub-cooled regions.

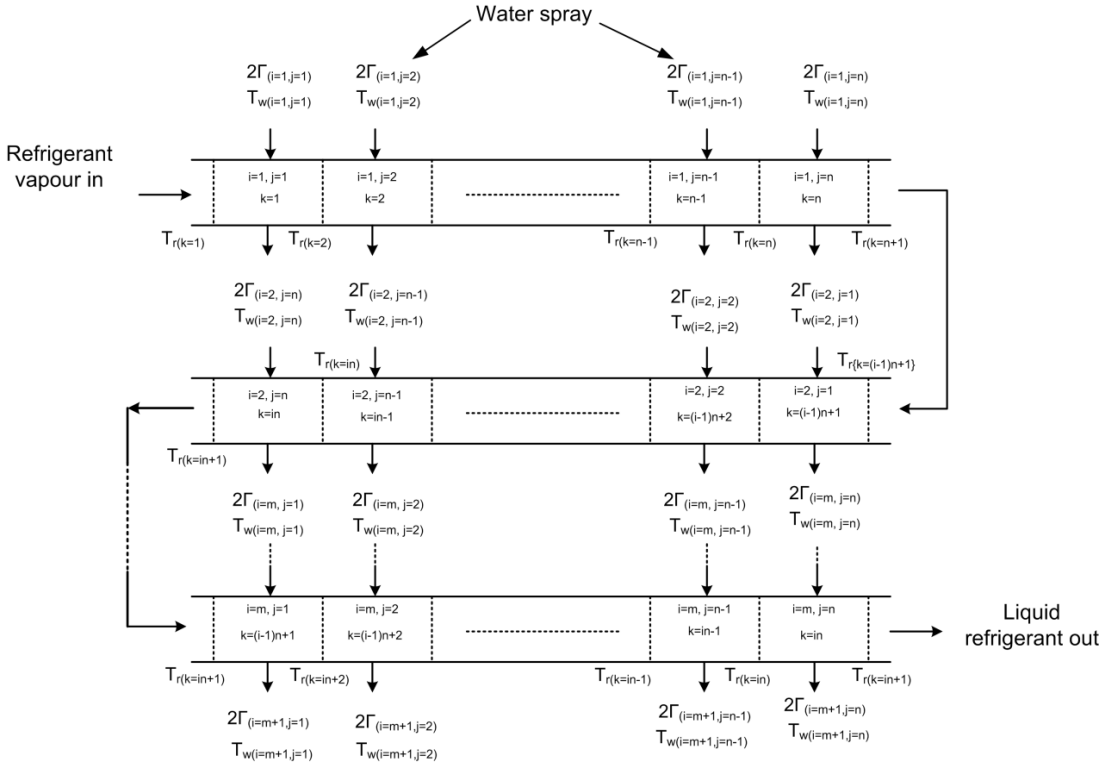

Figure 3.7 *Falling water film and variation of properties at different stages of the evaporative cooling*

3.3.1 Governing equations for the single-phase region (superheated and sub-cooled) of the condenser

Expression for the refrigerant outlet temperature at the kth segment of the tubes for the single-phase region can be established from an energy balance of the segment shown in Figure 3.8 as follows:

$$2\Gamma_{(i,j)} C_{pw} T_{w(i,j)} \Delta L + M_r C_{pr} T_{r(k)} =$$

$$2\Gamma_{(i+1,j)} C_{pw} T_{w(i+1,j)} \Delta L + M_r C_{pr} T_{r(k+1)} + 2M_v h_{fg,w} + Q_a \tag{3.53}$$

$$T_{r(k+1)} = \frac{\left\lfloor C_{pw} \Delta L \left(2\Gamma_{(i,j)} T_{w(i,j)} - 2\Gamma_{(i+1,j)} T_{w(i+1,j)}\right) + M_r C_{pr} T_{r(k)} - 2M_v h_{fg,w} - Q_a \right\rfloor}{M_r C_{pr}} \tag{3.54}$$

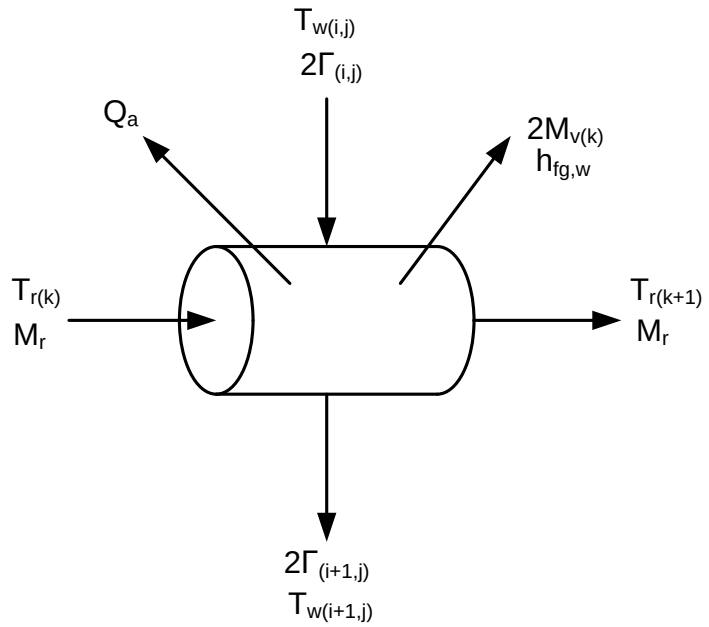

Figure 3.8 *Energy balance on the k^{th} segment of the condenser tube (single-phase region)*

where, $Q_a = h_a \pi D_o \Delta L (T_{w,av} - T_a)$ (3.55)

Heat transfer from the refrigerant to the inner wall of the condenser tube in the single-phase region can be expressed with reference to Figure 3.9, as follows:

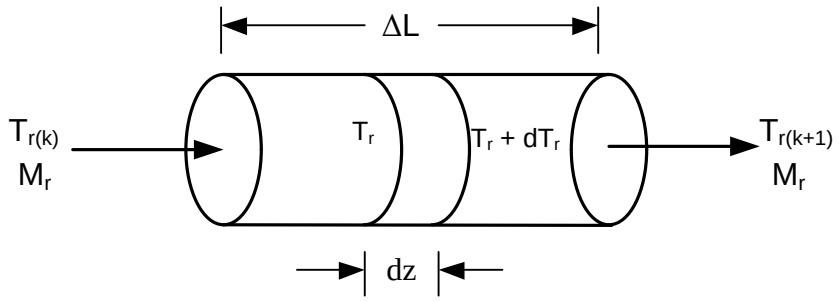

Figure 3.9 *Variation of refrigerant temperature on the k^{th} segment of the condenser tube (single-phase region)*

$$dQ = h_{r,1-phase}\pi D_i dz\left(T_r - T_{wall,i}\right) = M_r C_{pr} dT_r \tag{3.56}$$

Heat transfer through the wall of the segment can be written as:

$$dQ = \frac{2\pi k_{wall} dz}{\ln\left(\frac{D_o}{D_i}\right)}\left(T_{wall,i} - T_{wall,o}\right) \tag{3.57}$$

From equations (3.56) and (3.57),

$$\left(T_r - T_{wall,o}\right) = F_1 \frac{dT_r}{dz} \tag{3.58}$$

Integrating equation (3.58) over the length of the segment as shown in Figure 3.9 gives outside tube wall temperature as:

$$T_{wall,o} = \frac{T_{r(k)} \exp\left[\frac{\Delta L}{F_1}\right] - T_{r(k+1)}}{\exp\left[\frac{\Delta L}{F_1}\right] - 1} \tag{3.59}$$

where, $$F_1 = M_r C_{pr}\left[\frac{1}{h_{r,1-phase}\pi D_i} + \frac{\ln\left(\frac{D_o}{D_i}\right)}{2\pi k_{wall}}\right] \tag{3.60}$$

3.3.2 Governing equations for the two-phase region of the condenser (condensation)

An energy balance on the two-phase region element shown in Figure 3.10 gives:

$$2\Gamma_{(i,j)} C_{pw} T_{w(i,j)} \Delta L + M_r X_k h_{g,r} + M_r\left(1 - X_k\right) h_{f,r} \;=$$

$$2\Gamma_{(i+1,j)} C_{pw} T_{w(i+1,j)} \Delta L + M_r\left(X_{k+1}\right) h_{g,r} + M_r\left(1 - X_{k+1}\right) h_{f,r} + 2M_v h_{fg,w} + Q_a \tag{3.61}$$

Simplification and rearrangement of equation (3.61) gives:

$$X_{k+1} = \frac{2C_{pw}\Delta L\left(\Gamma_{w(i,j)}T_{w(i,j)} - \Gamma_{w(i+1,j)}T_{w(i+1,j)}\right) + M_r X_k h_{fg,r} - 2M_v h_{fg,w} - Q_a}{M_r h_{fg,r}} \tag{3.62}$$

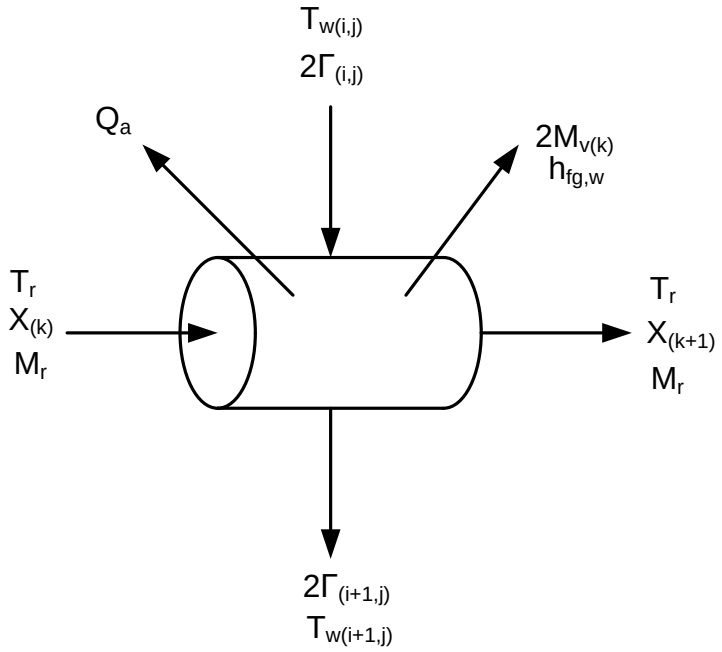

Figure 3.10 *Energy balance on the k^{th} segment of the condenser tube (two-phase region)*

Heat transfer from the inner wall of the condenser tube to the refrigerant in the two-phase region from the element of Figure 3.11 can be expressed as:

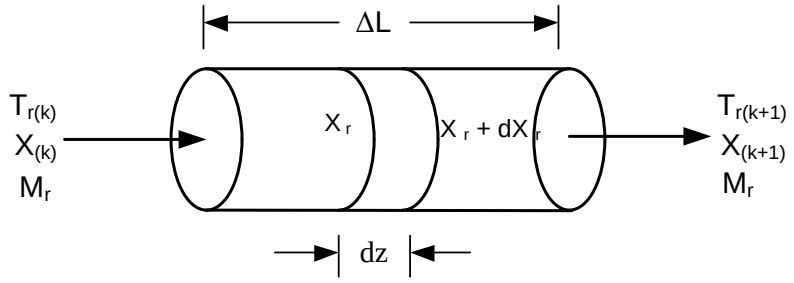

Figure 3.11 *Variation of refrigerant temperature on the k^{th} segment of the condenser tube (two-phase region)*

$$dQ = h_{r,2-phase}\pi D_i dz\left(T_r - T_{wall,i}\right) = M_r\, h_{fg,r}\, dX \tag{3.63}$$

From equations (3.57) and (3.63),

$$\left(T_r - T_{wall,o}\right) = F_2 \frac{dX}{dz} \tag{3.64}$$

Integrating equation (3.64) over the length of the segment ΔL gives:

$$T_{wall,o} = T_r - \frac{F_2\left(X_{r(k+1)} - X_{r(k)}\right)}{\Delta L} \tag{3.65}$$

where, $$F_2 = M_r h_{fgr}\left[\frac{1}{h_{r,2-phase}\pi D_i} + \frac{\ln\left(\frac{D_o}{D_i}\right)}{2\pi k_{wall}}\right] \tag{3.66}$$

Refrigerant side heat transfer coefficients are determined using the following expressions (Arora, 2000):

$$h_{r,1-phase} = 0.023\frac{k_r}{D_i}\mathrm{Re}^{0.8}\,\pi\,\mathrm{Pr}^{0.3} \tag{3.67}$$

$$h_{r,2-phase} = h_{r,liquid}\left(1 + X\left(\frac{\rho_{r,l}}{\rho_{r,v}} - 1\right)\right)^{0.5} \tag{3.68}$$

All the thermo-physical properties of the refrigerant, R134a, and water are determined using the property equations given in Appendix B and Appendix C, respectively.

3.3.3 Solution procedure for the bare condenser tubes (multiple rows)

Based on the detailed models presented in the preceding sections, a FORTRAN computer code is written for the numerical simulation of the bare

serpentine tube of the evaporatively-cooled condenser. Using the FORTRAN code, the model equations are numerically solved for the temperature distribution of the thin water film and subsequently for the heat transfer coefficients of the tube elements. The mass flux of water evaporated from the film-air interface as well as the water film temperature and flow rate at the bottom of the tube segment are also determined. Now, with the known inlet refrigerant conditions (pressure, temperature, and mass flow rate) at the first tube segment, equations (3.54) and (3.59) are used to determine the exit refrigerant temperature and the outside tube wall temperature for the bare tubes, respectively. The computation for the superheated region is continued until the refrigerant vapour attains saturated vapour state (the point where the exit refrigerant temperature reaches the condensing temperature, determined from the inlet pressure of the superheated refrigerant vapour). At this point, the refrigerant quality is taken as unity and the computation is proceeded for the refrigerant quality and outside tube wall temperature with equations (3.62) and (3.65). The computation for the sub-cooled region starts when the quality of the refrigerant reaches zero, and the computation continues until the last segment of the serpentine tube as shown in Figure 3.7. The flow rate and temperature of the falling film from one segment to the corresponding segment in the tube below are transferred in the computation as depicted in Figure 3.7. The above computational procedure for the bare tubes of an evaporatively-cooled condenser is depicted in detail in a flow chart in Figures 3.12.

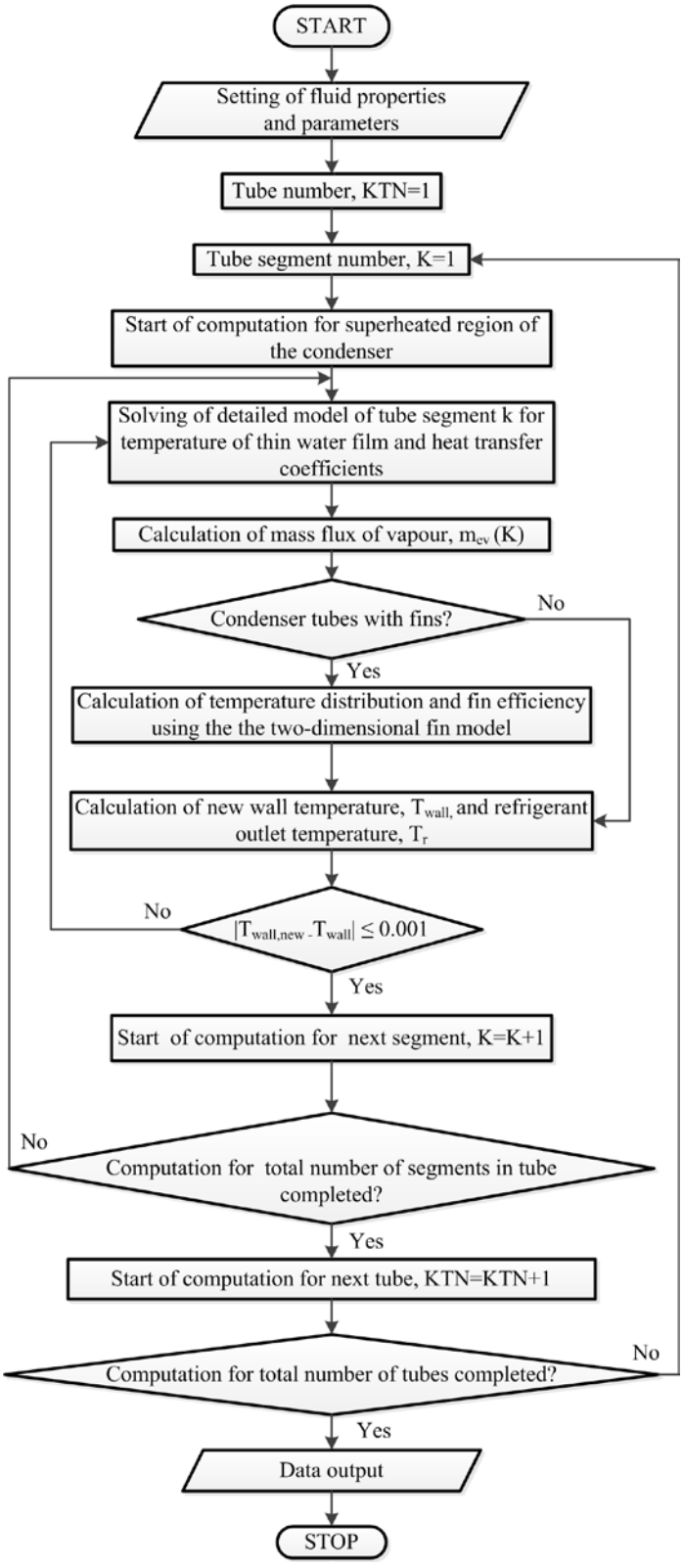

Figure 3.12 *Flow diagram for the computation of the serpentine tube model*

3.4 Numerical Results from the Detailed Model for a Tube Element of Evaporatively-Cooled Condenser

The detailed model developed for a small tube segment is used to quantify the simultaneous heat and mass transfer in the falling film of the evaporatively-cooled condenser. In the numerical simulation using the detailed model of the tube element, a constant wall temperature is assumed due to the smallness of the element. The discretized energy equation presented in the preceding section is numerically solved in the computational domain for the temperature distribution of the thin water film. Subsequently, the temperature distribution obtained is used to determine the film-tube interface (h_i) and film-air interface (h_o) heat transfer coefficients. Rate of water evaporated from the film-air interface is also determined from the numerically obtained film-air interface temperature. The two heat transfer coefficients and the rate of water evaporated from the film-air interface establish the performance of the evaporatively-cooled condenser using the extended detailed models for the evaporatively-cooled condensers with serpentine tubes. The numerical results for the heat and mass transfer characteristics obtained from the detailed model developed for the small representative evaporatively-cooled tube element are presented in the following sections.

3.4.1 Temperature distribution and heat transfer coefficients

The temperature profiles of the thin water film obtained for initial film thicknesses δ_w of 0.1mm and 0.15 mm are shown in Figures 3.13 and 3.14, respectively. The film Reynolds number, Re_f, as defined by equation (3.26), corresponding to the above film thicknesses are 3 and 9, respectively. As can be seen

from the temperature distribution profiles, the temperature varies quite consistently along the flow direction and across the film thickness up to more than half of the periphery of the tube. After that, as evident from the figures, there is a gradual drop in the interface temperature resulting from the increase in film thickness at the trailing section of the condenser tube periphery. For the film temperature profile for the 0.15 mm thick film, the rate of increase in temperature is slower compared to that for the 0.1mm thick film due to the added water film resistance resulting from the increase in film thickness.

The temperature distribution information of Figures 3.13 and 3.14 are used to determine the film-tube interface (h_i) and film-air interface (h_o) heat transfer coefficients. Variations of h_i, h_o and the combined heat transfer coefficient h ($h = 1/h_i + 1/h_o$) around the periphery of the condenser tube are shown in Figures 3.15 and 3.16. Figure 3.15 shows the variation of the heat transfer coefficients for an entry film thickness $\delta_{w,i}$ of 0.1 mm. As evident from the figure, the highest values of the heat transfer coefficients occur at the 90^o location on the periphery. The value of film thickness, δ is minimum at the 90^o mark as can be evaluated from equation (3.25); the maximum value of the heat transfer at this location can be attributed to this. The highest values of h_o, h_i, and h as seen from Figure 3.15 are about 32,000, 16,000, and 10,660 W/m^2 K, respectively. For this run of simulation, the air velocity was kept at 4 m/s, which is typical in an average capacity split air-conditioning system. As can be seen from Figure 3.16, the heat transfer coefficients decrease quite significantly when the film thickness is increased to 0.15 mm.

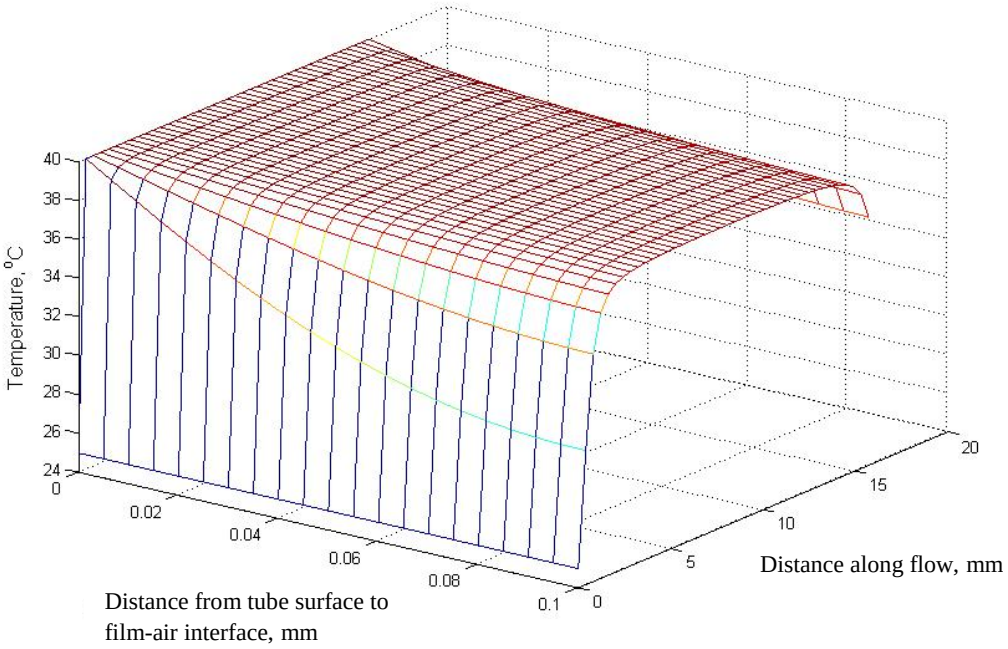

Figure 3.13 *Simulated water film temperature distribution for T_a = 30 ^oC, T_{wall} = 40 ^oC, T_{wi} =25 ^oC, RH = 80%, δ_w=0.1 mm (Re_f = 3), V=4m/s, R = 5 mm*

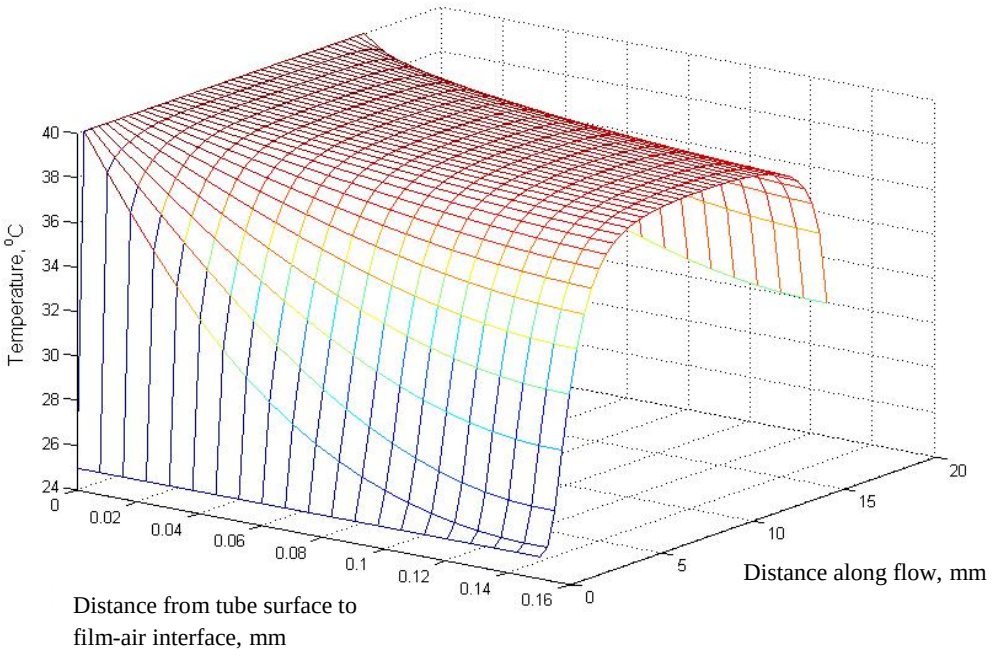

Figure 3.14 *Simulated water film temperature distribution for T_a = 30 ^oC, T_{wall} = 40 ^oC, T_{wi} =25 ^oC, RH = 80%, δ_w=0.15 mm (Re_f = 9), V=4m/s, R = 5 mm*

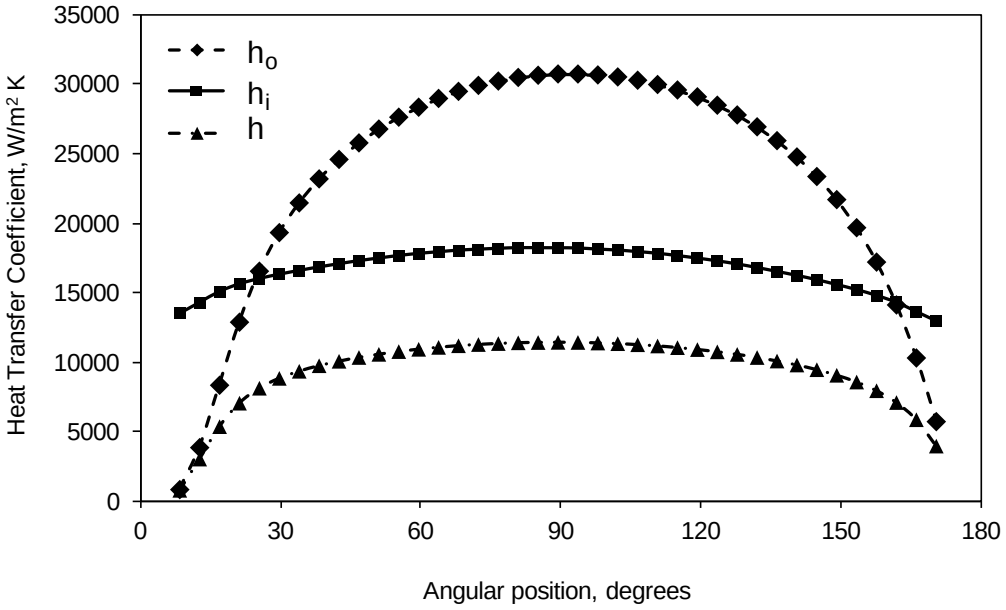

Figure 3.15 *Simulated variation of heat transfer coefficients along the tube periphery in the water flow direction for T_a = 30 ^oC, T_{wall} = 40 ^oC, T_{wi} =25 ^oC, RH = 80%, δ_w=0.1 mm (R_{ef}= 3), R = 5 mm*

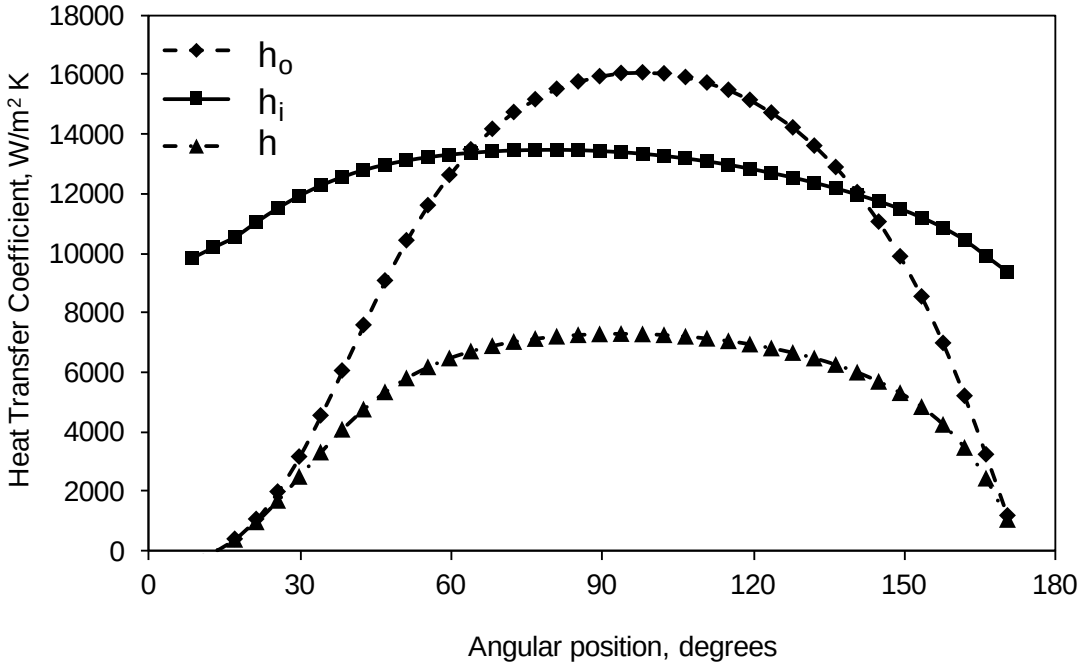

Figure 3.16 *Simulated variation of heat transfer coefficients along the tube periphery in the water flow direction for T_a = 30 ^oC, T_{wall} = 40 ^oC, T_{wi} =25 ^oC, RH = 80%, δ_w=0.15 mm (Re_f = 9), R = 5 mm*

The highest values of h_o, h_i, and h obtained for δ_w = 0.15 mm are about 16,000, 13,000, and 7,170 W/m^2 K, respectively.

The theory and the simulation results presented for the small tube segment is compared with the experimental and numerical results from published literature. In Figure 3.17, the combined heat transfer coefficient, h, of the present study is compared with that reported by Chun and Seban (1971) and Nusselt (Oosthuizen et al. 1999). The Chun and Seban result is for water film flowing along the outside of a vertical tube, where the flow is thermally developed. Whereas, in the Nusselt's and present work, the water film flowing circumferentially on a horizontal tube, where there is the existence of a thermally developing region as shown by Chyu and Bergles (1987) in their work. Chyu and Bergles also reported that the heat transfer coefficient for the case of thermally developing condition is greater than for the case of thermally developed condition. As can be seen from Figure 3.17, Chun and Seban's finding is reflected in this comparison, as the heat transfer coefficient obtained from Nusselt's work and the present study is greater than that from Chun and Seban. As can also be seen from the figure, the value of the average heat transfer coefficient from the present study is greater than those from Chun et al. and Nusselt when the mass flow of the water is low. This can be attributed to: (i) existence of thermally developing region as reported by Chyu and Bergles, (ii) the water film entry point as shown in the Figure 3.2 is at 9^o from the top of the tube, thereby a low film thickness causing a low thermal resistance and better heat transfer characteristics compared to the above work, where the water enters vertically resulting in higher film thickness at the entry region.

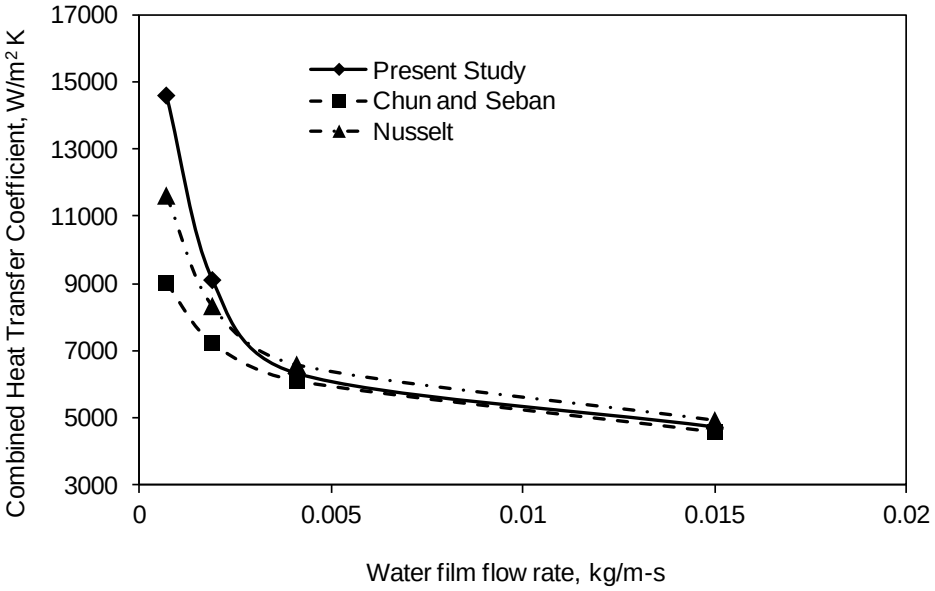

Figure 3.17 *Comparison of Simulated variation of average combined heat transfer coefficient from present detailed model with the model from literature for T_a = 30 ^oC, V = 0.1 m/s (Natural Convection), T_{wi} =25 ^oC, T_{wall} =40 ^oC, RH= 80 %, R = 5 mm*

Figure 3.18 shows a comparison of the combined heat transfer coefficients from the present investigations with those from Fletcher and Serna's (1974) experimental results for tubes of diameters 25.4 mm and 50.8 mm. The Figure shows the variation of the heat transfer coefficients with the saturation temperature of the water being sprayed on to the tube with a constant wall temperature range of 55 to 130 ^oC. It is important to note that to prevent boiling of water and its effects, the pressure of the chamber housing the tube was maintained at a pressure corresponding to the saturation temperature of the feed water. As can be seen from the figure, the present theory and the experimental results of Fletcher and Sernas shows good agreement except for a few points, which could be due to the fact that variations in thermo-physical properties of water with temperature were accounted in the present

study. In addition to this, the consideration of the temperature gradient in the thin water film in the present study could also be a contributing factor. In Fletcher and Sernas' work, the variations of the thermo-physical properties with temperature as well as the temperature gradient across the water film were not considered.

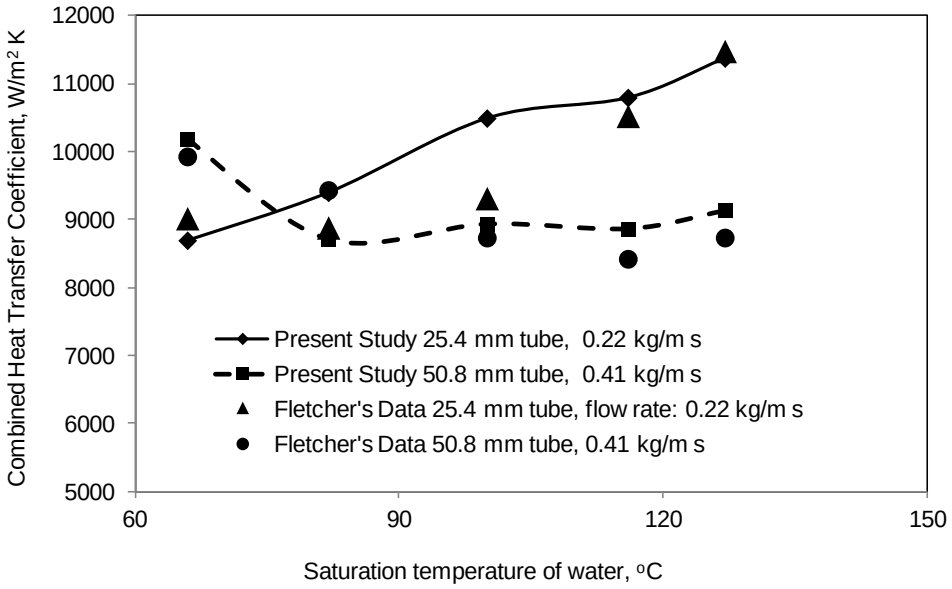

Figure 3.18 *Comparison of simulated average combined heat transfer coefficient from present detailed model with Fletcher and Serna's experimental data for T_a = 30 ^oC, V = 0.1 m/s (Natural Convection), RH= 80 %*

3.4.2 Effect of operating conditions on the heat and mass transfer

To establish how the heat and mass transfer in the falling film of the evaporatively-cooled condenser are affected by the main operating parameters of the condenser such as air flow rate, temperature, relative humidity as well as the tube wall temperature, a parametric study involving them is undertaken. The effect of each of the above mentioned parameters on the local Nusselt numbers (Nu_o and Nu_i) and water evaporation rate at the film-air interface are described in the following sections.

3.4.2.1 Effect of air velocity

The effect of air velocity on the film-air interface local Nusselt number (Nu_o) for an entry film Reynolds number of 3 is depicted in Figure 3.19. The local Nusselt number (Nu_o) changes from 2.5 to about 3.0 when the velocity is increased from 1 to 4 m/s. The corresponding variations of film-tube local Nusselt number (Nu_i) are shown in Figure 3.20.

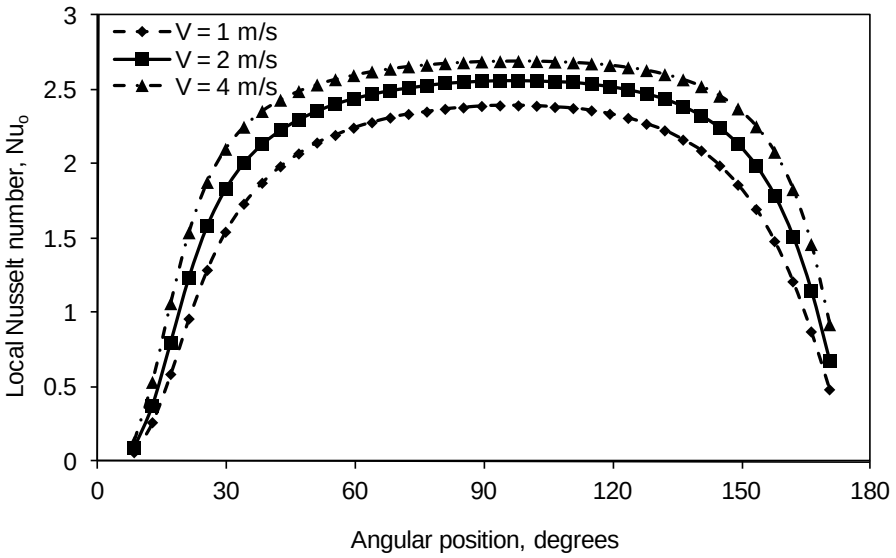

Figure 3.19 *Simulated variation of film-air interface local Nusselt number, Nu_o along the tube periphery in the water flow direction for different air velocity for δ_w=0.1 mm (Re_f = 3), T_a = 30 ^oC, T_{wall} = 40 ^oC, T_{wi} =25 ^oC*

Figure 3.20 shows the effect of velocity on film-tube interface local Nusselt number, Nu_i. As can be seen from the figure a reverse trend is observed compared to that of the local Nusselt number, Nu_o seen in Figure 3.19. This can be attributed to the combined diminishing effect of the ratio of film thickness and film thermal conductivity, which increases with the film temperature along the periphery of the tube.

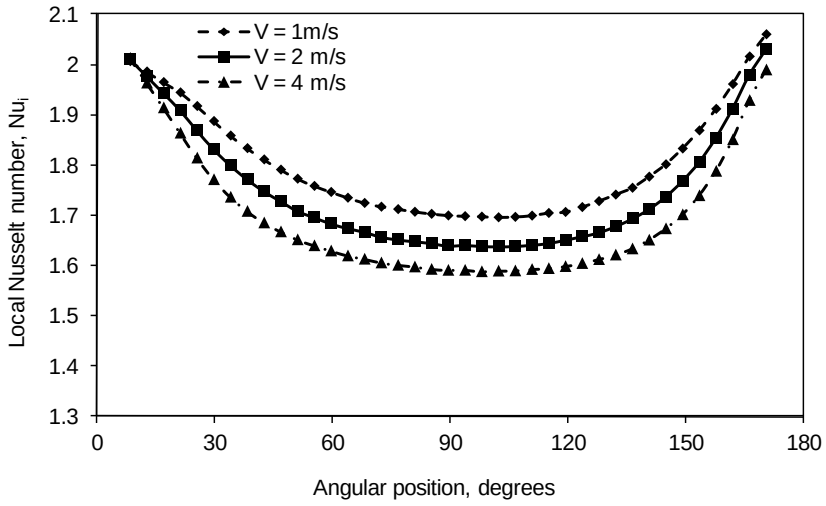

Figure 3.20 *Simulated variation of film-tube interface local Nusselt number, Nu_i along the tube periphery in the water flow direction for different air velocity for δ_w=0.1mm (Re_f = 3), T_a = 30 ^oC, T_{wall} = 40 ^oC, T_{wi} =25 ^oC*

Figure 3.21 shows the variation of the film water evaporation rate with different air velocities and as evident from the Figure, the water evaporation rate increases with the increase in air inlet velocity. As can be seen from the figure, the highest water evaporation rate obtained is: 3.5 and 8 kg/m^2 h, corresponding to the velocities of 1 and 4 m/s, respectively.

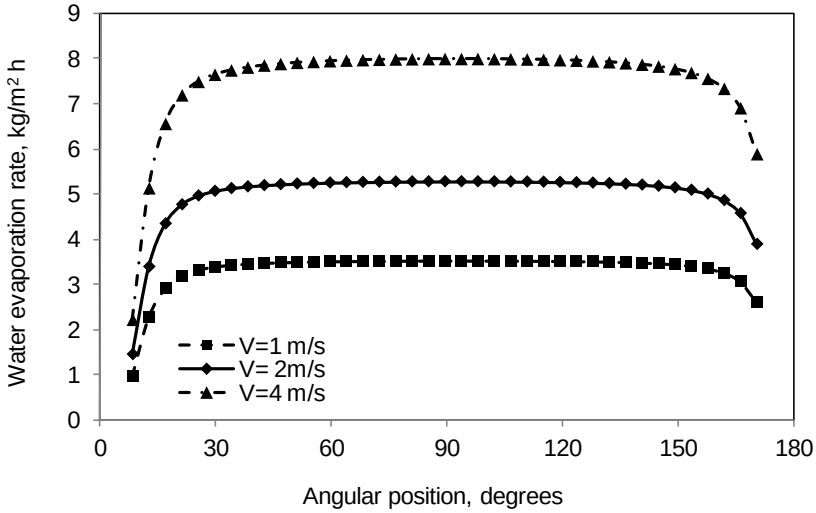

Figure 3.21 *Simulated variation of interface water evaporation rate along the tube periphery in the water flow direction for different air velocity for δ_w=0.1 mm (Re_f = 3), T_a = 30 ^oC, T_{wall} = 40 ^oC, T_{wi} =25 ^oC, RH=80%*

3.4.2.2 Effect of air temperature

The effect of ambient air temperature on the local Nusselt numbers is shown in Figures 3.22 and 3.23. As can be seen from the figures, the ambient temperature change from 30 ^{o}C to 40 ^{o}C does not cause significant changes in the local Nusselt number. This trend is consistent with the local heat transfer equations (3.34) and (3.35) given in the theoretical model chapter resulting from the unchanged average water film temperature. For a constant air flow rate, relative humidity and wall temperature, the rate of water evaporated from the water-air interface is increased for lower air temperature. However, as can be seen from the film-air interface heat transfer equation (3.35), there is a corresponding increase in the difference in average water film temperature and the film-air interface temperature resulting in a very marginal improvement in h_o and hence, the associated local Nusselt number, Nu_o.

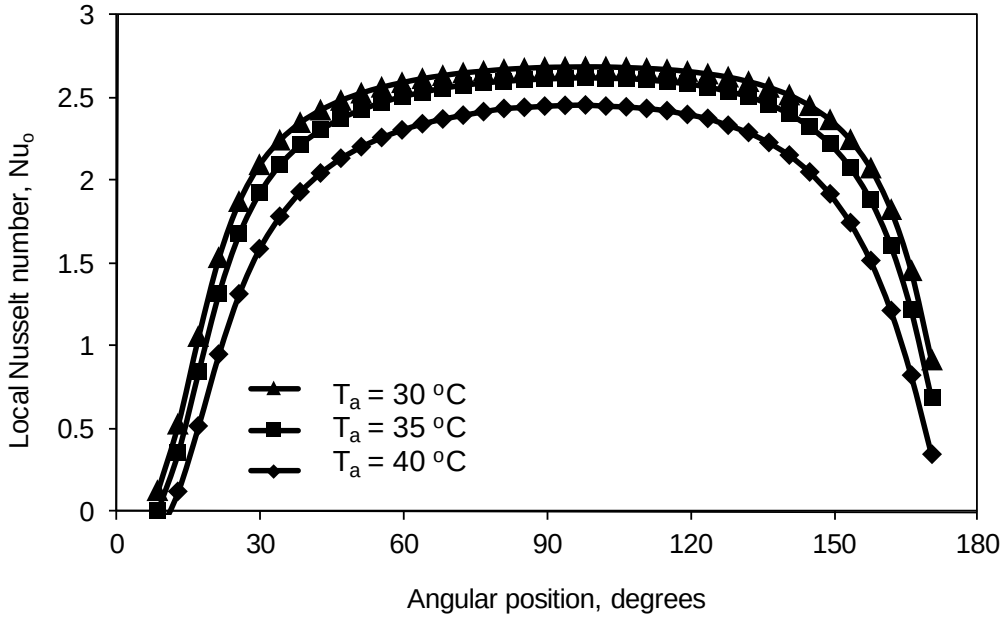

Figure 3.22 *Simulated variation of film-air interface local Nusselt number, Nu_o along the tube periphery in the water flow direction for different air temperature for δ_w=0.1 mm (Re_f = 3), T_{wall} = 40 ^{o}C, V = 4 m/s, T_{wi} =25 ^{o}C, RH= 80 %*

As for the film-tube interface local Nusselt number trend in Figure 3.23, there is a marginal increase in the average water film temperature when the ambient temperature increases. This results in a smaller difference between wall and average bulk temperature resulting in marginally higher value of film-tube heat transfer coefficient as can be seen from the equation of the heat transfer coefficient and a corresponding increase in the associated local Nusselt number.

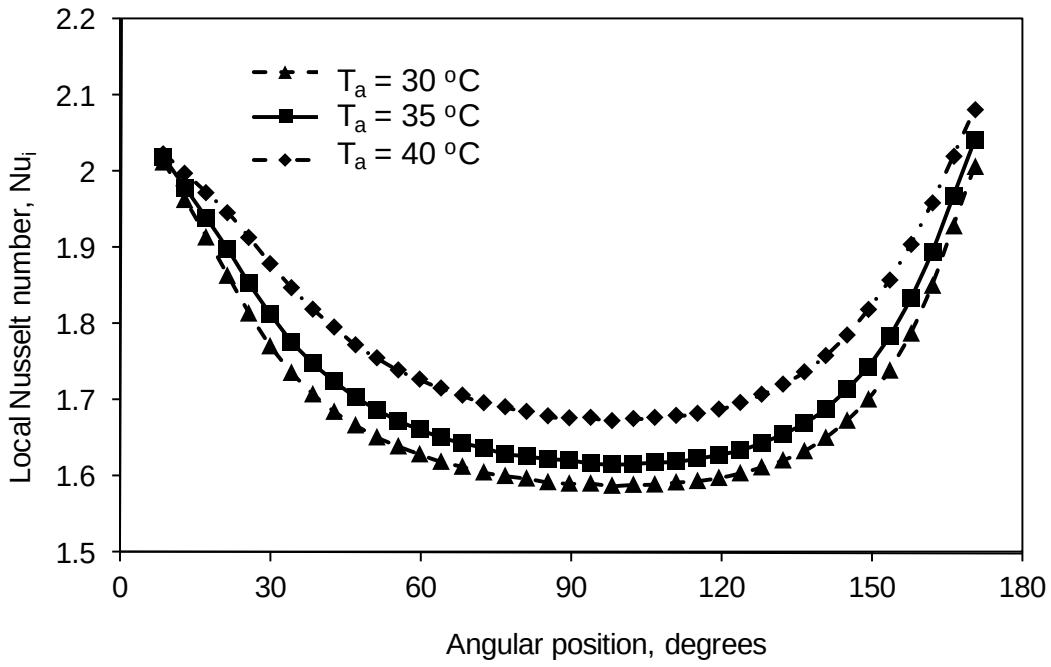

Figure 3.23 *Simulated variation of film-air interface local Nusselt number, Nu_i along the tube periphery in the water flow direction for different air temperature δ_w=0.1 mm (Re_f = 3), T_{wall} = 40 °C, V = 4 m/s, T_{wi} =25 °C, RH= 80 %*

Figure 3.24 shows the effect of the ambient temperature on the film evaporation rate. As evident from the Figure, the evaporation rate increases quite significantly around the periphery of the tube. This increase in the rate of water evaporated can be attributed to the favourable enthalpy potential developed at the film-air interface resulting from the reduced ambient temperature.

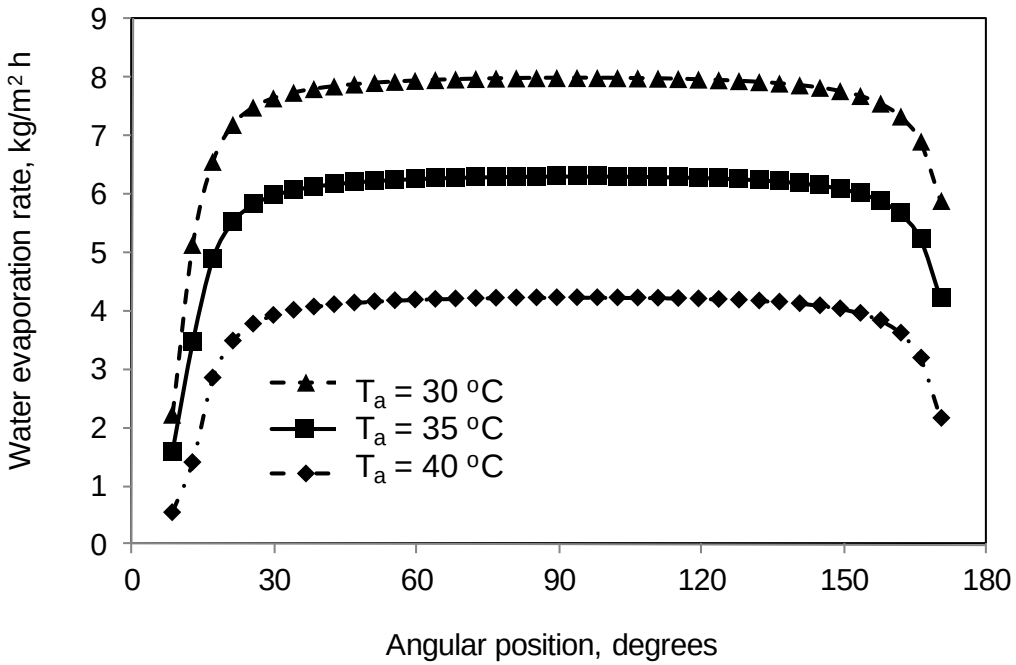

Figure 3.24 *Simulated variation of interface water evaporation rate along the tube periphery in the water flow direction for different ambient temperature for δ_w=0.1 mm (Re_f = 3), T_{wall} = 40 ^oC, T_{wi} =25 ^oC, RH = 80%, V=4m/s*

3.4.2.3 Effect of air relative humidity

As for the effect of ambient temperature on the local Nusselt numbers, the change in relative humidity has very little effect on the local Nusselt numbers. The same reasons as in the case of the ambient temperature effect can be cited for these trends as well.

The effect of relative humidity on the film-air interface evaporation rate is shown in Figure 3.25. As evident from the figure, better evaporation potential is developed when the relative humidity of the air is lowered and vice versa with the increase in relative humidity.

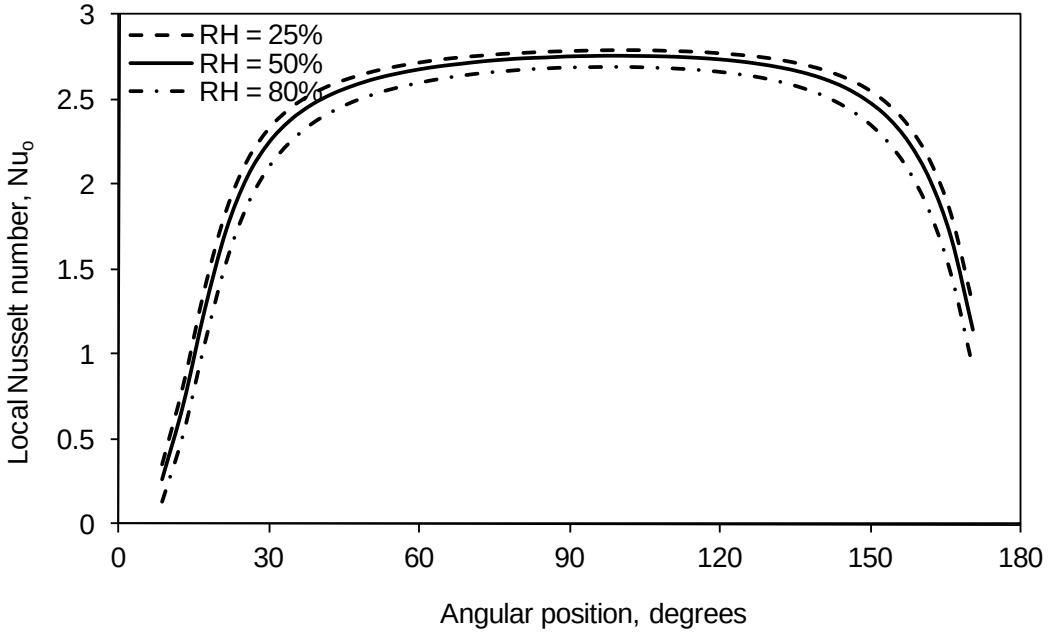

Figure 3.25 *Simulated variation of film-air interface local Nusselt number, Nu_o along the tube curvature in the water flow direction for different relative humidity for δ_w=0.1mm (Re_f = 3), T_a = 32 ^oC, V = 4 m/s, T_{wi} =25 ^oC, T_{wall} = 40 ^oC*

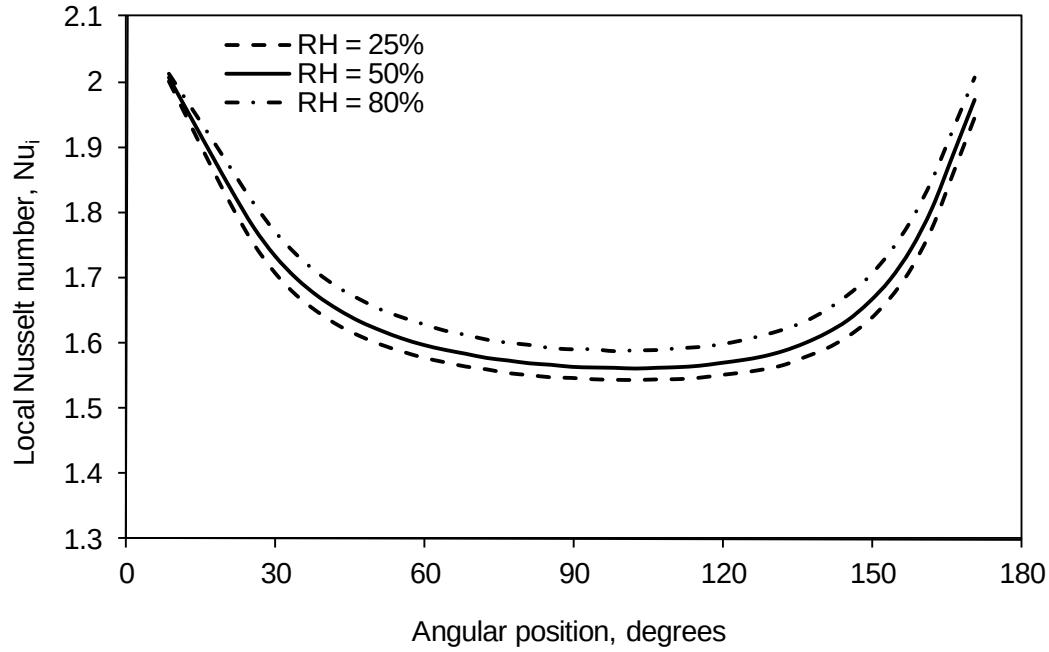

Figure 3.26 *Simulated variation of film-tube interface local Nusselt number, Nu_i along the tube periphery in the water flow direction for different relative humidity for δ_w=0.1 mm (Re_f = 3), T_a = 32 ^oC, V = 4 m/s, T_{wi} =25 ^oC, T_{wall} = 40 ^oC*

Figure 3.27 shows the variation of the interface water evaporation rate with the angular position around the periphery of the tube element for different relative humidities. As can be seen from the figure, for a given air temperature, a lower relative humidity of the air creates favourable water evaporation conditions at the film surface due to the better enthalpy potential of the air.

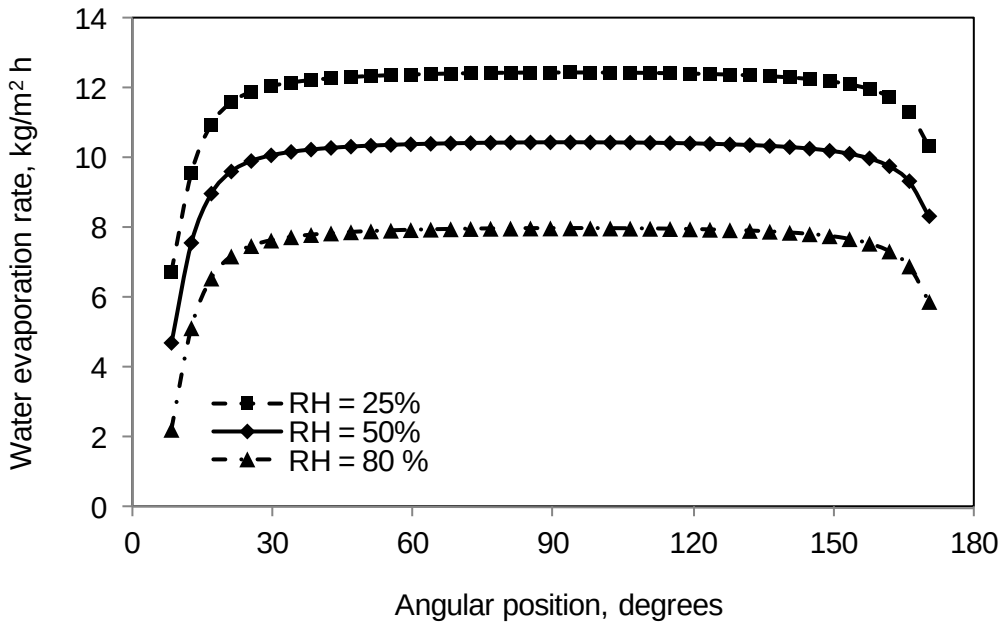

Figure 3.27 *Simulated variation of interface water evaporation rate along the tube periphery in the water flow direction for different RH for δ_w = 0.1mm (Re_f= 3), T_{wall} = 40 ^oC, T_{wi} =25 ^oC, T_a = 30 ^oC, V=4m/s)*

3.4.2.4 Effect of film Reynolds Number (Re_f)

Figures 3.28 to 3.30 show the effect of film Reynolds number at the top of the small tube segment (at the flow entry location) on the local Nusselt numbers as well as the water evaporation rate. The film- air interface local Nusselt number, Nu_o shows

an inversely proportional trend with the film Reynolds number as a result of the better evaporation conditions developed at the film surface due to the increased rate of heat transfer. This increase in heat transfer rate can be attributed to the lower thermal resistance existing for the smaller film thickness for the lower film Reynolds number as determined from Bird's equation (3.25).

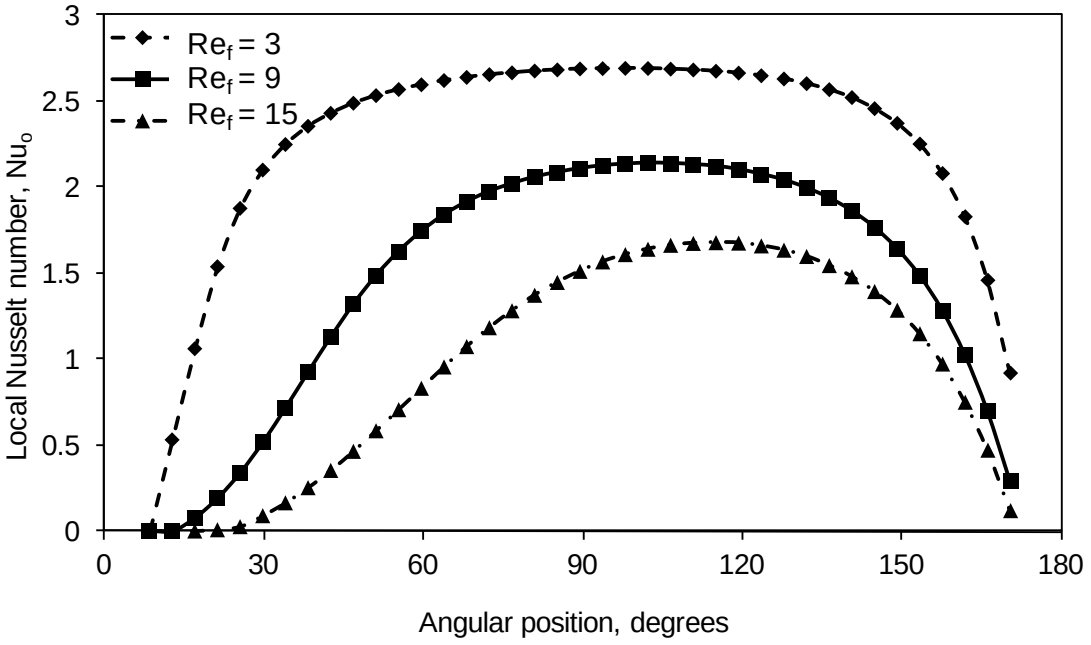

Figure 3.28 *Simulated variation of film-air interface local Nusselt number, Nu_o along the tube periphery in the water flow direction for different film Reynolds number for T_a = 30 ^oC, T_{wall} = 40 ^oC, T_{wi} =25 ^oC, RH = 80%, V=4m/s*

The film-tube interface local Nusselt number Nu_i shows a decreasing trend when the film Reynolds number is raised. For the higher thermal resistance formed causes a gradual build up of the average bulk water temperature which in turn increases the film-tube interface heat transfer coefficient as seen from the convective heat transfer coefficient equation (3.35). Higher film-tube heat transfer coefficient

translates into a higher film-tube interface local Nusselt number. Figure 3.30 shows the comparison of the interface water evaporation rate for the three film Reynolds numbers; 3, 9 and 15. As can be seen from the figure, the trend goes against one's intuitive thinking that a higher evaporation rate would occur for a higher film Reynolds number. The reason behind this trend shall well be explained with the fact that though more flow is available in the case of a higher Re_f , the higher thermal resistance due to the higher film thickness inhibits the heat transfer rate across the film. The opposite happens when the film Reynolds number is 3, where more heat is available at the interface resulting in greater water evaporation.

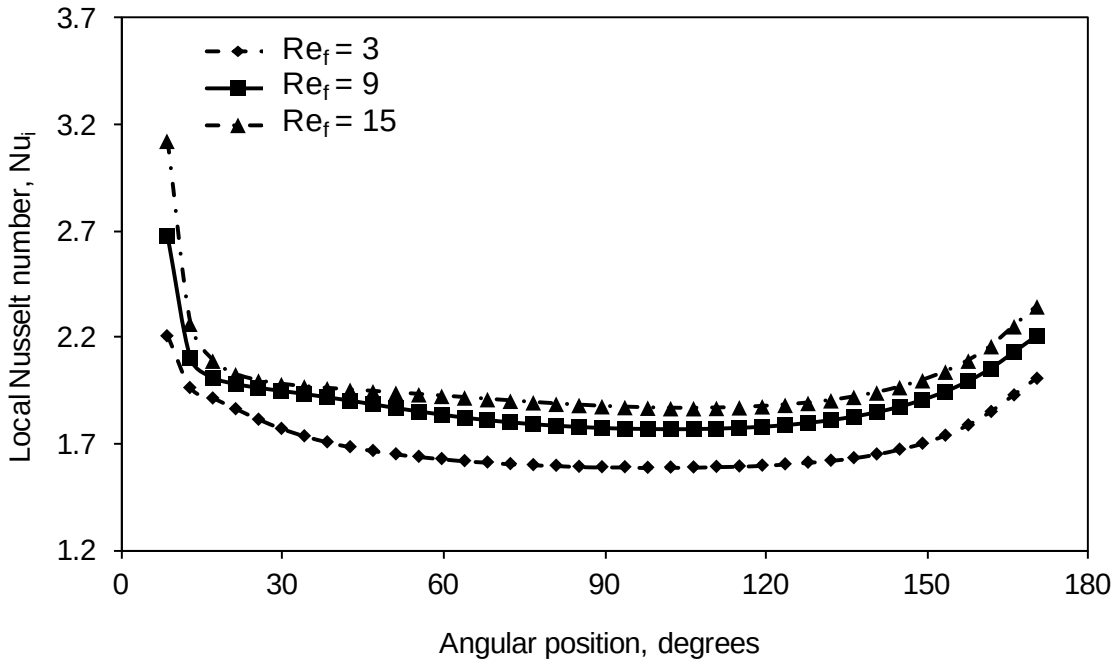

Figure 3.29 *Simulated variation of film-tube interface local Nusselt number, Nu_i along the tube periphery in the water flow direction for different film Reynolds number for T_a = 30 ^oC, T_{wall} = 40 ^oC, T_{wi} =25 ^oC, RH = 80%, V=4m/s*

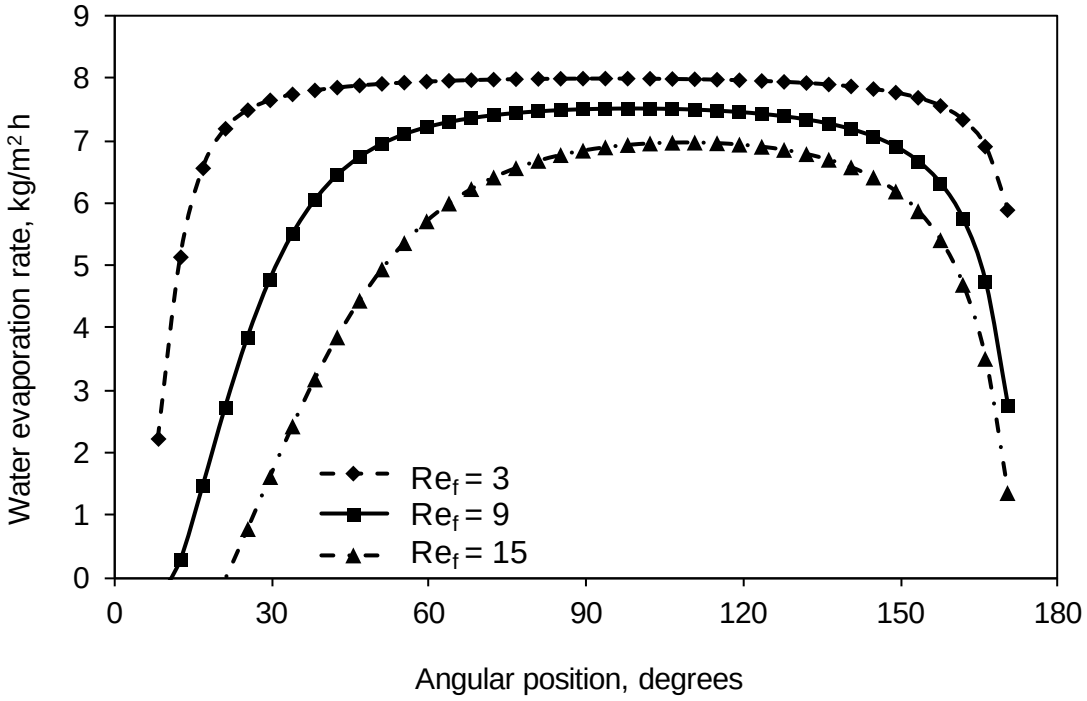

Figure 3.30 *Simulated variation of water film surface evaporation rate along the tube periphery in the water flow direction for different film Reynolds number for RH=80%, T_{wall} = 55 ^{o}C, T_{wi} =25 ^{o}C, T_a = 30 ^{o}C, V=4m/s*

3.4.2.5 Effect of wall temperature (T_{wall})

The variations of the local Nusselt numbers (Nu_o and Nu_i) for different tube wall surface temperatures are shown in Figures 3.31-3.33. As can be seen from Figure 3.31, the Nu_o peak shifts downwards on the periphery of the tube as the wall temperature is increased from 35 to 45 ^{o}C, with a maximum of about 2.8 for a wall temperature of 45 ^{o}C. The corresponding Nusselt numbers for 35 ^{o}C and 45 ^{o}C cases are 2.1 and 2.4, respectively.

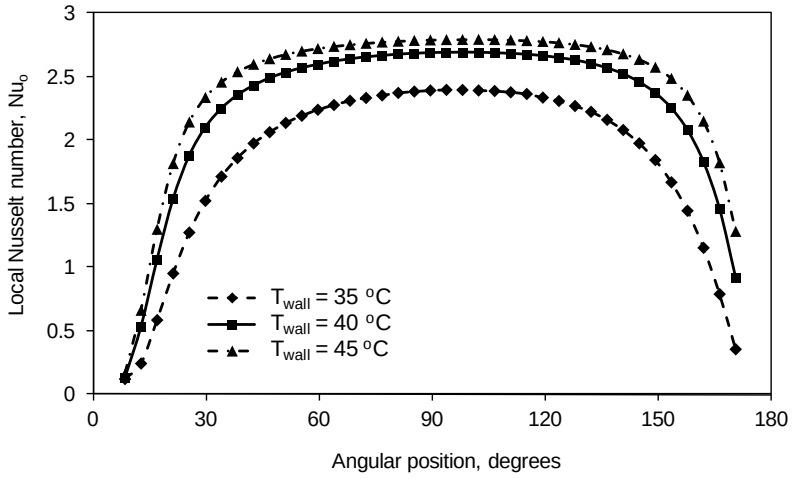

Figure 3.31 *Simulated variation of water film-air interface local Nusselt number, Nu_o along the tube periphery in the water flow direction for different wall temperature for δ_w = 0.1mm (R_{ef}= 3) T_a = 30 ^oC, V = 4 m/s, T_{wi} =25 ^oC, RH= 80 %*

The effect of tube wall temperature on the film-tube interface Nusselt number is depicted in Figure 3.32. The trend in this figure is an inverse trend as expected due to the increase in the temperature difference between wall and the average water film temperature.

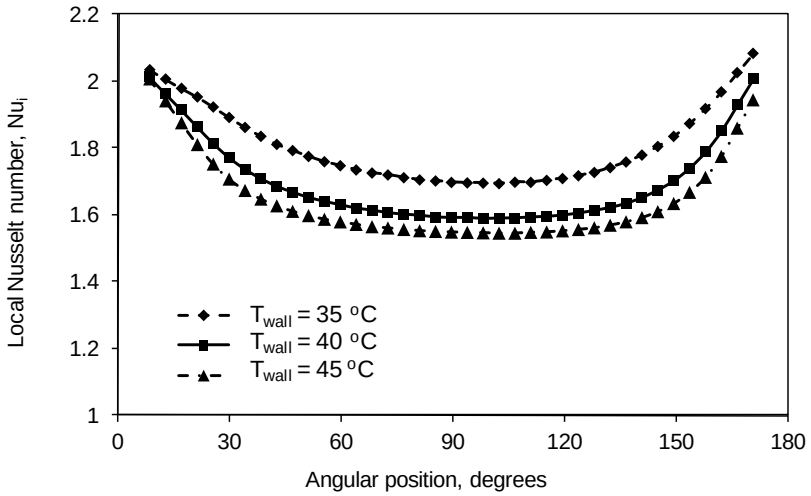

Figure 3.32 *Simulated variation of water film-air interface local Nusselt number, Nu_i along the tube periphery in the water flow direction for different wall temperature for δ_w = 0.1mm (R_{ef} = 3), T_a = 30 ^oC, V = 4 m/s, T_{wi} =25 ^oC, RH= 80 %*

Wall temperature as the varying parameter and the corresponding water film surface evaporation rates are depicted in Figure 3.33. As can be seen from the Figure, with the other system parameters kept constant, the increase in wall temperature causes significant increase in the film evaporation rate of up to 12 kg/m^2 h.

To investigate how the evaporative cooling incorporated in the condenser of the air-conditioning system performs in the absence of the air being blown across the condenser coil, the simulation is run with the air velocity set to a value of 0.1 m/s. The air-side heat transfer coefficient corresponding to this air velocity is 10 W/m^2 K (Incropera, 2007), which is a typical value for natural convection heat transfer. Figure 3.34 shows the comparison of film evaporation rate for forced (FC) and natural convection (NC) modes. As can be seen from the result of Figure 3.34, a drastic reduction in evaporation rate is observed when the FC mode is switched to NC mode. As can be seen, a reduction of about 90 % is observed.

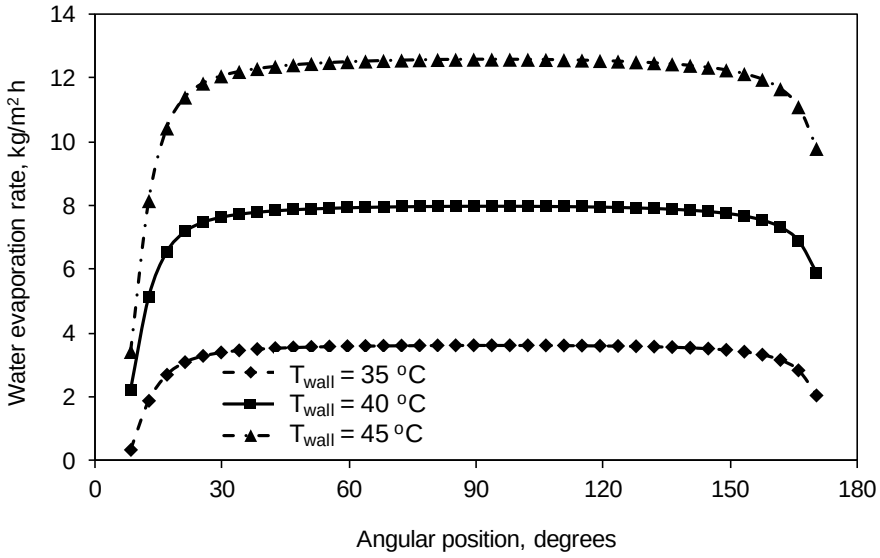

Figure 3.33 *Simulated variation of water film surface evaporation rate along the tube periphery in the water flow direction for different wall temperature for δ_w = 0.1mm (R_{ef}= 3), T_a = 30 ^{o}C, V = 4 m/s, T_{wi} =25 ^{o}C, RH= 80 %*

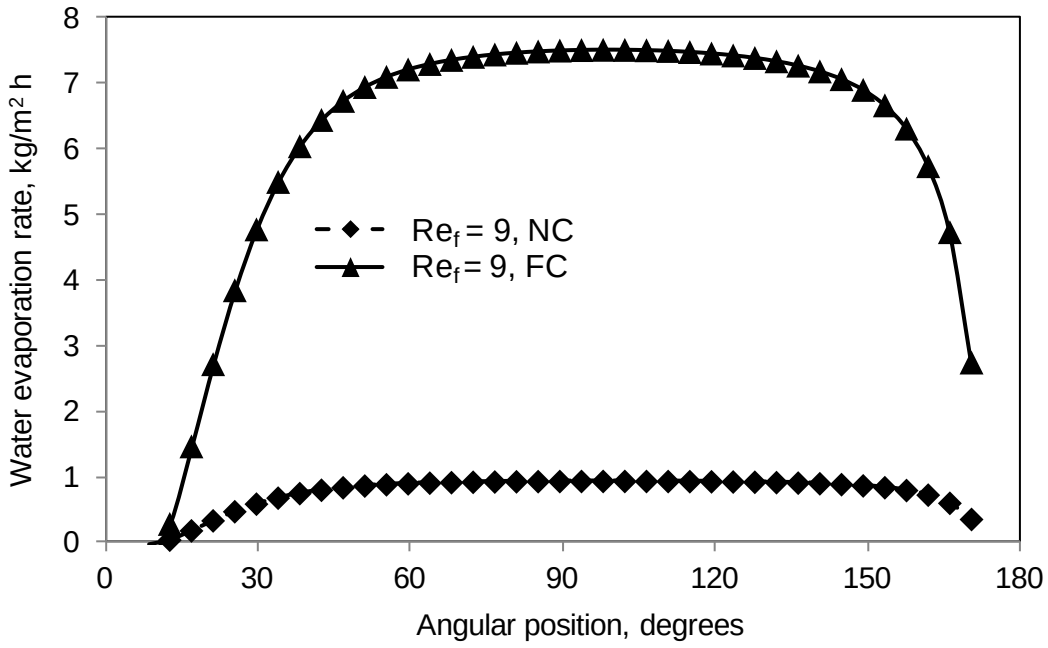

Figure 3.34 *Simulated variation of water film surface evaporation rate along the tube periphery in the water flow direction for natural and forced convection with evaporative cooling for δ_w = 0.15mm (R_{ef} = 9), T_a = 30 ^oC, V = 0.1 m/s (NC), V = 4.0 m/s (FC), T_{wi} =25 ^oC, RH= 80 %, T_{wall} = 40 ^oC*

3.5 Numerical Parametric Study of the Serpentine Bare-Tube Evaporatively-Cooled Condenser

To establish the overall performance of the bare-tube evaporatively-cooled condenser, a numerical parametric study is undertaken using the detailed model presented in the preceding section. The salient results from the numerical investigations performed on the serpentine bare condenser tubes are presented in the following sections.

The refrigerant R-134a enters the serpentine condenser tubes as superheated refrigerant vapour as shown in Figure 3.7 and emerges from the condenser as sub-cooled liquid. Fine water sprays cover the top tubes with a thin water film at predetermined flow rate determined by Bird's equation (3.25). The higher the mass of

water evaporated from the tube surface, the faster the heat rejected by the condenser to the surroundings, resulting in a lower condensing temperature of the air-conditioning system. The lower the condensation temperature, the lower is the pressure lift between the evaporator and condenser resulting in an improved COP of the air-conditioning system.

Numerically simulated variations of the film-air interface (h_o) and the film-tube interface (h_i) heat transfer coefficients are shown in Figure 3.35 for a thin water film flowing from the top to bottom of the condenser tubes. The initial falling film water flow rate of 13.88 kg/m h, (corresponding film Reynolds number, $Re_f = 9$) is set to have a film thickness of 0.15 mm at the topmost tube. An average combined heat transfer coefficient, h, of about 7,900 W/m^2 K is observed, as can be seen from the figure. It is interesting to note that without evaporative cooling, for an air velocity of 4 m/s, calculated forced convection heat transfer coefficient (h_a) is just 86 W/m^2 K (Incropera et al. 2007), which is very much lower than that with evaporative cooling.

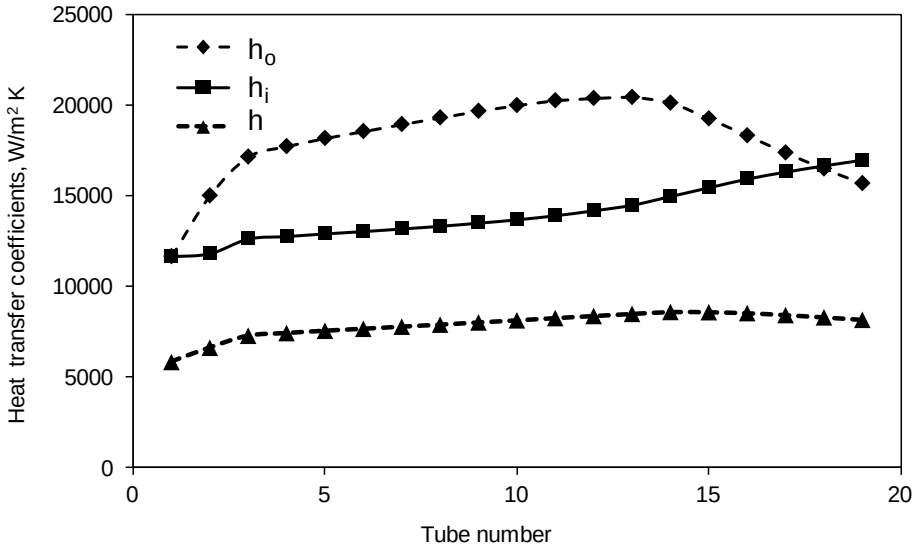

Figure 3.35 *Simulated variation of heat transfer coefficients in the condenser tubes for T_a = 30 ^{o}C, T_{wi} =25 ^{o}C, RH = 70%, Re_f = 9, V=4m/s, R = 5 mm*

Variations of the combined heat transfer coefficients, h, from the first to the last tube of the condenser are shown in Figure 3.36. As can be seen from the figure, higher values of the heat transfer coefficients are obtained for lower values of film thicknesses resulting from smaller thermal resistance.

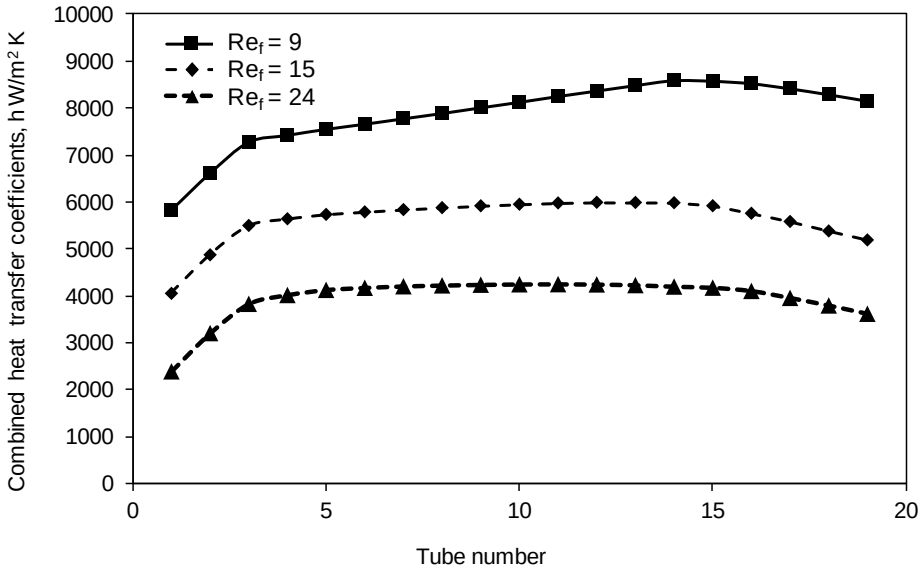

Figure 3.36 *Simulated variation of combined heat transfer coefficient along the tubes for different film Reynolds number for T_a = 30 ^oC, T_{wi} =25 ^oC, RH = 70%, V=4m/s, R = 5 m)*

Figures 3.37 to 3.40 show the results of a parametric study of the variation of average Nusselt number at the film-tube interface ($Nu_{i,av}$) and film-air interface ($Nu_{o,av}$) with the film Reynolds number for different temperatures and relative humidities. Figure 3.37 shows the variation of $Nu_{i,av}$ with film Reynolds number and as can be seen from the figure, the average film-tube interface Nusselt number increases with the film Reynolds number.

The opposite trend was observed for the case of film-air interface Nusselt number, Nu_o as shown in Figure 3.38. The reason behind this trend could be due to the fact that the value of h_o is likely to be more dependent on the film thickness and,

therefore, the water mass flow rate and film Reynolds number. In addition, the nature of the film interface such as the presence of waves and ripples at the surface may be other contributors to the value of the film- air interface heat transfer coefficient, h_o.

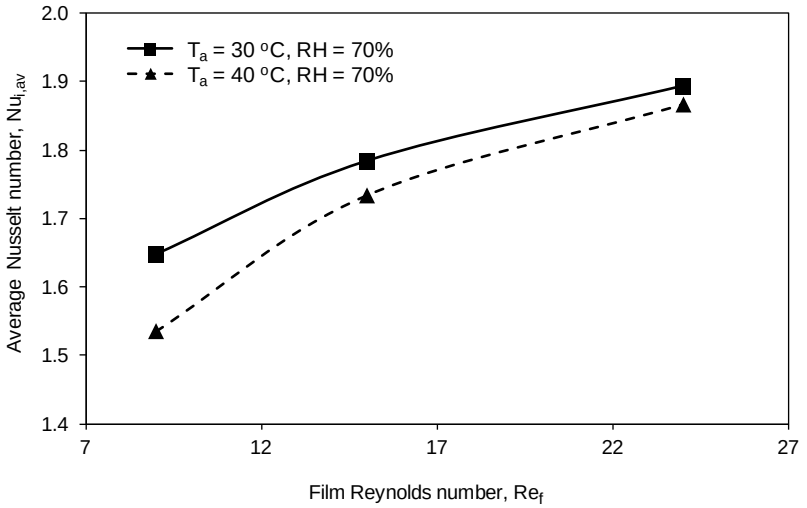

Figure 3.37 *Simulated variation of average film-tube interface Nusselt number with the film Reynolds number for different air temperature for T_{wi} =25 ^oC, Re_f = 9, V=4m/s, R = 5 mm*

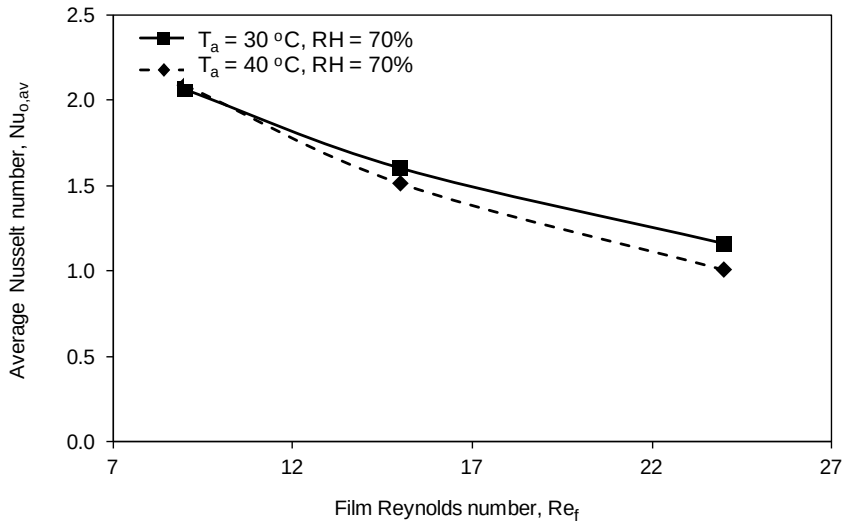

Figure 3.38 *Simulated variation of average film-air interface Nusselt number with the film Reynolds number for different air temperature for T_{wi} =25 ^oC, V=4m/s, R = 5 mm*

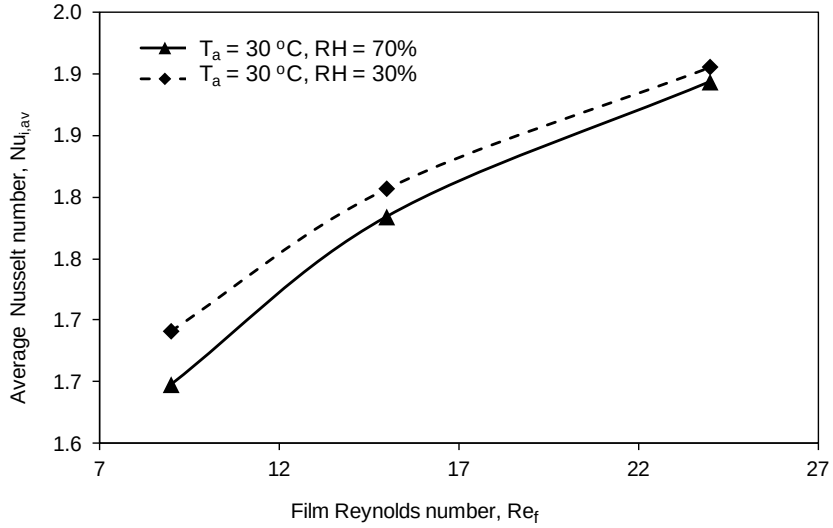

Figure 3.39 *Simulated variation of average film-tube interface Nusselt number with the film Reynolds number for different air relative humidity for T_{wi} =25 ^oC, V=4m/s, R = 5 mm*

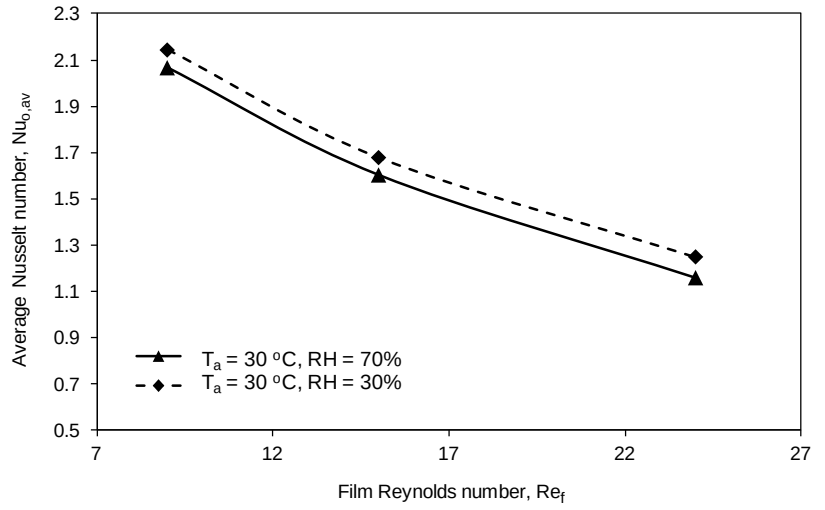

Figure 3.40 *Simulated variation of average film-tube interface Nusselt number with the film Reynolds number for different air relative humidity for T_{wi} =25 ^oC, V=4m/s, R = 5 mm*

The simulated variations of rate of water evaporated from the condenser tube surface with the film Reynolds number and the various operating conditions are plotted in Figures 3.41 to 3.43. The underlying trend in these figures can be well explained by the enthalpy potential of the air; i.e. air with lower relative humidity and

temperature possesses a favourable enthalpy potential which allows more water to evaporate from the film over the condenser tube surfaces. This in turn causes faster heat rejection rate.

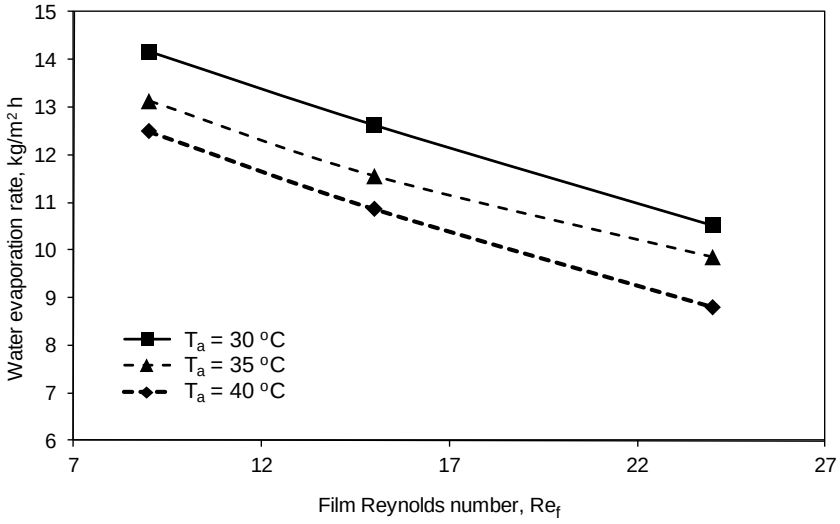

Figure 3.41 *Simulated variations of mass of water evaporated from the condenser tube surface with film Reynolds number and air temperature for T_{wi} =25 ^{o}C, V=4m/s, RH = 70%*

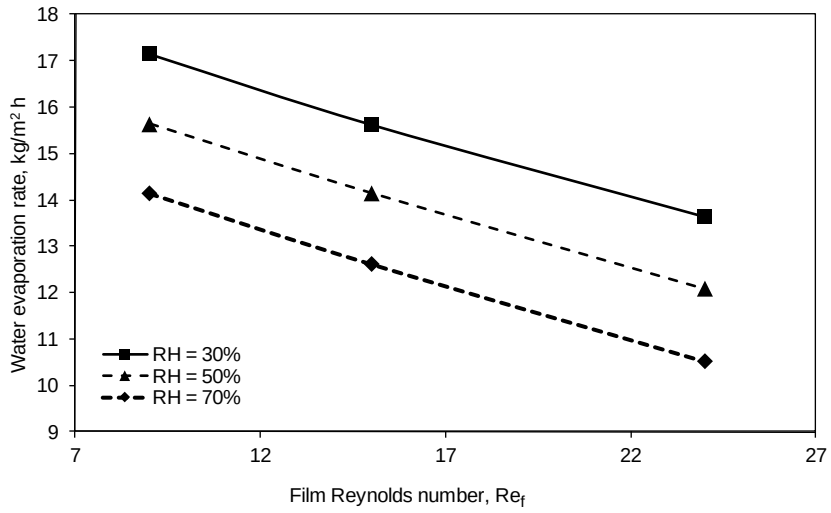

Figure 3.42 *Simulated variation of mass of water evaporated from the condenser tube surface with film Reynolds number and relative humidity of air for T_{wi} =25 ^{o}C, V=4m/s, T_a=30 ^{o}C*

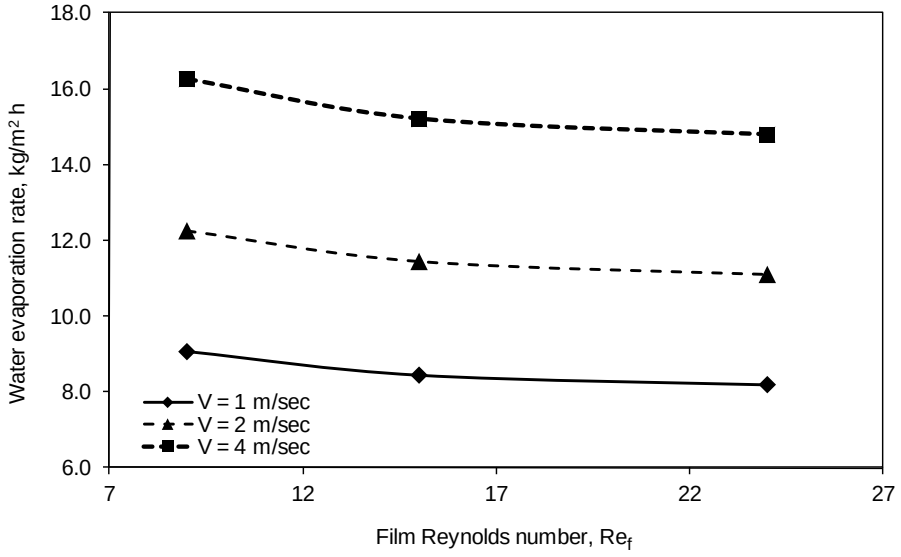

Figure 3.43 *Simulated variation of mass of water evaporated with film Reynolds number and air velocity for T_{wi} =25 ^{o}C, V=4m/s, RH = 70%*

Figures 3.44 to 3.46 show the simulated variation of the required bare-tube condenser tube length with the main operating variables of the evaporatively-cooled air-conditioner. For the same condenser heat rejection rate resulting from a change in refrigerant state from 80 ^{o}C, 15 bar superheated vapour to 42 ^{o}C subcooled liquid refrigerant is considered for these plots. Figure 3.44 shows the variation of the condenser tube length with film Reynolds number, Re_f and ambient air temperature. As expected and can be seen from the figure, lower air inlet temperatures and lower film Reynolds numbers give better performance requiring shorter tube lengths for the condenser.

Simulated variations of the condenser tube length with film Reynolds number and ambient air relative humidity is depicted in Figure 3.45. As can be seen in the figure, the required tube length is shortened for lower RH as the air possesses a better enthalpy potential resulting from lower air inlet relative humidity. As can be observed

from the figure, for the bare-tube evaporatively-cooled condenser investigated, a total tube length of just 10 m is required (about 15 nos. of 0.7 m straight tubes) for a 13 ^{o}C sub-cooled refrigerant outlet condition for the case of 30 % relative humidity.

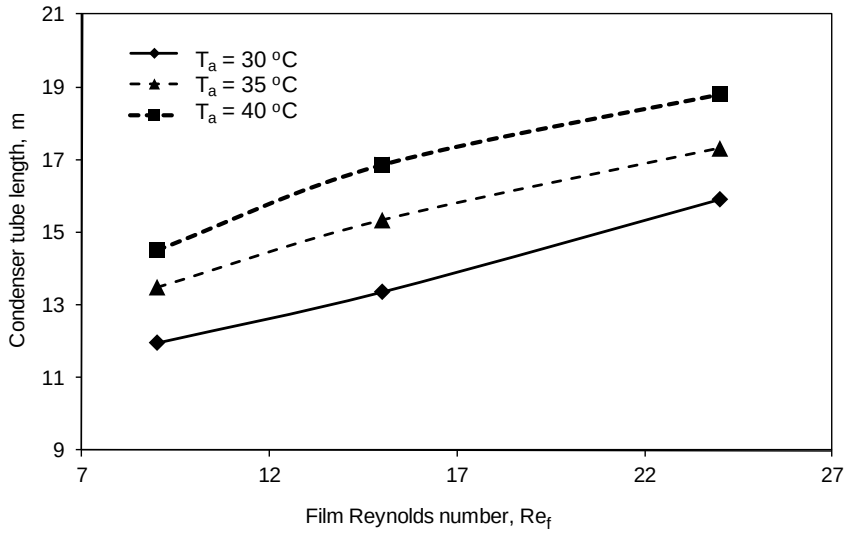

Figure 3.44 *Simulated variation of condenser tube length with film Reynolds number and air temperature for T_{wi} =25 ^{o}C, V=4m/s, RH = 70%*

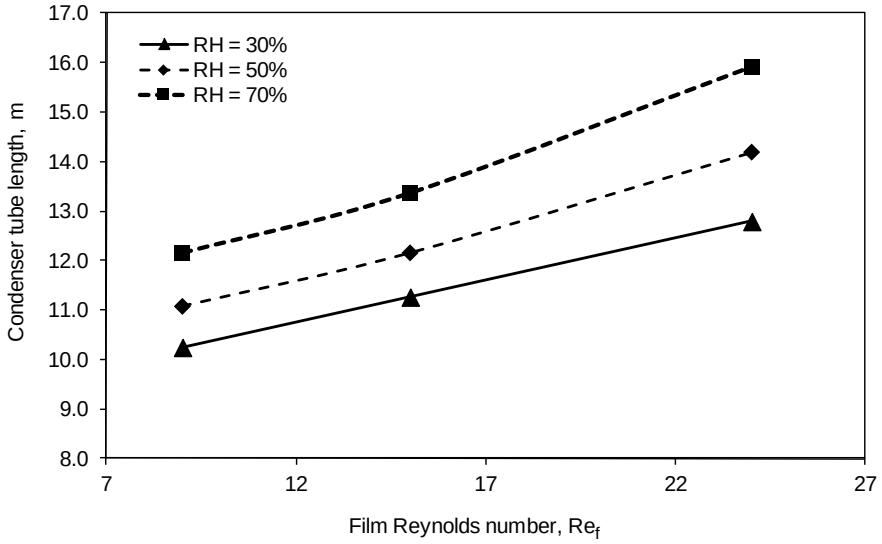

Figure 3.45 *Simulated variation of condenser tube length with film Reynolds number and air relative humidity for T_{wi} =25 ^{o}C, V=4m/s, T_a = 30 ^{o}C*

Figure 3.46 shows the simulated variation of required condenser tube length with the film Reynolds number and air velocity. As can be seen from the

figure, for a given film Reynolds number, the required condenser tube length is decreased with increase in air velocity and vice versa.

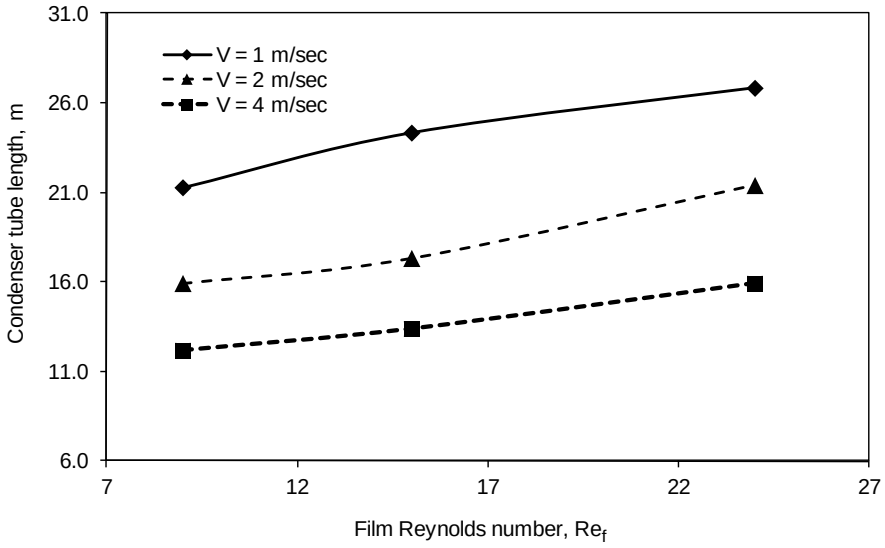

Figure 3.46 *Simulated variation of condenser tube length with film Reynolds number and air velocity for T_{wi} =25 ^{o}C, RH=70%, T_a = 30 ^{o}C*

Figures 3.47 and 3.48 show the comparison of the performances of the bare-tube evaporatively-cooled condenser with and without evaporative cooling. Figure 3.47 shows the variation of refrigerant temperature along the serpentine condenser tube with and without evaporative cooling. Figure 3.48 shows the variation of refrigerant quality along the serpentine condenser tube for the cases with and without evaporative cooling. As can be observed from Figures 3.47 and 3.48, improvement in performance is very significant due to the evaporative cooling in terms of the required condenser tube length.

Figures 3.49 and 3.50 show the simulated variation of condenser tube length with ambient air temperature and velocity for the bare-tube condenser with and without evaporative cooling. As can be seen from the figures, the required bare-tube

length without evaporative cooling is unrealistically high when the air temperature and velocity values are approaching to 40 ^{o}C and 1 m/s, respectively.

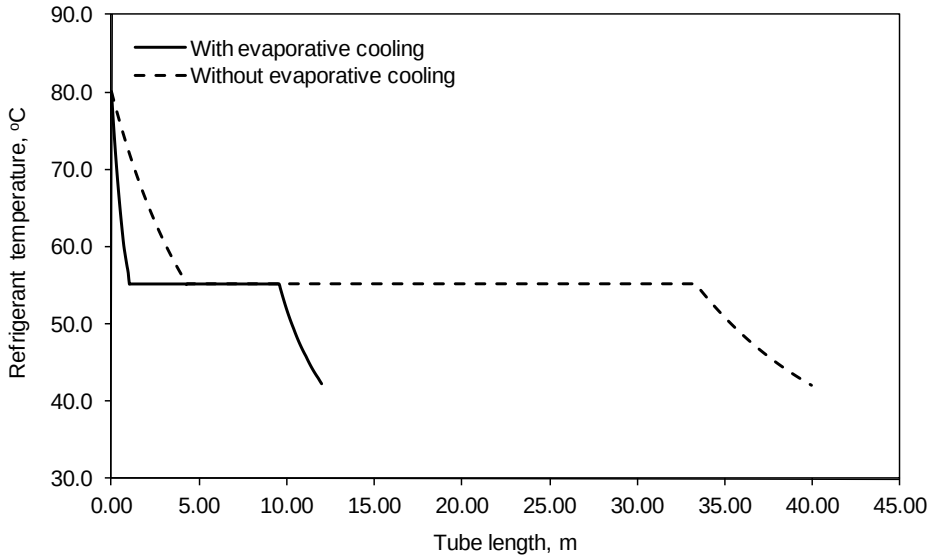

Figure 3.47 *Simulated variation of refrigerant temperature along the tube length with and without evaporative cooling for T_{wi} =25 ^{o}C, Re_f = 9, V=4m/s, T_a = 30 ^{o}C, RH = 70%*

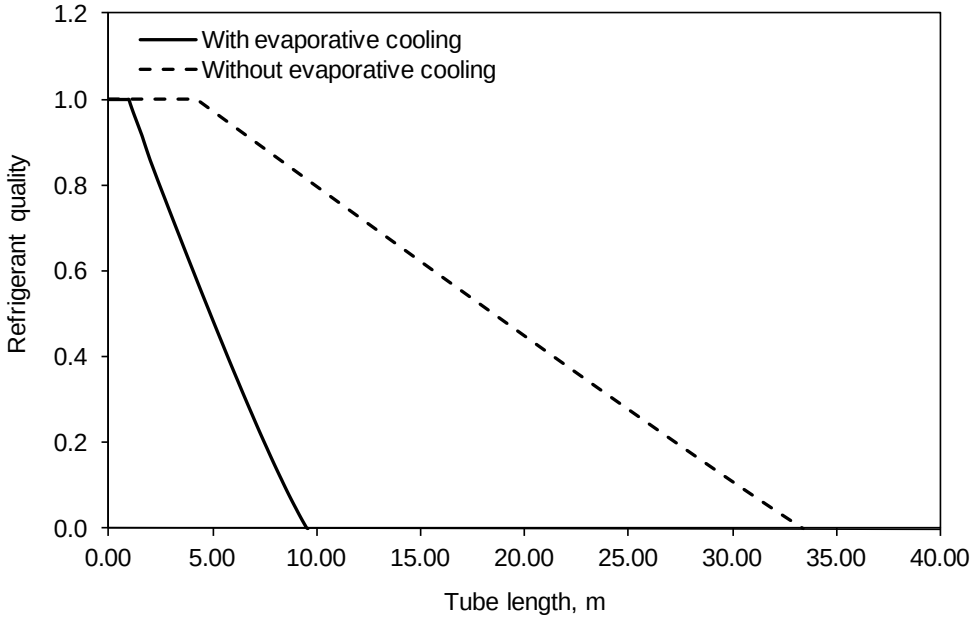

Figure 3.48 *Simulated variation of refrigerant quality along the tube length with and without evaporative cooling (bare tube condenser) for T_{wi} =25 ^{o}C, Re_f = 9, V=4m/s, T_a = 30 ^{o}C, RH = 70%*

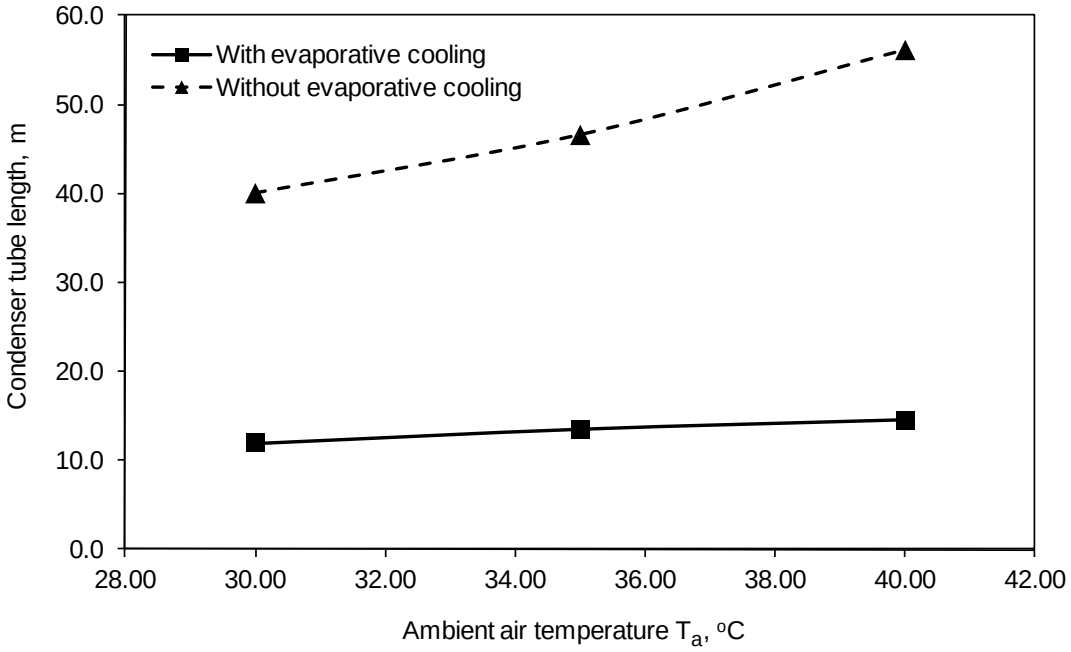

Figure 3.49 *Simulated variation of condenser tube length with air temperature with and without evaporative cooling for T_{wi} =25 °C, Re_f = 9, V=4m/s, RH = 70%*

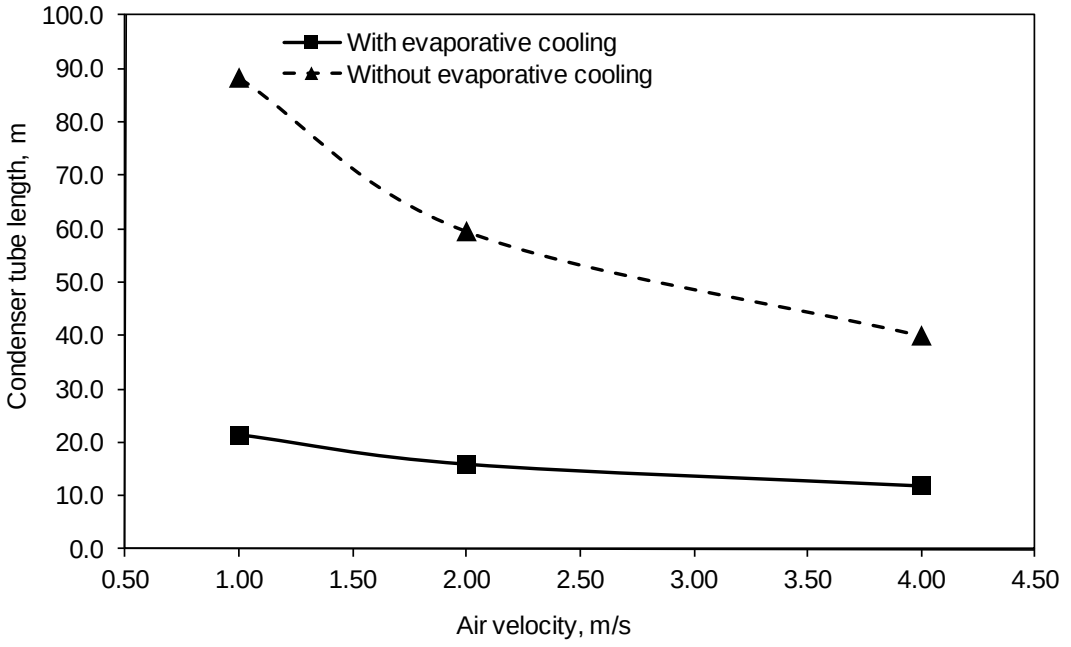

Figure 3.50 *Simulated variation of condenser tube length with air velocity with and without evaporative cooling for T_{wi} =25 °C, Re_f = 9, T_a = 30 °C, RH = 70%*

3.6 Summary

A numerical model for a small representative element of an evaporatively-cooled bare-tube serpentine condenser was developed from the conservation of mass, momentum and energy. The energy equation was transformed to a regular computational domain using a coordinated transformation system adopted from the published literature. The transformed energy equation was discretised using an implicit finite difference scheme and numerically solved for the temperature profile of the water film with the help of a written FORTRAN computer code. Subsequently, the detailed model developed for the tube element was integrated over a full serpentine tube of an evaporatively-cooled condenser. Using the full tube detailed model, a numerical study involving main operating parameters of the serpentine condenser tube of evaporatively-cooled condenser was carried out.

Numerical results obtained for the heat and mass transfer using the detailed model developed for a small representative tube element along with those of the serpentine bare tube of an evaporatively-cooled condenser were also presented in this chapter. The temperature distribution obtained from the numerical solution of the discretized energy equation was used to determine the two important heat transfer coefficients, namely, film-tube interface (h_i) and film-air interface (h_o) as well as the rate of water evaporated from the tube element. The results from the numerical simulation were also compared with the published results available in the literature. A parametric study was also undertaken to establish the effect of the main operating conditions on the heat and mass transfer characteristics of the evaporatively-cooled condenser tube for three different thin water film thicknesses, with the corresponding

film Reynolds numbers 3, 9 and 15. It was also observed from the numerical model that the simultaneous cross flow of air in the evaporatively-cooled condenser could improve the performance of the evaporatively-cooled condenser tremendously.

Chapter 4
DETAILED MODEL FOR EVAPORATIVELY-COOLED SERPENTINE FINNED-TUBE CONDENSERS

Currently, most of the small and medium-sized air-conditioners are fitted with finned air-cooled condensers. Hence, the detailed model developed for evaporatively-cooled bare-tube condenser in Chapter 3 is extended to the case where the condenser tubes are finned. For this investigation of the finned serpentine tube with evaporative cooling, initially, a two-dimensional wet fin model is developed. The wet fin model is used to determine the heat transfer from the wet fin surface during evaporative cooling of condensers.

The serpentine bare-tube condenser discussed in Chapter 3 is now fitted with N_f number of fins per segment of length ΔL of fin thickness of δ_f. In the following section, for the determination of the wet fin heat transfer, a two-dimensional model for the temperature distribution of the wet fin is developed from first principles.

4.1 Horizontal Finned-Condenser Tube with the Falling Film

4.1.1 Two-Dimensional Wet Fin Model

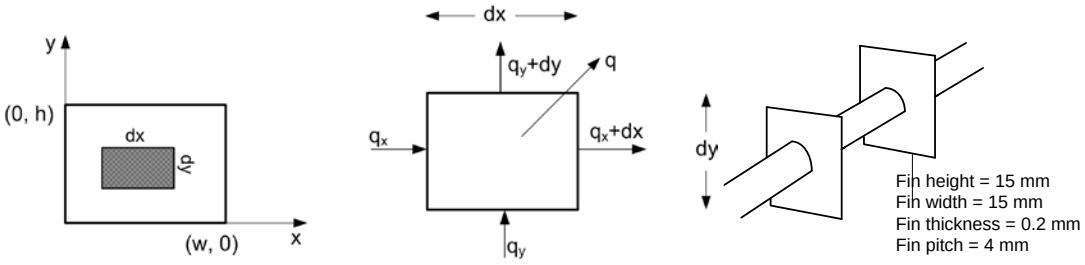

Figure 4.1 *Control element for the two-dimensional wet fin model*

Various energy components entering and leaving the control element of the fin with width *w* and height *h*, shown in Figure 4.1 are:

Incoming conduction heat transfer rate in the x-direction,

$$q_x = -k_f \delta_f dy \frac{\partial T_f}{\partial x} \tag{4.1}$$

Outgoing conduction heat transfer rate in the x-direction,

$$q_{x+dx} = -k_f \delta_f dy \frac{\partial T_f}{\partial x} + \frac{d\left(-k \delta_f dy \frac{\partial T_f}{\partial x} \right)}{\partial x} dx \tag{4.2}$$

Net conduction heat transfer rate in the x-direction = $k_f \delta_f dx\, dy \frac{\partial^2 T_f}{\partial x^2}$ (4.3)

Similarly, incoming conduction heat transfer rate in the y-direction,

$$q_y = -k_f \delta_f dx \frac{\partial T_f}{\partial y} \tag{4.4}$$

Outgoing conduction heat transfer rate in the y-direction,

$$q_{y+dy} = -k_f \delta_f dx \frac{\partial T_f}{\partial y} + \frac{d\left(-k_f \delta_f dx \frac{\partial T_f}{\partial y} \right)}{\partial y} dy \tag{4.5}$$

And the net conduction heat transfer rate in the y-direction = $k_f \delta_f dx\, dy \frac{\partial^2 T_f}{\partial y^2}$ (4.6)

The total heat energy convected and evaporated from the 2 faces of the fin element is:

$$2\,q\,dx\,dy \tag{4.7}$$

An energy balance for the control volume around the fin element will give:

Net rate of heat conducted in = Sum of rate of heat convected and evaporated out

$$\text{i.e.} \quad k_f \delta_f dx\,dy \frac{\partial^2 T_f}{\partial x^2} + k_f \delta_f dx\,dy \frac{\partial^2 T_f}{\partial y^2} = 2\ q\,dx\,dy \tag{4.8}$$

Simplification and rearrangement of equation (4.8) give:

$$\frac{\partial^2 T_f}{\partial x^2} + \frac{\partial^2 T_f}{\partial y^2} - \frac{2\ q}{k_f . \delta_f} = 0 \tag{4.9}$$

An energy balance on the evaporative surface of the fin as shown in Figure 4.1 gives:

$$q = k_w \frac{\left(T_f - T_{ws}\right)}{\delta_w} = h_a\left(T_{ws} - T_a\right) + h_d\left(\omega_{ws} - \omega_a\right)h_{fg,w} \tag{4.10}$$

where, δ_w and T_{ws} are the water film thickness and temperature, respectively.

From (4.10), $$\left(T_f - T_{ws}\right) = \frac{\delta_w\, q}{k_w} \tag{4.11}$$

For evaporation involving water and air, Lewis Number, L_e =1 (Incropera, 2007) and

h_d is defined as: $$h_d = \frac{h_a}{C_{pm}} \tag{4.12}$$

From equations (4.10) and (4.12), we get:

$$\left(T_{ws}-T_a\right)=\frac{q}{h_a}-\frac{h_{fg,w}\left(\omega_{ws}-\omega_a\right)}{C_{pm}} \tag{4.13}$$

Adding equations (4.11) and (4.13) and using equation (4.10), an expression for q can be written as:

$$q=\left(T_f-T_a\right)\frac{\left(1+\left(\frac{h_{fg}}{C_{pm}}\right)\frac{\left(\omega_{ws}-\omega_a\right)}{\left(T_f-T_a\right)}\right)}{\left(\frac{\delta_w}{k_w}+\frac{1}{h_a}\right)} \tag{4.14}$$

Substituting for q in (4.9) yields:

$$\frac{\partial^2 T_f}{\partial x^2}+\frac{\partial^2 T_f}{\partial y^2}-\left[\frac{2}{k_f\delta_f}\frac{\left(1+\left(\frac{h_{fg}}{C_{pm}}\right)\frac{\left(\omega_{ws}-\omega_a\right)}{\left(T_f-T_a\right)}\right)}{\left(\frac{\delta_w}{k_w}+\frac{1}{h_a}\right)}\right]\left(T_f-T_a\right)=0 \tag{4.15}$$

As the water film is very thin, the ratio $\frac{\delta_w}{k_w}$ is much smaller than $\frac{1}{h_a}$ and can be neglected. For example, for a film thickness δ_w = 0.1 mm, water thermal conductivity k_w = 0.638 W/m K and h_a = 86 W/m^2 K, the error occurred by neglecting the $\frac{\delta_w}{k_w}$ is about 1.3%.

Hence, equation (4.15) becomes:

$$\frac{\partial^2 T_f}{\partial x^2}+\frac{\partial^2 T_f}{\partial y^2}-\frac{2h_a}{k_f\delta_f}\left(1+\left(\frac{h_{fg,w}}{C_{pm}}\right)\frac{(\omega_{ws}-\omega_a)}{(T_f-T_a)}\right)(T_f-T_a)=0 \tag{4.16}$$

$$\frac{\partial^2 T_f}{\partial x^2}+\frac{\partial^2 T_f}{\partial y^2}-m^2(1+\alpha E)(T_f-T_a)=0 \tag{4.17}$$

$$\text{where, } m^2=\frac{2h_a}{k_f\delta_f} \qquad E=\frac{(\omega_{ws}-\omega_a)}{(T_f-T_a)}=\frac{(\omega_{sf}-\omega_a)}{(T_{ws}-T_a)} \text{ and } \alpha=\frac{h_{fg,w}}{C_{pm}} \tag{4.18}$$

Equation (4.17) is discretised using the finite difference technique. The second order central difference scheme is employed for the descretisation and the final form of the equation is:

$$\begin{aligned}&T_{f(i-1,j)}+\left(-2-(m\Delta x)^2(1+\alpha E_{(i,j)})-2\beta^2\right)T_{f(i,j)}+T_{f(i+1,j)}\\&=-\beta^2T_{f(i,j-1)}-\beta^2T_{f(i,j+1)}-(m\Delta x)^2(1+\alpha E_{(i,j)})T_a\end{aligned} \tag{4.19}$$

$$\text{where, } m=\sqrt{\frac{2h_a}{k_f\delta_f}} \qquad E_{i,j}=\frac{(\omega_{ws(i,j)}-\omega_a)}{(T_{f(i,j)}-T_a)}=\frac{(\omega_{sf(i,j)}-\omega_a)}{(T_{ws(i,j)}-T_a)} \text{ , and } \beta=\frac{\Delta x}{\Delta y} \tag{4.20}$$

The computation domain used for the numerical simulation of the fin along with the grids is shown in Figure 4.2. For the simplicity of the numerical disretization and subsequent applying of the boundary conditions of the fin model, an equivalent square section corresponding to the condenser tube diameter is taken as shown in Figure 4.2. Equation (4.19) is written for all the grid points resulting in an equal number of algebraic equations as the number of unknowns $T_{f(i,j)}$.

The boundary conditions used for numerically solving the discretized algebraic equations with reference to Figure 4.2 are as follows:

Along the line c-d-e, $T_f = T_{wall}$ (4.21)

Due to symmetry, along line b-c, $\frac{\partial T_f}{\partial x} = 0$ (4.22)

Due to symmetry, along the line e-f, $\frac{\partial T_f}{\partial y} = 0$ (4.23)

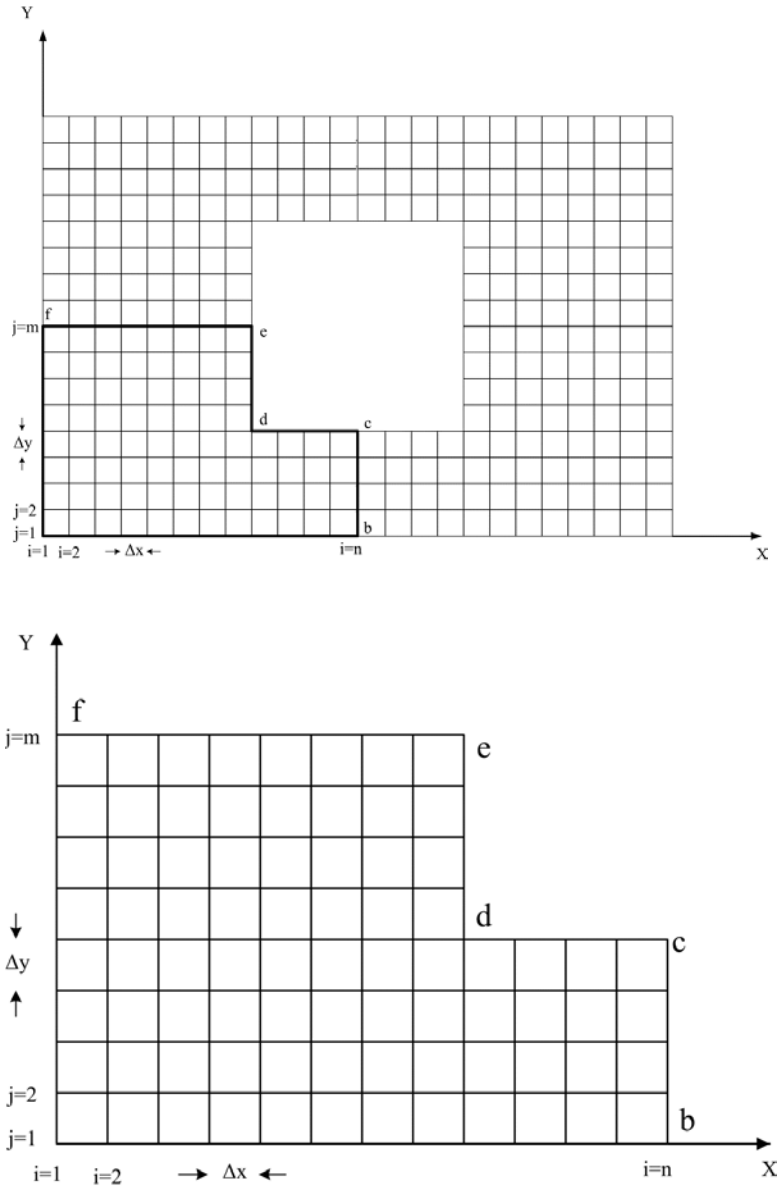

Figure 4.2 *Computational domain for the two-dimensional wet fin model*

In conjunction with the boundary conditions given by equations (4.21), (4.22) and (4.23), the algebraic equations are solved using the Gauss-Siedel iteration method. An initial guess of unknown temperature at all the grid points is made and the iteration is carried out until the solution is converged to within the specified error of 0.001. The solution obtained is the temperature distribution in the fin and the fin heat transfer and the fin efficiency are calculated as follows:

Actual and maximum possible heat transfer from the wet fin surface can be written as:

$$q_f = h_a(T_{ws} - T_a) + h_d(\omega_{ws} - \omega_a)h_{fg,w} \tag{4.24}$$

where, q_f *is* the heat transfer per unit area from one side of the fin surface.

$$Q_f = 2q_f A_f \tag{4.25}$$

where, Q_f is the heat transfer rate from both sides of the fin surface.

$$q_{\max} = h_a(T_{wall} - T_a) + h_d(\omega_{@T_{wall}} - \omega_a)h_{fg,w} \tag{4.26}$$

Fin efficiency is defined as: $\eta_f = \dfrac{q_f}{q_{\max}}$ (4.27)

4.1.2 Governing equations for the single-phase region (superheated and sub-cooled) of the condenser tube

With the fin thickness δ_f and number of fins per segment N_f known, the length of the bare segment in the previous model without fin will be reduced and can be written as:

$$\Delta L_1 = \Delta L - N_f.\delta_f \tag{4.28}$$

Expression for the refrigerant outlet temperature at the k^{th} segment of the tubes for the single phase region of the condenser tube can be written from an energy balance for the segment shown in Figure 4.3 as:

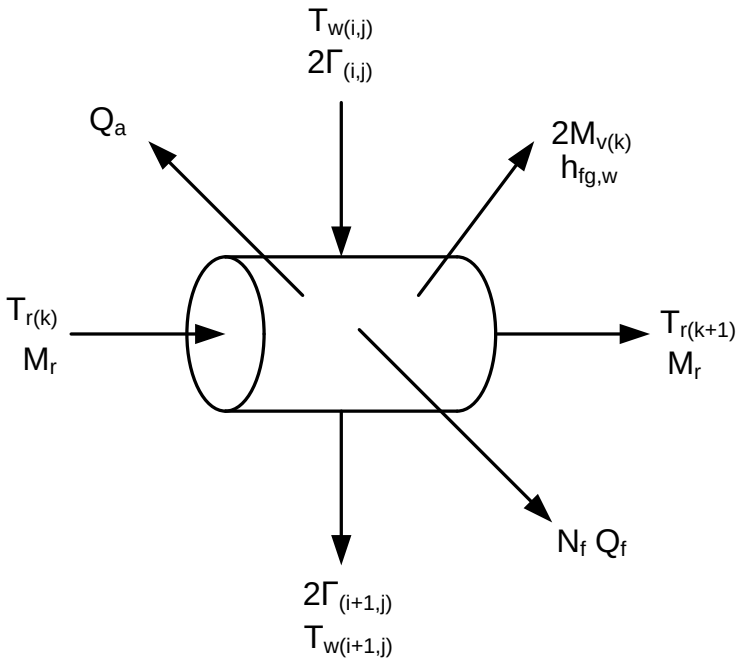

Figure 4.3 *Energy balance on the k^{th} segment of the finned condenser tube (single phase region)*

$$2\Gamma_{(i,j)} C_{pw} T_{w(i,j)} \Delta L_1 + M_r C_{pr} T_{r(k)} =$$

$$2\Gamma_{(i+1,j)} C_{pw} T_{w(i+1,j)} \Delta L_1 + M_r C_{pr} T_{r(k+1)} + 2M_v h_{fg,w} + N_f Q_f + Q_a \qquad (4.29)$$

$$T_{r(k+1)} = \frac{\left[C_{pw} \Delta L_1 \left(2\Gamma_{(i,j)} T_{w(i,j)} - 2\Gamma_{(i+1,j)} T_{w(i+1,j)}\right) + M_r C_{pr} T_{r(k)} - 2M_v h_{fg,w} - N_f Q_f - Q_a\right]}{M_r C_{pr}} \qquad (4.30)$$

where, $Q_a = h_a \pi D_o \Delta L_1 \left(T_{w,av} - T_a\right)$ (4.31)

Similar to equation (3.63) in Chapter 3, the wall temperature for the finned tube in the single phase regions of the condenser can be expressed as:

$$T_{wall,o} = \frac{T_{r(k)} \exp\left[\frac{\Delta L_1}{F_1}\right] - T_{r(k+1)}}{\exp\left[\frac{\Delta L_1}{F_1}\right] - 1} \tag{4.32}$$

where, the definition of F_1 is same as that in equation (3.63).

4.1.3 Governing equations for the two-phase region (condensation region) of the finned-tube

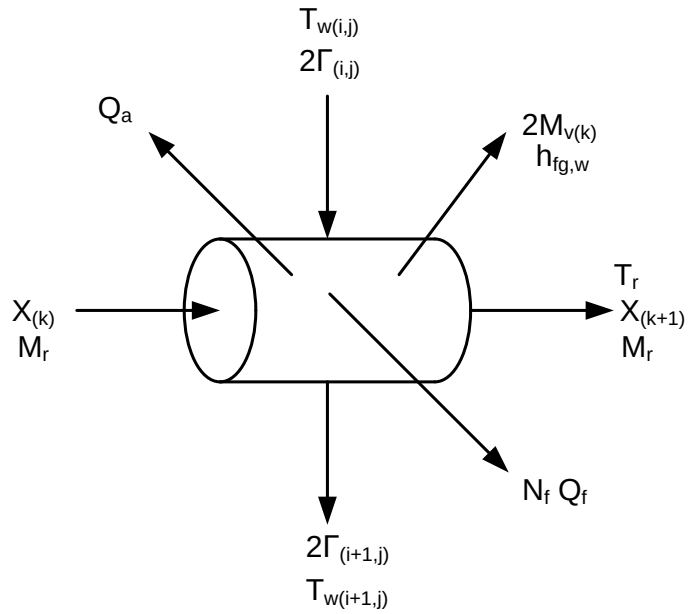

Figure 4.4 *Variation of refrigerant temperature on the k^{th} segment of the condenser tube (two-phase region)*

An energy balance on the two-phase region of the condenser for the segment shown in Figure 4.4 gives:

$$2\Gamma_{(i,j)} C_{pw} T_{w(i,j)} \Delta L_1 + M_r X_k h_{g,r} + M_r (1 - X_k) h_{f,r} =$$

$$2\Gamma_{(i+1,j)} C_{pw} T_{w(i+1,j)} \Delta L_1 + M_r (X_{k+1}) h_{g,r} + M_r (1 - X_{k+1}) h_{f,r} + 2M_v h_{fg,w} + N_f Q_f + Q_a \tag{4.33}$$

Simplification and rearrangement of equation (4.33) yield:

$$X_{k+1} = \frac{2C_{pw}\Delta L_1\left(\Gamma_{(i,j)}T_{w(i,j)} - \Gamma_{(i+1,j)}T_{w(i+1,j)}\right) + M_r X_k h_{fg,r} - 2M_v h_{fg,w} - N_f Q_f - Q_a}{M_r h_{fg,r}} \quad (4.34)$$

Similar to equation 3.66 in Chapter 3, the wall temperature for the finned tube condenser in the two-phase region can be written as:

$$T_{wall,o} = T_r - \frac{M_r h_{fg,r}\left(\frac{\ln(D_o/D_i)}{2\pi k_{wall}} + \frac{1}{h_{r,2-phase}\pi D_i}\right)\left(X_{r(k+1)} - X_{r(k)}\right)}{\Delta L_1} \quad (4.35)$$

4.1.4 Solution procedure for serpentine finned condenser tubes (multiple rows)

As in the case of the serpentine bare-tube condenser, the refrigerant and water flow path for the finned serpentine condenser tube can be computed with reference to Figure 3.7. Water mass flow rate per unit length of the tube, 2Γ kg/m s, falls on the top tube and is split into two paths on either side of the tube with a flow rate of Γ kg/m s each. As shown in the figure, the serpentine finned tube is divided into small segments of length ΔL for numerical determination of the heat and mass transfer in the evaporatively-cooled condenser. Based on the detailed models presented in the preceding section, a FORTRAN computer code is written for the numerical simulation of the finned serpentine tube of the evaporatively-cooled condenser. For this case of the serpentine tube with the fins, the 2-dimensional wet fin model is also used to investigate the effect of fins in the evaporative cooling process. The fin subroutine is called from the main program for the numerical determination of the wet fin temperature distribution, fin efficiency and ultimately the actual heat transfer from the wet fin.

Using the FORTRAN code, the model equations are numerically solved for the temperature distribution of the thin water film and subsequently for the heat transfer coefficients of the tube segment. The mass flux of water evaporated from the film-air interface as well as the water film temperature and flow rate at the bottom of the tube segment are also determined using the detailed model. Now, with the known inlet refrigerant conditions (pressure, temperature, and mass flow rate) at the first tube segment, equations (4.30) and (4.32) are used to determine the exit refrigerant temperature and the outside tube wall temperature for the finned-tubes. The computation for the superheated region is continued until the refrigerant vapour attains saturated vapour state (the point where the exit refrigerant temperature reaches the condensing temperature, determined from the inlet pressure of the superheated refrigerant vapour). At this point, the refrigerant quality is taken as unity and the computation is proceeded for the refrigerant quality and outside tube wall temperature using the equations (4.34) and (4.35). The computation for the sub-cooled region starts when the quality of the refrigerant reaches zero, the computation continues until the last segment of the serpentine tube. The flow rate and temperature of the falling film from one segment to the corresponding segment in the next tube are transferred in the computation as depicted in Figure 3.7. The above computational procedure for the evaporatively-cooled condenser for the three regions of the condenser is depicted in detail in the flow chart of Figures 3.12.

4.2 Numerical Parametric Study of the Serpentine Finned-Tube Evaporatively-Cooled Condenser

A detailed parametric study taking the important operating conditions as parameters is conducted using the detailed model for the finned evaporatively-cooled

condensers presented in the preceding section of this chapter. The important findings are plotted and described below.

Figures 4.5 to 4.8 shows the simulated variation of average film-tube interface Nusselt number ($Nu_{i,av}$) with film Reynolds number and relative humidity. As can be seen from Figure 4.5, the film-tube interface Nusselt number steadily increases with the film Reynolds number, Re_f. This is attributed to the fact that the water film-wall heat transfer coefficient, h_i, is a function of bulk water film temperature and tube wall temperature as well as the temperature gradient at the wall. Increase in the h_i value indicates that the change of temperature gradient at the wall is more dominant than the difference in bulk water and wall temperature. Relatively higher thermal resistance developed coupled with the change in thermo-physical properties of water with temperature also could contribute to the increasing trend of the local Nusselt number Nu_i with film Reynolds number in the figure.

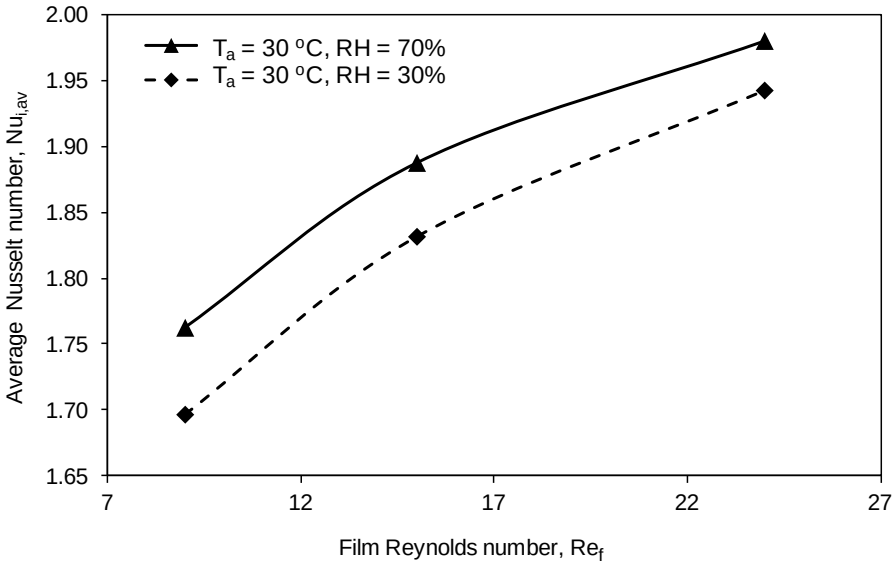

Figure 4.5 *Simulated variation of film-tube interface Nusselt number from the top to bottom condenser tubes for different air relative humidity for δ_w=0.15mm (Re_f = 9), V = 4 m/s, T_{wi} = 25 ^oC*

The effect of film Reynolds number on the average film-air interface Nusselt number (Nu_o) is shown in Figure 4.6. As can be seen from the figure, the water film - air interface Nusselt number, Nu_o, decreases with Re_f which is exactly the opposite trend seen for the film-tube interface Nusselt number of Figure 4.7. This average Nusselt number value is essentially governed by the mass of water evaporated from the film-air interface. For a smaller film Reynolds number, the mass of water evaporated from the water film-air interface is larger as compared to the mass flux of water evaporation for a larger film Reynolds number. As the film Reynolds number is increased, the rate of heat dissipation from the tube wall is diminished due to the development of an increased thermal resistance between the tube wall and the film-air interface.

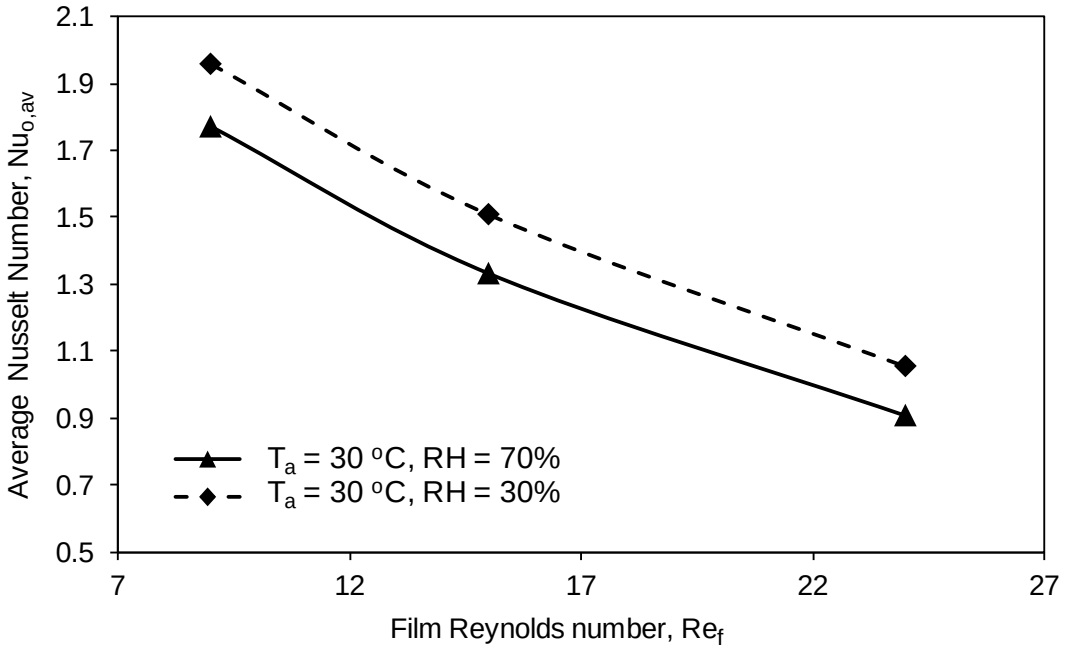

Figure 4.6 *Simulated variation of film-air interface Nusselt number from the top to bottom condenser tubes for different air relative humidity for δ_w=0.15mm (Re_f = 9), V = 4 m/s, T_{wi} = 25 ^oC*

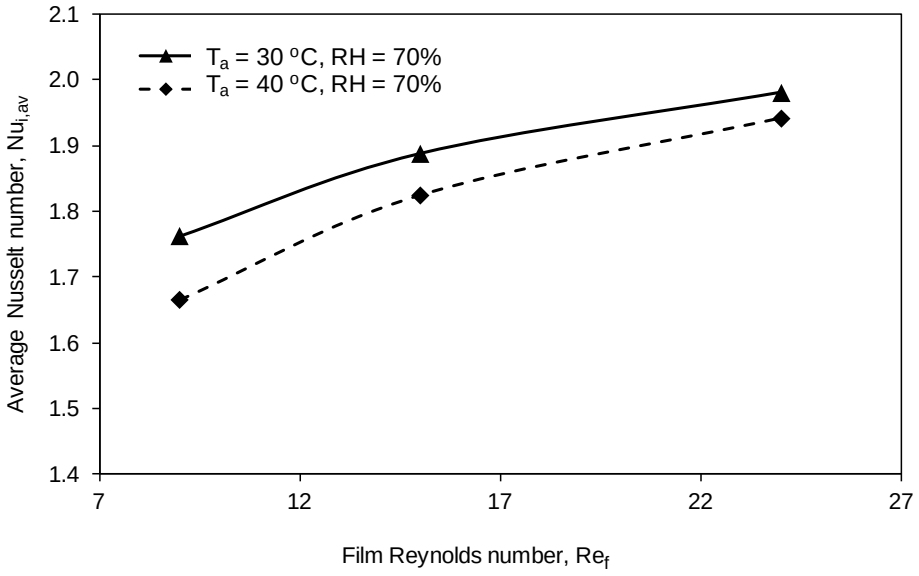

Figure 4.7 *Simulated variation of film-tube interface Nusselt number from the top to bottom condenser tubes for different air temperature for δ_w=0.15mm (Re_f = 9), V = 4 m/s, T_{wi} = 25 °C*

Trends observed in Figures 4.7 and 4.8 are consistent with the trends obtained in Figures 4.5 and 4.6.

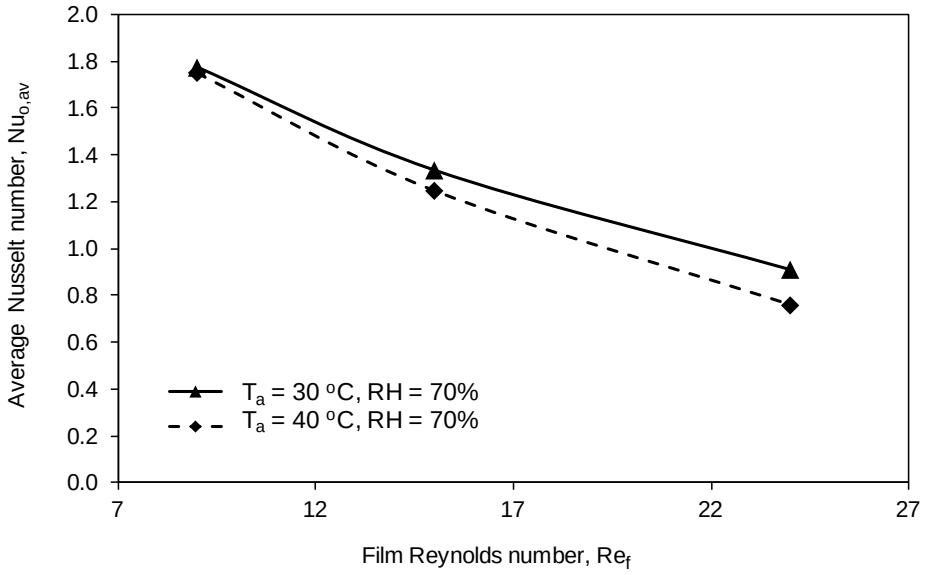

Figure 4.8 *Simulated variation of film-air interface Nusselt number from the top to bottom condenser tubes for different air temperature for δ_w=0.15mm (Re_f = 9), V = 4 m/s, T_{wi} = 25 °C*

Some of the results extracted from the simulation runs involving the two dimensional wet fin model presented in the preceding section are plotted in Figures 4.9 to 4.11. Figure 4.9 shows the effect of air inlet velocity on the fin heat transfer and efficiency for dry and wet fins. As can be seen from the figure, the fin heat transfer increases with the air velocity; whereas, the fin efficiency decreases with the air inlet velocity. A wet fin efficiency of about 65% was observed for the nominal air velocity of 4 m/s which is typical for small and medium size air-conditioners.

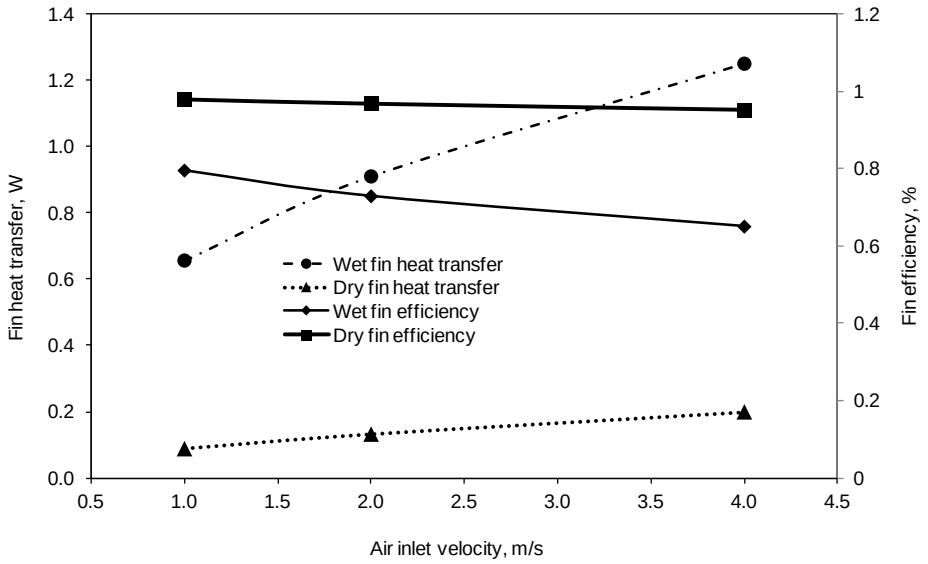

Figure 4.9 *Simulated variation of wet fin efficiency and heat transfer with inlet air velocity for* $T_a = 30\ ^oC$, $T_{wi} = 25\ ^oC$, $T_{wall} = 50\ ^oC$

Figure 4.10 shows the effect of fin thickness on the fin heat transfer and efficiency. As evident from the figure, both the fin heat transfer and efficiency increases with the increase in fin thickness. Fin efficiencies of 62 % and 88 % were observed for fin thicknesses of 0.1 mm and 0.5 mm, respectively. Figure 4.11 shows the variation of fin heat transfer and efficiency with fin base temperature. As can be

seen from the figure, fin efficiency drops almost in a linear fashion with increase in fin base temperature. As also can be seen in the figure, heat transferred by the fin increases with the fin base temperature.

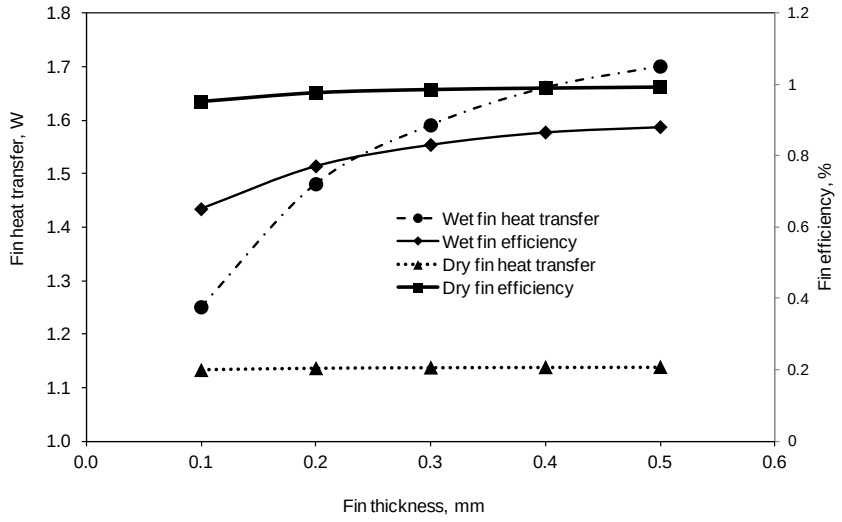

Figure 4.10 *Simulated variation of wet fin efficiency and heat transfer with fin thickness for T_a= 30 ^oC, T_{wi} = 25 ^oC, $T_{b,fin}$ = 50 ^oC, V = 4 m/s*

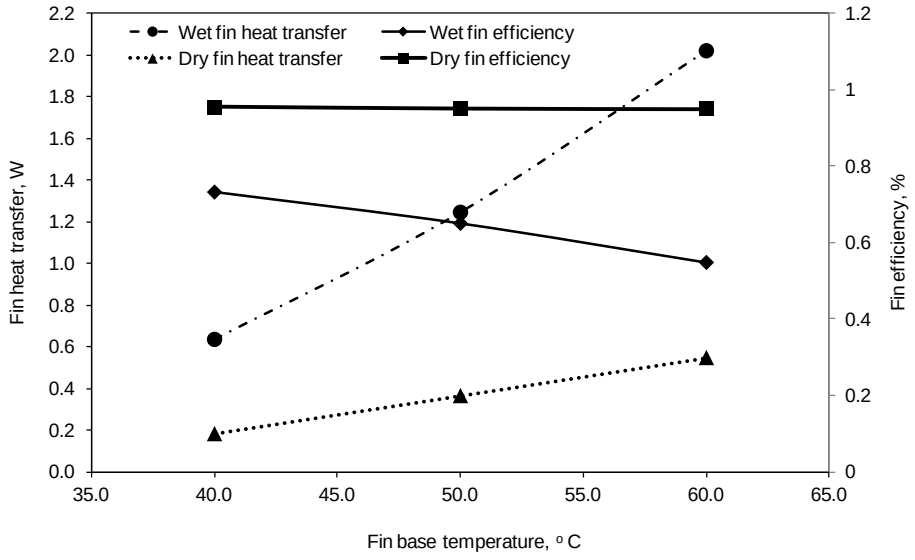

Figure 4.11 *Simulated variation of wet fin efficiency and heat transfer with fin base temperature for T_a= 30 ^oC, T_{wi} = 25 ^oC, V = 4 m/s*

The effect of the fin parameters and ambient conditions on the rate of water evaporated from the condenser tube surface and the corresponding required condenser tube length for the fixed sub-cooled refrigerant condition at the condenser outlet is shown in Figures 4.12 to 4.19. Other parameters considered for the graphs of Figures 4.12 to 4.19 are given in the figure captions.

Variation of the numerically simulated condenser tube length with fin pitch and air relative humidity is depicted in Figure 4.12. As can be seen from the figure, the required condenser tube length for complete condensation of the refrigerant from a superheated state of 80 ^{0}C and 15 bar to a sub-cooled state of 40 ^{0}C, increases with fin pitch and relative humidity.

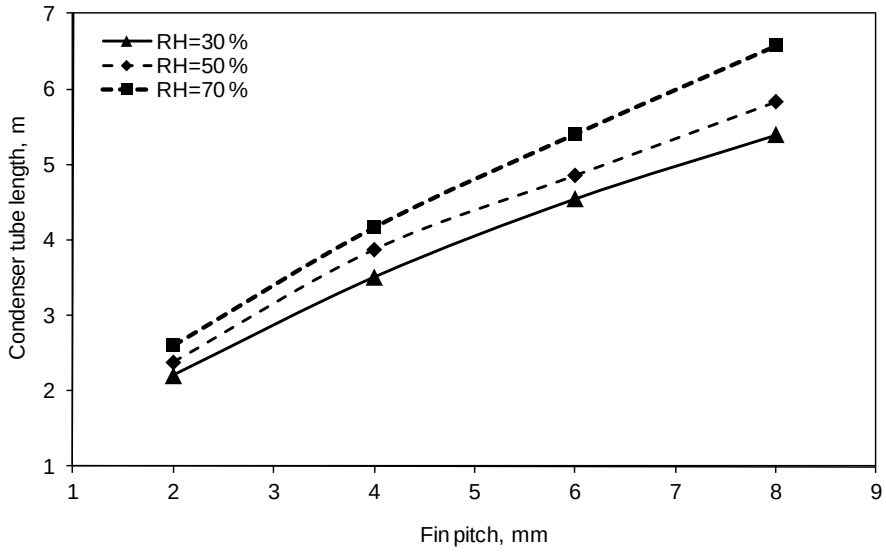

Figure 4.12 *Simulated variation of required condenser tube length with fin pitch for different air relative humidity for δ_w=0.15mm (Re_f = 9), V = 4 m/s, T_{wi} = 25 ^{o}C, T_a = 30 ^{o}C*

The effect of film Reynolds number on the required condenser tube length for different fin thickness is shown in Figure 4.13. As can be seen from the figure, for a given fin thickness, the condenser tube length variation with the film Reynolds

number is not that significant. This can be due to the fact that, for a given fin geometry and heat load, the net sum of the heat taken away by the falling water spray leaving the condenser tubes and the mass of water evaporated from the tube surface remains almost constant. However, as evident from the figure, as the fin becomes thicker the required condenser tube length is reduced.

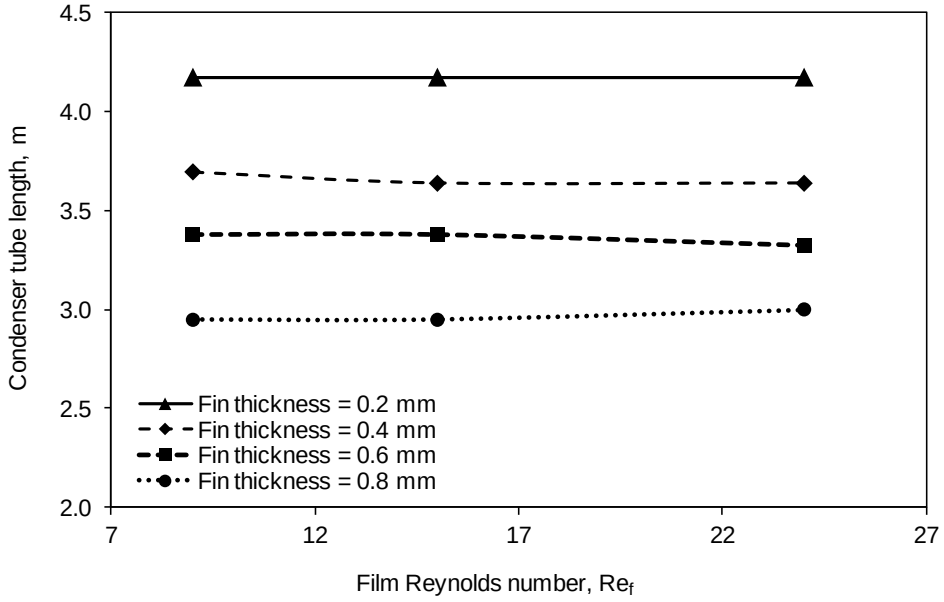

Figure 4.13 *Simulated variation of required condenser tube length with film Reynolds number for different fin thickness for V = 4 m/s, T_{wi} = 25 ^{o}C, T_a = 30 ^{o}C, RH = 70%*

The simulated variation of required condenser tube length with film Reynolds number and fin pitch is illustrated in Figure 4.14. Same as that of the trend in the previous figure, there is negligible effect of film Reynolds number on the condenser tube length for a given fin pitch.

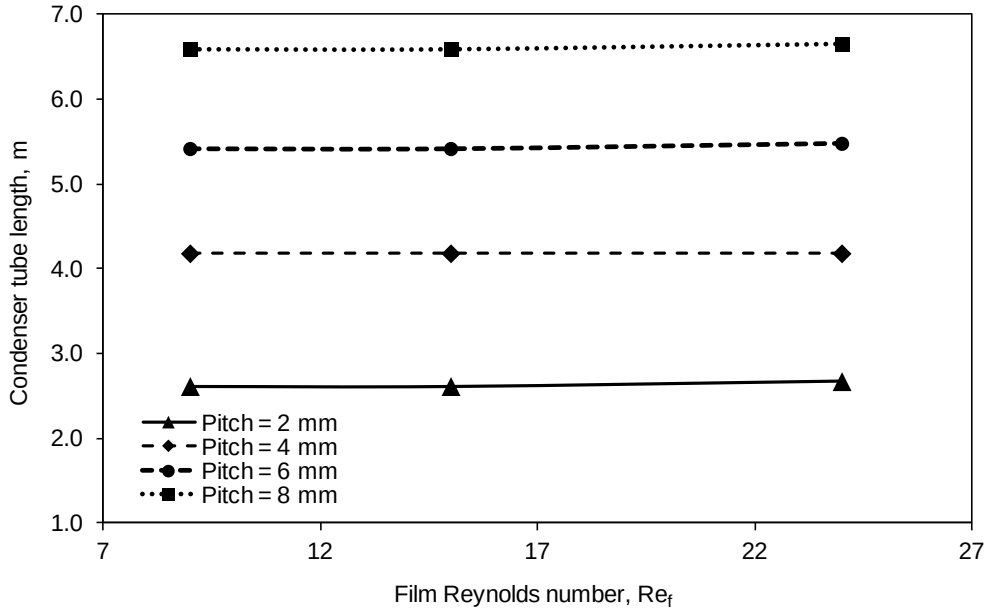

Figure 4.14 *Simulated variation of required condenser tube length with film Reynolds number for different fin pitches for V = 4 m/s, T_{wi} = 25 ^{o}C, T_a = 30 ^{o}C, RH = 70%*

The effect of fin pitch and air temperature on the rate of water evaporated from the condenser tube surface is shown in Figure 4.15. For a given air temperature, the mass of water evaporated decreases with increase in the fin pitch, which is consistent with the trend obtained previously. As also evident from the figure, for lower ambient temperature, better water evaporation rate is obtained due to the favourable enthalpy potential existing at the film-air interface.

The simulated variation of the rate of water evaporated from the tube surface with fin thickness and relative humidity of air is shown in Figure 4.16. As can be seen from the figure, there is a significant improvement in the water evaporation rate when the relative humidity of the air is reduced to 30 %. Figure 4.17 establishes the variation of the required condenser tube length with fin pitch and air temperature. As can be seen from the figure, a combination of a low fin pitch and low air temperature

brings about a significant reduction in the required condenser tube length for a particular heat rejection rate in the condenser.

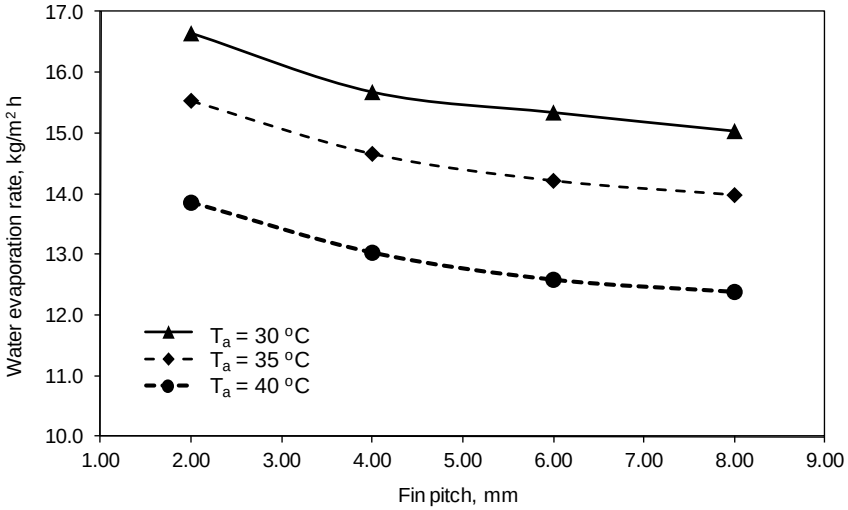

Figure 4.15 *Simulated variation of mass of water evaporated with fin pitch for different air temperatures for δ_w=0.15mm (Re_f = 9), V = 4 m/s, T_{wi} = 25 ^oC, RH = 70%*

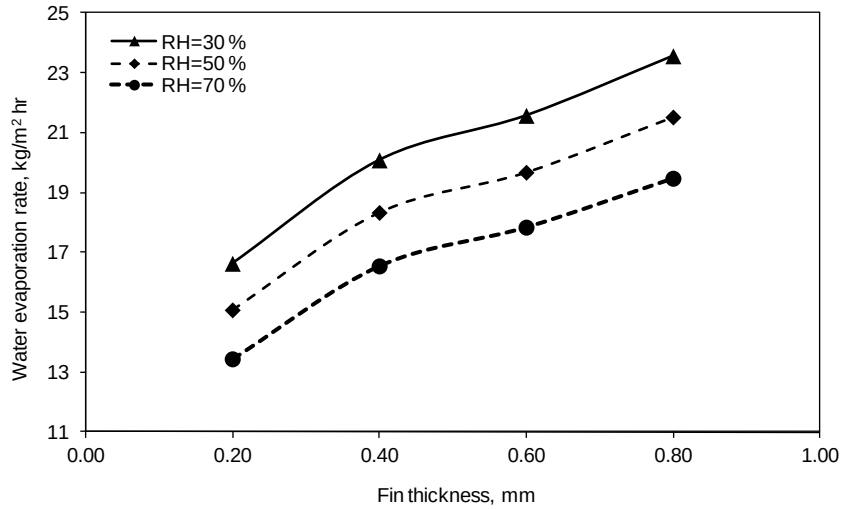

Figure 4.16 *Simulated variation of mass of water evaporated with fin thickness for different air relative humidity for δ_w=0.15mm (Re_f = 9), V = 4 m/s, T_{wi} = 25 ^oC, T_a = 30 ^oC*

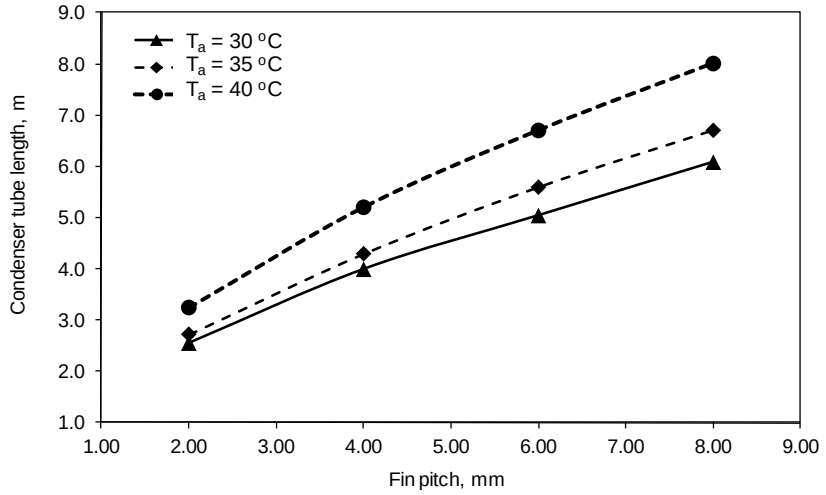

Figure 4.17 *Simulated variation of required condenser tube length with fin pitch for different air temperatures δ_w=0.15mm (Re_f = 9), V = 4 m/s, T_{wi} = 25 ^oC, RH = 70%*

Figures 4.18 and 4.19 show the effect of air velocity on the performance of the evaporatively-cooled finned condenser performance in terms of the rate of water evaporated and the associated condenser tube length requirement for a given heat rejection rate at the condenser. As expected and can be seen from Figure 4.18, the increase in air velocity causes better total water evaporation rate from the condenser tube surface for a given fin geometry.

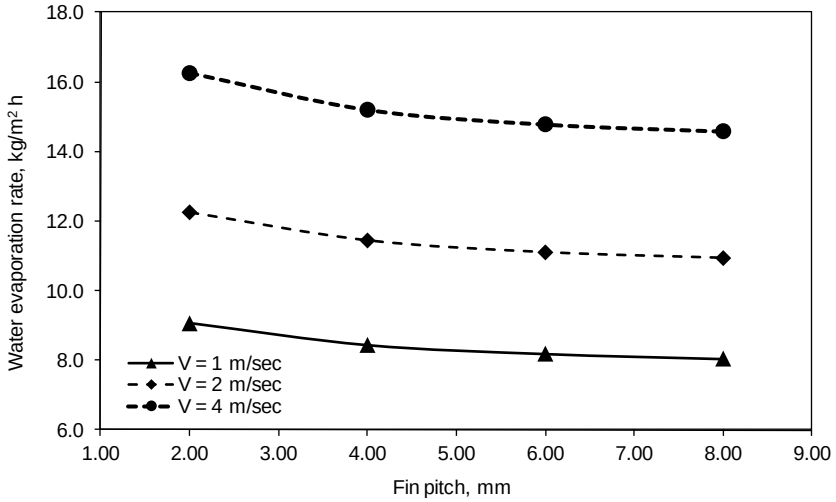

Figure 4.18 *Simulated variation of mass of water evaporated with fin pitch for different air velocities for δ_w=0.15mm (Re_f = 9), T_{wi} = 25 ^oC, T_a = 30 ^oC, RH = 70%*

The variation of the required condenser tube length with fin pitch for different velocities is depicted in Figure 4.19. As can be seen from the figure, the required condenser tube length increases with the fin pitch due to the reduction in the surface area available for the water evaporation. As seen from the previous results, a higher velocity causes the required condenser tube length to reduce significantly.

The simulated variation of refrigerant temperature and quality with the required condenser tube length is shown in Figures 4.20 and 4.21, respectively for the cases with and without evaporative cooling of the finned condenser tube. As evident from the figures, the evaporatively-cooled finned condenser tube length required is significantly reduced compared to the cases of evaporatively-cooled bare-tube condensers and finned-tube condenser without evaporative cooling.

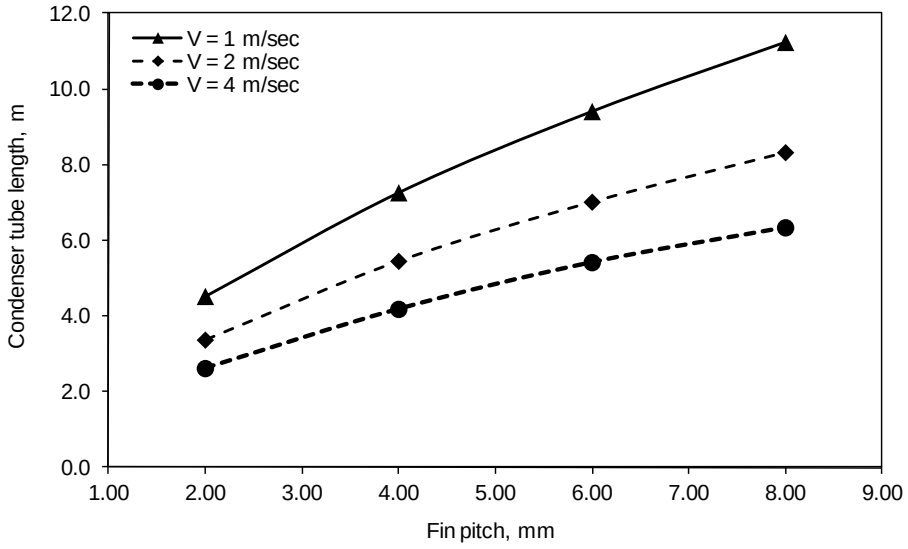

Figure 4.19 *Simulated variation of required condenser tube length with fin pitch for different air velocities for* δ_w*=0.15mm (*Re_f *= 9),* T_{wi} *= 25* ^oC*,* T_a *= 30* ^oC*, RH = 70%*

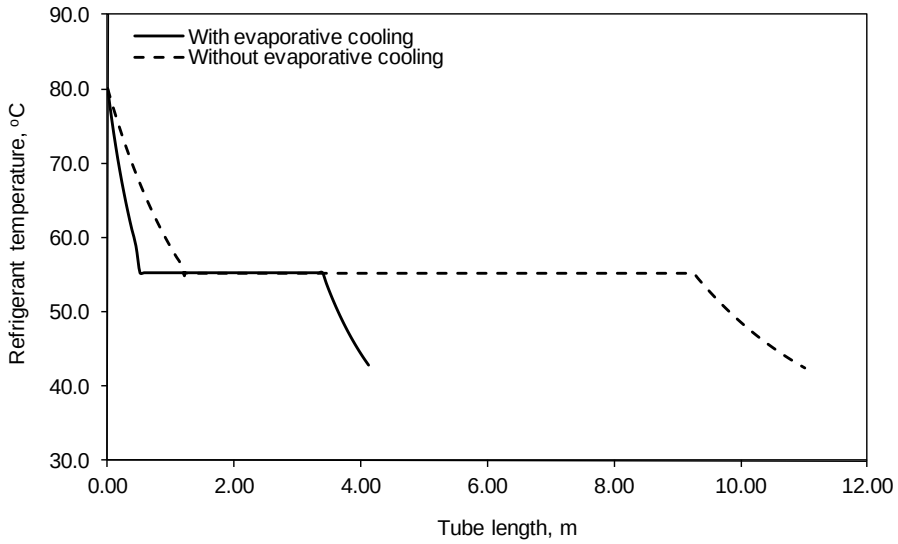

Figure 4.20 *Simulated variation of refrigerant temperature along the tube length with and without evaporative cooling for δ_w=0.15mm (Re_f = 9), V = 4 m/s, T_{wi} = 25 ^oC, T_a = 30 ^oC, RH = 70%*

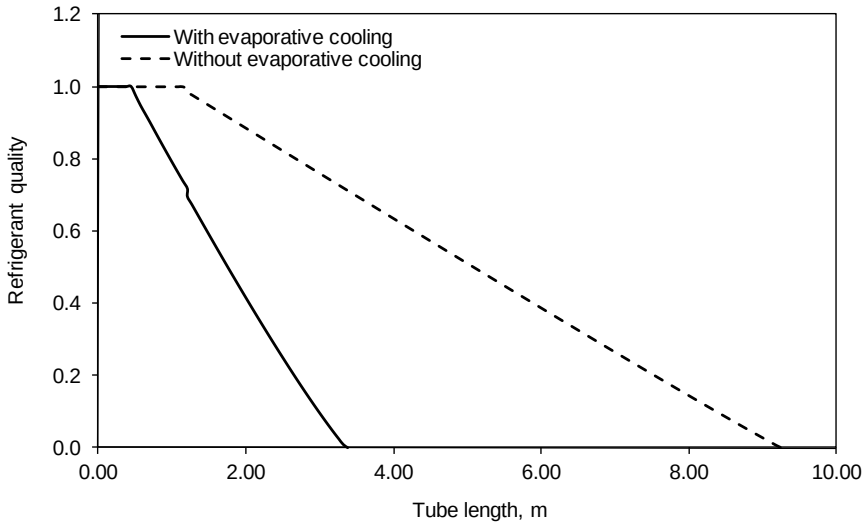

Figure 4.21 *Simulated variation of refrigerant quality along the tube length with and without evaporative cooling for δw=0.15mm (Re_f = 9), V = 4 m/s, T_{wi} = 25 ^oC, T_a = 30 ^oC, RH = 70%*

The effect of ambient air temperature and velocity on the condenser tube length requirement for the finned condenser with and without evaporative cooling is depicted in Figures 4.22 and 4.23, respectively. Trends in Figures 4.22 and 4.23 are

consistent with the trends seen in the preceding sections for the ambient air temperature and velocity.

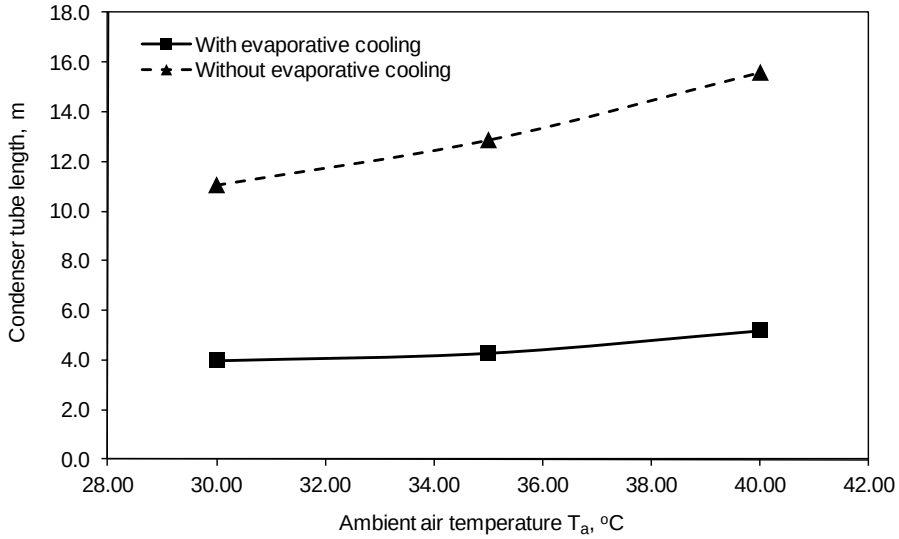

Figure 4.22 *Simulated variation of required condenser tube length with air temperature with and without evaporative cooling for δ_w=0.15mm (Re_f = 9), V = 4 m/s, T_{wi} = 25 ^oC, RH = 70%*

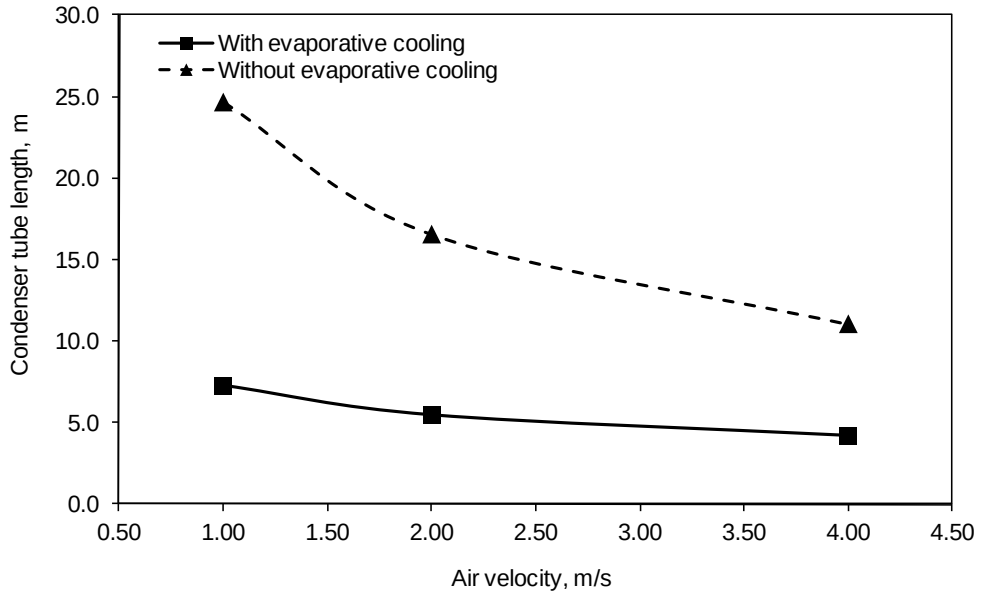

Figure 4.23 *Simulated variation of required condenser tube length with air velocity with and without evaporative cooling (finned tube condenser) for δ_w=0.15mm (Re_f = 9), T_{wi} = 25 ^oC, T_a = 30 ^oC, RH = 70%*

4.3 Summary

The detailed model developed for bare-tube evaporatively-cooled condenser was extended to the finned-tube evaporatively-cooled condenser. For this, at first, a two-dimensional wet fin model was developed for obtaining the wet fin heat transfer rate during evaporative cooling of the condenser. The detailed numerical model was used to conduct a detailed parametric study involving the main operating parameters to establish the heat and mass transfer characteristics of the finned evaporatively-cooled condenser. The parametric study was also extended to determine the required condenser tube length for a fixed heat rejection rate from the condenser. It was observed from the parametric study that with the evaporative cooling, the condenser shows improved heat and mass transfer characteristics requiring shorter condenser tube length for a fixed heat rejection rate in the condenser.

Chapter 5
EXPERIMENTAL PROGRAM

Prior to the implementation of any simulation system developed from theoretical developments, the validation of the simulation program using a well-equipped experimental set-up is a good practice. In the present work, a fully equipped experimental set-up has been built to validate the results from the numerical investigation of the evaporatively-cooled condenser. There are two evaporatively-cooled condensers, with and without fins, which are part of a 5.8 kW split air-conditioning system. These two condensers are installed in such a way that they can be operated simultaneously or one at a time as required in the investigation. A schematic diagram and photographs of the experimental set up along with the photographs of the two condensers are shown in Figures 5.1, 5.2 and 5.3, respectively.

5.1 Description of the Experimental System

An experimental set up for the purpose of investigating the evaporatively-cooled condensers experimentally as well as to validate the numerical models is designed and built as shown in the schematic diagram in Figure 5.1. The set up, as shown in the figure, is essentially a split air conditioning system with the two condensers placed inside a rectangular duct. The duct also contains a 20 kW heater controller assembly to heat the air to be blown across the two condensers. A PID temperature controller attached to the heater circuit controls the air temperature to the set value. A fan interlock system installed in the set-up keeps the heater in an off position in the absence of the air flow. The other main components in the test rig is the water spray circuit for spraying water on to the condenser tubes with the help of a small pump. The spray system is designed in such a way that the spraying can be done

from the top of the condenser at a preset water flow rate. The hot air at the set temperature is blown across the condenser tube surface. The air blown across the condensers are subsequently vented into the ambient. Details of the different components of the set-up are described in the next sections.

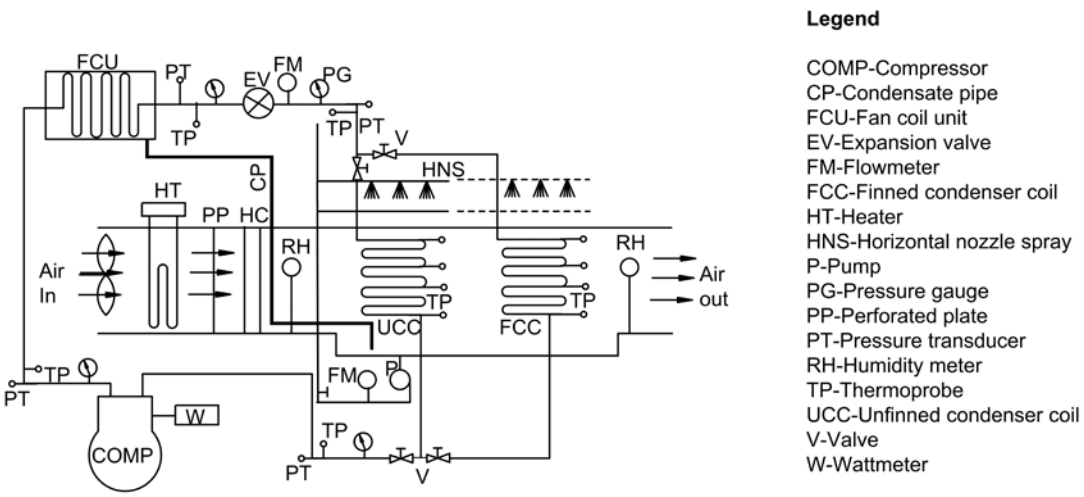

Figure 5.1 *Schematic diagram of the evaporatively cooled condenser split air-conditioner*

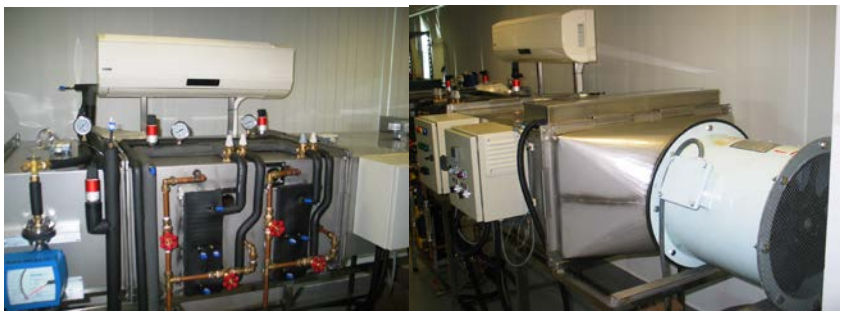

Figure 5.2 *Photograph of the evaporatively cooled condenser split air-conditioner*

The different components of the experimental rig can be grouped into three as follows:

5.1.1 Air-conditioning system

The air-conditioning system is essentially a modified vapour compression single split unit of 5.8 kW capacity with the two custom made condensers fitted in series with a bypass arrangement to isolate one of them during the experiments. The

other components in the air-conditioner are a centrifugal compressor, a fan coil unit and the thermostatic expansion device.

Behind the fan coil unit, a PVC condensate pipe is fitted to collect the condensate from the fan coil unit (FCU) and the condensate and the collected condensate water is mixed with the spraying water in the pump sump. The compressor used in the system is a hermetic 1.5 kW constant speed compressor.

The photographs of the custom-made finned and bare tube condensers are shown in Figures 5.3 and 5.4, respectively. The schematic diagrams of the finned and bare-tube condensers are shown in Figures 5.5 and 5.6, respectively. In the finned condenser, rectangular aluminium fins are used as shown in the Figure 5.3. More details on the two condensers including the fin dimensions are given in Table 5.1.

Figure 5.3 *Photograph of the finned evaporatively-cooled condenser*

Figure 5.4 *Photograph of the finned evaporatively-cooled condenser*

5.1.2 Water spray circuit

The Spraying System used for the evaporative cooling of the two condensers consists of a pump nozzle circuit as shown in the photograph of Figure 5.5. Main components in the spraying circuit are: 8 hollow cone nozzles with a cone angle of

70^{o} arranged on top of the condenser tubes. The height of the nozzle is fixed based on the cone angle such that there is no overlapping of the sprays from the nozzle and a fine spray of water is available on the top most condenser tube at a predetermined flow rate controlled by a valve and measured by a rotameter. A 0.75 hp centrifugal pump is included in the spraying circuit to circulate the used water collected in the pump sump.

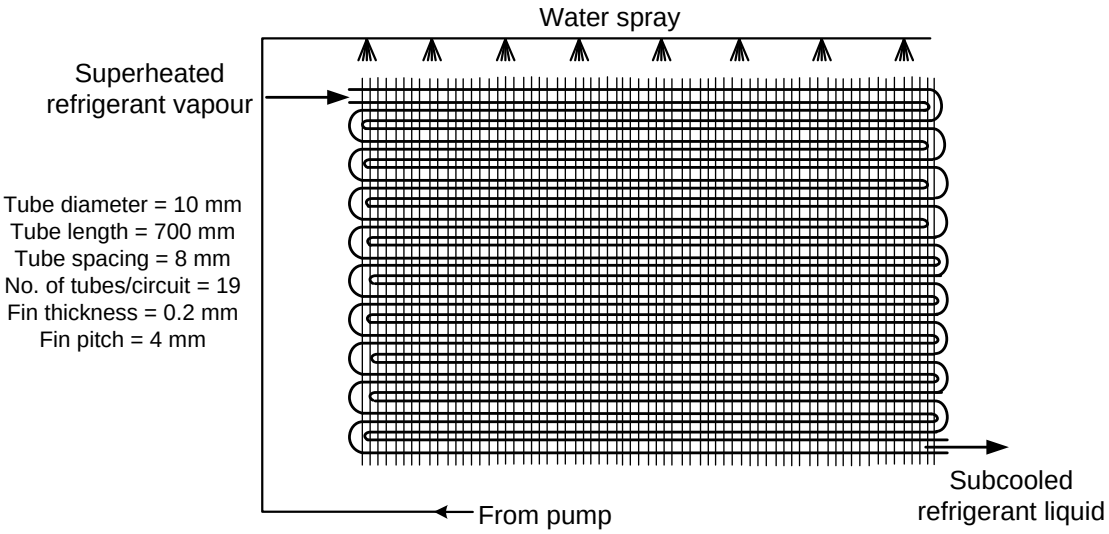

Figure 5.5 *Schematic diagram of the finned evaporatively-cooled condenser*

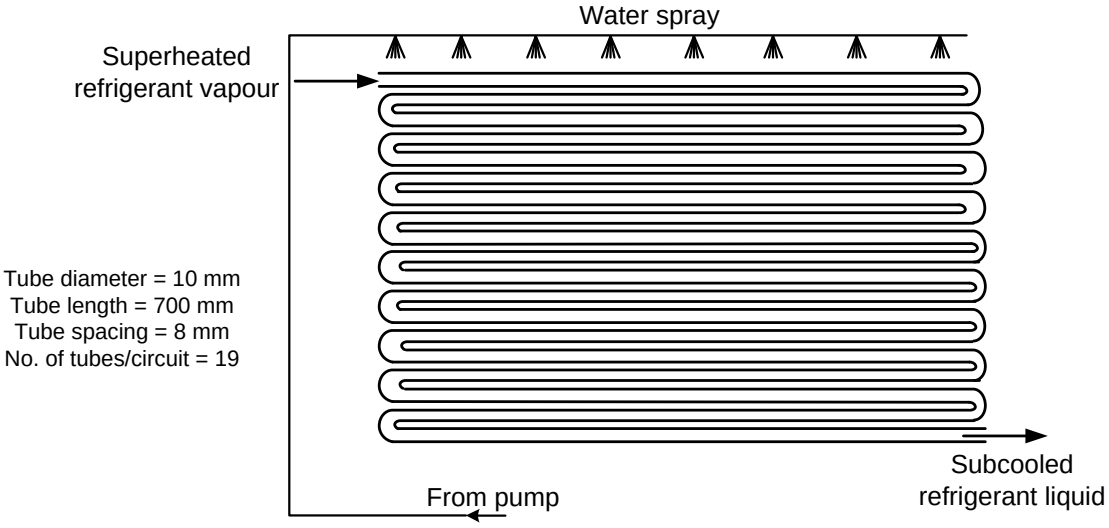

Figure 5.6 *Schematic diagram of the bare evaporatively-cooled condenser*

5.1.3 Air circuit

The air circuit is an open circuit with a blower-PID-heater control system housed in a stainless steel duct to blow air across the condensers at a predetermined air flow rate and temperature. A hot wire anemometer system is used to measure the air velocity and two humidity transmitters are mounted in the air circuit to measure the relative humidity and temperature of the air at the inlet and outlet, respectively. An axial blower as shown in Figure 5.2 with a variable speed motor inverter assembly is used to control the air velocity. A PID-controlled heater system controls the air temperature as required. The air emerging from the outlet of the duct is vented out to the ambient.

The specifications and characteristics of the system components are shown in Table 5.1.

Table 5.1 *Component specifications of the experimental set-up*

1. Condensers
   - i) Bare-tube
   - a. Tube inside diameter : 9.0 mm
   - b. Tube outside diameter : 10.0 mm
   - c. No. of tubes : 19
   - d. No. of circuit : 2

   - ii) Finned

   - a. Tube inside diameter : 9.0 mm
   - b. Tube outside diameter : 10.0 mm
   - c. No. of tubes : 19
   - d. No of circuit : 2
   - e. Fin material : Aluminium
   - f. Fin thickness : 0.2 mm
   - g. Fin height : 15 mm
   - h. Fin pitch : 4 mm
   - iii) Tube material : Copper
2. Fan Coil Unit
   - a. Type : Cross flow fin and tube
   - b. Fins : 1550 per m^2
   - c. Cooling capacity : 5.8 kW

3. Compressor
   - a. Bore : 0.035 m
   - b. Stroke : 0.026 m
   - c. Capacity : 3.0 kW
   - d. Speed(RPM) : 2800
   - e. Refrigerant : R134a

4. Pump
   - a. Type : Centrifugal
   - b. Capacity : 0.75 hp

5. Spraying Nozzles
   - a. Flow rate : 0.032-0.517 L/min
   - b. Spray angle : 70^{o}
   - c. No. of nozzles/condenser : 8

6. Blower and controller
   - a. Type : Axial
   - b. Capacity : 260 cu.m/h; static head: 300 Pa
   - c. Controller : Variable speed motor with inverter

7. Heater and controller
   - a. Capacity : 20 KW
   - b. Controller : PID

5.1.4 Measuring equipment

The primary objective of the experimental set-up is to investigate and evaluate the performance of the evaporatively-cooled condensers and subsequently the performance of the air-conditioning system. For the same, it is necessary to measure the flow rate of refrigerant and spraying water, temperature and pressure of the refrigerant flowing through the system at different locations of the air-conditioning circuits. The instruments deployed in the experimental set up for these measurements are described below.

5.1.4.1 Refrigerant flow meter

To measure the volume flow rate of the refrigerant, a magnetic type volume flow meter of capacity 21 to 210 L/h is used. Maximum working temperature of the flow meter is about 100 ^{o}C. The flow meter which was calibrated with refrigerant R134a under atmospheric pressure has an accuracy of ± 1.6%.

5.1.4.2 Rotameter

Two rotameters whose measuring range is from 0 to 1.0 liters/minute are connected in parallel, as shown in Figure 5.1. These measure the volume flow rate of the spraying water. Each rotameter has a valve to control the flow of cooling water through it. These rotameters are calibrated separately using standard measuring volumes of accuracy 0.01 liters. The rotameters have an accuracy of ± 1.5 percent.

5.1.4.3 Hot wire anemometer

To facilitate the practical calculation of the moisture absorbed by the air in the system, the measurement of volume flow rate of air is very important. For this, a vane type anemometer is used. It is calibrated by the manufacturer and has a velocity ranege of 0 to 25 m/s. Using the measured average velocity at different points (in the present study, measured at 8 points and averaged) along with the area of cross-section of the duct, the volume flow rate can be determined.

5.1.4.4 Humidity sensors

In order to fix the thermodynamic state of the air blown across the condenser tubes, one more property other than temperature is essential. So the second property selected is relative humidity. With the knowledge of the above two, the moisture content of air can be determined. In this set-up the relative humidity of the air at the inlet and outlet of the condenser tubes is measured with the help of two humidity transmitters. The humidity transmitter calibration is in such a way that 4 to 20 mA corresponds to 0 to 100 % relative humidity. A calibration equation is developed using these points and this equation is used to convert the output signal into relative humidity. The accuracy of the relative humidity sensors is ± 2.0 %.

5.1.4.5 Temperature measurement

Fourteen type-T (copper-constantan) thermocouples are used to measure the temperature of the refrigerant at different locations of the experimental set-up, as shown in Figures 5.1. All thermocouples are calibrated using a standard liquid-in-glass thermometer with an accuracy of ± 0.05 ^{o}C. The calibration equations for the thermocouples are tabulated in Appendix D.

5.1.4.6 Electronic pressure transducer

To measure the absolute pressure of the refrigerant at important locations of the air-conditioner, two electronic pressure transducers each of operating ranges 0-10 bars and 0-20 bars are used. The output signals corresponding to the absolute pressure ranges in bars are 0 and 10.0 V DC. The accuracy of the electronic pressure transducers is ± 0.1 %.

5.1.4.7 Compressor power measurement

To measure the compressor motor power input, a HIOKI clamp-on power meter with accuracy of ± 2.0 % is used.

5.1.4.8 Data acquisition system

A data acquisition system consisting of a high-speed data logger (Agilent, Model 34970A) and a computer was used in the experimental set-up. The data logger can accommodate a maximum of three detachable multiplexes of modules and each module can accept a combination of sixteen a.c and d.c voltage, a.c and d.c current, thermocouples and thermistor signals. However, of the sixteen channels, only two are reserved for current signals. Other current signals have to be converted to voltage signals with suitable precision resistors connected in series. For data acquisition and real time monitoring of the system variables during the experiment, a software program (DATALINK) supplied by the manufacturer of data logger was used. The software was

capable of displaying the parameters being measured in graphical and the numerical form. All thermocouples and the pressure transducers were connected to the data logger and the data sampling speed and time interval were controlled by the computer.

The calibration charts and equations for the thermoprobes, humidity transmitters and pressure transducers are given in Appendix D.

5.2 Details of the Experiments Carried Out

For the convenience of presentation, the experiments carried out may be broadly grouped into two categories. These are (i) experimental investigation of the evaporatively-cooled condenser without fins and (ii) experimental investigation of the evaporatively-cooled condenser with fins. The procedures of the above experiments are described in the following sections.

5.2.1 Experimental investigation on the bare-tube evaporatively-cooled condenser

The test rig was designed and constructed in a manner that allowed the testing of the evaporatively-cooled condenser with and without fins independently. The performance of the 5.8 kW modified split air-conditioner with the bare tube evaporatively-cooled condenser has been investigated experimentally under different operating conditions. At the beginning of each test, the fan speed and the air temperature are set to predetermined values with the help of the fan inverter and heater PID controller, respectively. The bare-tube condenser is first tested without evaporative cooling (spraying of water). The air-conditioner is switched on and allowed to run for 30 to 45 minutes to attain steady state. Once the steady state condition is reached, scanning of the temperatures and pressures at different locations in the refrigeration circuit as well as the air inlet and outlet conditions into a personal computer every 20 s interval with the help of an Agilent 40 channel data acquisition unit is started. The refrigerant flow rate is read from the magnetic refrigerant flow meter. The duration of each experimental run is fixed

at about 90 minutes. Matching experiments are conducted on the bare tube condenser on the evaporative cooling mode. Before the evaporative cooling experiments are commenced, water level in the pump sump is checked for adequate water level. Using the control valve and the rotameter in the spraying circuit, the water flow rate is adjusted to the predetermined flow rate to have the required water film thickness on the top tube of the condenser calculated using the Bird's equation given in the Chapter 3. As in the previous case, the fan speed and air temperature are set and the air-conditioner is turned on, the data scanning is commenced once the system attained steady state operating conditions. It is worthwhile to note that, in these runs of experiments on the bare tube the entire refrigerant flow path is diverted into the bare tube condenser with the help of the bypass valves.

5.2.2 Experimental investigation on the finned-tube evaporatively-cooled condenser

For these runs of experiments, the entire refrigerant flow is diverted into the finned tube condenser. Similar to the experimental runs in the previous section on the bare tube condenser, experiments on the finned tube condenser is conducted initially without evaporative cooling and subsequently with evaporative cooling.

Upon completion of each run of the experiments, the data is checked for quality and saved and processed for the determination of the coefficient of performance with and without evaporative cooling for both the condensers. Mass flow rate of water evaporated from the condenser tube surface is determined from the measured air inlet and outlet conditions data. The variation of measured condenser temperature in the condenser tubes along with the experimental mass flux of water evaporated are used for the validation of the present numerical investigation as well as those from the experimental results of other researchers' work.

A detailed uncertainty analysis for the derived parameters from the measurements is described in Appendix E. Based on the uncertainty analysis performed using the given

individual uncertainties in the preceding section, the uncertainties of the derived parameters; COP and rate of water evaporated from the film-air interface are found to be within 5% and 7%, respectively.

5.3 Summary

In this chapter, the details of the experimental program to evaluate the performance of a 5.8 kW air-conditioner with bare and finned tube condensers on both non-evaporative and evaporative cooling modes was presented. The test facility consisted of a stainless steel duct housing the two condensers, blower, heater coils, spraying nozzles as well as the humidity and temperature sensors. The other components of the test facility included the fan coil unit (FCU), reciprocating compressor, rotameter, refrigerant flow meter as well as a water pump. The flow rates were measured with rotameters while the air inlet and outlet conditions were measured with the help of humidity transmitters. A hot wire anemometer measures the air velocity, which is used subsequently to establish the air mass flow rate. The air temperature and fan speeds are controlled by a PID temperature controller and inverter, respectively. Fine water spray is formed with the help of the nozzle-pump system and is sprayed on to the top condenser tube at controlled flow rate to have a predetermined water film thickness on the top condenser tube surface. Tests are carried out for a series of operating conditions, which include varying air inlet temperature, air velocity, cooling water flow rate and fixed cooling water temperature.

Chapter 6
COMPARISON OF SIMULATED AND EXPERIMENTAL RESULTS FOR BARE AND FINNED-TUBE EVAPORATIVELY-COOLED CONDENSERS

In this chapter, results from the experimental and numerical investigations performed on the serpentine condenser tubes with and without fins are presented. The detailed theoretical model is validated with experiments performed for the range of variables listed in Table 6.1 and Table 6.3. The full theoretical model simulation and matching experiments on the condenser tubes establish the performance of the evaporatively-cooled condenser by determining the heat and mass transfer characteristics in the finned and bare serpentine tubes. The refrigerant R-134a enters the serpentine condenser tubes as superheated refrigerant vapour and emerges from the condenser as sub-cooled liquid. Fine water sprays cover the top tubes with water at a predetermined flow rate. The measured rate of water evaporated from the film-air interface on the tube surface is determined using equation 3.27. The higher the mass of water evaporated from the film-air interface, the faster the heat rejected by the condenser to the surroundings resulting in a lower condensing temperature of the air-conditioning system. The lower the condensation temperature, the lower is the pressure lift between the evaporator and condenser resulting in an improved COP of the air-conditioning system.

6.1 Experimental Validation of the Numerical Model of the Bare-tube Condenser

The variation of the simulated and experimental refrigerant temperature along the bare-tube for two different parameters is depicted in Figures 6.1 to 6.3. Figure 6.1 shows the variation of temperature along the condenser tube for two different air

temperatures. As can be seen from the figure there is good agreement between the measured and simulated refrigerant temperatures for both the 30 and 35 ^{o}C ambient air temperature cases, with relative humidity of 42 % and 33 %, respectively. The regions 1, 2 and 3 marked on the figures are the superheated, condensation and sub-cooled regions in the condenser, respectively.

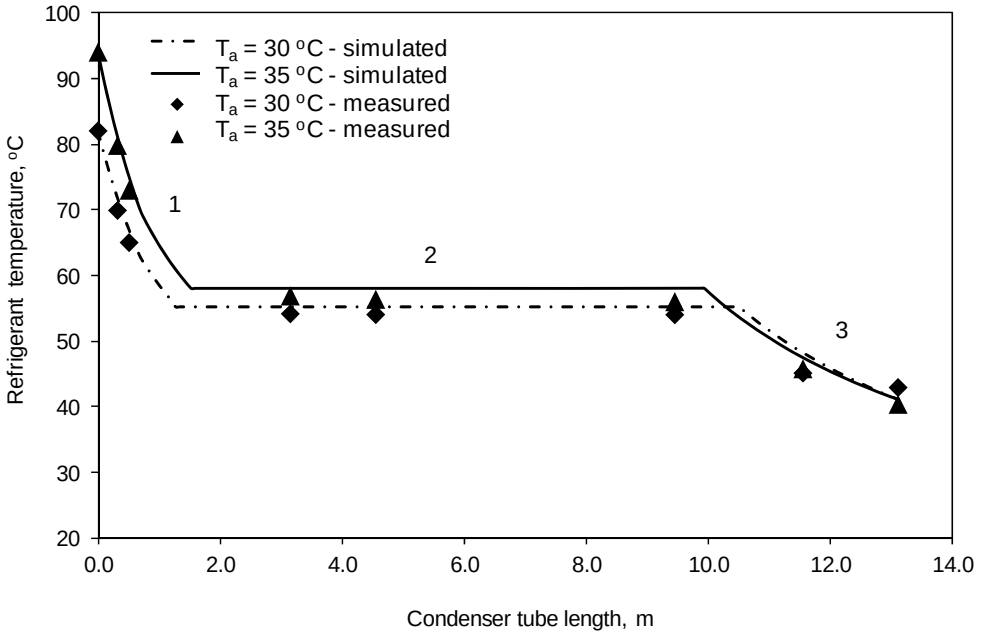

Figure 6.1 *The simulated and measured variations of refrigerant temperature along the condenser tube length for different air temperature for δ_w=0.18 mm (Re_f = 15), RH=43%, $T_{w,i}$=25 ^{o}C, V = 4 m/s, $P_{r,in}$=16 bar*

Table 6.1 Experimental conditions and variables (bare-tube)

Variables	Range
Γ (kg/mh)	8.0-38.3
$T_{w,in}$ (^{o}C)	20.0- 25.0
$M_{r,in}$ (kg/h)	124.0
$P_{r,in}$ (bar)	15.0- 16.8
T_{cond} (^{o}C)	55.0 - 60
V (m/s)	2.0-4.0
T_a (^{o}C)	30.0-40.0
RH (%)	30.0 - 50

Figure 6.2 shows the variation of measured and simulated refrigerant temperature along the condenser tube length for two air velocities. As can be seen from the figure, the predicted and measured refrigerant temperatures are in good agreement.

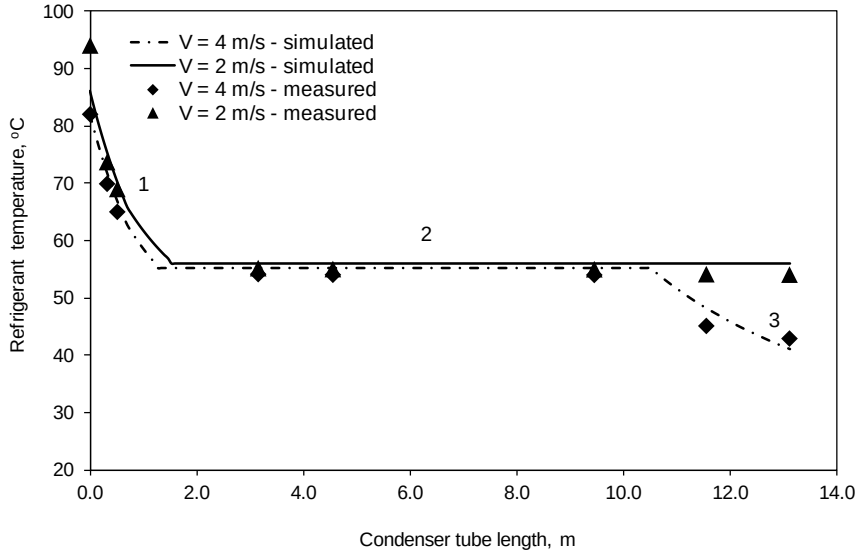

Figure 6.2 *The simulated and measured variation of refrigerant temperature along the condenser tube length for two different air velocities for δ_w=0.18 mm (Re_f = 15), RH=43%, $T_{w,i}$=25 ^oC, T_a = 35 ^oC, $P_{r,in}$=16 bar*

Variation of measured and simulated refrigerant temperatures for two film Reynolds numbers; Re_f = 9 and 15 is shown in Figure 6.3 and as in the previous cases of air temperature and velocity, they are also in good agreement. Figure 6.4 shows the experimental and simulated water evaporation rates from the film-air interface for the experimental conditions given in Table 6.1. The experimental water evaporation rate is determined from the measured air relative humidity (RH) and temperature at the inlet and exit of the condenser coil. As can be seen from the figure, the simulated and experimental values of the total water evaporation rate are in satisfactory agreement within 13 %.

From the measured and simulated temperature distributions along the tube in Figures 6.1 to 6.3 as well as the measured mass flux of water evaporated in Figure 6.4 validate the present model for the serpentine condenser tubes without fins.

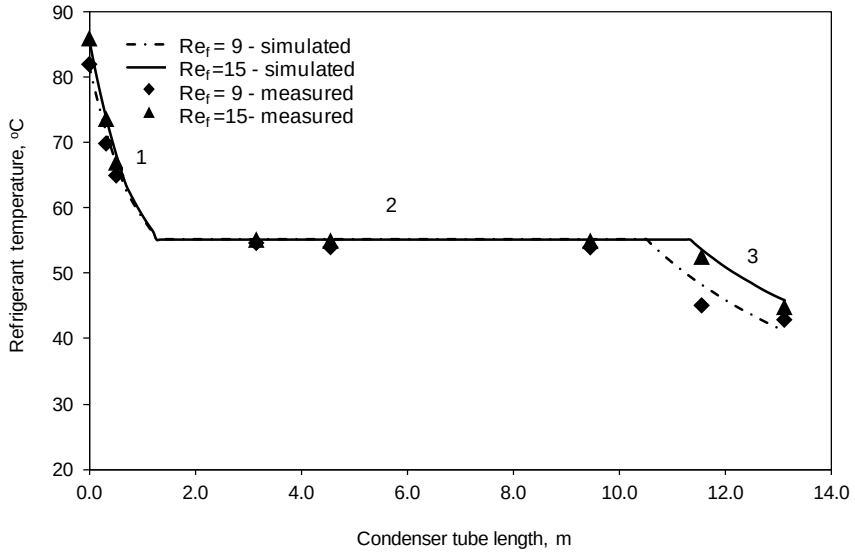

Figure 6.3 *The simulated and measured variation of refrigerant temperature along the condenser tube length for two different film Reynolds numbers, RH=43%, $T_{w,i}$=25 ^oC, T_a = 35 ^oC, V= 4 m/s $P_{r,in}$=16 bar*

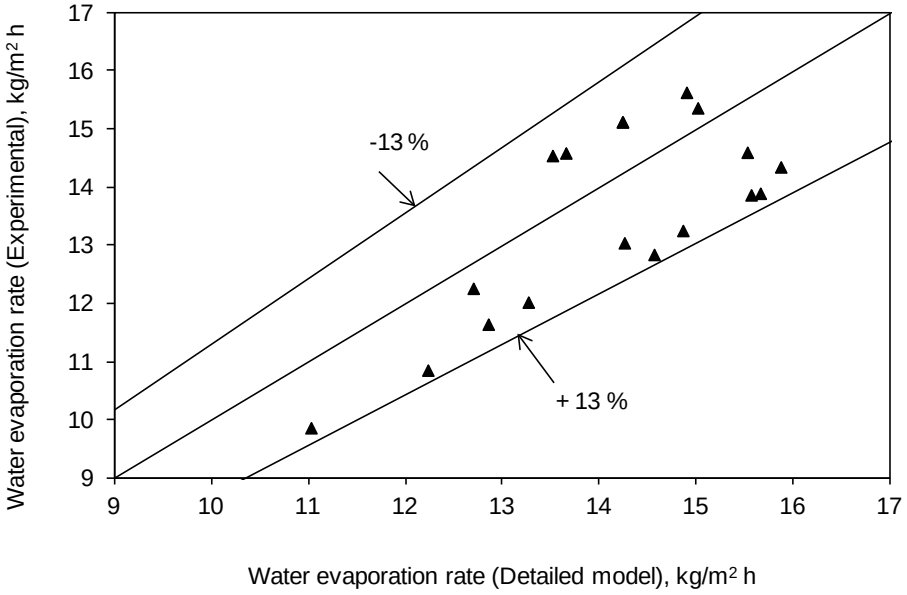

Figure 6.4 *Comparison of numerical and experimental total mass flux of water evaporated from the tubes for the experimental conditions given in Table 6.1*

Numerically and experimentally determined COP, measured mass flux of water evaporated from the film-air interface, cooling capacity and compressor motor power input for the bare-tube evaporatively-cooled condenser are presented in the following section. Average values of steady-state experimental data for 16 runs of experiments each for the bare-tube and evaporatively-cooled condensers are attached as Appendix F. An uncertainty analysis of the 32 runs are carried out and tabulated in Appendix E.

Figure 6.5 shows simulated and measured variations of the rate of mass of water evaporated from the condenser tube surface with ambient air temperature for the condenser with evaporative cooling. The other parameters for the experiments are shown in parenthesis. As can be seen from the figure, the mass of water evaporated shows an inverse relationship with the air inlet temperature. A water evaporation rate of 14.5 kg/m^2 h is obtained for an air inlet temperature of 30 ^{0}C. As can also be seen from the figure, the simulated and measured rate of water evaporated is in good agreement.

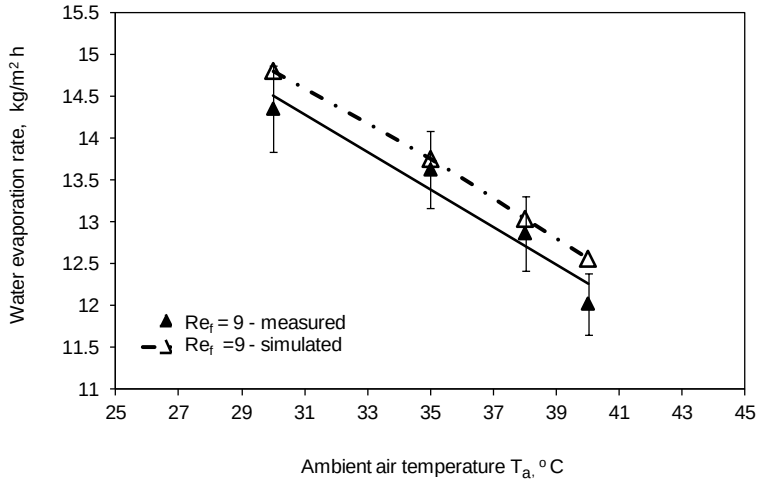

Figure 6.5 *The simulated and measured variations of mass of water evaporated from the condenser tube surface with air inlet temperature for T_{wi} =25 ^{o}C, δ_w=0.15mm (Re_f = 9), R = 5 mm, V = 4 m/s*

Simulated and measured variations of mass of water evaporated from the condenser tube surface with the film Reynolds number, is shown in Figure 6.6. The range of film Reynolds numbers considered here is 5 to 24, which corresponds to top tube water film thicknesses of 0.12 to 0.21 mm as determined from the Bird equation. As observed from Figure 6.6, a better evaporation rate is observed for a lower film Reynolds number because of the low thermal resistance existing for the lower film thickness. As can be seen from the Figure, the simulated and measured rates of water evaporated from the condenser tube surface are in satisfactory agreement.

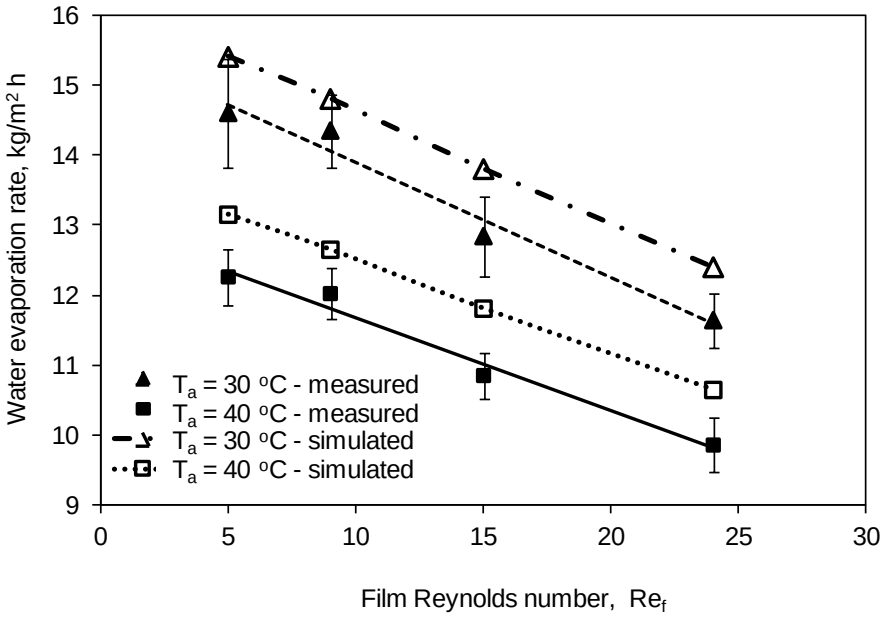

Figure 6.6 *Simulated and measured variations of mass of water evaporated from the condenser tube surface with film Reynolds number for T_{wi} =25 ^{o}C, T_a = 30 ^{o}C, R = 5 mm, V = 4 m/s*

Figure 6.7 shows the P-h diagrams obtained experimentally from the measured evaporator and condenser pressures and temperature for the cases with and without evaporative cooling of the condenser. As can be seen from the figure, the vapour compression air-conditioning cycles 1-2-3-4 and 1'-2'-3'-4' are for the cases without and with evaporative cooling, respectively. The points 1, 2, 3 and 1', 2', 3' are fixed

from the measured pressures and temperature. However, due to the difficulty in the measurement of refrigerant quality, the points 4 and 4' are fixed assuming the expansion processes 3-4 and 3'-4' as isenthalpic. For this, the thermostatic expansion valve was well insulated during the experiments.

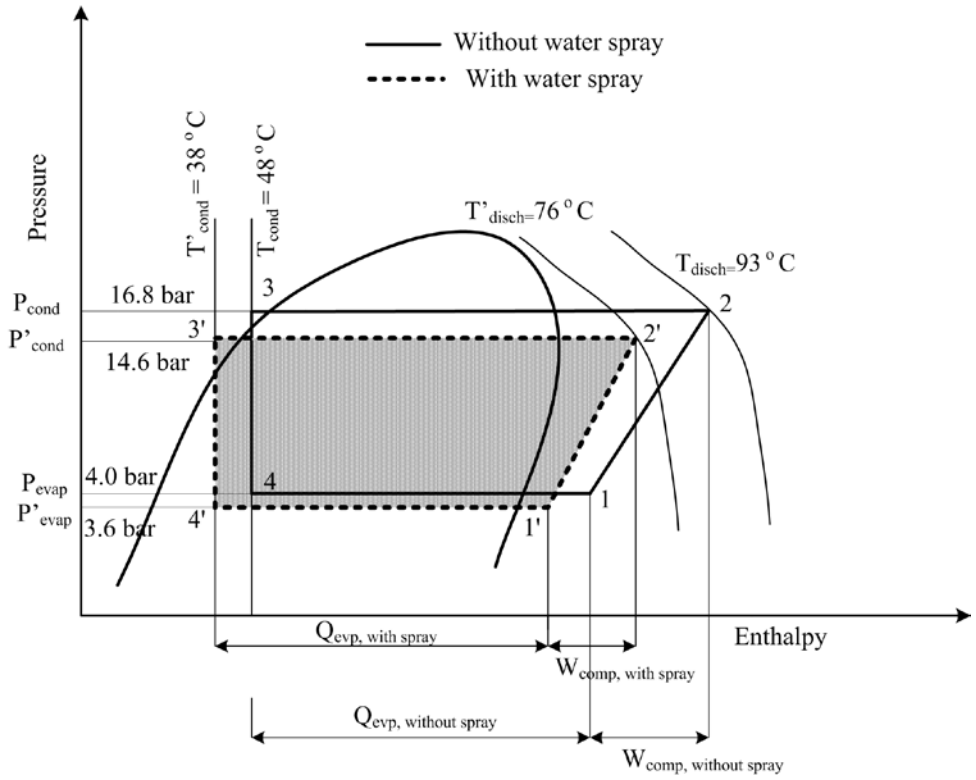

Figure 6.7 *P-h diagram with the condenser and evaporator pressure changes for T_{wi} =25 ^{o}C, δ_w=0.15mm (Re_f = 9, mm), R = 5 mm, V_f = 30 m^3/min (measured average volume flow rate 8 points), T_a =30 ^{o}C*

As can be seen from Figure 6.7, the condensing pressures observed from the experiments were 16.8 bars and 14.6 bars, without and with evaporative cooling, respectively. The observed drops in the evaporator and condenser pressures due to evaporative cooling are similar to that observed by Hajidavalloo (2007). The corresponding evaporative pressures were 4.0 bars and 3.6 bars, respectively. It is also evident from the figure that an improvement in the cooling capacity (Q_{ev}) as well as a reduction in the compressor work input (W_{comp}) resulted from the reduced condensing

pressure with evaporative cooling. The data points as well as the determined COP for the experimental run are listed in Table 6.2. From the determined values, an improvement in COP of about 28 % is observed.

Figures 6.8 shows the simulated and measured COP plotted against air inlet temperature, with and without evaporative cooling. The simulated COP and cooling capacities are determined from the numerically obtained condenser exit temperature in conjunction with the measured evaporator and compressor exit conditions as well as the measured compressor motor power. As can be seen from the figure, a COP value of 2.82 is obtained with the evaporative cooling of the condenser compared to the COP of 2.2 without the evaporative cooling, with the other experimental conditions kept constant. As also can be seen from Figure 6.8, the lowest value of COP is 1.96, which is observed for the case without evaporative cooling notably for an ambient temperature of 40 ^{0}C. Experimental variation of the COP with the film Reynolds number, Re_f is shown in Figure 6.9.

Table 6.2 *Typical data points and COP with and without evaporative-cooling (bare-tube)*

Data Point	Without Evaporative cooling	With Evaporative cooling
Inlet air temperature, ^{o}C	30.0	30.0
Inlet air relative humidity, %	42.0	42.0
Outlet air temperature, ^{o}C	35.0	31.3
Outlet air relative humidity, %	32.0	82.0
Condensing Pressure, bar	16.8	14.6
Evaporating Pressure, bar	4.0	3.6
Compressor discharge temperature,	93.0	76.0
Condensing Temperature, ^{o}C	60.0	54.0
Condenser exit temperature, ^{o}C	48.0	38.0
Evaporator inlet temperature, ^{o}C	9.0	6.0
Evaporator exit temperature, ^{o}C	19.0	15.0
Evaporator inlet enthalpy, h_4, kJ/kg	268.8	253.6
Evaporator outlet enthalpy, h_1,	414.4	410.5
Compressor power , kW	2.23	1.97
Refrigerant mass flow rate, kg/h	120.24	127.08
Coefficient of Performance, COP	2.21	2.82
% increase in COP	-	27.6%

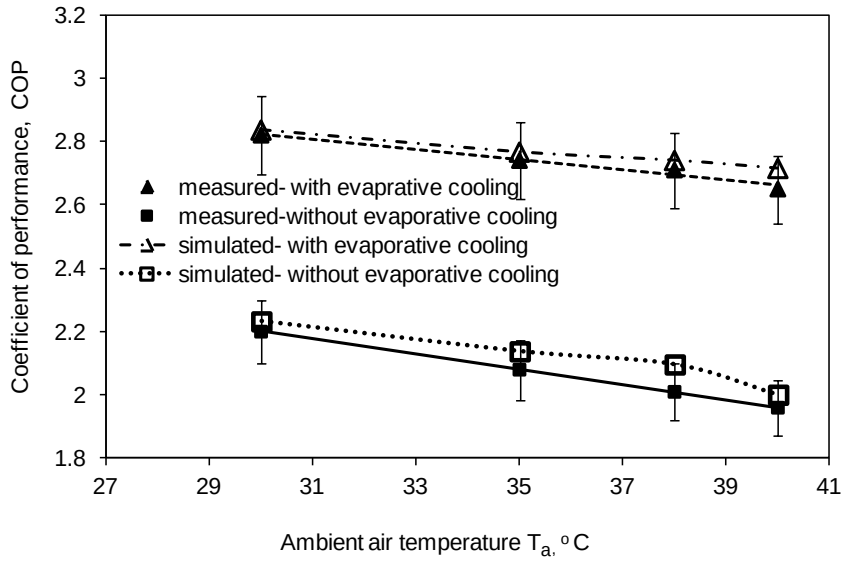

Figure 6.8 *Simulated and measured variation of COP with air inlet temperature for T_{wi} =25 °C, δ_w=0.15mm (Re_f = 9), R = 5 mm, V_f = 30 m^3/min (measured average volume flow rate 8 points)*

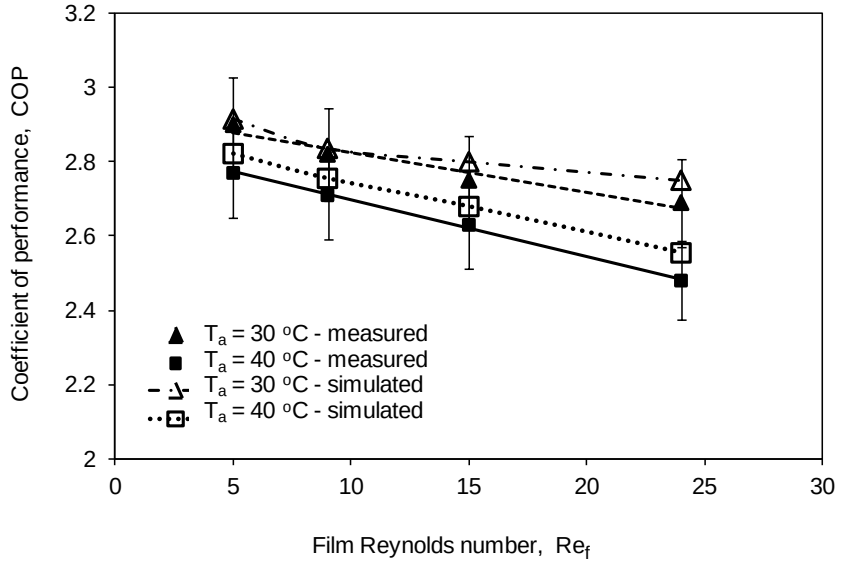

Figure 6.9 *Simulated and measured variation of COP with film Reynolds number for T_{wi} =25 °C, T_a = 30 °C, R = 5 mm, V_f = 30 m^3/min (measured average volume flow rate 8 points)*

The effect of film Reynolds number, Re_f, on cooling capacity from both the simulation and experiments is shown in Figure 6.10. As can be seen, the cooling capacity decreases with the film Reynolds number due to the change in the evaporator inlet conditions caused by the relatively higher condensing temperature. The higher

condensing temperature is due to the increase in thermal resistance caused by increase in water film thickness, which in turn lowers the heat transfer rate in the condenser.

The variation of cooling capacity with air inlet temperature, with and without evaporative cooling, is shown in Figure 6.11. As can be seen from the figure, better cooling capacity is observed in the presence of evaporative cooling due to the better heat transfer characteristics at the condenser. However, as expected and also can be seen from the figure, with increase in air temperature, the cooling capacity is reduced with and without evaporative cooling.

Figure 6.12 shows the variation of the measured input electrical power with the air inlet temperature, with and without evaporative cooling. In both the cases, as expected, the compressor power input increases as the air blown across the condenser tubes becomes warmer. The highest electrical power input of 2.31 kW is observed from the figure for an air inlet temperature of 40 ^{o}C.

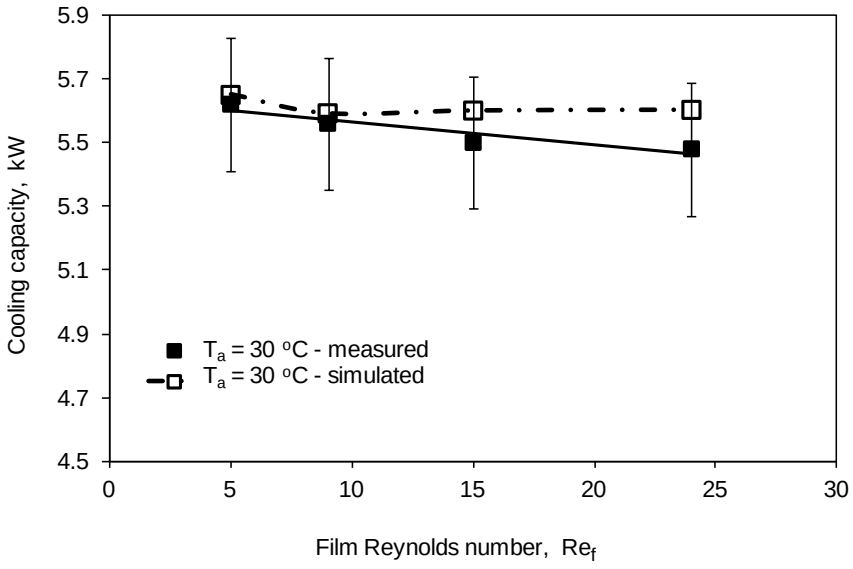

Figure 6.10 *Simulated and Measured variation of cooling capacity with film Reynolds number with evaporative cooling for T_{wi} =25 ^{o}C, T_a = 30 ^{o}C, R = 5 mm, V_f = 30 m^3/min (measured average volume flow rate 8 points)*

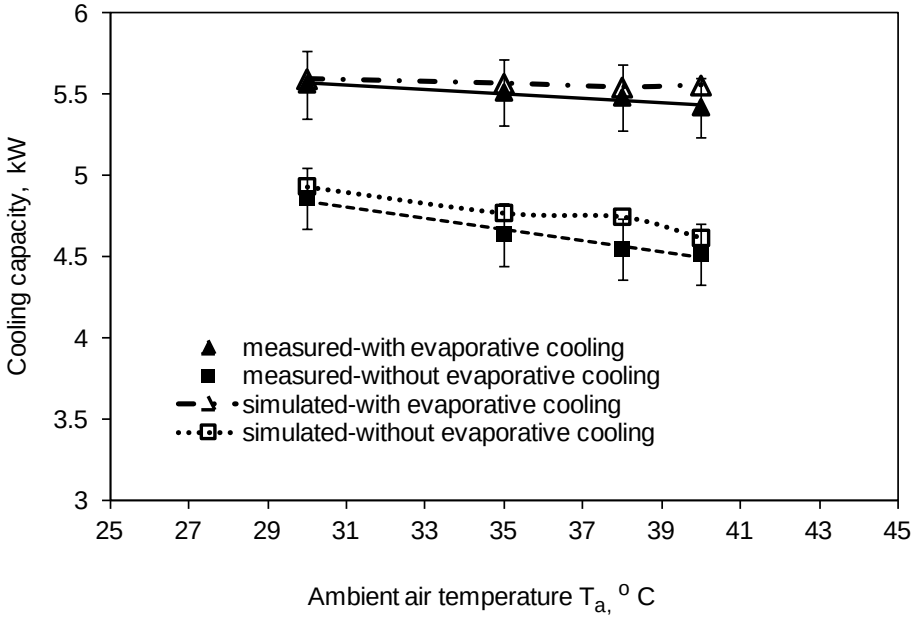

Figure 6.11 *Simulated and measured variation of cooling capacity with air temperature with and without evaporative cooling for T_{wi} =25 ^{o}C, T_a = 30 ^{o}C, R = 5 mm, Re_f = 9, V_f = 30 m^3/min (measured average volume flow rate 8 points)*

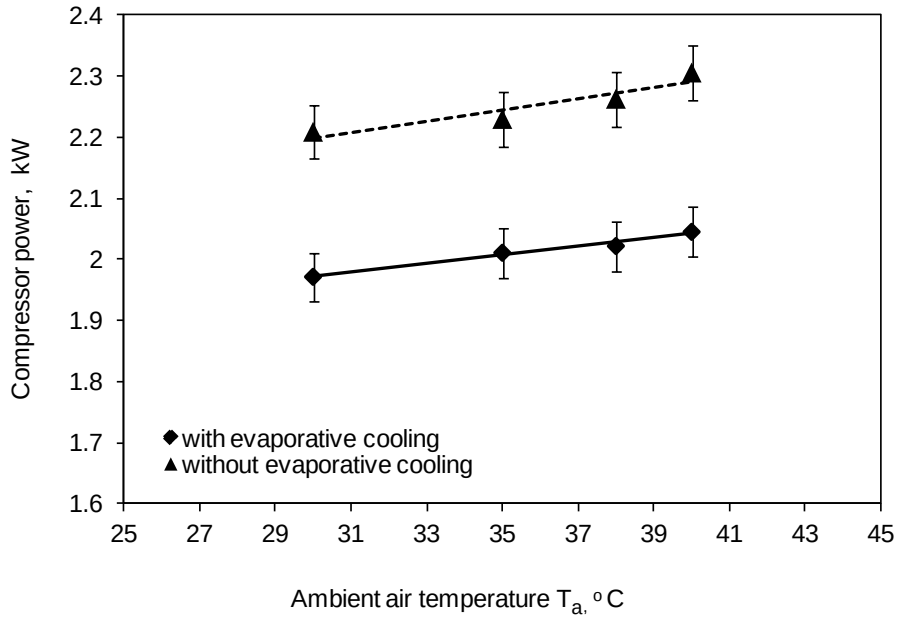

Figure 6.12 *Measured variation of compressor power with air inlet temperature for R_{ef} = 9, T_a = 30 ^{o}C, R = 5 mm, V_f = 30 m^3/min (measured average volume flow rate 8 points)*

Measured variation of the electrical power input with film Reynolds number for the bare tube evaporatively-cooled air-conditioner is depicted in Figure 6.13. The input power and film Reynolds number shows an inverse relationship because of the higher thermal resistance existing for higher film Reynolds number (higher film thickness). The minimum and maximum values of the compressor power input observed from the figure are 1.93 and 2.17 kW for film Reynolds number values of 5 and 24, respectively.

The effect of the air inlet temperature on the percentage increase in cooling capacity, compressor power input and COP due to evaporative cooling for the bare tube condenser is shown in Figure 6.14. As can be seen from the figure, because of the combined double effect of improvements in both the cooling capacity and compressor power input due to evaporative cooling, the COP of the air-conditioning system shows significant improvement of up to 35%.

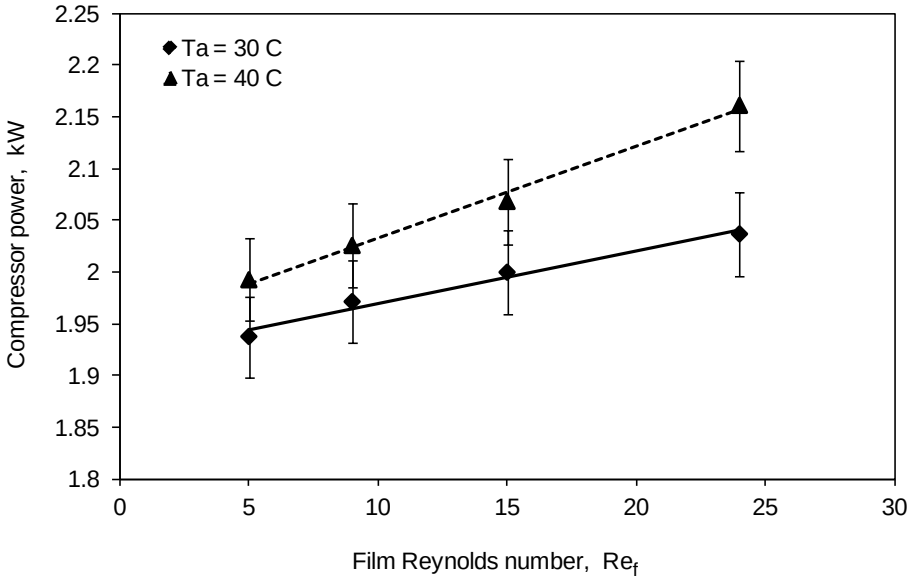

Figure 6.13 *Measured variation of compressor power with film Reynolds number for T_{wi} =25 ^oC, R = 5 mm, V_f = 30 m^3/min (measured average volume flow rate 8 points)*

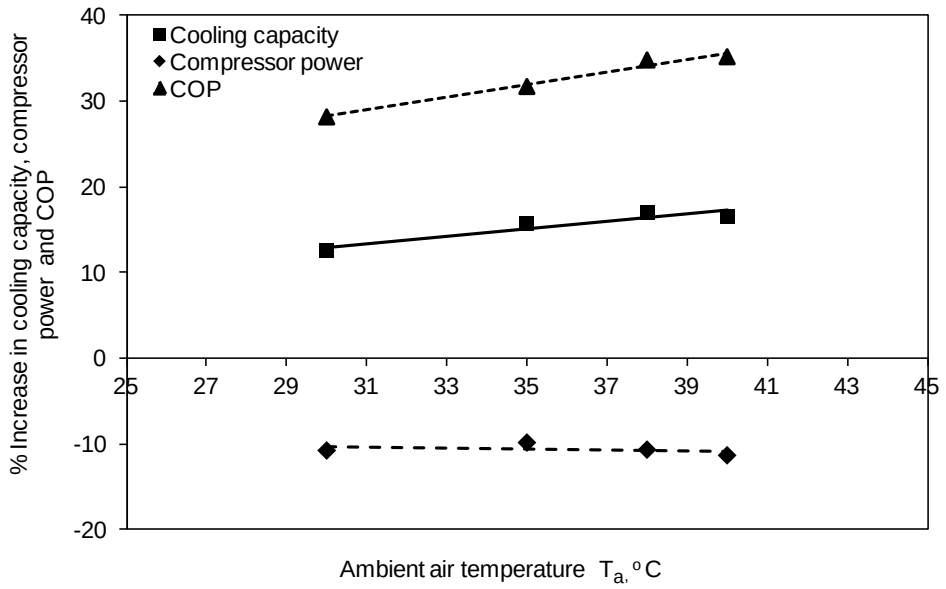

Figure 6.14 *Effect of the air inlet temperature on the percentage increase in measured cooling capacity, compressor power input and COP due to evaporative cooling for T_{wi} =25 °C, Re_f = 9, R = 5 mm, V_f = 30 m^3/min (measured average volume flow rate 8 points)*

6.2 Experimental Validation of the Numerical Model of the Finned-tube Condenser

As in the previous section, the measured key system performance parameters and the matching simulated parameters for the finned evaporatively-cooled condensers are presented in the following paragraphs.

The variation of the simulated and measured refrigerant temperatures along the tube with parametric variations of the air temperature, velocity and spraying water mass flow rate are shown in Figures 6.15 to 6.17. As can be seen, there is good agreement between the measured and computed refrigerant temperatures for the operating parameters considered. The ambient air relative humidity as measured from the experiments ranged from 30 to 45%. The other input parameters for the experiments are shown in Table 6.3.

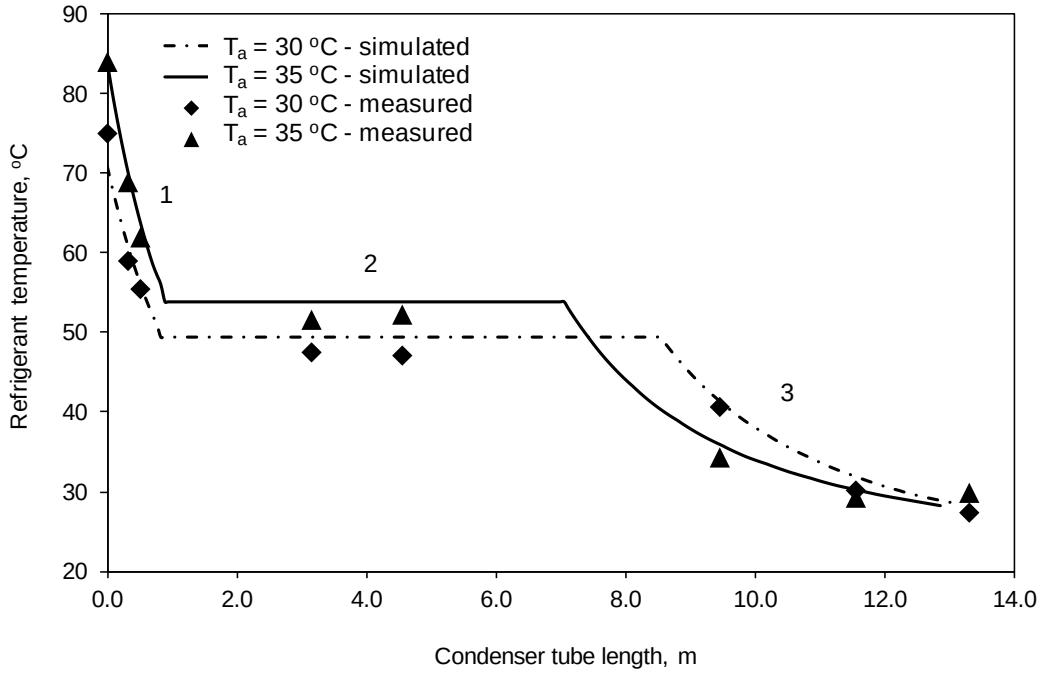

Figure 6.15 *Simulated and measured variations of refrigerant temperature along the condenser tube length for different ambient temperature for δ_w=0.18 mm (Re_f = 15), RH=43%, $T_{w,i}$=25 °C, T_a = 35 °C, $P_{r,in}$=14 bar*

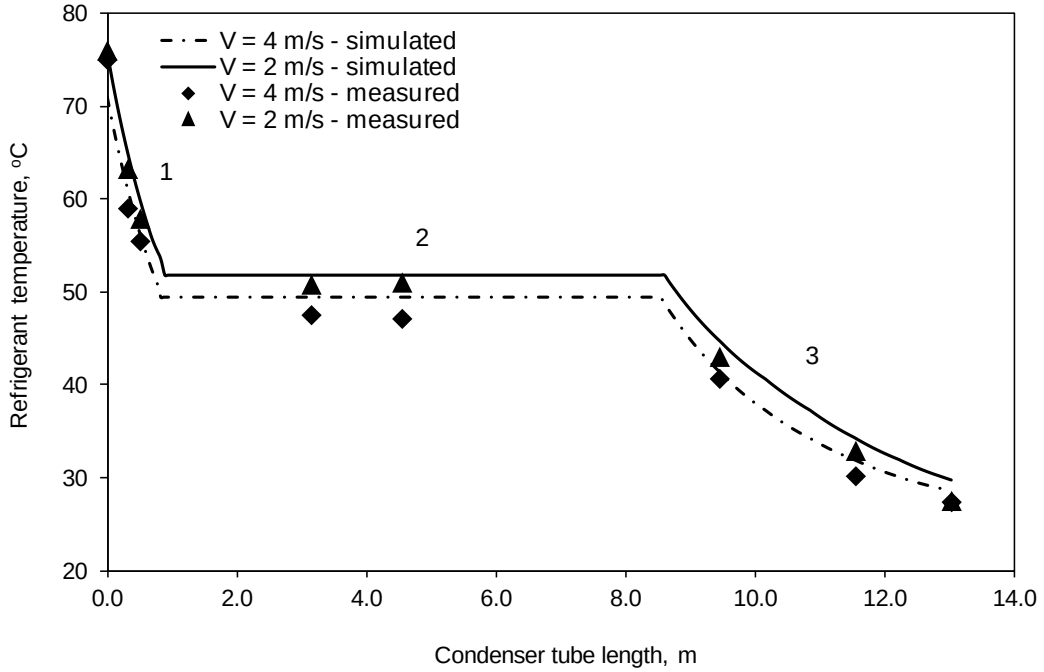

Figure 6.16 *Simulated and measured variations of refrigerant temperature along the condenser tube length for different air velocity for δ_w=0.18 mm (Re_f = 15), RH=43%, $T_{w,i}$=25 °C, T_a = 35 °C, $P_{r,in}$=14 bar*

Table 6.3 Experimental conditions and variables (finned-tube)

Variables		Range
Γ	(kg/mh)	8.1– 38.2
$T_{w,in}$	(^oC)	25.0
$M_{r,in}$	(kg/h)	145.5
$P_{r,in}$	(Bar)	9.5 – 14.0
$T_{r,in}$	(^oC)	70.0 – 90.0
T_{cond}	(^oC)	37.5 – 53.0
V	(m/s)	2.0 – 4.0
T_a	(^oC)	30.0 – 40.0
RH	(%)	30.0 – 60.0
Fin pitch (mm)		4.0
Fin thickness (mm)		0.2
Fin length		15

Figure 6.18 shows the measured and simulated water evaporation rates from the condenser tube surface for the experimental conditions given in Table 6.3. The experimental water evaporation rate is determined from the measured relative humidity (RH) and temperature at the inlet and exit of the condenser coil. As can be seen from the figure, the simulated and experimental values of the total water evaporation rate are in satisfactory agreement within 15.0 %.

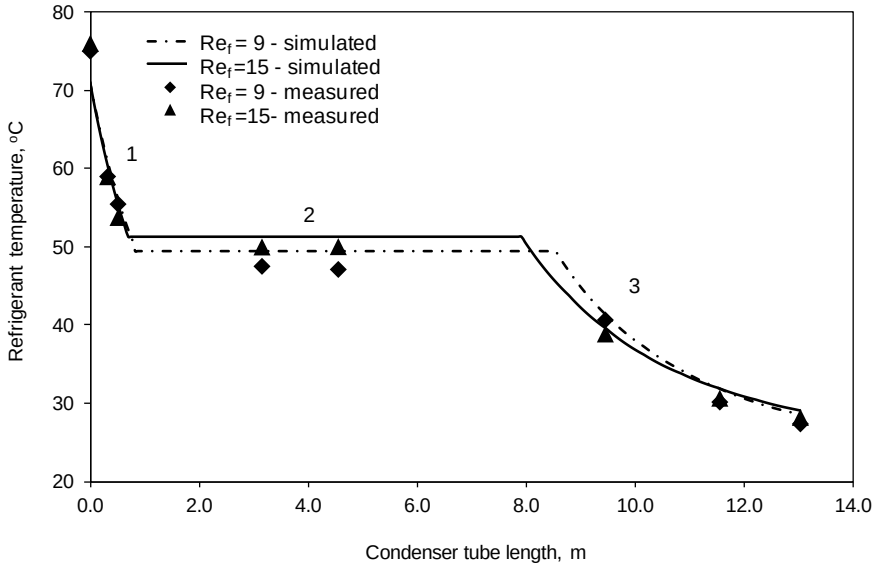

Figure 6.17 *Variation of refrigerant temperature along the condenser tube length for different air velocity for RH=43%, $T_{w,i}$=25 ^{o}C, T_a = 35 ^{o}C, $P_{r,in}$=14 bar, V = 4 m/s*

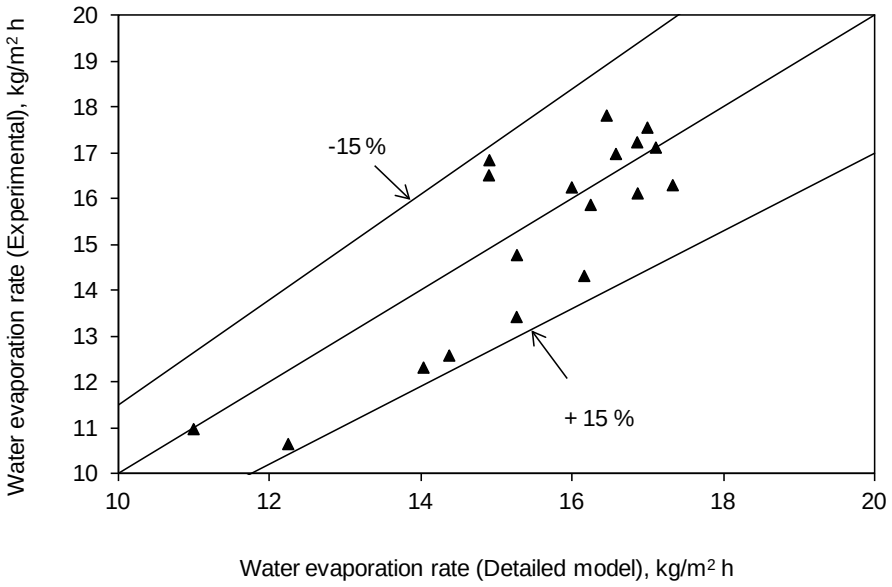

Figure 6.18 *Comparison of numerical and experimental total water evaporation rate from the tubes for the experimental conditions given in Table 6.3.*

The simulated and measured key system performance parameters of the 5.81 kW split air-conditioner with a finned evaporatively-cooled condenser are presented in the following section. As in the case of the bare-tube condenser, Figure 6.19 shows P-h diagrams labeled with the vapour compression cycles 1-2-3-4 and 1'-2'-3'-4' for the cases of with and without evaporative cooling. Due to the same reason given for the case of the bare-tube condenser, the expansion processes 3-4 and 3'-4' are assumed to be isenthalpic. As can be seen from the figure, there are drops in both the condenser and evaporator pressures as a result of the evaporative cooling. A similar phenomenon was observed even in the case of the bare tube condenser presented in the preceding chapter as well as in the research work of Hajidavalloo (2007). The drops in evaporator pressure can be due to the fact that the thermostatic expansion valve in the air-conditioner was set at a constant set point.

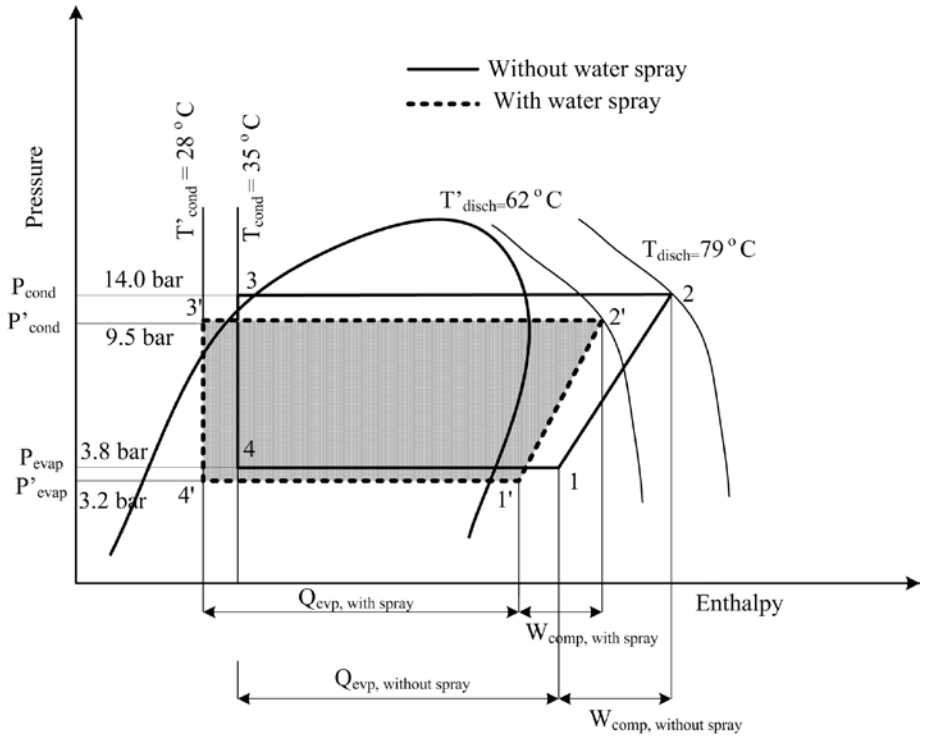

Figure 6.19 *P-h diagrams with the condenser and evaporator pressure changes for T_{wi} =25 ^oC, Re_f = 9, $V_{f,a}$ = 30 m^3/min (measured average volume flow rate 8 points)T_a =30 ^oC*

Table 6.4 Typical data points and COP with and without evaporative-cooling (finned-tube)

Data Point	Without Evaporative cooling	With Evaporative cooling
Inlet air temperature, ^oC	30.0	30.0
Inlet air relative humidity, %	42.0	42.0
Outlet air temperature, ^oC	36.0	31.0
Outlet air relative humidity, %	29.0	91.0
Condensing Pressure, bar	14.0	9.5
Evaporating Pressure, bar	3.8	3.2
Compressor discharge temperature,	79.0	62.0
Condensing temperature, ^oC	53.0	37.5
Condenser exit temperature, ^oC	35.0	28.0
Evaporator inlet temperature, ^oC	8.0	6.0
Evaporator exit temperature, ^oC	17.0	16.0
Evaporator inlet enthalpy, h_4, kJ/kg	249.2	238.9
Evaporator outlet enthalpy, h_2,	411.6	410.4
Condenser inlet enthalpy, h_3, kJ/kg	455.8	442.7
Compressor power, kW	1.63	1.25
Refrigerant mass flow rate, kg/s	0.0402	0.0406
Coefficient of Performance, COP	2.8	4.03
% Increase in COP	-	44%

Simulated and measured COP, rate of water evaporated from the condenser tube surface as well as the compressor power are depicted in Figures 6.20 to 6.24.

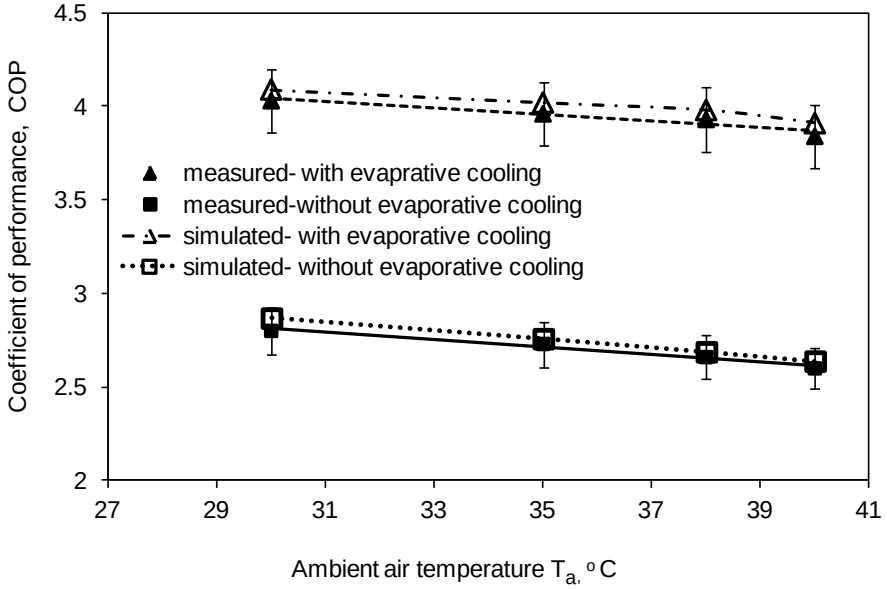

Figure 6.20 *Simulated and measured variation of COP with air temperature with and without evaporative cooling for T_{wi} =25 ^{o}C, Re_f = 9, $V_{f,a}$ = 30 m^3/min (measured average volume flow rate 8 points)*

The effect of ambient air temperature on COP with and without the incorporation of evaporative cooling in the finned condenser is depicted in Figure 6.20. As can be seen from the figure, a COP value of over 4.0 is obtained with the evaporative cooling incorporated while the corresponding COP for the case without evaporative cooling is about 2.8. The lowest value of COP is 2.6, which is observed for the case without evaporative cooling for an ambient temperature of 40 ^{0}C. As can be seen from the figure, the simulated and measured COP for the evaporatively-cooled condenser are in good agreement.

The simulated and measured variations of rate of water evaporated with film Reynolds number and air temperature is shown in Figure 6.21. Consistent with the results in the preceding sections and as evident from the figure, the better evaporation

performance is observed in both the simulated and meaured water evaporation rate for a combination of lower film Reynolds number, Re_f and lower air temperature. The corresponding variation in the COP is shown in Figure 6.22.

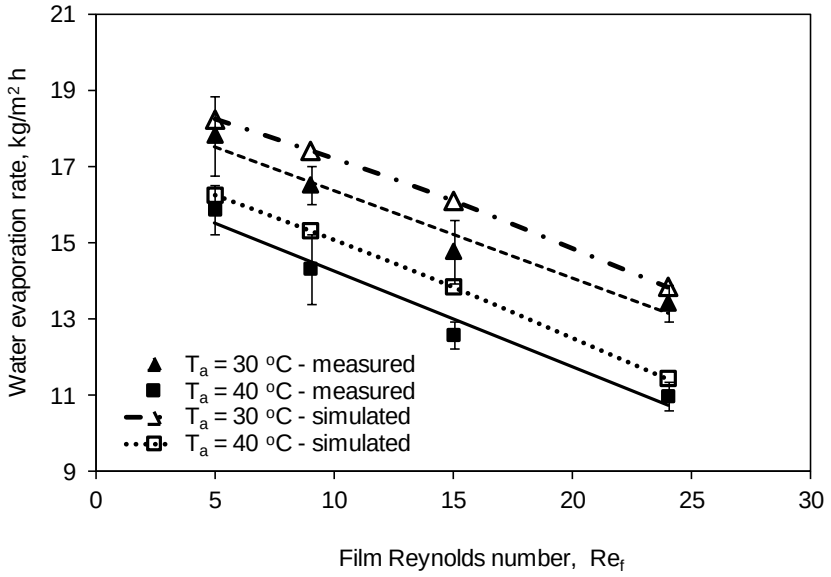

Figure 6.21 *Simulated and measured variation of mass of water evaporated with film Reynolds number with evaporative cooling for T_{wi} =25 ^oC, T_a = 30 ^oC , $V_{f,a}$ = 30 m^3/min (measured average volume flow rate 8 points)*

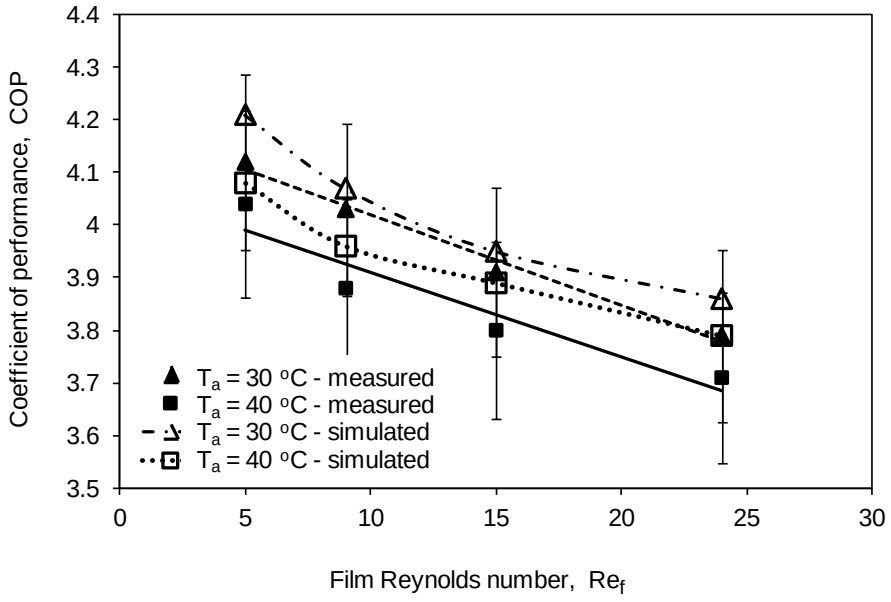

Figure 6.22 *Simulated and measured variation of COP with film Reynolds number with evaporative cooling for T_{wi} =25 ^oC, T_a = 30 ^oC , $V_{f,a}$ = 30 m^3/min (measured average volume flow rate 8 points)*

The effect of film Reynolds number, Re_f, on cooling capacity of the air-conditioner for the finned evaporatively-cooled condenser is shown in Figure 6.23. As can be seen from Figure 6.23, the cooling capacity decreases with the film Reynolds number due to the change in the evaporator inlet conditions brought about by the relatively higher condensing temperature. The existence of higher condensing temperature can again be attributed to the less favourable heat transfer conditions developed due to increase in the water film thickness.

The Simulated and measured variation of cooling capacity with air inlet temperature, with and without evaporative cooling, is shown in Figure 6.24. As can be seen from the figure, better cooling capacity is obtained in the presence of evaporative cooling due to the better heat transfer characteristics at the condenser. However, as also can be seen from the figure, with increase in ambient air temperature, the cooling capacity is reduced, with and without evaporative cooling.

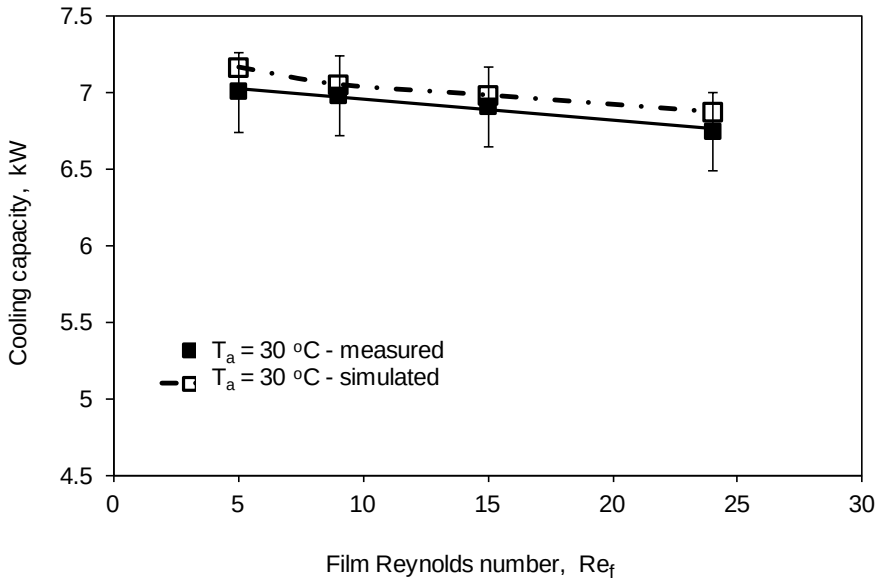

Figure 6.23 *Measured variation of cooling capacity with film Reynolds number with evaporative cooling for T_{wi} =25 ^oC, T_a = 30 ^oC, $V_{f,a}$ = 30 m^3/min*

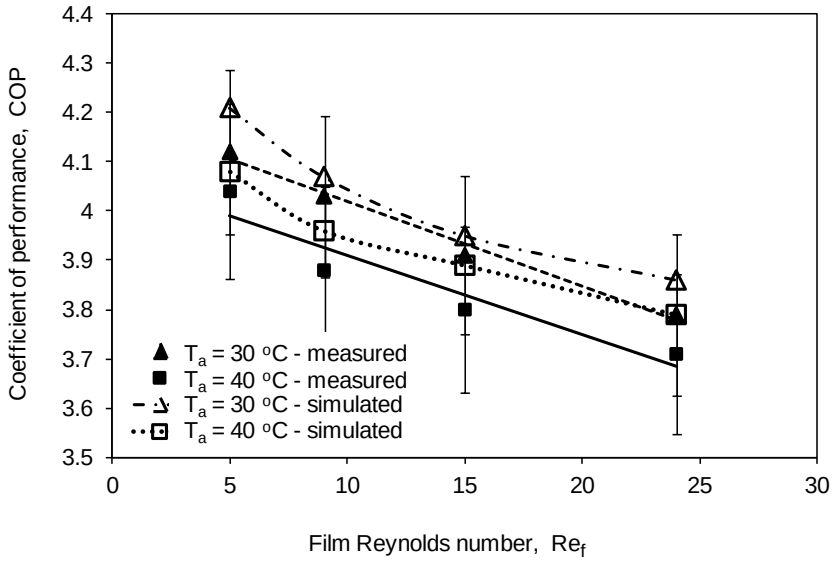

Figure 6.24 *Measured variation of cooling capacity with air temperature with and without evaporative cooling for T_{wi} =25 ^{o}C, Re_f = 9, $V_{f,a}$ = 30 m^3/min (measured average volume flow rate 8 points)*

Figures 6.25 shows the variation of the compressor power input with ambient air temperature with and without evaporative cooling. A compressor power as high as 2.45 kW was observed for air temperature of 40 ^{o}C. As can be seen from the figure, the compressor power input increases slightly as the air blown across the condenser tubes become warmer.

The measured variation of compressor power with film Reynolds number and air temperature for the evaporatively-cooled air-conditioner is depicted in Figure 6.26. As expected, and cited in the preceding sections, the compressor power increases with the film Reynolds number because of the higher thermal resistance existing for higher film Reynolds number (higher film thickness). Minimum and maximum values of the compressor power input in the air-conditioner for this set of experiments are 1.7 and 1.82 kW for film Reynolds number (Re_f) values of 5 and 24, respectively.

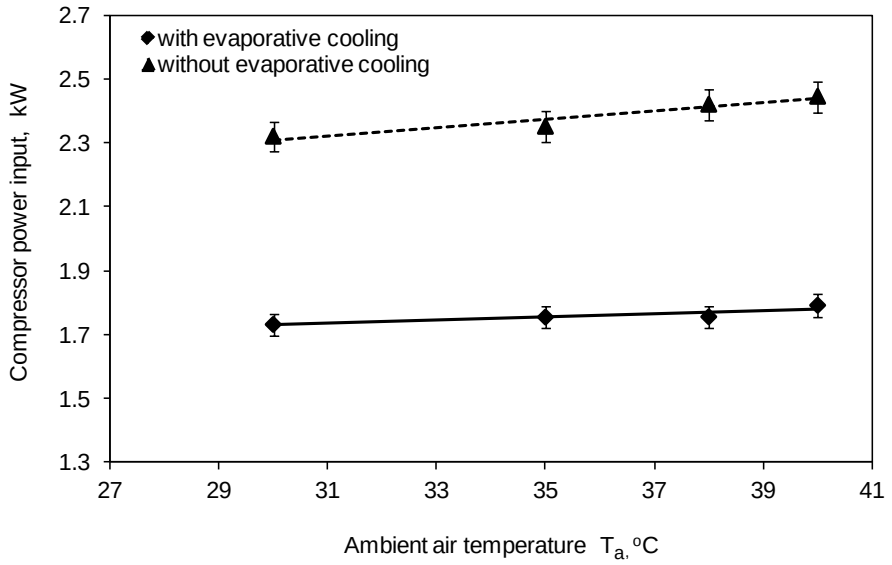

Figure 6.25 *Measured variation of compressor power input with air temperature with and without evaporative cooling for T_{wi} =25 °C, Re_f = 9, $V_{f,a}$ = 30 m^3/min (measured average volume flow rate 8 points)*

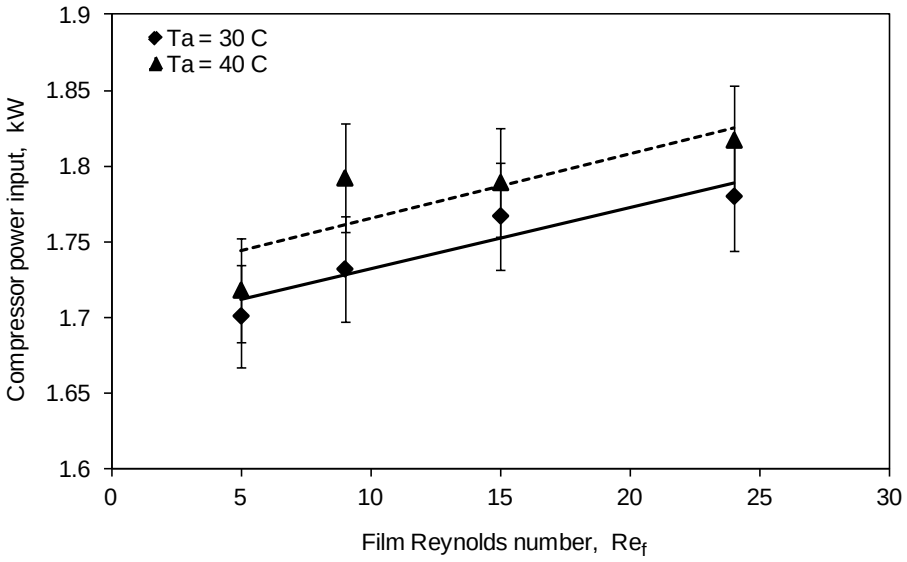

Figure 6.26 *Measured variation of compressor power input with film Reynolds number with evaporative cooling for T_{wi} =25 °C, T_a = 30 °C, $V_{f,a}$ = 30 m^3/min (measured average volume flow rate 8 points)*

The effect of the air inlet temperature on the percentage increase in cooling capacity, compressor power and COP due to evaporative cooling is shown in Figure 6.27. As can be seen from Figure 6.27, the combined double effect of improvements in both the cooling capacity and compressor power due to evaporative cooling, the COP of the air-conditioning system shows significant improvements of up to 47 %.

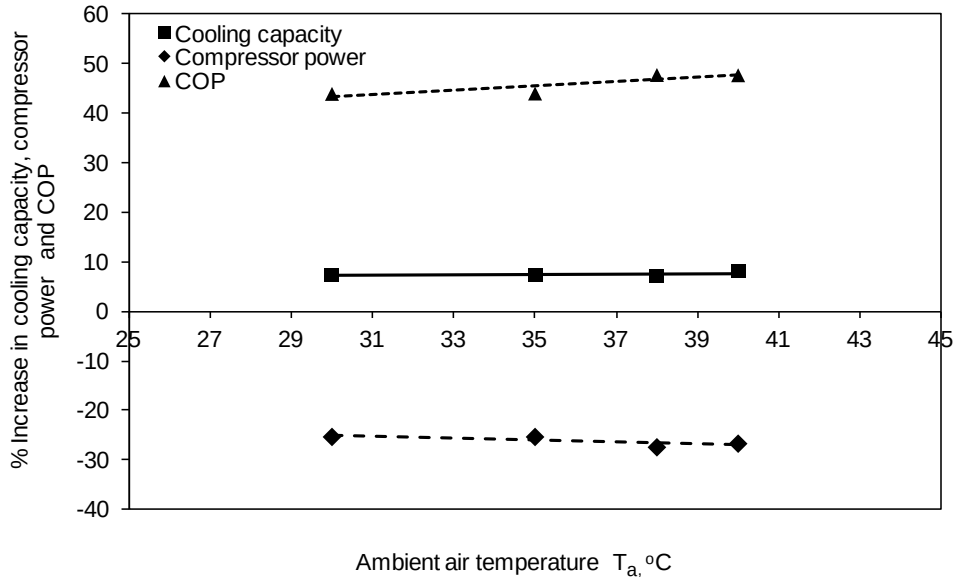

Figure 6.27 *Effect of the air inlet temperature on the percentage increase in cooling capacity, compressor power input and COP due to evaporative cooling for T_{wi} =25 ^{o}C, Re_f = 9, $V_{f,a}$ = 30 m^3/min (measured average volume flow rate 8 points)*

6.3 Comparison of Evaporatively-Cooled Finned and Bare-Tube Condensers

Important numerical results for the bare and finned-tube evaporatively cooled condensers presented in the preceding sections are combined here for the purpose of comparison and are briefly described in the following sections.

Figures 6.28 and 6.29 show the variation of refrigerant temperature and quality for the bare and finned condensers, with and without evaporative-cooling. As can be seen from the figure, the performance of the finned evaporatively-cooled

condenser is superior in comparison to that of bare-tube evaporatively-cooled condenser for the same heat rejection conditions used in the numerical simulation.

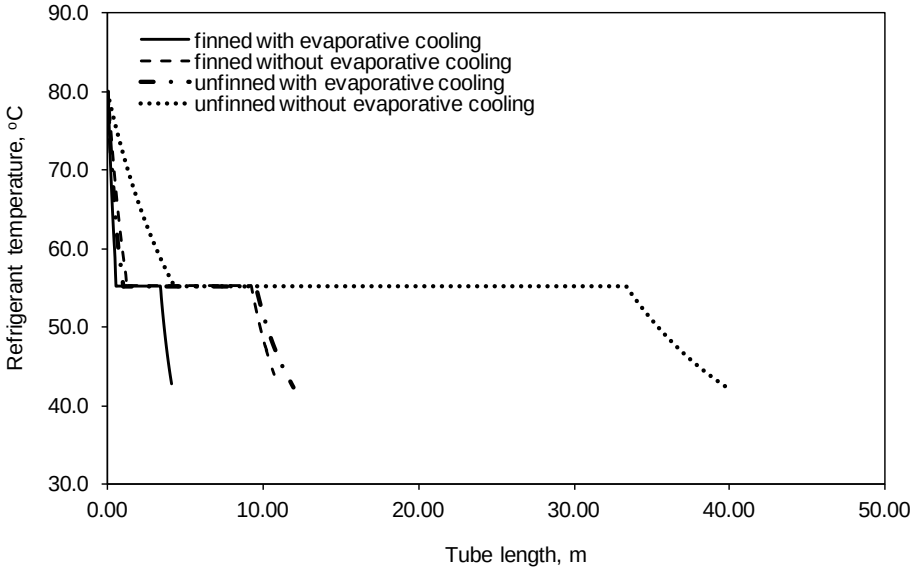

Figure 6.28 *Simulated variation of refrigerant temperature along the condenser tube length for the finned and unfinned condensers for* T_{wi} *=25* ^{o}*C,* Re_f *= 9, V = 4 m/s,* T_a *= 30* ^{o}*C, RH = 70%*

The effect of ambient air temperature and velocity is depicted in Figures 6.30 and 6.31, respectively.

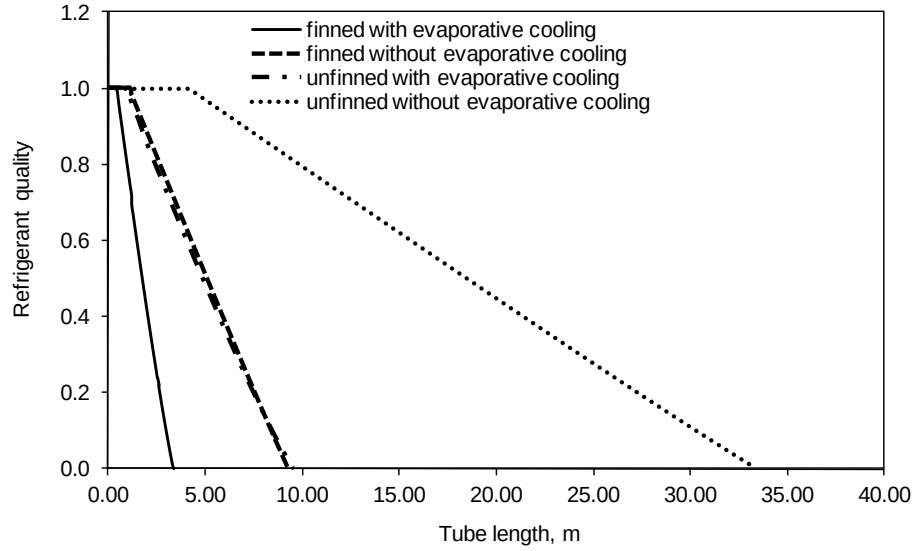

Figure 6.29 *Simulated variation of refrigerant quality along the condenser tube length for the finned and unfinned condensers for* T_{wi} *=25* ^{o}*C,* Re_f *= 9, V = 4 m/s,* T_a *= 30* ^{o}*C, RH = 70%*

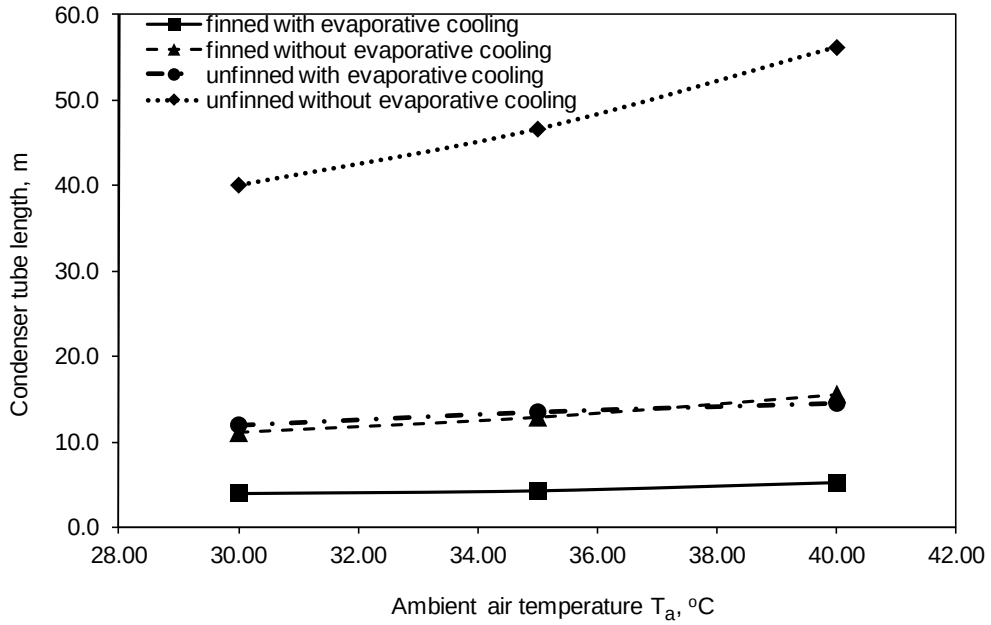

Figure 6.30 *Simulated variation of condenser tube length with air inlet temperature for the finned and unfinned condensers for T_{wi} =25 ^{o}C, Re_f = 9, V = 4 m/s, RH = 70%*

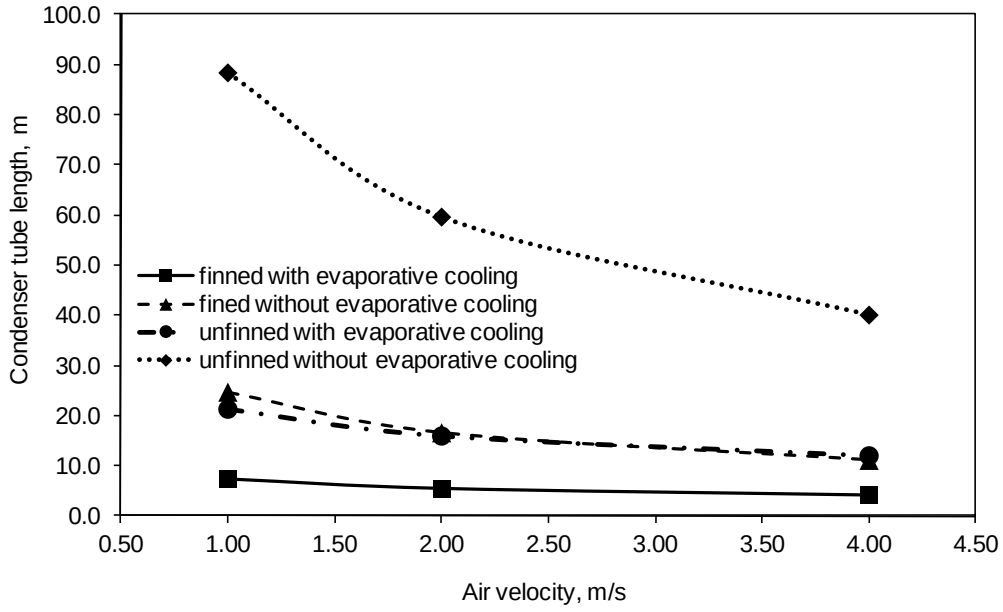

Figure 6.31 *Simulated variation of condenser tube length with ambient air temperature for the finned and unfinned condensers for T_{wi} =25 ^{o}C, Re_f = 9, T_a = 30 ^{o}C, RH = 70%*

Figures 6.32 to 6.34 show the effect of film Reynolds number on the required condenser tube length as a function of the operating conditions in the condenser. As can be seen from the figures, for the case of bare-tube condenser, the film Reynolds number affects the required condenser tube length. Whereas, for the case of finned tube condenser, the film Reynolds number does not affect the required condenser tube length significantly. Besides the reason cited previously, (i.e. for a given fin geometry and heat load, the nett heat taken away by the falling water spray leaving the condenser tubes and the mass of water evaporated from the tube remains almost constant) this can also be due to the fact that for unit tube length increment, the increment in surface area of the finned tube is much larger than that of the bare tube.

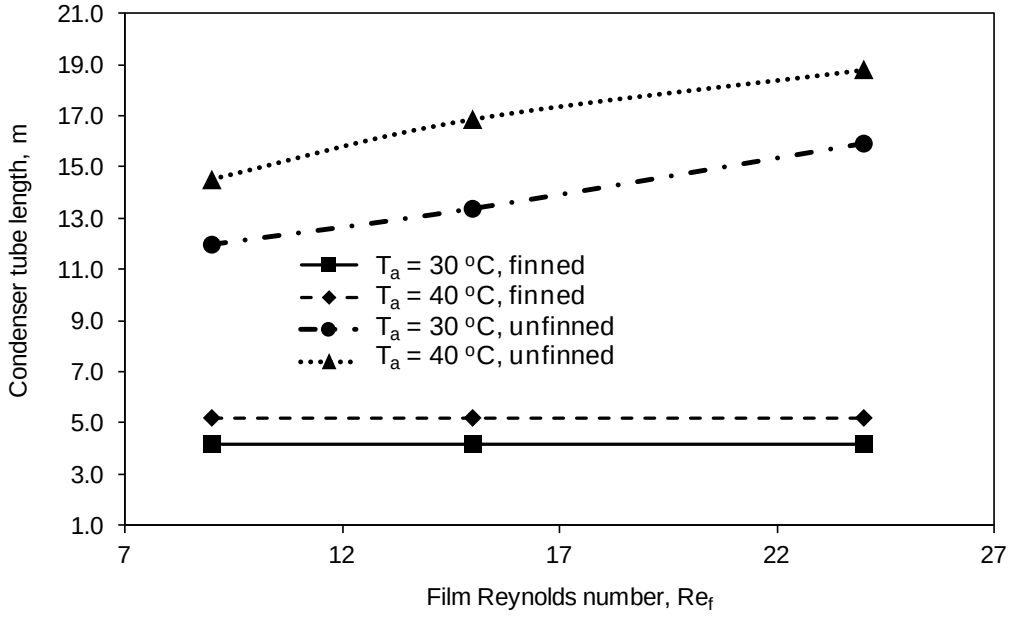

Figure 6.32 *Simulated variation of condenser tube length with film Reynolds number and air inlet temperature for the finned and unfinned condensers for T_{wi} =25 °C, V = 4 m/s, RH = 70%*

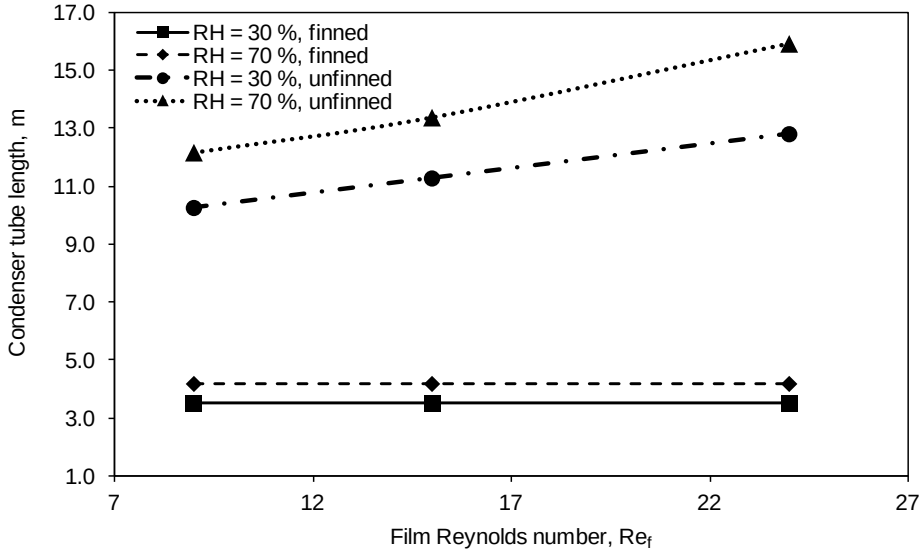

Figure 6.33 *Simulated variation of condenser tube length with film Reynolds number and air relative humidity for the finned and unfinned condensers forT_{wi} =25 ^oC, V = 4 m/s, T_a = 30 ^oC*

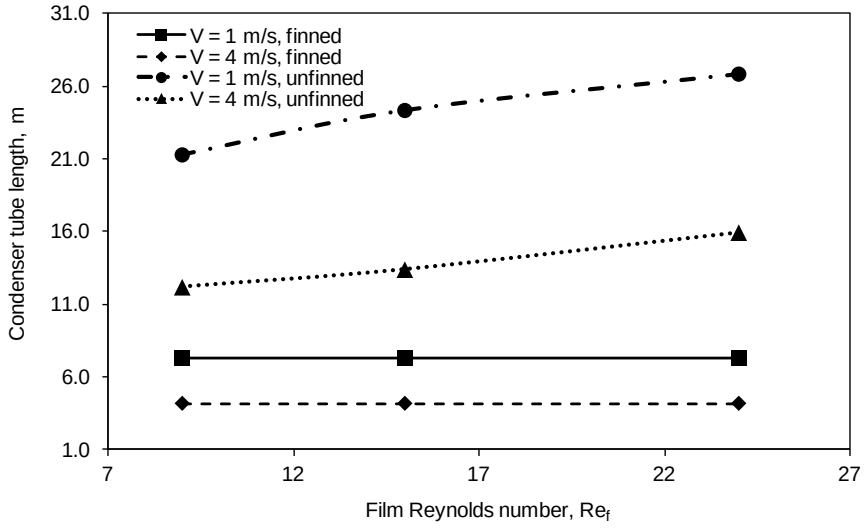

Figure 6.34 *Simulated variation of condenser tube length with film Reynolds number and air velocity for the finned and unfinned condensers for T_{wi} =25 ^oC, V = 4 m/s, T_a = 30 ^oC, RH = 70%*

The important performance parameters obtained from the experiments for both the bare-tube and finned-tube condensers are combined and plotted in Figures 6.35 to 6.37. As can be seen from the figures, there are marked and significant performance

superiority for the finned-tube evaporatively-cooled condenser compared to the bare-tube condenser for the same operating conditions.

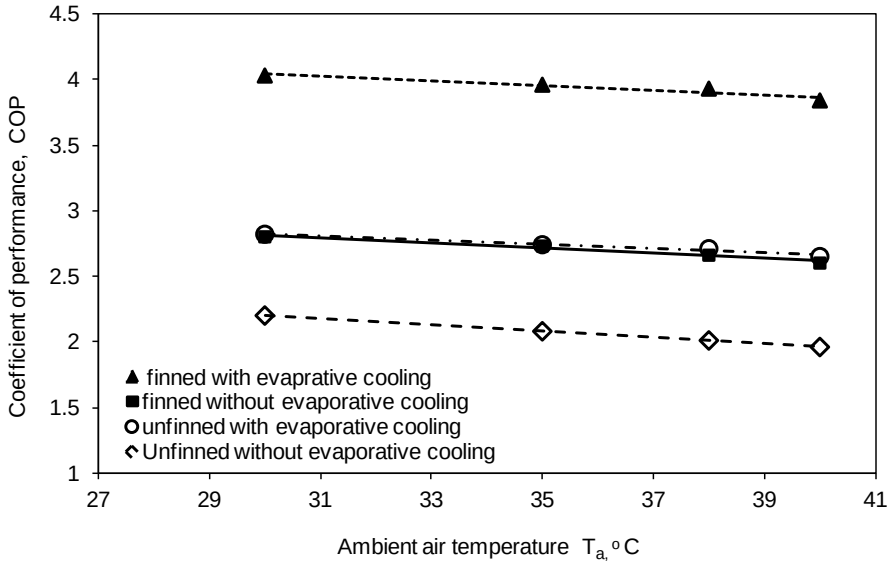

Figure 6.35 *Measured variation of COP with air inlet temperature with and without evaporative cooling for T_{wi} =25 °C, Re_f = 9, V = 4 m/s*

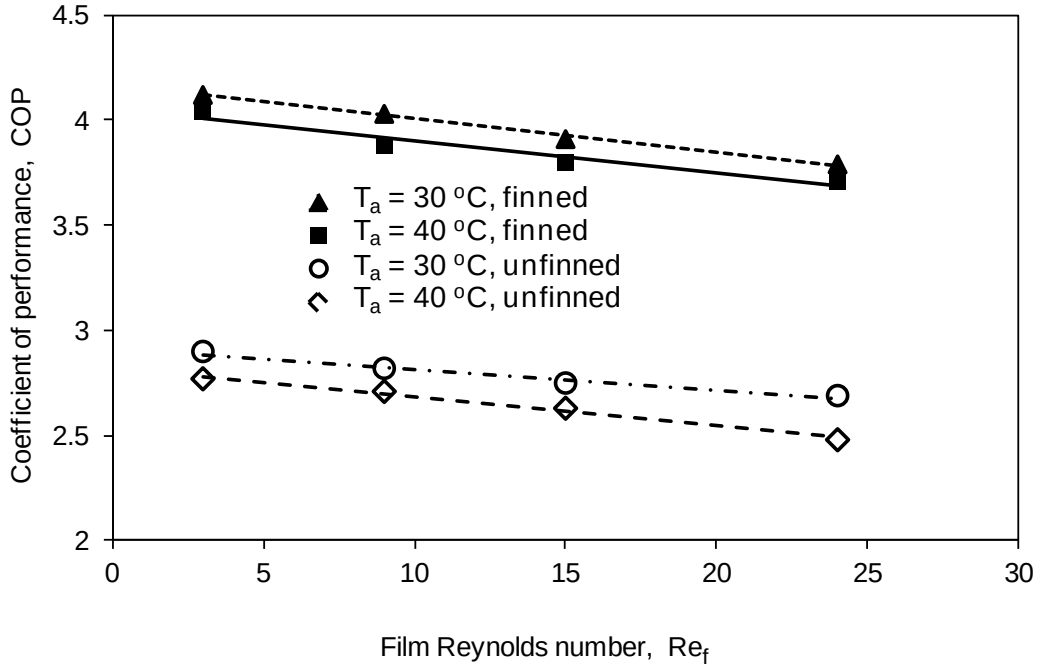

Figure 6.36 *Measured variation of COP with film Reynolds number with air inlet temperature for T_{wi} =25 °C, T_a = 30 °C, V = 4 m/s*

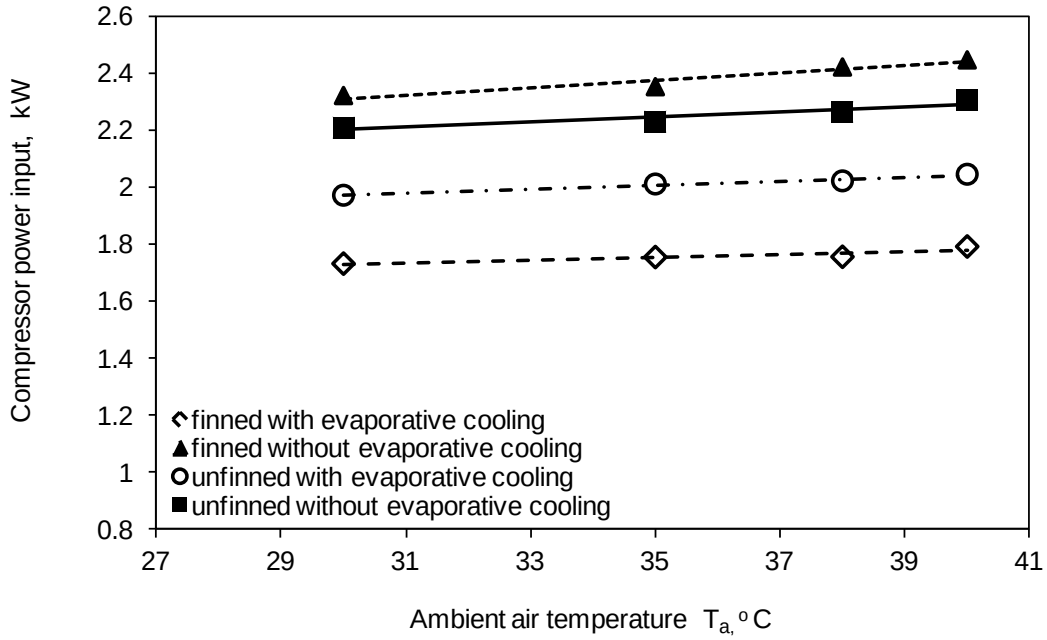

Figure 6.37 *Measured variation of compressor power input with air inlet temperature for with and without evaporative cooling for the condensers for T_{wi} =25 ^oC, Re_f = 9, V = 4 m/s*

6.4 Summary

In this Chapter, the detailed models developed for both bare and finned-tube condensers were verified with experiments. For this, the variation of the refrigerant condenser tube and the rate of water evaporated from the condenser were considered. The measured and simulated refrigerant temperatures were found to be in good agreement. The rate of water evaporated from the film-air interface determined from the experiments and corresponding numerical values matched each other within 13% and 15 % for the bare and finned-tube condensers, respectively.

The simulated and measured Coefficient of Performance (COP) and cooling capacity for the evaporatively-cooled condenser were also presented. Both the simulated and measured COP and cooling capacity were in good agreement. The performance results of the air-conditioner, namely, COP, cooling capacity and the compressor power input showed a significant improvement with the evaporative

cooling incorporated. COP improvements over 30 % and 45% for bare and finned-tube condensers, respectively, were observed with the evaporatively-cooled condenser incorporated in to the air-conditioner. It was also observed from the experiments that a reduction in compressor power input up to 17 to 20 % can be obtained with the evaporatively-cooled condenser.

Finally, a comparison of the bare and finned-tube condensers in terms of the condenser tube length requirement for a particular state change (fixed heat rejection) of the refrigerant as well as their experimentally obtained performance was also presented. The comparison showed better performance with the finned evaporatively-cooled condensers in terms of the required tube length for complete condensation of the refrigerant.

Chapter 7
SIMPLIFIED MODEL FOR BARE-TUBE EVAPORATIVELY-COOLED CONDENSERS

The detailed model developed in Chapter 3 for the serpentine bare-tube condenser is computationally intensive and can be difficult to implement in practice by average technical personals. However, for typical design conditions as discussed in the numerical parametric study of Chapter 3 and 6, the film-tube interface and film-air interface heat transfer coefficients can be extracted from the detailed model. Development of a simple one-dimensional model, henceforth referred as simplified model, in which the extracted heat transfer coefficients from the detailed model can be used as input is explored. The simplified model can be a design tool for the easy design of serpentine bare-tube evaporatively-cooled condensers. The development of a simplified model is described in the following sections.

7.1 Simplified Model for Serpentine Bare-Tube Evaporatively-Cooled Condenser

A simplified model for the design and analysis of evaporatively-cooled bare-tube condensers is developed and presented below. In the simplified model, the evaporative-cooled condenser tubes can be idealized as a vertical conduit with the evaporating falling film on both sides of the conduit and the phase changing refrigerant flowing through the conduit as shown in Figure 7.1. This assumption is well justified considering the temperature trend of refrigerant inside the actual condenser tubes and the falling film on the condenser tubes. The film-tube interface (h_i) and film-air interface (h_o) heat transfer coefficients required as input parameters

in the simplified model are obtained from the equations (3.35) and (3.34), respectively, presented in the Chapter 3.

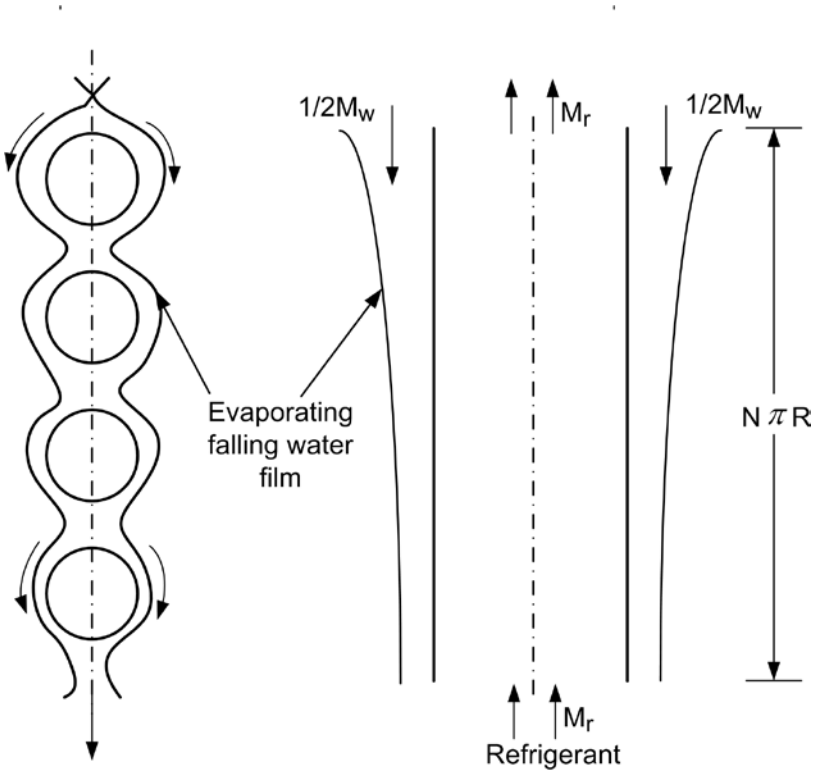

(a) Condenser tube bundle *(b) The equivalent conduit*

Figure 7.1 *Condenser tube bundle and the equivalent conduit with water film in the simplified model*

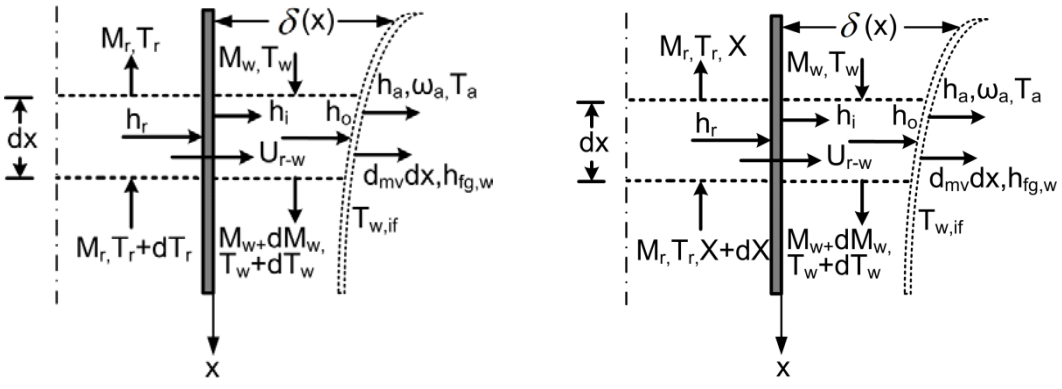

(a) The Single phase region *(b) The two phase region*

Figure 7.2 *Elements for the simplified model*

7.1.1 Energy balance for the refrigerant

Referring to Figure 7.2, energy balance for the single phase region of refrigerant flowing through the vertical conduit of width *W* yields:

$$M_r C_{pr}\left(T_r + dT_r\right) = M_r C_{pr} T_r + U_{r-w}\, dx\, 2W\left(T_r - T_w\right) \tag{7.1}$$

Simplification and re-arrangement of equation (7.1) gives:

$$\frac{dT_r}{dx} = \frac{U_{r-w}\, 2W}{M_r C_{pr}}\left(T_r - T_w\right) \tag{7.2}$$

Heat balance for the two-phase region of refrigerant flowing through the conduit gives:

$$\begin{aligned} &M_r\left(X + dX\right)h_{g,r} + M_r\left(1 - X - dX\right)h_{f,r} = \\ &U_{r-w}\, dx W\left(T_r - T_w\right) + M_r X h_{g,r} + M_r\left(1 - X\right)h_{f,r} \end{aligned} \tag{7.3}$$

Simplifying equation (3.104) gives: $\dfrac{dX}{dx} = \dfrac{U_{r-w}\, 2W}{M_r h_{fg,r}}\left(T_r - T_w\right)$ (7.4)

7.1.2 Energy balance for the falling water film

Energy balance on an element of the falling film shown in Figure 7.2 gives:

$$\begin{aligned} &M_w C_{pw} T_w 2W + U_{r-w}\, dx\, 2W\left(T_r - T_w\right) = \\ &\left(M_w + dM_w\right)C_{pw}\left(T_w + dT_w\right)2W + dm_v\, 2W dx h_{fg,w} + h_a dx 2W\left(T_{w,if} - T_a\right) \end{aligned} \tag{7.5}$$

Simplification and rearranging of equation (7.5) give:

$$M_w C_{pw}\frac{dT_w}{dx} + C_{pw} T_w \frac{dM_w}{dx} + h_{fg,w} dm_v = \left[U_{r-w}\left(T_r - T_w\right) - h_a\left(T_{w,if} - T_a\right)\right] \tag{7.6}$$

7.1.3 Mass balance for the water film

Mass balance of water film over an elemental area Wdx of the conduit gives:

$M_w 2W = dm_v dx 2W + \left(M_w + dM_w\right)2W$, therefore $dm_v dx = -dM_w$ (7.7)

Rate of water vapour evaporated from the water-air interface for the differential area $2Wdx$ can be expressed as:

$$dm_v = h_d\left(\omega_{w,if} - \omega_a\right) \tag{7.8}$$

The change in mass flow rate of water along the conduit can be written as:

$$\frac{dM_w}{dx} = -h_d\left(\omega_{w,if} - \omega_a\right) \tag{7.9}$$

Substituting equations (7.8) and (7.9) in to equation (7.6) and simplifying give:

$$\frac{dT_w}{dx} = \frac{1}{M_w C_{pw}}\left[U_{r-w}\left(T_r - T_w\right) - h_a\left(T_{w,if} - T_a\right) + \left\{h_d\left(C_{pw}T_w - h_{fg,w}\right)\left(\omega_{w,if} - \omega_a\right)\right\}\right] \tag{7.10}$$

An energy balance for an element involving film-air interface gives:

$$h_o\, dx\, 2W\left(T_w - T_{w,if}\right) = dm_v dx 2W h_{fg,w} + h_a\, dx\, 2W\left(T_{w,if} - T_a\right) \tag{7.11}$$

7.1.4 Final form of the equations for solution using Runge-Kutte method

Equations (7.2), (7.4) and (7.10) are solved for various output parameters for the water, refrigerant and the water vapour evaporated from the interface. The output parameters obtained from the 4th order Runge-Kutte (R.K) scheme are: Refrigerant temperature (T_r), quality (X), mass flow rate of the water (M_w), rate of water vapour evaporated in the film flow direction (m_v) as well as the water-air interface temperature ($T_{w,if}$).

Equations (7.2), (7.4) and (7.10) are re-written in coefficient forms to solve using the 4th order R.K scheme as follows:

For the sub-cooled region of the condenser tube:

$$\frac{dT_r}{dx} = A_1 T_r + B_1 T_w + C_1 \tag{7.12}$$

$$\frac{dT_w}{dx} = A_2 T_r + B_2 T_w + C_2 \tag{7.13}$$

For the two-phase region:

$$\frac{dX}{dx} = A_3 T_w + B_3 X + C_3 \tag{7.14}$$

$$\frac{dT_w}{dx} = A_4 T_w + B_4 X + C_4 \tag{7.15}$$

For the super-heated region:

$$\frac{dT_r}{dx} = A_5 T_r + B_5 T_w + C_5 \tag{7.16}$$

$$\frac{dT_w}{dx} = A_6 T_r + B_6 T_w + C_6 \tag{7.17}$$

The coefficients A_1 , B_1 , C_1 through A_6 , B_6 , C_6 are defined as follows:

$$A_1 = A_5 = \frac{U_{r-w} 2W}{M_r C_{pr}} \qquad B_1 = B_5 = -\frac{U_{r-w} 2W}{M_r C_{pr}} \qquad C_1 = C_5 = 0 \tag{7.18}$$

$$A_2 = A_6 = \frac{U_{r-w}}{M_w C_{pw}} \qquad A_4 = B_2 = B_6 = \frac{h_d \omega_{if}}{M_w} - \frac{h_d \omega_a}{M_w} - \frac{U_{r-w}}{M_w C_{pw}} \tag{7.19}$$

$$C_2 = C_6 = \frac{h_d h_{fg} \omega_a}{M_w C_{pw}} - \frac{h_d h_{fg} \omega_{if}}{M_w C_{pw}} - \frac{h_a \left(T_{if} - T_a\right)}{M_w C_{pw}} \tag{7.20}$$

$$A_3 = -\frac{U_{r-w} 2W}{M_r h_{fgr}} \qquad B_3 = B_4 = 0 \qquad C_3 = \frac{U_{r-w} 2W T_r}{M_r h_{fgr}} \tag{7.21}$$

$$C_4 = \frac{U_{r-w} T_r}{M_w C_{pw}} + \frac{h_d h_{fg} \omega_a}{M_w C_{pw}} - \frac{h_d h_{fg} \omega_{if}}{M_w C_{pw}} - \frac{h_a \left(T_{if} - T_a\right)}{M_w C_{pw}} \tag{7.22}$$

The entry film thickness and flow rate per unit conduit width are related as follows (Raisul Islam, 2002):

$$\delta_{w,in} = \left(\frac{3 \Gamma \mu}{\rho_w^{\,2} g} \right)^{1/3} \tag{7.23}$$

7.1.5 The simplified model solution procedure

The simplified model developed in the preceding section is solved with the help of the 4th order Runge-Kutte scheme in an iterative manner. The equations (7.12) to (7.17) in conjunction with the coefficients given by equations (7.18) to (7.22) are used to formulate a MATLAB computer code with the incorporation of the 4th order Runge-Kutte scheme. The conduit is divided into three sections based on the refrigerant state. The superheated refrigerant vapour enters at the bottom of the vertical conduit and while traversing along the conduit, it gets de-superheated and become saturated. The first section of the conduit ends at the point, where the vapour reaches the saturation state. The second section is the two-phase region, where the saturated vapour loses its latent heat of vapourisation and gets condensed and the second section ends at the point of complete condensation. The third section is the region of sub-cooling.

The conduit length is divided into a number of small elemental lengths and the calculation is started by executing the written MATLAB computer code at the first element from the top of the conduit with known values of water film temperature (T_w), water flow rate (M_w), air temperature (T_a), relative humidity (RH) and refrigerant mass flow rate (M_r). The air-water interface temperature ($T_{w,if}$), and the refrigerant outlet temperature (T_r), are assumed to be known at the conduit inlet. The R-K scheme calculates the water and the refrigerant temperature as well as the water mass flow rate and the mass flux of water vapour evaporated from the elemental interface. The assumed interface temperature is fixed at the end of each element using the energy balance for an element involving film-air interface given by equation (7.11). The calculations are performed for the sub-cooled region of the condenser by solving the equations (7.12) and (7.13) with the associated equations for the relevant

coefficients. The calculation for the sub-cooled region is completed when the refrigerant temperature reaches the known condensing temperature. For the two-phase region of the condenser, the equations (7.14) and (7.15) in conjunction with the equations for the relevant coefficients are solved for all the output parameters. The computation for the two-phase region is completed when the refrigerant quality reaches one. Following the two-phase region, the computation for the superheated region is carried out using the equations (7.16) and (7.17) until the last element of the tube is reached. At the last element, the refrigerant temperature is compared with the known inlet super-heated refrigerant temperature. If the preset convergent criterion for the refrigerant temperature is achieved, the computation for the entire conduit is completed and the output data are retrieved for the subsequent analysis of the evaporatively-cooled condenser. If the solution has not converged, the entire computations are repeated with a refined assumption of the refrigerant outlet temperature until the convergence criterion is met. The systematic solution procedure for the simplified model is depicted in a flow chart in Figure 7.3.

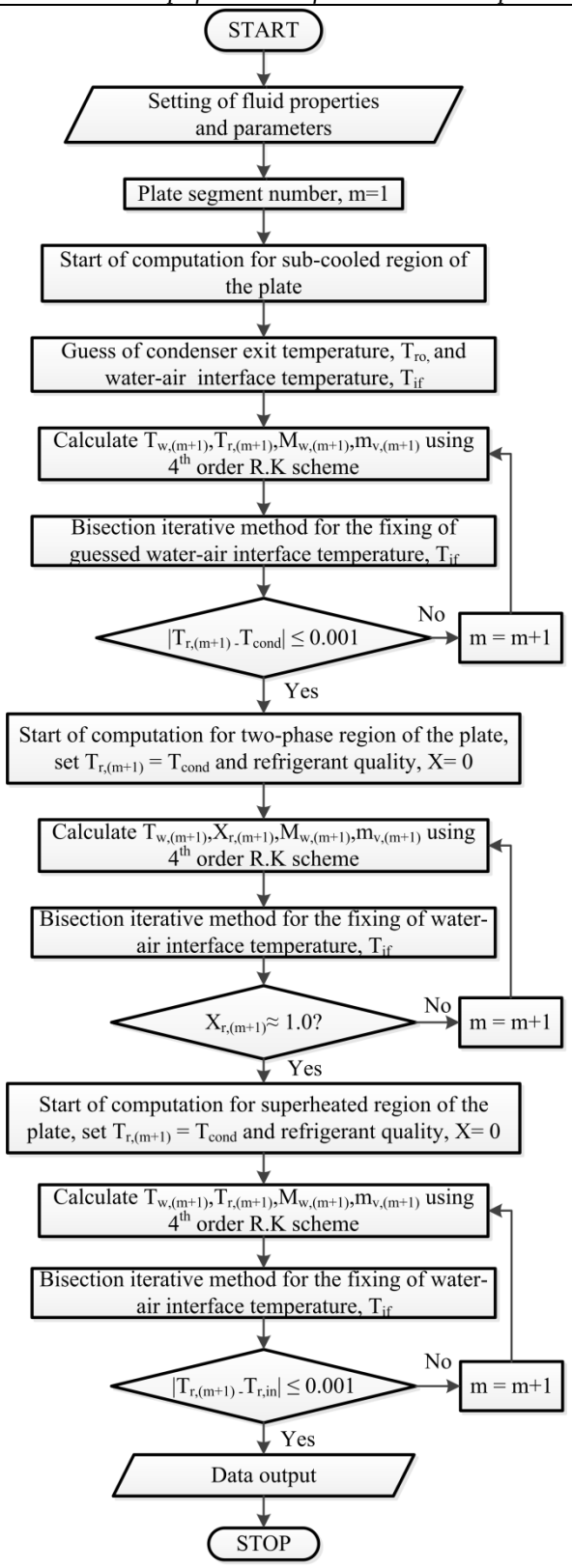

Figure 7.3 *Flow diagram for the computation of the simplified model*

7.2 Results for Simplified Model of the Evaporatively-Cooled Condenser

The predictions from the simplified model are compared with the experimental results and the results from the detailed model. The simulation and experiments were conducted on two parallel circuits of 19 tubes of 10 mm nominal outer diameter, 1 mm wall thickness and 700 mm effective length. In the simplified model simulation run, a vertical conduit is considered to be physically equivalent to the evaporatively-cooled condenser tube as presented in Chapter 3. Values of all the input parameters such as refrigerant inlet temperature, refrigerant mass flow rate, air inlet temperature, spraying water temperature and flow rate that are used in the simplified and detailed model are the same as those used in the experiments conducted in the present study. The film-tube interface heat transfer coefficient, h_i, and the film-air interface heat transfer coefficients, h_o, used in the simplified model have been calculated from the detailed model for the same set of input variables. Table 7.1 shows the comparison of the predictions of the simplified model with the results from the detailed model and experiments and there is good agreement. In the simplified model, the entry film Reynolds number Re_f at the top of the conduit corresponding to a film thickness of 0.15 mm is determined using equation (7.23) and (3.26) and is found to be 56. This is equivalent to the entry film Reynolds number of 9 calculated using equation 3.25 (Bird, 1960) for the case of falling film on a round tube.

7.2.1 Validation of the simplified model

The simulated refrigerant temperature along the tube length using the simplified and detailed models, and that obtained from the experiments are compared in Figure 7.4. As can be seen from the figure, the trends of the three sets of results agree very well.

Table 7.1 *Comparison of simulation results with experimental data for N = 19, T_{ri} = 90 ^{o}C, Mr =0.0172 kg/s, Re_f = 56, P_{cond} = 15 bar, T_{ai} = 30 ^{o}C*

Parameter	Experimental result	Detailed model	Simplified model
Refrigerant outlet temperature (^{o}C)	37.80	38.20	37.35
Mass of water evaporated (kg/m^{2}h)	14.20	14.60	15.80
Tube length required for the complete condensation of refrigerant (m)	8.78	8.61	7.95

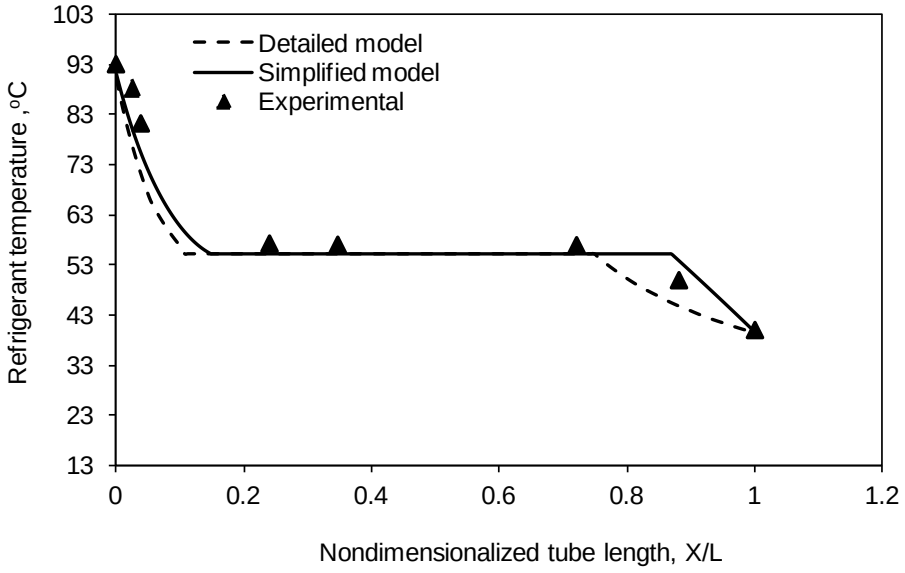

Figure 7.4 *Typical temperature profiles of the temperature for evaporatively- cooled condenser for N= 19, V = 4 m/s, T_{wi} = 25 ^{o}C, T_a = 30 ^{o}C*

Figure 7.5 shows the simulated variation of the rate of water evaporated from the condenser tube surface with the film Reynolds number for the simplified, detailed models and experiments. The trends of the results in the figure are satisfactory. However, as seen in the figure, the rate of water evaporated predicted from the simplified model shows slightly higher values compared to those from the detailed

model and experiments. This is presumably due to the use of averaged h_i and h_o values in the simplified model.

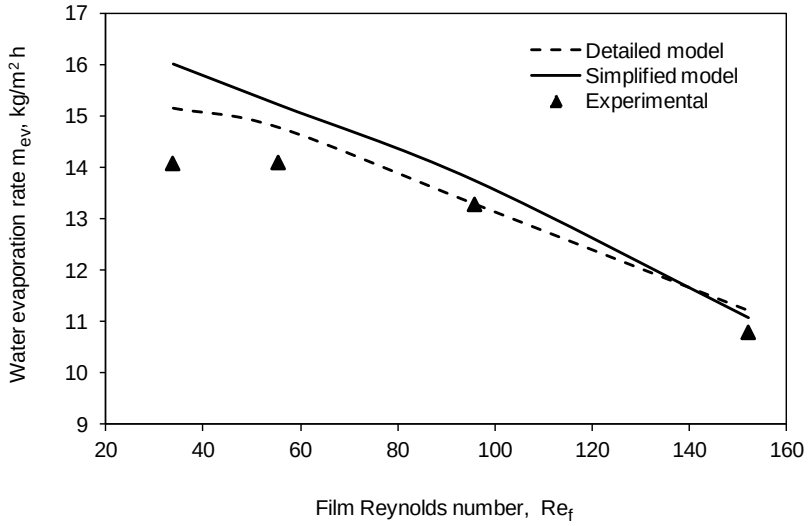

Figure 7.5 *Typical temperature profiles of the temperature for evaporatively- cooled condenser for V = 4 m/s, T_{wi} = 25 ^oC, T_a = 30 ^oC, RH=70%*

7.2.2 Numerical parametric study

Condenser tube length, water flow rate (for the spray), refrigerant inlet temperature and its flow rate, air inlet temperature, air inlet relative humidity are the main variables in the design of a practical evaporatively-cooled condenser. The effects of these design variables on the performance of the evaporatively-cooled condenser in terms of rate of water evaporated have been studied using the simplified model. Table 7.2 summarises the range of the variables considered in the parametric study.

The results of the parametric study are used to plot the graphs in Figures 7.6 to 7.10. Figure 7.6 shows the simulated variation of rate of water evaporated from the condenser tube surface with the change of refrigerant inlet temperature for different numbers of tubes or the total tube length (NL). As can be seen from the figure, a higher refrigerant inlet temperature leads to an increase in the water evaporation rate

resulting in better performance of the evaporatively-cooled condenser. For a larger number of tubes (larger evaporator length), there is a decrease in the water evaporation rate per unit area of the tube surface.

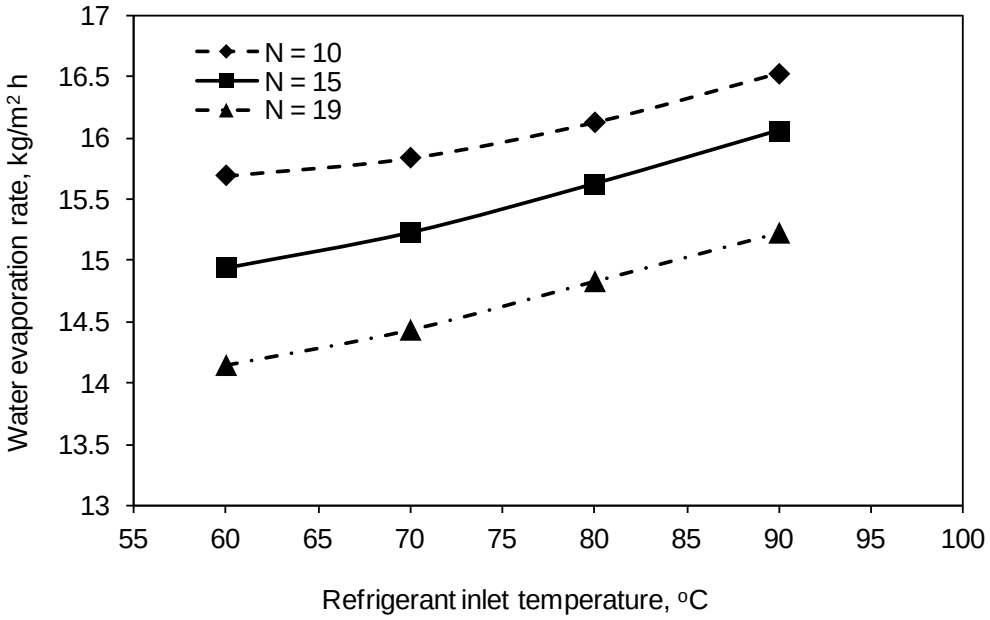

Figure 7.6 *Simulated variation of water evaporation rate with refrigerant inlet temperature*

Table 7.2 *Range of design variable used in the parametric study using the simplified model (P_{cond} = 15 bar)*

Figure	Design variables						
	N	$T_{r,in}$ (^oC)	M_r (kg/s)	Γ (kg/ms)	RH	$T_{a,in}$ (^oC)	V (m/s)
7.6	10-19	60-90	0.0172	0.012326	0.8	30.0	4.0
7.7	10-19	90.0	0.0137-0.0277	0.012326	0.8	30.0	4.0
7.8	10-19	90.0	0.0172	0.00370-0.03383	0.8	30.0	4.0
7.9	10-19	90.0	0.0172	0.012326	0.3 – 0.85	30.0	4.0
7.10	10-19	90.0	0.0172	0.012326	0.8	25.0 - 45.0	4.0

The effect of refrigerant flow rate on water evaporation rate is presented in Figure 7.7. For a constant heat rejection in the condenser, an increase of refrigerant

flow rate results in higher wall and water film temperature distribution along the tube resulting in an increased water evaporation rate. For a greater number of tubes, the wall temperature and, the water film temperature distribution are reduced resulting in a relatively reduced water evaporation rate compared to the evaporation rate for fewer tubes. This can be due to the fact that for a given refrigerant inlet conditions and water film flow rate, the average wall temperature is higher for a smaller number of tubes resulting in higher water evaporation rate.

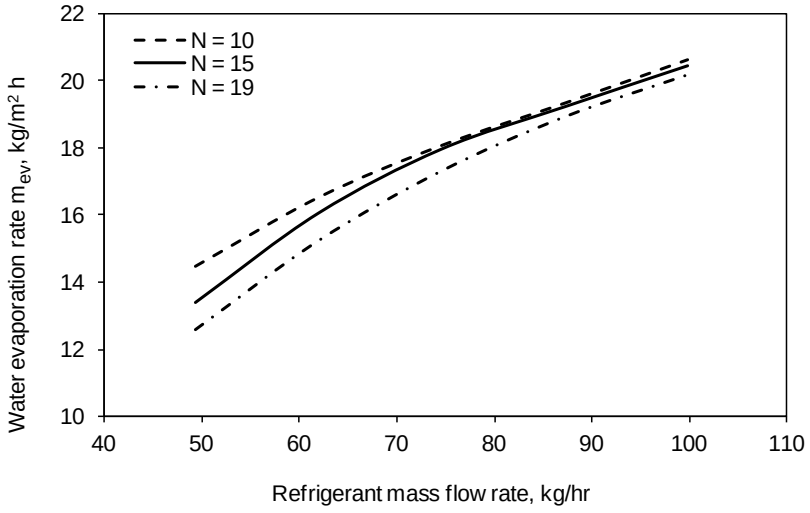

Figure 7.7 *Simulated variation of water evaporation rate with refrigerant mass flow rate*

The simulated variation of water evaporation rate with film Reynolds number and the number of tubes is depicted in Figure 7.8. For lower film Reynolds numbers, the evaporatively-cooled condenser with a fewer number of tubes performs better as can be seen from the figure. As the film Reynolds number is increased, the water evaporation rate for the three cases appears to approach the same value. This is presumably as a result of the existence of a higher film resistance and the mass transfer process is totally controlled by the water film-air interface heat transfer coefficient.

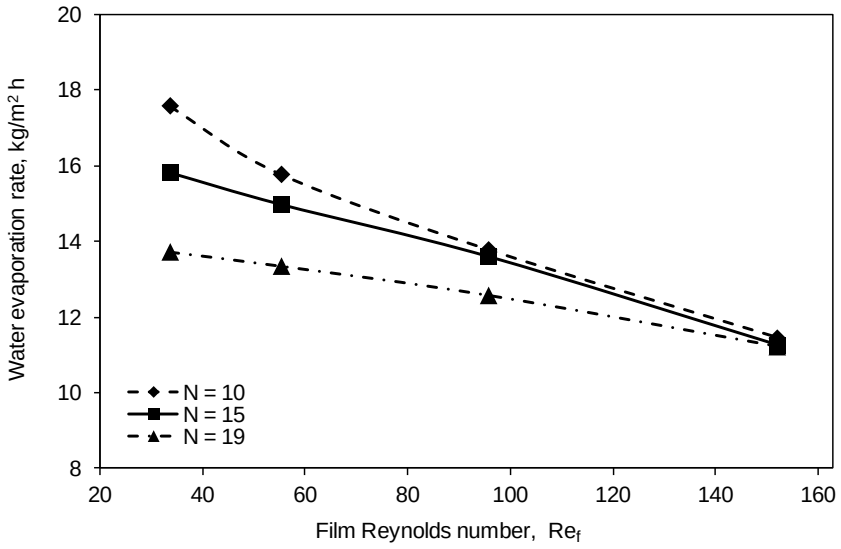

Figure 7.8 *Simulated variation of water evaporation rate with film Reynolds number*

The effect of air inlet temperature on the water evaporation rate is illustrated in Figure 7.9. As can be seen from the figure, as the air temperature increases keeping the humidity ratio constant, the enthalpy potential of the air is reduced resulting in lower water evaporation rate from the condenser tube surface.

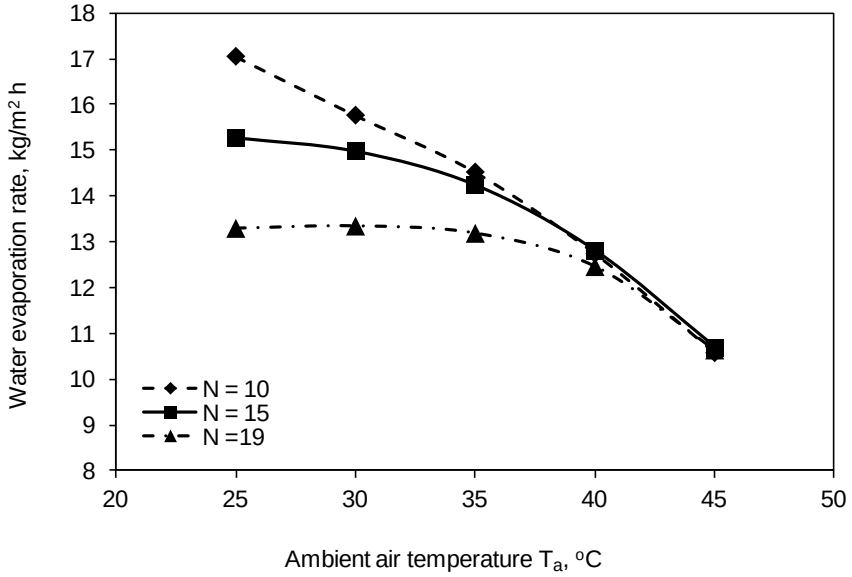

Figure 7.9 *Simulated variation of water evaporation rate with air inlet temperature*

Figure 7.10 shows the effect of air inlet relative humidity on the water evaporation rate for different numbers of condenser tubes. As in the previous case, the enthalpy potential of the air plays an important role in the water evaporation rate trend as seen in the figure. For a higher number of tubes, the trend is consistent with the previous cases because of a lower tube wall temperature and water film temperature distribution.

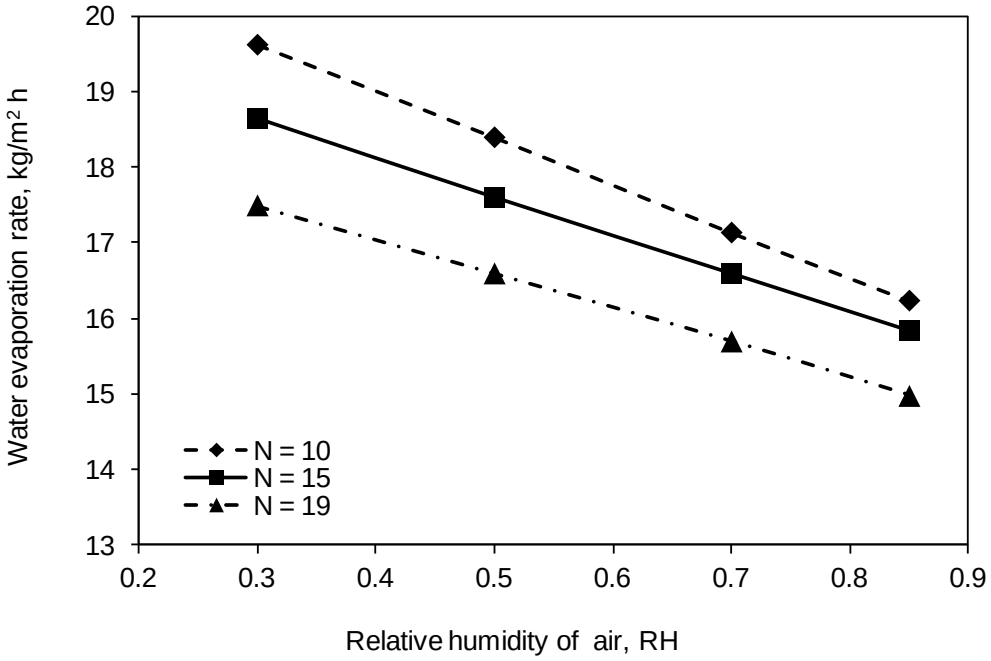

Figure 7.10 *Simulated variation of water evaporation rate with inlet air relative humidity*

7.3 Summary

The results from the numerical simulation based on the simplified model developed for the design of evaporatively-cooled condenser was presented in this chapter. The results were validated by comparing with those results obtained from the detailed model as well as experiments as shown in Table 7.1 and good agreement was observed. The simplified model was used to conduct a parametric study involving the important operating parameters of the condenser and the results were presented.

Chapter 8
INCORPORATION OF EVAPORATIVELY-COOLED CONDENSER IN AIR-CONDITIONERS

In the Copenhagen Summit on climate change in 2009, the Singapore government has committed to play a significant role in the reduction of green house gas emissions. Considering that 30 % of the total energy consumed in a building is for air- conditioning, every attempt should be made to reduce the energy consumed by the air- conditioners through the improvement of their energy efficiency. Based on the experimental study here, it was found that the COP of an air-cooled split unit air conditioning system can be increased by 20%-45% with spray cooling. The following is an illustration of how much savings in the cost of air conditioning of Singapore HDB apartments can be realized through the successful implementation of the evaporative cooling technique in all the air-conditioners. The benefits derived from the implementation of the evaporatively-cooled condenser in split air conditioning systems as well as the major potential challenges in the implementation are summarized in the following sections.

8.1. Benefits from Implementation of the Evaporatively-Cooled Condenser

Table 8.1 shows a conservative estimate of the number of air conditioned Housing Development Board (HDB) apartments in Singapore and the annual energy consumption of their air-conditioners. It is conservatively estimated that 25% of the HDB apartments in Singapore have air-conditioning systems installed and the average cooling load per apartment is 7.1 kW. Based on the current electricity tariff in Singapore of $0.27 per kWh, the annual expenditure on electricity for air-conditioning of HDB apartments is conservatively estimated to be $370,868,374.

Table 8.1 Energy consumption on air conditioning in Singapore HDB apartments

No. Of air-conditioned HDB apartments	250,000
Average cooling load (kW) of air-conditioning system installed	7.1
Coefficient of Performance (COP)	2.83
Average kW consumption per apartment on air-conditioning	2.508
No. Of hours of air-conditioning per day	6
Daily kWh per apartment used on air-conditioning	15.053
Yearly kWh per apartment used on air-conditioning	5494.34
Total annual kWh consumption on air-conditioning	1,373,586,572

With the successful implementation of the evaporatively-cooled condenser, the nett estimated monetary savings on the air-conditioning bill for HDB apartments is shown in Table 8.2 for various levels of improvements in the COP of the air-conditioning system. Besides the air-conditioning systems installed in HDB apartments in Singapore, there are also larger air-cooled air conditioning systems used in private residences and much larger air-cooled packaged air conditioning systems used in commercial and industrial establishments, which will mean even greater savings on cost of air-conditioning.

Table 8.2 *Total Singapore Residential Air-conditioner Electricity usage comparison with and without Evaporative-cooling (Singapore meteorological conditions)*

Improvement in COP (%)	Annual Consumption with Evaporative Cooling (kWh)	Total annual cost with Evaporative Cooling ($)	Total Annual Savings, ($)
50	915,724,381	264,745,583	106,122,792
40	981,133,266	282,405,982	88,462,393
30	1,056,605,055	302,783,365	68,085,010
20	1,144,655,477	326,556,979	44,311,396
10	1,248,715,065	354,653,068	16,215,307
5	1,308,177,688	370,707,976	160,399
0	1,373,586,572	388,368,375	0

Assuming that 0.0004 tonne of CO_2 is emitted for every kWh of electricity produced using natural gas (UNEP, 2002) the total annual production of CO_2 from the air-conditioning of HDB apartments is 592,212 tonne. Table 8.3 shows the carbon foot print comparison with the improvement in energy efficiency of the HDB residential air-conditioners alone (in Singapore). As can be seen from the table, the total annual reduction in CO_2 emission is significant and can definitely contribute towards Singapore's Copenhagen commitment. With the implementation of evaporatively-cooled air conditioning systems in private residences and commercial and industrial establishments, the reduction in CO_2 emission will be even greater.

Thus the successful implementation of the evaporatively-cooled condenser will enable Singapore to save millions of dollars per year in air-conditioning costs. It will also contribute greatly to the Green Building industry and the technologies developed have great potential for development.

Table 8.3 *Carbon footprint savings with evaporatively-cooled condensers*

Improv-ement in COP (%)	Annual Consumption with Evaporative Cooling (kWh)	Total Annual CO_2 Emission with Evaporative Cooling (tonne)	Total Annual CO_2 Emission Reduction (tonne)
50	915,724,381	394,808	197,404
40	981,133,266	423,008	169,203
30	1,056,605,055	455,547	136,664
20	1,144,655,477	493,510	98,702
10	1,248,715,065	538,374	53,837
5	1,308,177,688	564,011	28,200
0	1,373,586,572	592,212	0

8.2 Potential Challenges in the Implementation of the Evaporatively-cooled Condensers

It was established from the investigation on the finned and unfinned condensers with the evaporative cooling techniques that they are big energy savers when they are used as part of the air-conditioners. It was also described in the

preceding section of this chapter that they both provide significant economical and environmental benefits. However, there are certain technical obstacles on the successful operation after they are incorporated into the existing or new air-conditioners. The main technical obstacles that may be encountered during the operation of the evaporatively-cooled condensers as part of the air-conditioners are described in the following paragraphs.

8.2.1 Corrosion and fouling of condenser tubes

Corrosion is the chemical change in which the metal passes from the elementary to the combined condition like the formation of oxide (scale) on steel heated in air and rust (hydrous oxide) on iron exposed to water or moist air. Corrosion can be thought of as nature's way of trying to revert refined metals to their natural ore or compound state with minimum energy level. In cooling applications like air-conditioning, the damage caused by corrosion is enhanced whenever the attack is concentrated on small areas. There are occurrences of intense pitting under conditions intermediate between those that produce general corrosion and those that confer complete immunity. Hence, inadequate protective measures in the cooling systems would accelerate corrosive penetration leading to rapid perforation of the copper pipes in the evaporatively-cooled condensers.

There are two types of metal losses possible in the cooling systems involving evaporatively-cooled condensers. Although, the major mechanism behind corrosion is chemical in nature, there are also mechanical and electrical forces at work. The three kinds of metal losses in the evaporatively-cooled condensers can be:

1. Erosion corrosion as a result of low pH value of water.
2. Corrosion caused by electron flow due to the presence of oxygen
3. Finally, pump impeller deterioration as a result of cavitation.

Erosion corrosion involves a number of conditions that may cause uniform metal loss over a small or large area. Thinning of return bends of copper tubes of evaporatively-cooled condensers is a good example of erosion. To minimize erosion in this kind of situations, careful consideration should be given to water flow rate in the design stages of the evaporatively-cooled condensers. If the water is recirculated in the evaporatively-cooled condensers, it should be clean, falling at the right flow rate and free from air bubbles. pH is a measure of the relative concentration of the hydrogen and hydroxyl ions in water. When the pH of water is 4.0 or below, the hydrogen ions present are more than sufficient to cause metal loss in the evaporative cooling systems. Meanwhile, when the pH is more than 4.3, the hydroxyl ions present suppress the electrical currents that allow free electron flow. Corrosion in the cooling system involving water with a pH value of 4.3 is as a result of the oxygen effect.

Fouling in an evaporatively-cooled condenser is the process of deposition of foreign matter, including bio-growth, on the heat exchanger surface that inhibits the cooling process. The adverse effect of fouling is the offsetting of the benefits derived from the evaporative cooling by reducing the overall effectiveness of the evaporatively-cooled condenser. Hence, it is very important to eliminate excessive corrosion, scaling and biological fouling in the evaporatively-cooled condensers. Besides reducing the overall effectiveness of the cooling systems involving the affected evaporatively-cooled condensers, they could damage the equipment leading to catastrophical failure of the entire cooling system. As for the maintenance of the evaporatively-cooled condensers are concerned, it is very common that the owners and service providers are mostly concerned with the elimination of the Legionella's bacteria rather than putting effort on the important preventive maintenance against corrosion and scaling issues that reduces the efficiency of the cooling systems

drastically. In the maintenance of the cooling systems for the fouling and scaling, it is also an industrial practice to adopt a good water treatment programme that will address the threat of corrosion, scaling, microbiological growth and fouling, thus ensuring that each is addressed without prejudicing the other. However, water treatment for evaporative condensers poses different challenges as compared to an open-circuit cooling tower because of the volume of water to be treated is much smaller. This may suggest that the treatment should be easier but this is not necessarily the case. The volume may be smaller but the turnover of the water is much quicker and the materials of construction of the heat exchanger coil are of great importance and must be considered carefully. It is also interesting to note availability of state-of-the-art instrumentation to measure the scale thickness including indication of the coil tendencies regarding fouling. However, these superficial measures do not provide adequate quantification of performance degradation of the evaporatively-cooled condensers due to fouling and scaling. For effectively identifying and quantifying the effect of fouling and scaling on the degradation of the heat exchanger performance, the following factors should be determined:

(i) the correlation between scale thickness and fouling; (ii) loss in thermal performance; (iii) the effect of scale thickness on heat transfer capability. Calcium carbonate ($CaCO_3$) scaling on an evaporative condenser was investigated by Macleod-Smith (2002). He has given the percentage design heating capacity, which is defined as the ratio of the fouled heat capacity to the heat capacity at the clean state as a function of scale thickness. The scale thickness is a function of time. Figure 8.1 shows this heating capacity. As can be seen from the figure, the capacity of the evaporatively-cooled condenser decreases by almost 55% as a result of the scaling. Normally, $CaCO_3$ scaling is deposited very rapidly compared to any other scaling,

that is why a reduction in capacity as investigated by Macleod Smith is having such a significant reduction of 55%. However, it is to be noted that scaling is considered as one of the biggest challenges as far as the implementation of the evaporatively-cooled condensers in air-conditioners are concerned. Scaling not only reduces thermal effectiveness of the heat exchanger but also is a threat in shortening the life of evaporative cooled systems. Even a moderate amount of scaling significantly reduces thermal efficiency and promotes corrosion of the coil beneath a layer of scale, which can lead to a drastic shortening of the equipment life.

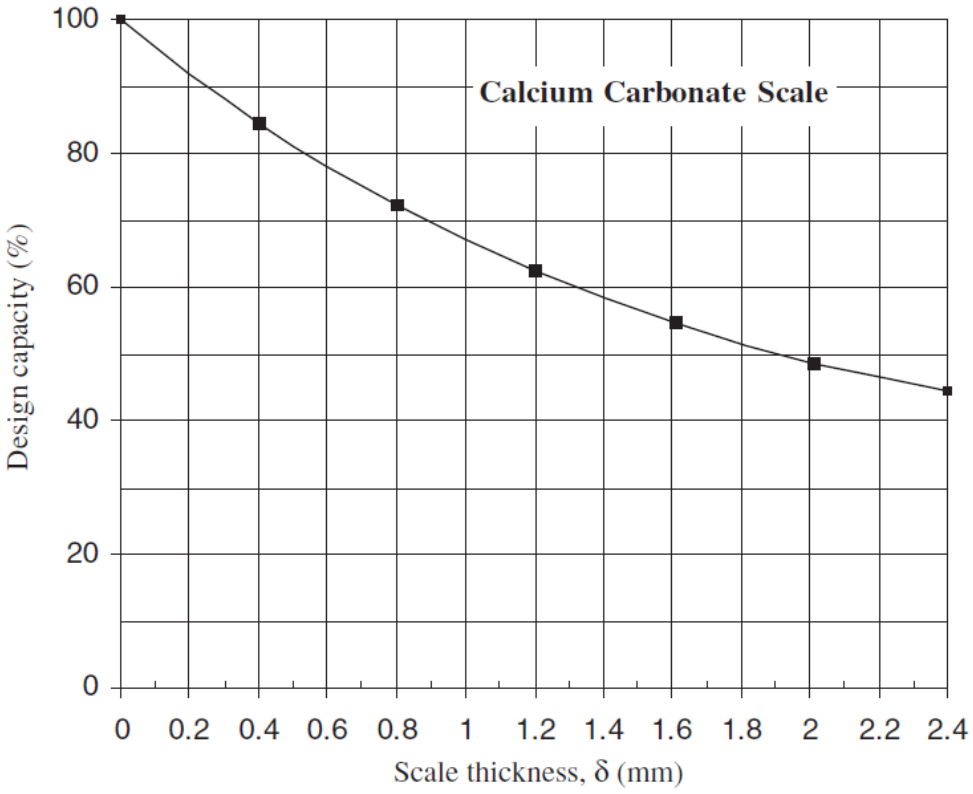

Figure 8.1 *Variation of decrease in percentage design capacity with scaling thickness for $CaCO_3$ scaling on heat exchanger surface (Macleod-Smith, 2002).*

Other measures for protecting the coil include keeping the coil in a wetted state continuously. Literature in the field of scaling emphasize that the more the coil surfaces are wetted, the lesser the chance of it getting scaled. Generally, as the evaporatively-cooled condensers consists of spraying systems, it is strongly recommended that the nozzles be frequently checked for any blockage caused by the partial unwetted coil surface, which is usually a favourable condition for scale formation. Scale and corrosion inhibitors can be used in scale and corrosion prevention of evaporatively-cooled condensers. Generally, the choice of inhibitor depends on the amount of make-up water and the type of heat exchanger material.

8.2.1.1 Fouling models

There are different detailed fouling and scaling models available to determine the loss of heat transfer effectiveness of evaporatively-cooled condensers. One such model has been developed by Bilal and Syed (2005) by following the method of Mizushina et al. (1968), Webb (1984) and Dreyer (1988), but without neglecting the water evaporation.

From the conservation of energy and mass for an evaporatively-cooled condenser system, Bilal and Syed developed the following expressions:

Fouling growth models:

The normalized evaporatively-cooled condenser performance index as a function of scale thickness as expressed by Khan and Zubair

$$\eta = \left(\frac{Q_{cl}-Q_{fl}}{Q_{cl}}\right) = C_1\left[1 - exp\ \left(\frac{-\delta}{C_2}\right)\right] \quad (8.1)$$

$$ln\left(\frac{1}{1-\left(\frac{\eta}{C_1}\right)}\right) = \left(\frac{\delta}{C_2}\right) \quad (8.2)$$

where, C_1 and C_2 are fouling characteristic constants for the evaporatively-cooled condenser. The maximum value of C_1 is taken as 0.73 where C_2 = 0.6

The overall heat transfer coefficient as a function of time is expressed as:

$$\frac{1}{U_o(t)} = \left(\frac{1}{h_a}\right)\left(\frac{D_o}{D_i}\right) + \left(\frac{D_o}{2k_t}\right) ln\left(\frac{D_o}{D_i}\right) + \frac{1}{h} + R_{if} + R_f(t) \qquad (8.3)$$

The effectiveness of the evaporatively-cooled condenser is defined as the ratio of actual energy to the maximum possible energy transfer from the fluid in the tubes and is expressed as:

$$\varepsilon\mathcal{E}_{ec} = \left(\frac{h_{r,i} - h_{r,o}}{h_{r,i} - h_{w,i}}\right) \qquad (8.4)$$

The effectiveness of these heat exchangers is based on the assumption that the lowest possible temperature achievable for the fluid in the pipes is the water temperature. Bilal and Syed used their fouling model for both design and rating calculations of an evaporatively-cooled condenser.

Table 8.5 shows the effectiveness and heat transfer for an evaporatively cooled-condenser calculated by Bilal and Syed for the input parameters of Table 8.4

Table 8.4 *Input parameters for the effectiveness heat transfer by Bilal and Syed (2005)*

Parameters	Value
$T_{db,in}$	25 ^oC
$T_{wb,\ in}$	18 ^oC
T_r	50 ^oC
A	9.7 m^2
Le	1.0
m_r	0.11 kg/s
m_w	2.67 kg/s
m_a	1.88 kg/s

Table 8.5 *Percentage change of ε_{ec} for different values of C_1 for an evaporatively-cooled condenser with C_2=0.6*

	Q (kW)		ε_{ec}		
C_1	Clean	Fouled	Clean	Fouled	Change (%)
0.25	113.661	91.980	0.9394	0.7518	18.94
0.37	113.661	81.573	0.9394	0.6629	28.53
0.49	113.661	71.166	0.9394	0.5747	38.04
0.61	113.661	60.759	0.9394	0.4874	47.45
0.73	113.661	50.178	0.9394	0.3996	56.91

8.3 Economic Analysis

Air-conditioning systems with evaporatively-cooled condenser require an initial investment, compared to conventional energy conversion equipment. Therefore, an economic analysis is carried out to determine the practical feasibility of such a system as well as the return on investment. For this purpose an economic analysis has been carried out for the evaporatively-cooled air-conditioning system. The main cost involved in the analysis of the air-conditioning system is capital equipment cost and operating cost.

The various economic figures of merit used for the performance evaluation of thermal energy systems may be described as follows:

1. The net life cycle savings
2. The payback period
3. Total annualized cost
4. The internal rate of return

It can be seen from analysis available from the literature (White, 2010) that the governing equation describing the optimum condition becomes identical for annualized life cycle cost and net life cycle savings and predicts the same optimum economic analysis parameter. Similarly, the analysis of internal rate of returns and

payback period leads to an identical equation, giving the same value for the optimized parameter. For this reason, one of these, either life cycle savings or payback period can be considered. In this analysis, the payback period is considered.

8.3.1 Economic evaluation methodology

The optimization of evaporatively-cooled air-conditioning systems involves multiple variables. Economic optimization procedure in a particular evaporatively-cooled air- conditioning system design is based on a comparison with the total expenditures of conventional systems during the life-cycle. In general, all the components in the system will have some effect on the cooling performance and thus on costs. In practice, the problem often reduces to a simpler one of determining the size of a cooling system for a known cooling load, and other parameters are fixed in relation to the optimized parameter. For evaporatively-cooled air-conditioning systems, the performance is more sensitive to mass of water evaporated from the tube surface than any other variables.

The economic analysis in terms of payback period is carried out for both the cases; the evaporatively-cooled condenser with and without fins.

The economic analysis of the evaporatively-cooled condensers with and without fins, is carried out based on the measured coefficient of performance (COP) values for a 5.8 kW split air-conditioner. At first, the base system COP without evaporative cooling is established. Subsequently, the COP of the bare and finned tube condensers are determined in evaporative cooling mode for different air temperature and film Reynolds number. The water requirement for the evaporative cooling is also determined experimentally, which gives the annual water requirement. From the COP values with and without evaporative cooling, the annual energy savings is then established. The annual savings minus the additional expenses for the water as well as

the additional power consumption gives the nett annual savings. The capital cost divided by the nett annual savings gives the payback period of the evaporatively-cooled air-conditioning system. The various parameters used for the economic analysis of the bare and finned tube condensers are listed in Tables 8.6 and 8.7, respectively.

8.3.1.1 Evaporatively-cooled condenser without fins

Figure 8.2 shows the variation of payback period with film Reynolds number and air temperature for the evaporatively-cooled air conditioner with the bare tube condenser.

As expected and seen from the figure, lower payback period is observed for lower air temperature and film Reynolds number. Figure 8.3 shows the payback period when the system capacity is increased to 19.4 kW. An extra capital cost of 25 % is assumed for the higher capacity condenser as an adjustment for the extra numbers of nozzles and slightly higher capacity pump. Another assumption made for the higher capacity air-conditioner case is the same COP improvement.

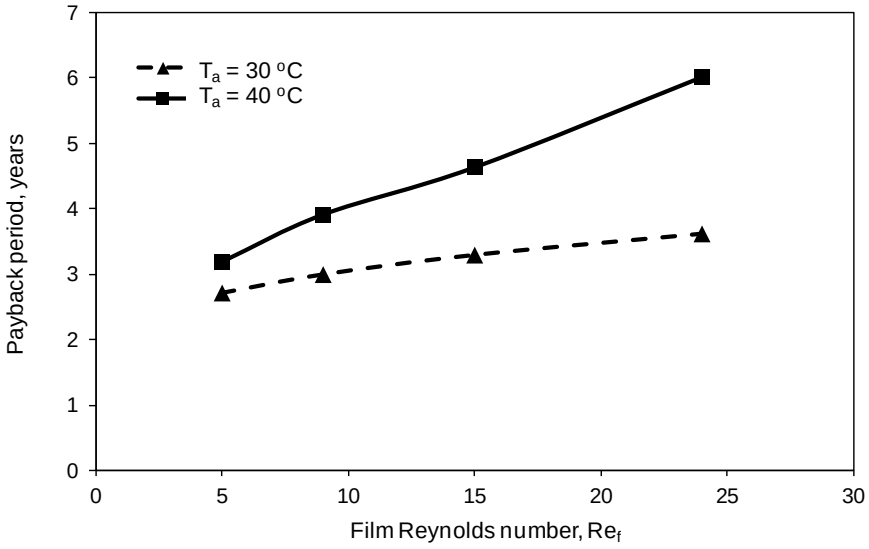

Figure 8.2 *Variation of payback period with film Reynolds number and ambient temperature (cooling capacity = 5.8 kW) for the evaporatively-cooled condenser without fins.*

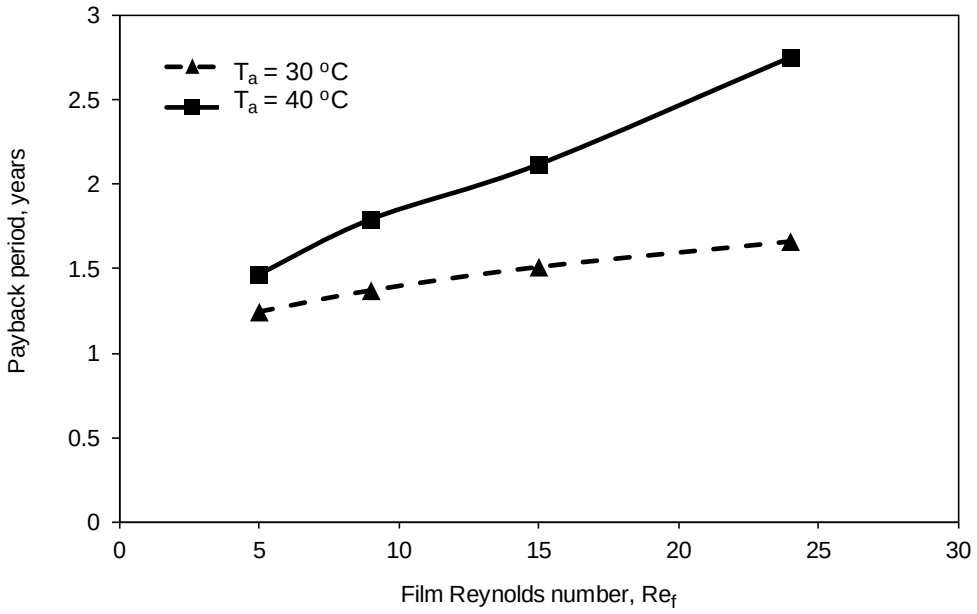

Figure 8.3 *Variation of payback period with film Reynolds number and ambient temperature (cooling capacity = 19.4 kW) for the evaporatively-cooled condenser without fins.*

Figure 8.4 shows the comparison of the variation of the payback period with air temperature for the 5.8 kW and 19.4 kW air conditioners.

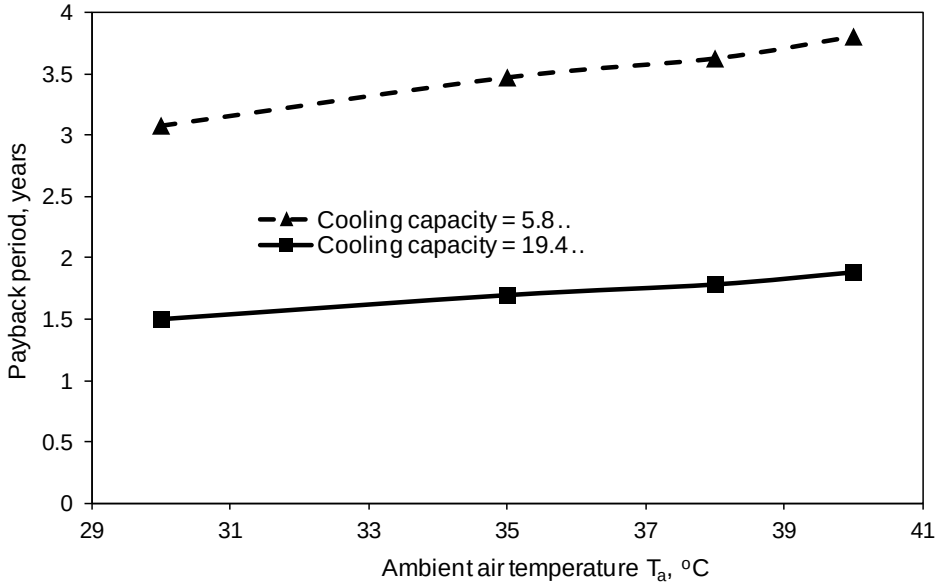

Figure 8.4 *Variation of payback period with air temperature and cooling capacity for the evaporatively-cooled condenser without fins.*

8.3.1.2 Evaporatively-cooled condenser with fins

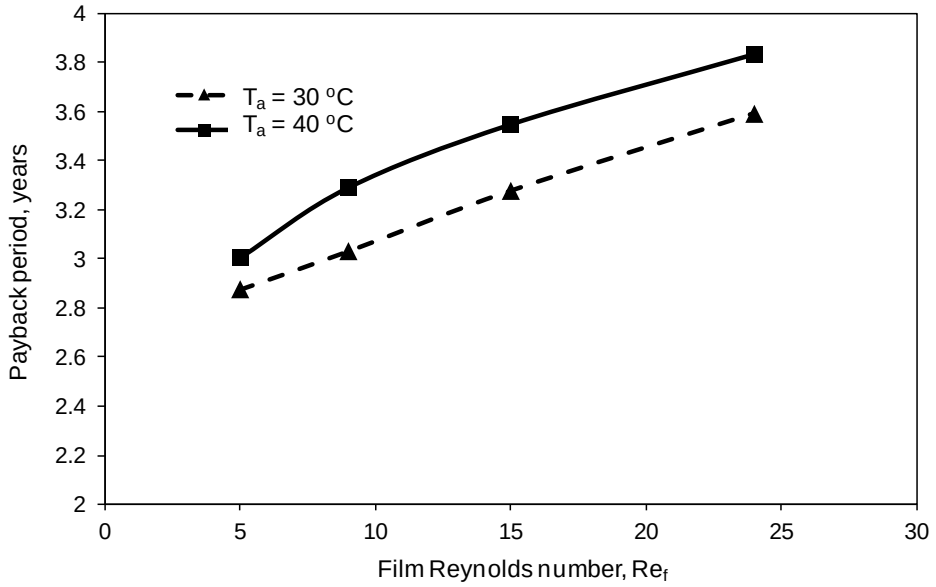

Figure 8.5 *Variation of payback period with film Reynolds number and ambient temperature (cooling capacity = 5.8 kW) for the evaporatively-cooled condenser with fins.*

Figures 8.6 to 8.8 show the variation of the payback period with film Reynolds number and air temperature for the air-conditioner with finned tube condenser.

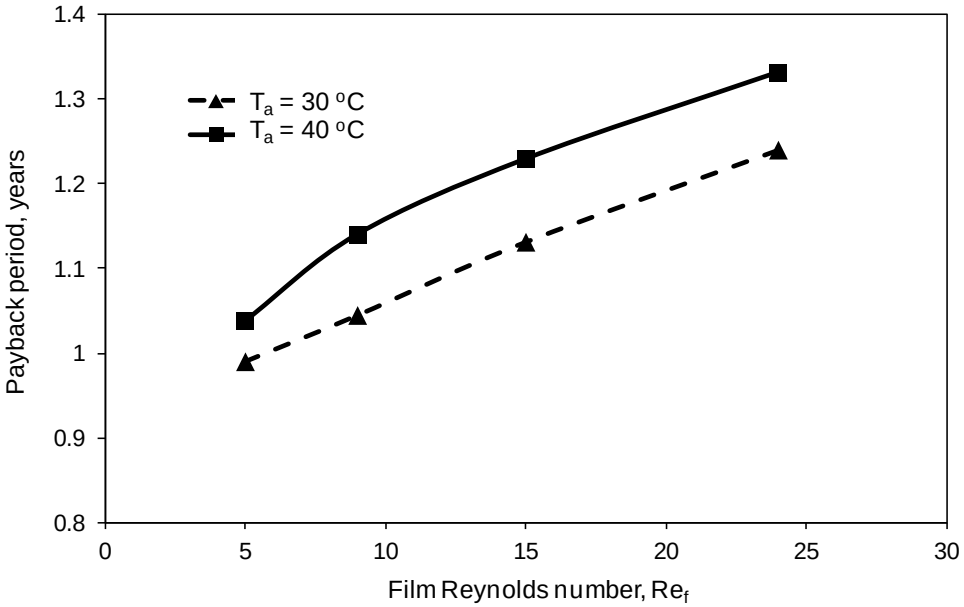

Figure 8.6 *Variation of payback period with film Reynolds number and ambient temperature (cooling capacity = 19.4 kW) for the evaporatively-cooled condenser with fins.*

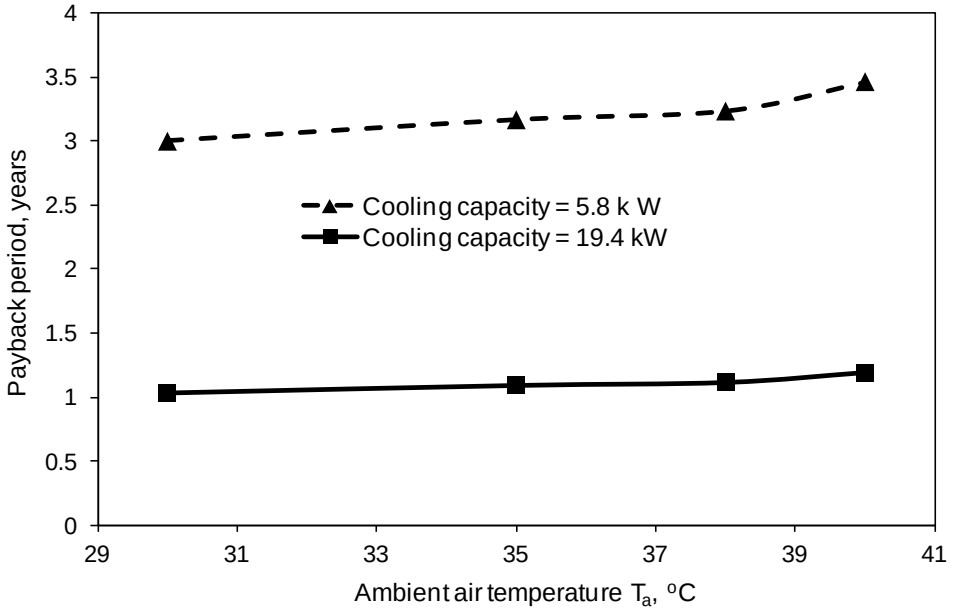

Figure 8.7 *Variation of payback period with air temperature and cooling capacity for the evaporatively-cooled condenser with fins.*

Table 8.6 *Economic analysis of evaporatively-cooled air-conditioner (bare tube condenser)*

Variables	Values
Air-conditioner capacity	5.8 kW
Film Reynolds number ($4\Gamma/\mu$)	9
Ambient air temperature and relative humidity	30 C, 70%
COP without evaporative cooling	2.20
COP with evaporative cooling	2.82
Percentage improvement in COP	28.2%
Compressor power required without evaporative cooling	2.64 kW
Compressor power required with evaporative cooling	2.06 kW
Power savings due to evaporative cooling	0.58 kW
Additional power required for evaporative cooling	0.06 kW
Air conditioner run-days	200 days/year
Air conditioner run-time	8 h/day x 200 = 1600 h
Electricity tariff (Singapore)	S$ 0.27/kWh
Water tariff (Singapore)	S$ 1.17/m^3
Required water quantity for evaporative cooling	12.0 m^3
Water cost	S$ 14.04
Additional power cost	S$ 25.92
Savings in operational cost due to reduction in compressor power	S$ 250.56
Net savings	S$ 210.60
Equipment and maintenance cost	S$ 700.00
Payback period	3.32 years

Table 8.7 *Economic analysis of evaporatively cooled ai- conditioner (condenser with fins)*

Variables	Values
Air-conditioner capacity	5.8 kW
Film Reynolds number ($4\Gamma/\mu$)	9
Ambient air temperature and relative humidity	30 C, 70%
Fin pitch	4 mm
Fin thickness	0.2 mm
COP without evaporative cooling	2.8
COP with evaporative cooling	4.03
Percentage improvement in COP	43.4%
Compressor power required without evaporative cooling	2.08 kW
Compressor power required with evaporative cooling	1.44 kW
Power savings due to evaporative cooling	0.64 kW
Additional power required for evaporative cooling	0.06 kW
Air conditioner run-days	200 days/year
Air conditioner run-time	8 h/day x 200 = 1600 h
Electricity tariff (Singapore)	S$ 0.27/kWh
Water tariff (Singapore)	S$ 1.17/m^3
Required water quantity for evaporative cooling	9.9 m^3
Water cost	S$ 16.14
Additional power cost	S$ 25.92
Savings in operational cost due to reduction in compressor power	S$ 276.48
Net savings	S$ 234.42
Equipment and maintenance cost	S$ 700.00
Payback period	2.98 years

8.4 Summary

Various issues pertaining to the implementation of the investigated evaporatively-cooled condensers in air-conditioners were described in this chapter. At first, the benefits derived through such implementation were illustrated with reference to the residential air-conditoner application in Singapore. The benefits derived were quantified in terms of the annual energy and carbon foot print reduction from the statistics available from the Housing Development Board (HDB) of Singapore. Various challenges in the implementation of the evaporatively-cooled condensers were also identified and described briefly. The main challenges include those arising from the corrosion as well as fouling and scaling. Some of the fouling and scaling

related models available from the literature for the quantification of the heat transfer deterioration were also included. Finally, an economic analysis in terms of a simple payback period was carried out for both the bare and finned tube evaporatively-cooled condensers. The economic analysis suggested that the incorporation of the evaporatively-cooled condensers is economically feasible.

Chapter 9
CONCLUSIONS AND RECOMMENDATIONS

9.1 CONCLUSIONS

The main conclusions of the study carried out to evaluate the performance of an evaporatively-cooled condenser of vapour compression air-conditioning systems are as follows:

1. Based on the findings of the literature survey on theoretical studies and mathematical modeling of the evaporatively-cooled air-conditioning system and falling film evaporation with tubes of different configurations, a detailed numerical formulation was developed considering the practical configuration of the evaporatively-cooled condensers. These numerical formulations are used to analyze the heat and mass transfer processes and investigate the impact of the main operating variables on their performance.
2. A detailed model for a small element of the condenser tube was developed from which the temperature distribution of the thin water film on the tube surface was obtained. The two important heat transfer coefficients; film-tube interface (h_i) and film-air interface (h_o) were determined from the above temperature distribution. Subsequently, the above detailed model was extended to both finned and unfinned serpentine condenser tubes of evaporatively-cooled condensers. For the finned condenser tube, a two-dimensional wet fin model was also developed to study the effect of fins in evaporative cooling.
3. For the design and development of evaporatively-cooled condensers by practising engineers, a simplified model was developed in which the two heat transfer coefficients obtained from the detailed model were used as input for

the purpose of sizing of the condenser. The simplified model was numerically solved using the 4^{th} order R-K scheme. There was good agreement between the predictions of the detailed and simplified models.

4. An experimental test rig was designed and constructed around a real split air-conditioner of 5.8 kW capacity. In the test rig, the necessary modifications were carried out at the condenser side to house the finned and unfinned condensers subjected to evaporative cooling. The test set-up was comprehensively instrumented to measure as many operating variables as possible. The performance of the condensers was experimentally investigated with and without evaporative cooling. The key performance indicators considered in the experiments were the condensing temperature as well as the power consumed by the compressor. With these the Coefficient of Performance of the air-conditioning system was determined to evaluate the COP improvement of the system with and without evaporative cooling.
5. In the published literature a number of procedures are used to estimate the heat and mass transfer coefficients where the evaporatively-cooled condenser is usually treated as a heat and mass exchanger and the two transfer processes are uncoupled. In the present study, the simplified coupled-model with constant mass flow rate of refrigerant was used to analyze the experimental and numerical data to determine the heat transfer coefficients and the mass exchange from the condenser tube surface.
6. In real small or medium-sized air-conditioners generally used in a residential or commercial setup, the condensers used are air-cooled condensers. In the present study, two condensers with and without fins were tested with and without evaporative cooling technique incorporated. An improvement of

Coefficient of Performance (COP) of over 30% and 45% were observed for the unfinned (bare) and finned-tube condensers, respectively. A reduction in compressor power input of about 17% and 27% were observed for the bare and finned-tube condensers, respectively.The results from the present numerical and experimental study also suggested that the currently used air-cooled condensers can either be retrofitted with evaporative cooling or totally replaced with a bare-tube evaporatively-cooled condenser. In the present study, the evaporatively-cooled condenser with fins was also studied with different fin dimensions and their performance in terms of condenser tube length was determined.

7. In the present study, the benefits of incorporation of the evaporative cooling technique in air-conditioning systems with respect to the usage of small and medium-scale air-conditioners in the Singapore context is statistically established with the help of the statistics obtained from the Housing Development Board (HDB) of Singapore. The benefits were quantified in terms of the annual electricity savings as well as the carbon foot print savings in Singapore. While air-conditioners with evaporative cooling are advantageous as far as energy efficiency and carbon emission are concerned, there are also challenges to overcome in their incorporation and maintenance. The main potential challenges in terms of corrosion and fouling were also addressed in this present study. A simple economical analysis was carried out to determine the payback period of the evaporatively-cooled air-conditioning system.

9.2 RECOMMENDATIONS

1. In the present study, in the development of the detailed model, it was assumed that the water spray enters the first tube at an entry angle gently and forms a thin film and flows around the circumference and enters the subsequent bottom tubes with a reduced film thickness. The above simplified entrance effect of the water spray as well as the conservative assumption of negligible inter tubular heat transfer from the water can be studied to check the performance variation of the evaporatively-cooled condensers.
2. The simplified model developed in this study is for the purpose of design and development of evaporatively-cooled condensers. The validity of the model could be further investigated using the experimental data available in the published literature. An attempt can be made to modify the simplified model to establish a generalized correlation to determine the heat transfer coefficients as well as the mass exchange in the falling film of the evaporative cooling process.
3. In an application point of view, as most of the modern small and medium size air-conditioners are fitted with the inverter technologies to modulate the compressor operation in an energy efficient manner, a matching control system could also be devised to regulate the water spraying rate based on the compressor speed during the evaporative cooling.

REFERENCES

Adrian, B. Advanced Engineering Thermodynamics Third Edition. John Wiley and Sons Inc, 2006.

Alhusseini, A.A., Tuzla. K., Chen, J.C. Falling film evaporation of single component liquids. Int J Heat Mass Transfer Vol.41, pp.1624–1632, 1998.

Anderson, J. D. Computational fluid dynamics, MacGraw-Hill Companies Inc, 1995.

Armbruster, R. and Mitrovic, J. Heat Transfer in Falling Film on a Horizontal Tube, National Heat Transfer Conference, vol.314, pp. 13-21.1995.

Arora, C.P. Refrigeration and air conditioning, Tata Mcgraw-Hill publishing company limited, second edition, 2000.

ASHRAE Fundamentals. American Society of Heating, Refrigeration and Air conditioning Engineers 2009.

Assad, M.E.H., and Lampinen, M.J. Mathematical modeling of falling liquid film evaporation process, International Journal of Refrigeration. 25, pp. 985–991, 2002.

Bird, R.B., Stewart, W.E, and Lightfoot, E.N. Transport Phenomena, Wiley International ed., New York: Wiley & Sons, Inc. 1960.

Chan, H.S., Lee, D.W., and Ro, S.T. Cooling enhancement in an air-cooled finned heat exchanger by thin water film evaporation, vol.46, pp.1241-1249, 2003.

Chato, J.C. Laminar Condensation inside Horizontal and Inclined Tubes, ASHRAE Journal, Vol. 4 (2), pp.52-60, 1962

Clealand, A.C. Computer subroutines for rapid evaluation of refrigerant thermodynamic properties, International journal of refrigeration, vol.9, pp.346-351, 1986.

Chowdhury, S.K., Hisajima, D, Ohuchi, T, Nishiguchi, A, Fukushima, T, and Sakaguchi, S. Absorption of Vapors into Liquid Films Flowing Over Cooled Horizontal Tubes, ASHRAE Transaction: Research 99-2, pp.81-89, 1993.

Chun, K.R., and Seban, R.A. Heat transfer to evaporating liquid films, Journal of Heat Transfer 98, pp.391-396, 1971.

Chyu, M.C., and Bergles, A.E. An analytical and experimental study of falling film evaporation on a horizontal tube, Journal of Heat Transfer 109, pp.415-421, 1987.

El-Baky, M.A.A., Mohamed, M.M. Heat pipe heat exchanger for heat recovery in air conditioning, Applied Thermal Engineering, Vol. 27, pp.795–801, 2007.

Fletcher, L.S., Sernas, V, and Galowin, S. Evaporation of thin water films on horizontal tubes, Ind. Eng. Chem. Process Des. Dev. 13 pp. 265-269, 1974.

Hajidavalloo, E. Application of evaporative cooling on the condenser of window-air-conditioner. Applied Thermal Engineering vol.27 pp. 1937-1943, 2006

He, S., An, P., Li, J., and Jackson, J.D. Combined heat and mass transfer in a uniformly heated vertical tube with water film cooling, International Journal of Heat and Fluid Flow. 19, pp.401-417, 1998.

Hsu, S.T., and Lavan, Z. Optimization of wet-surface heat exchangers, Energy, vol 14, pp. 757-770, 1989.

Incropera, Dewitt, Bergmann, Lavine, Fundamentals of Heat and Mass Transfer, sixth ed. Wiley publishers Inc, New York, 2007.

Islam, M.R. Performance evaluation of absorber for vapour absorption cooling systems, Doctor of philosophy thesis, National University of Singapore, 2002.

Islam, M.R., Wijeysundera, N.E., and Ho, J.C. Evaluation of Heat and Mass Transfer Coefficients for Falling-Films on Tubular Absorbers, Int. J. Refrigeration., vol. 26, pp. 197-204. 2003.

Kachhwaha, S.S., Dhar, P.L., and Kale, S.R.. Experimental studies and numerical simulation of evaporative cooling of air with a water spray, International Journal of Heat and Mass Transfer, vol.41, pp.447-464, 1997.

Kocamustafaogullari, A. and Chen, I.Y. Falling Film Heat Transfer Analysis on a Bank of Horizontal Tube Evaporator, AiChE Journal, Vol. 34 (9), 1988.

Kutateladze, S.S. Gogonin, I.I. Heat transfer in film condensation of slowly moving vapor, Int J Heat Mass Transfer Vol. 22, pp.1593–1599, 1979.

Labuntsov, D.A. Heat Transfer in Film Condensation of Steam on a Vertical Surface and Horizontal Tubes, Teplonergetica, vol.4, No. 7, pp.72-80,1957.

Leidenfrost,W., Lee K.H., and Korenic, B. Conservation of energy estimated by second law analysis of a power consuming process, Energy, vol.5, pp. 47-61, 1980

Liu, Z.H., Zhu, Q.Z., and Chen, Y.M. Evaporation heat transfer of falling film on a horizontal tube bundle, Heat Transfer—Asian Res 3, 42–55, 2002.

Lorenz, J.J., and Yung, D. A note on combined boiling evaporation of liquid films on horizontal tubes, ASME J. Heat Transfer 101, pp.178-180, 1979.

Maclaine-cross, I.L., and Banks, P.J.A General Theory of Wet Surface Heat Exchangers and its Application to Regenerative Evaporative Cooling, Journal of Heat Transfer, Vol.103, pp.579-585, 1981.

Mathur, G.D. Performance Enhancement of Existing Air conditioning Systems, Energy Conversion Engineering Conference, 1997. IECEC-97., Proceedings of the 32nd Intersociety. Vol 3, pp. 1618 – 1623, 1997.

Miller, W.A., and Keyhani, M. The Correlation of Simultaneous Heat and Mass Transfer Experimental Data for Aqueous Lithium Bromide Vertical Falling Film Absorption, Journal of Solar Energy Engineering, vol. 123, pp.30-42, 2001.

Moalem, D., and Sideman, S. Performance Improvement of Horizotal Evaporator-condenser Desalination Units, Proceedings of 5th International Symposium on Fresh Water from the Sea, Vol.2, pp. 315-324, 1976.

Moffat, R.J. Using uncertainty analysis in the planning of an experiment, Journal of fluids engineering, vol.107, pp. 173-180, 1985.

Moffat, R.J. Describing uncertainties in experimental results, Experimental thermal and fluid science, vol.1, pp. 3-17, 1988.

Nakayama, W., Kuwahara, H. and Hirasawa, S. International Journal of Heat and Mass Transfer, vol.31, pp. 449-460, 1988.

Oosthuizen, Patric H., and David Naylor. Edwards, Convective Heat Transfer Analysis, pp. 5756-577, McGraw-Hill International Editions, 1999.

Ozisik, M.N. Heat Transfer a Basic Approach, Mcgraw-Hill publishers, International edition, 1985.

Parken, W.H., and Fletcher, L.S. Heat transfer in thin liquid films flowing over horizontal tubes, proceedings of 7th Int. Heat Transfer Conference, Munich 4, pp.415-420, 1982.

Patankar, S.V. Numerical Heat Transfer and Fluid Flow, first ed. Hemisphere Publishing Corporation, 1980.

Perry, R.H. Perry's Chemical Engineers' Handbook, eighth ed. MacGraw-Hill Companies Inc, New York, 2008.

Prasad, M., and Kumar, P. An Experimental and Analytical Study of Non-conventional Air conditioning System, Energy Conversion Management, Vol. 24, No. 3, pp. 165-170, 1984.

Qureshi, B.A., and Zubair, S.M. The impact of fouling on performance evaluation of evaporative coolers and condensers, Int J Energy Research 29, pp.1313–1330, 2005.

Rana, R.S., Charan, V., and Varma, H.K. International Journal of Heat and Mass Transfer, vol.29, pp.555-562, 1985.

Rogers, J.T. Laminar falling film and heat transfer characteristics on horizontal tubes, Canadian J. Chemical Engineering 59 pp. 213-222,1981.

Sadik, K. Boilers, Evaporators and Condensers. Canada: John Wiley and Sons Inc, 1991.

Sandall, O.C., Hanna, O.T., and Ibanex, G.R. Heating and evaporation of turbulent falling liquid films, AICHE Journal, Vol.34, pp.502-505, 1988.

Sarma, P.K., and Saibabu, J. Evaporation of laminar, falling liquid film on a horizontal cylinder, Warme-und Stoffubertragung 27, pp.347-355, 1992.

Solan, A. and Zfati, A. Heat Transfer in a Laminar Flow of a Liquid Film on a Horizontal cylinder. Proceedings of 5th International Heat Transfer Conference, Japan, pp.90-93, 1974.

Stoecker, W.F., Jerold, W.J. Thermal system design, second edition, 1982.

Stoitchkov, N.J., and Dimitrov, G.I. Effectiveness of crossflow plate heat exchanger for indirect evaporative cooling, International journal of Refrigeration, vol.21, pp. 463-471, 1998.

Stoecker, W.F., Jerold, W.J. Refrigeration and air conditioning, second edition, 1982.

Sweetland, M. and Lienhard V.J.H. Evaporative cooling of continously drawn glass fibres by water sprays, International Journal of Heat and Mass Transfer, vol.43, pp. 777-790, 2000.

Sultana, P. Study of thermal performance of falling film absorbers with and without film inversion, Doctor of philosophy thesis, National University of Singapore, 2006.

Tiwari, G.N., and Ghosal, M.K. Fundamentals of Renewable Energy Sources, Alpha Science International Ltd, 2001.

Tsay, Y.L. Analysis of heat and mass transfer in a counter current-flow wet surface heat exchanger, International Journal of Heat and Fluid Flow, vol.15, pp.149-156, 1994.

Tsay, Y.L., and Lin, T.F. Evaporation of a Heated Falling Liquid Film into a Laminar Gas Stream, Experimental Thermal and Fluid Science. 11, pp.61-71, 1995.

Uche, J., Artal, J., and Luis, S. Comparison of Heat Transfer Coefficient Correlations for Thermal Desalination units, Desalination, Vol. 152, pp.195-200, 2002.

Vrachopoulos, M.G., Filios, A.E., Kotsiovelos,G.T., and Kravvaritis. Incorporated evaporative condenser. Applied Thermal Engineering vol.27 pp. 823-828, 2007

Wang, C.C., and Chang, C.T. Heat and mass transfer for plate fin-and-tube heat exchanger, with and without hydrophilic coating. International Journal of Heat and Mass Transfer vol.41 pp.3109-3120,1998

White J.A., Case K.E., Pratt D.B. Principles of engineering economic analysis, fiftth ed. Wiley publishers Inc, New York, 2010.

William M.G., and Weirum, F.A. Liquid spray cooling of a heated surface, International Jornal of Heat and Mass Transfer, vol.24, pp.261-271, 1981.

Common carbon metric, Protocol for measuring Energy Use and reporting Greenhouse Gas Emissions from building operations (http://www.unep.org), 2002

Yan, W. M. Effects of film vaporization on turbulent mixed convection heat and mass transfer in a vertical channel, International Journal of Heat and Mass Transfer, vol.38, pp.713-772, 1994.

Yang, W.J., and Clark, D.W. Spray cooling of air-cooled compact heat exchangers, International Journal of Heat and Mass Transfer, vol.18, pp.311-317, 1974.

Youbi-Idrissi, M., Macchi-Tejeda, H., Fournaison, L., and Guilpart, J. Numerical model of sprayed air cooled condenser coupled to refrigerating system. Energy Conversion and Management vol.48 1943-1951, 2007

Yu, F.W. Application of direct evaporative coolers for improving for the energy efficiency of air-cooled chillers, Transaction of the ASME, vol.27, pp. 430-433,2005.

Yunus, A.C. Heat Transfer A Practical Approach. MacGraw-Hill Companies Inc, 1998

Appendix A
CO-ORDINATE TRANSFORMATION AND TEMPERATURE COEFFICIENTS IN THE DISCRETIZED EQUATION OF THE DETAILED MODEL

A.1 Co-ordinate Transformation Derivation

The one-to-one co-ordinate transformation of the velocity components u and v as well as the energy equation is described below.

The velocity u in the flow direction can be expressed as:

$$u = \frac{\rho_w g \sin\theta}{\mu}\left(\delta y - \frac{y^2}{2}\right) \tag{A.1}$$

With the help of the momentum equation and the boundary conditions listed above, the y-component of the velocity can be written as:

$$v = -\frac{\rho_w g y^2}{2\mu R}\left(\sin\theta\frac{d\delta}{d\theta} + \delta\cos\theta - \frac{y}{3}\cos\theta\right) \tag{A.2}$$

The falling film thickness is expressed as:

$$\delta = \left(\frac{3.\Gamma.\mu}{\rho_w{}^2 g \sin\theta}\right)^{1/3} \tag{A.3}$$

The final form of energy equation as:

$$\frac{\partial}{R.\partial\theta}\left(uT_w\right) + \frac{\partial}{\partial y}\left(vT_w\right) = \alpha\frac{\partial^2 T_w}{\partial y^2} \tag{A.4}$$

The transformation relations are as follows, Choudhury et al. (1995):

$$\xi = \frac{\theta}{\pi} \qquad \eta = \frac{Y}{\delta} \tag{A.5}$$

Substituting the transformation co-ordinates in the u-component of the velocity gives,

$$u = \frac{\rho_w g \sin\theta}{\mu}\left(\delta\delta\eta - \frac{(\eta\delta)^2}{2}\right) \tag{A.6}$$

$$u=\frac{\rho_w g\sin\theta}{\mu}\left(\eta\delta^2-\frac{\eta^2\delta^2}{2}\right) \tag{A.7}$$

Transformed velocity component in the θ direction can be expressed as:

$$u=\frac{\rho_w g\delta^2\sin\theta}{2\mu}\left(2\eta-\eta^2\right) \tag{A.8}$$

Similarly, the velocity in the y direction, v, is transformed as follows:

Differentiating the film thickness, δ with respect to θ gives,

$$\frac{d\delta}{d\theta}=\left(\frac{3\Gamma\nu}{\rho g}\right)^{1/3}\left(\frac{-1}{3}\right)\sin\theta^{-4/3}\cos\theta \tag{A.9}$$

Substituting equation (A.9) in the equation (A.2) gives,

$$v=-\frac{\rho_w g\delta^2\eta^2}{2\mu R}\left[\left(\frac{\Gamma\nu}{9\rho g}\right)^{1/3}\sin\theta\sin\theta^{-4/3}\cos\theta+\delta\cos\theta-\cos\theta\frac{\eta\delta}{3}\right] \tag{A.10}$$

$$v=-\frac{\rho_w g\delta^2\eta^2}{2\mu R}\left[\left(\frac{\Gamma\nu}{9\rho g}\right)^{1/3}\sin\theta\sin\theta^{-4/3}\cos\theta+\delta\cos\theta-\cos\theta\frac{\eta\delta}{3}\right] \tag{A.11}$$

Simplification of equation (A.11) yields the y-component of the velocity in the transformed co-ordinate as,

$$v=\frac{\rho_w g\delta^2\eta^2\cos(\pi\xi)}{6\mu R}\left[\left(\frac{3\Gamma\mu}{\rho^2 g\sin(\pi\xi)}\right)^{1/3}-\delta\left(3-\eta\right)\right] \tag{A.12}$$

For the transformation of the energy equation (A.4), the following transformation derivative expressions are used:

$$\frac{\partial}{\partial\theta}=\frac{\partial}{\partial\xi}\times\frac{\partial\xi}{\partial\theta}+\frac{\partial}{\partial\eta}\times\frac{\partial\eta}{\partial\theta} \tag{A.13}$$

$$\frac{\partial}{\partial y}=\frac{\partial}{\partial \xi}\times\frac{\partial \xi}{\partial y}+\frac{\partial}{\partial \eta}\times\frac{\partial \eta}{\partial y} \tag{A.14}$$

Using equation (A.13) and (A.14), the different derivative terms in the energy equation are expressed as:

$$\frac{\partial(uT_w)}{\partial \theta}=\frac{\partial(uT_w)}{\partial \xi}\times\frac{\partial \xi}{\partial \theta}+\frac{\partial(uT_w)}{\partial \eta}\times\frac{\partial \eta}{\partial \theta} \tag{A.15}$$

$$\frac{\partial(uT_w)}{\partial \theta}=\frac{1}{\pi}\frac{\partial(uT_w)}{\partial \xi}+\frac{\partial(uT_w)}{\partial \eta}\times\frac{\partial \eta}{\partial \theta} \tag{A.16}$$

But, $$\frac{\partial(\eta)}{\partial \theta}=\frac{-\eta}{\delta}\frac{d\delta}{d\theta} \tag{A.17}$$

From the film thickness expression,

$$\frac{d\delta}{d\theta}=\left(\frac{3\Gamma\nu}{\rho g}\right)^{1/3}\left[\frac{d\left(\sin\theta^{-1/3}\right)}{d\theta}\right] \tag{A.18}$$

Differentiating and simplifying (A.18) yields,

$$\frac{d\delta}{d\theta}=-\left(\frac{\Gamma\nu}{9\rho g}\right)^{1/3}\sin\theta^{-4/3}\cos\theta \tag{A.19}$$

Therefore, $$\frac{\partial(\eta)}{\partial \theta}=\frac{\eta}{\delta}\left(\frac{\Gamma\nu}{9\rho g}\right)^{1/3}\sin\theta^{-4/3}\cos\theta \tag{A.20}$$

$$\frac{\partial(\eta)}{\partial \theta}=\frac{\eta}{\delta}\left(\frac{\Gamma\nu}{9\rho g\sin\theta}\right)^{1/3}\cot\theta \tag{A.21}$$

And $$\frac{\partial(uT_w)}{\partial \theta}=\frac{1}{\pi}\frac{\partial(uT_w)}{\partial \xi}+\frac{\eta\partial(uT_w)}{\partial \eta}\times\frac{1}{\delta}\left(\frac{\Gamma\nu}{9\rho g\sin\theta}\right)^{1/3}\cot\theta \tag{A.22}$$

$$\frac{\eta\partial(uT_w)}{\partial \eta}=\frac{\partial(\eta uT_w)}{\partial \eta}-uT_w \tag{A.23}$$

$$\frac{\partial(uT_w)}{\partial \theta}=\frac{1}{\pi}\frac{\partial(uT_w)}{\partial \xi}+\frac{1}{\delta}\left(\frac{\Gamma\nu}{9\rho g\sin\theta}\right)^{1/3}\cot\theta\left(\frac{\partial(\eta uT_w)}{\partial \eta}-uT_w\right) \tag{A.24}$$

$$\frac{\partial(vT_w)}{\partial y}=\frac{\partial(vT_w)}{\partial \xi}\times\frac{\partial \xi}{\partial y}+\frac{\partial(vT_w)}{\partial \eta}\times\frac{\partial \eta}{\partial y}=\frac{1}{\delta}\frac{\partial(vT_w)}{\partial \eta} \tag{A.25}$$

$$\alpha\frac{\partial^2 T_w}{\partial y^2}=\alpha\frac{\partial}{\partial y}\left(\frac{\partial T_w}{\partial y}\right) \tag{A.26}$$

$$\alpha\frac{\partial^2 T_w}{\partial y^2}=\alpha\left[\frac{\partial}{\partial \xi}\left(\frac{1}{\delta}\frac{\partial(T_w)}{\partial \eta}\right)\times\frac{\partial \xi}{\partial y}+\frac{\partial}{\partial \eta}\left(\frac{1}{\delta}\frac{\partial(T_w)}{\partial \eta}\right)\times\frac{1}{\delta}\right] \tag{A.27}$$

$$\alpha\frac{\partial^2 T_w}{\partial y^2}=\frac{\alpha}{\delta^2}\frac{\partial^2 T_w}{\partial \eta^2} \tag{A.28}$$

Substituting (A.24), (A.25) and (A.28) in the energy equation (A.4) and simplifying yields the transformed energy equation in the computational domain as:

$$\frac{1}{\pi R}\frac{\partial}{\partial \xi}(uT_w)+\frac{1}{\delta}\frac{\partial}{\partial \eta}(vT_w)-\left(\frac{\Gamma\mu}{9\rho_w{}^2 g\sin(\pi\xi)}\right)^{1/3}\frac{1}{\delta R\tan(\pi\xi)}\left(uT_w-\frac{\partial}{\partial \eta}(\eta uT_w)\right)$$
$$=\frac{\alpha}{\delta^2}\frac{\partial}{\partial \eta}\left(\frac{\partial T_w}{\partial \eta}\right) \tag{A.29}$$

The boundary conditions, equations (3.13) to (3.17) are transformed as follows:

a) $\left.\begin{matrix}\xi=\xi_i\\ 0\le\eta\le 1\end{matrix}\right\}$ $T_w = T_{w,in},\ \Gamma=\Gamma_0$ (A.30)

b) $\left.\begin{matrix}\xi_i\le\xi\le\xi_o\\ \eta=0\end{matrix}\right\}$ $T_w = T_{wall}$, u = 0, v = 0 (A.31)

c) $\left.\begin{matrix}\xi_i\le\xi\le\xi_o\\ \eta=1\end{matrix}\right\}$ $m_{ev}=\frac{h_a}{C_{pm}}(\omega_{if}-\omega_a)_{\eta=1}$ (A.32)

$$k_w\left(\frac{\partial T_w}{\partial \eta}\right)_{\eta=1}=m_{ev}h_{fg,w}+h_a(T_{w,if}-T_a) \tag{A.33}$$

$$T_{w,if}=f(\omega_{if}) \tag{A.34}$$

A.2 Temperature coefficients in the discretized equation

The coefficients of the temperature in the discretized energy equation are described below:

Coefficients in the energy equation for the general nodes; $2 \le i \le n-2$ **and** $1 \le j \le m$

$$W_e = \frac{-V_{i-1,j}}{\delta \Delta\eta} + Q(1-i)U_{i-1,j} - \frac{\alpha}{\delta^2 \Delta\eta^2} \tag{A.35}$$

$$P_e = \frac{V_{i,j}}{\delta \Delta\eta} + \frac{U_{i,j}}{\pi R \Delta\xi} + Q(i-1)U_{i,j} + \frac{2\alpha}{\delta^2 \Delta\eta^2} \tag{A.36}$$

$$E_e = -\frac{\alpha}{\delta^2 \Delta\eta^2} \tag{A.37}$$

$$C_e = \frac{U_{i,j-1}T_{i,j-1}}{\pi R \Delta\xi} \tag{A.38}$$

Coefficients in the energy equation for the first column of nodes; $i = 1$ **and** $1 \le j \le m$

$$W_e = 0 \tag{A.39}$$

$$P_e = \frac{V_{1,j}}{\delta_{1,j} \Delta\eta} + \frac{U_{1,j}}{\pi R \Delta\xi} + \frac{2\alpha}{{\delta_{1,j}}^2 \Delta\eta^2} \tag{A.40}$$

$$E_e = -\frac{\alpha}{{\delta_{1,j}}^2 \Delta\eta^2} \tag{A.41}$$

$$C_e = \frac{U_{1,j-1}T_{1,j-1}}{\pi R \Delta\xi} + \frac{\alpha T_{wall}}{\delta_{1,j}{}^2 \Delta\eta^2} \tag{A.42}$$

Coefficients in the energy equation for the last column of nodes; $i = n-1$ **and** $1 \le j \le m$

$$W_e = \frac{-V_{n-2,j}}{\delta_{n-1,j}\Delta\eta} + Q(2-n)U_{n-2,j} - \frac{\alpha}{\delta_{n-1,j}{}^2 \Delta\eta^2} \tag{A.43}$$

$$P_e = \frac{V_{n-1,j}}{\delta_{n-1,j}\Delta\eta} + \frac{U_{n-1,j}}{\pi R \Delta\xi} + Q(n-2)U_{n-1,j} + \frac{2\alpha}{\delta_{n-1,j}{}^2 \Delta\eta^2} \tag{A.44}$$

$$E_e = 0 \tag{A.45}$$

$$C_e = \frac{U_{n-1,j-1}T_{n-1,j-1}}{\pi R \Delta\xi} + \frac{\alpha T_{iff}}{\delta_{n-1,j}{}^2 \Delta\eta^2} \tag{A.46}$$

where, $$Q = \left(\frac{\Gamma\mu}{9\rho^2 g \sin(\pi\xi)}\right)^{1/3} \frac{1}{\delta R \tan(\pi\xi)} \tag{A.47}$$

Appendix B
REFRIGERANT, R-134a, PROPERTY EQUATIONS

B1. Saturated pressure and temperature

$$P_{sat} = \exp\left(21.51297 - \frac{2200.9809}{246.61 + T_{sat}}\right) \quad \text{(B.1)}$$

$$T_{sat} = \left(\frac{-2200.9809}{\ln(P_{sat}) - 21.51297}\right) - 246.61 \quad \text{(B.2)}$$

B2. Liquid enthalpy

$$h_L = 200{,}000 + 1335.29T_{sat} + 1.70650\ T^{2}{}_{sat} + 7.6741 \times 10^{-3}\ T^{3}{}_{sat} \quad \text{(B.3)}$$

B3. Saturated vapour enthalpy

$$h_{il} = 249{,}455 + 606.163T_{sat} + 1.05644\ T^{2}{}_{sat} + 1.05644 \times T^{2}{}_{sat} - 1.82426 \times 10^{-2}\ T^{3}{}_{sat}$$

(B.4)

$$h_v = h_{il} + 149{,}048 \quad \text{(B.5)}$$

B4. Superheated vapour enthalpy

$$h_{i2} = h_{il}\begin{pmatrix} 1 + 3.48186 \times 10^{-3}\Delta T_s + 1.6886 \times 10^{-6}\Delta T^{2}{}_{sar} + 9.2642 \times 10^{-6}\Delta T_s T_{sat} \\ - 7.698 \times 10^{-8}\Delta T^{2}{}_{s} T_{sat} + 1.7070 \times 10^{-7}\Delta T_s T^{2}{}_{sat} - 1.2130 \times 10^{-9}\Delta T^{2} T^{2}{}_{sat} \end{pmatrix}$$

(B.6)

$$h_s = h_{i2} + 149{,}048 \quad \text{(B.7)}$$

B5. Saturated vapour specific volume

$$v_v = \exp\left(-12.4539 + \frac{2669.0}{273.15 + T_{sat}}\right) \times \begin{pmatrix} 1.101357 + 1.06736 \times 10^{-3} T_{sat} \\ - 9.2532 \times 10^{-6} T^{2}{}_{sat} - 3.2192 \times 10^{-7} T^{3}{}_{sat} \end{pmatrix}$$

(B.8)

B6. Superheated vapour specific volume

$$v_s = v_v \begin{pmatrix} 1 + 4.7881\times10^{-3}\Delta T_s - 3.965\times10^{-6}\Delta T^2{}_s + 2.5817\times10^{-5}\Delta T_s T_{sat} \\ -1.8506\times10^{-7}\Delta T^2{}_s T_{sat} + 8.5739\times10^{-7}\Delta T_s T^2{}_{sat} - 5.401\times10^{-9}\Delta T_s{}^2 T^2{}_{sat} \end{pmatrix}$$

(B.9)

B7. Thermal conductivity

$$k_f = 0.0934 - 0.0005T_{sat} - 4\times10^{-7}T^2{}_{sat} + 2\times10^{-8}T^3{}_{sat} + 2\times10^{-10}T^4{}_{sat} + 1\times10^{-12}T^5{}_{sat}$$

(B.10)

$$k_g = 2.9742 - 0.17962T_{sat} + 0.4265\times10^{-3}T^2{}_{sat} \quad \text{(B.11)}$$

B8. Specific heat

$$C_{p_f} = 1311.6 + 6.018T_{sat} - 0.0972T^2{}_{sat} + 0.0016T^3{}_{sat} \quad \text{(B.12)}$$

$$C_{pf} = -0.005257455 + 0.00329657T_{sat} - 2.017321\times10^{-6}T^2{}_{sat} + 15.82170T^{-1}{}_{sat}$$

(B.13)

B9. Viscosity

$$\mu_f = 0.0003 - 4\times10^{-6}T_{sat} + 3\times10^{-8}T^2{}_{sat} - 2\times10^{-10}T^3{}_{sat} + 5\times10^{-13}T^4{}_{sat}$$

(B.14)

$$\mu_g = (575.67T^{0.5}{}_{sat} - 3.619)\times10^{-8} \quad \text{(B.15)}$$

All the above relations are valid for -40 $°C \le T_{sat} \le 70\,°C$

Appendix C
WATER AND AIR PROPERTY EQUATIONS

C1. Saturated pressure and temperature of water

$$P_s = \exp\left(23.19 - \frac{3830.0}{(T_s - 44.83)}\right) \quad \text{(C.1)}$$

$$T_s = 44.83 + \left(\frac{3830.0}{23.19 - \ln(P_s)}\right) \quad \text{(C.2)}$$

C2. Enthalpy of vapor and water vapor mixture

$$h_v = 1.7719 \times T_s + 2502.6 \quad \text{(C.3)}$$

$$h_{fg} = -2.4108 \times T_s + 2502.4 \quad \text{(C.4)}$$

C3. Density of water

$$\rho_w = 1000.6 + 0.0024 \times T_w - 0.0058 \times T_w^{\,2} + 2.0 \times 10^{-5} \times T_w^{\,3} \quad \text{(C.5)}$$

C4. Dynamic viscosity of water

$$\mu_w = \left(1673.2 - 41.411 \times T_w + 0.4707 \times T_w^{\,2} - 2.0 \times 10^{-3} \times T_w^{\,3}\right) \times 10^{-6} \quad \text{(C.6)}$$

C5. Thermal conductivity of water

$$k_w = 0.5685 + 0.0019 \times T_w - 9.0 \times 10^{-6} \times T_w^{\,2} - 2.0 \times 10^{-8} \times T_w^{\,3} \quad \text{(C.7)}$$

C6. Specific heat capacity of water

$$C_{pw} = \left(4.2145 - 0.0027 \times T_w + 7.0 \times 10^{-5} \times T_w^{\,2} - 7.0 \times 10^{-7} \times T_w^{\,3}\right) \times 10^3 \quad \text{(C.8)}$$

C7. Moisture content of air with and without Relative Humidity

$$\omega_s = \frac{0.622 \times P_s}{P - P_s} \quad \text{(C.9)}$$

$$\omega_a = \frac{0.622 \times P_s \times RH}{P - P_s \times RH} \quad \text{(C.10)}$$

C8. Enthalpy of air and the temperature of air

$$h_a = T_a + \omega_a \times (2501.0 + 1.805 \times T_a) \quad \text{(C.11)}$$

$$T_a = \frac{h_a - (2501.0 \times \omega_a)}{1.0 + (1.805 \times \omega_a)} \quad \text{(C.12)}$$

Appendix D
CALIBRATION CHART AND EQUATIONS

D.1 Thermoprobes

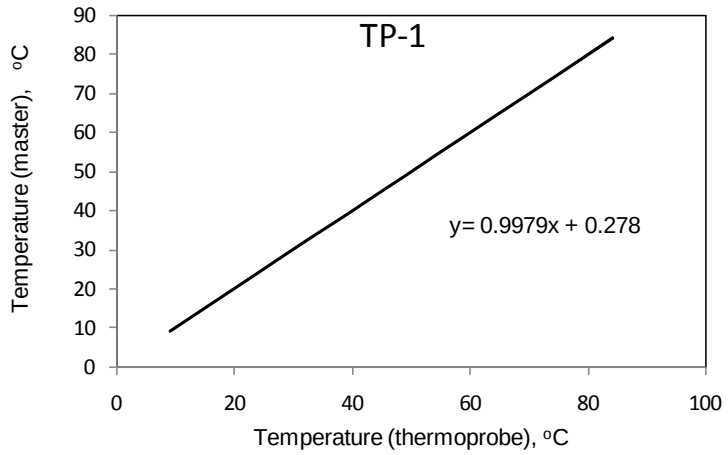

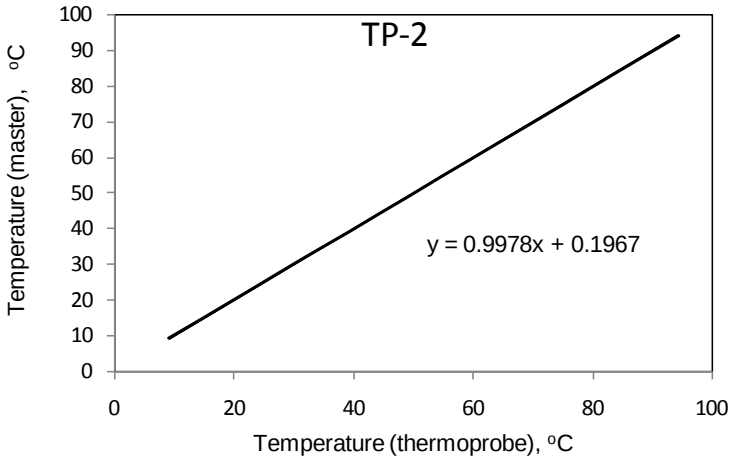

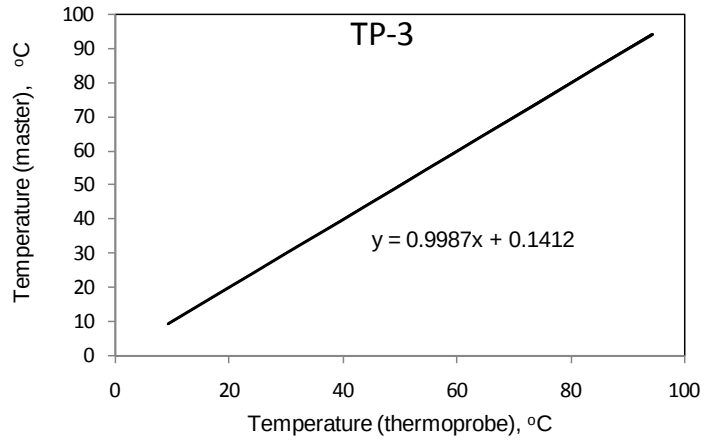

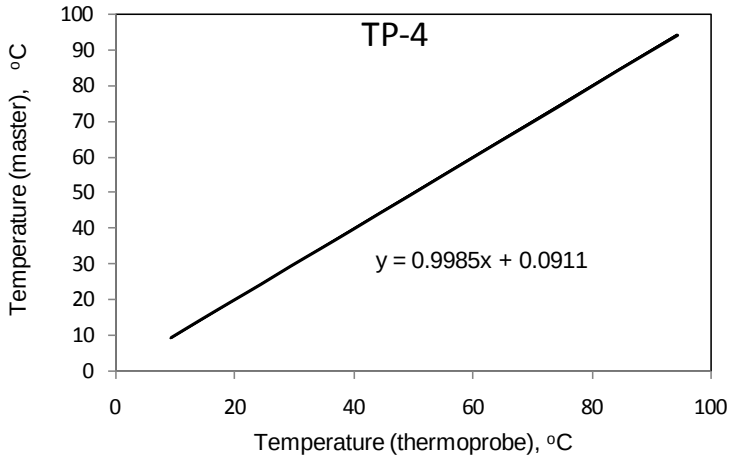
TP-4
y = 0.9985x + 0.0911
Temperature (master), °C
Temperature (thermoprobe), °C
0
10
20
30
40
50
60
70
80
90
100
0
20
40
60
80
100

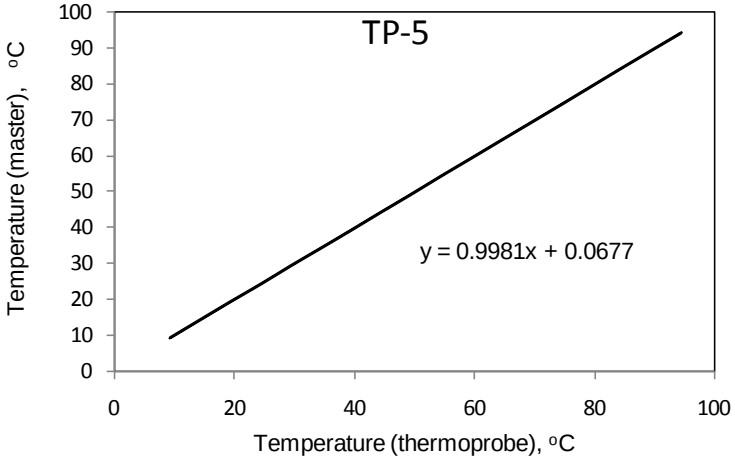
TP-5
y = 0.9981x + 0.0677
Temperature (master), °C
Temperature (thermoprobe), °C
0
10
20
30
40
50
60
70
80
90
100
0
20
40
60
80
100

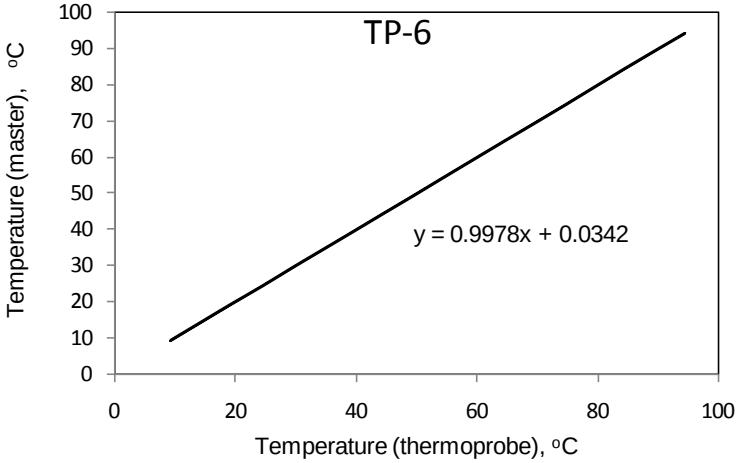
TP-6
y = 0.9978x + 0.0342
Temperature (master), °C
Temperature (thermoprobe), °C
0
10
20
30
40
50
60
70
80
90
100
0
20
40
60
80
100

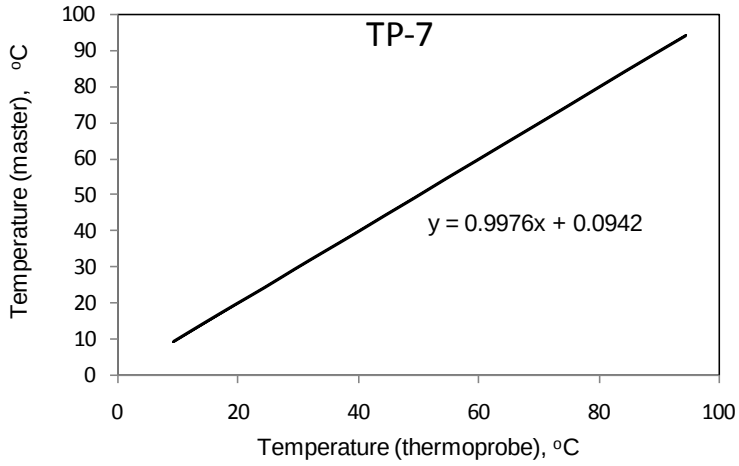
TP-7
y = 0.9976x + 0.0942
Temperature (master), °C
Temperature (thermoprobe), °C
0
10
20
30
40
50
60
70
80
90
100
0
20
40
60
80
100

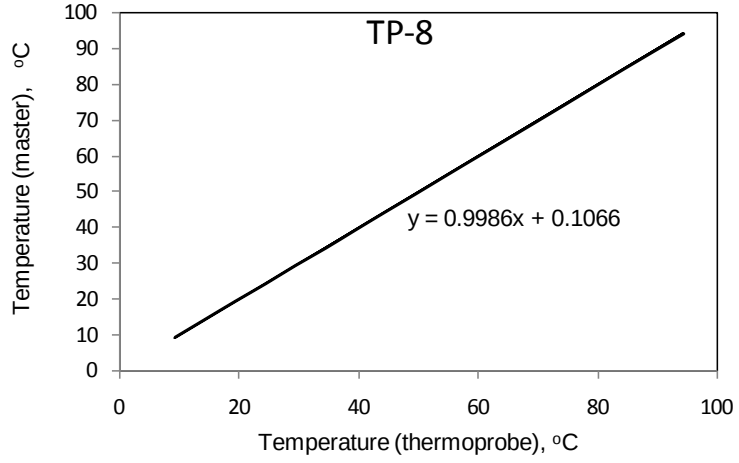
TP-8
y = 0.9986x + 0.1066
Temperature (master), °C
Temperature (thermoprobe), °C
0
10
20
30
40
50
60
70
80
90
100
0
20
40
60
80
100

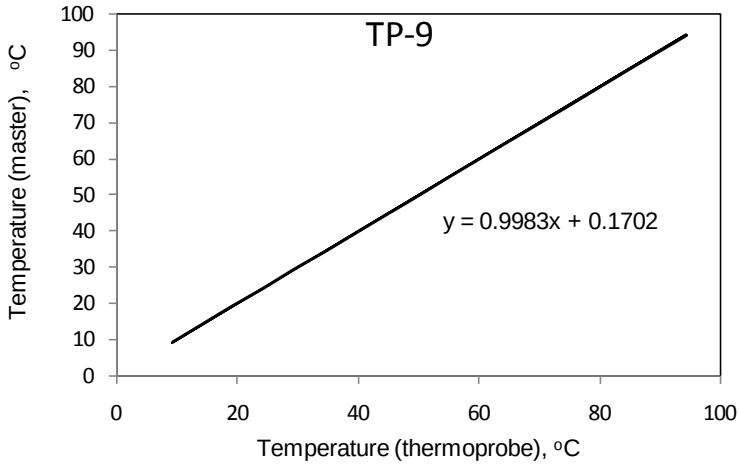
TP-9
y = 0.9983x + 0.1702
Temperature (master), °C
Temperature (thermoprobe), °C
0
10
20
30
40
50
60
70
80
90
100
0
20
40
60
80
100

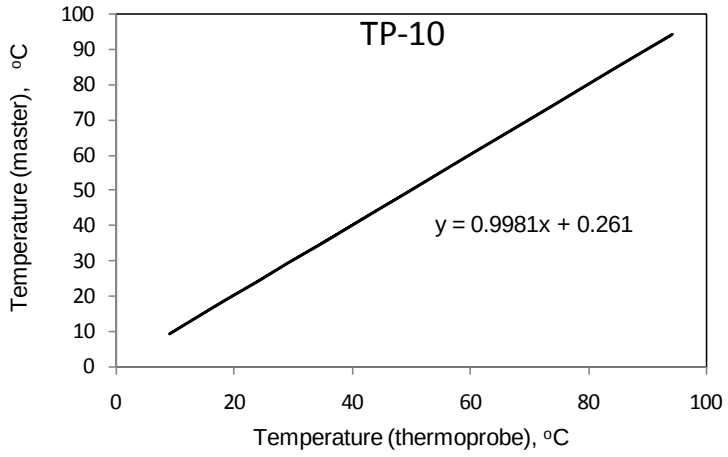
TP-10
y = 0.9981x + 0.261
Temperature (master), °C
Temperature (thermoprobe), °C
0
10
20
30
40
50
60
70
80
90
100
0
20
40
60
80
100

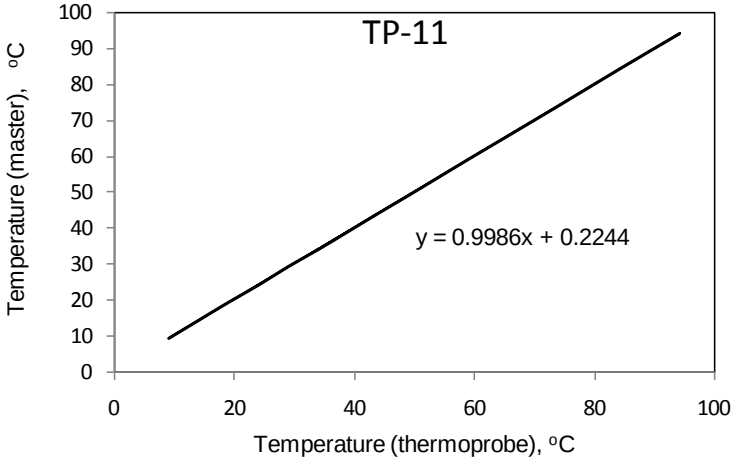
TP-11
y = 0.9986x + 0.2244
Temperature (master), °C
Temperature (thermoprobe), °C
0
10
20
30
40
50
60
70
80
90
100
0
20
40
60
80
100

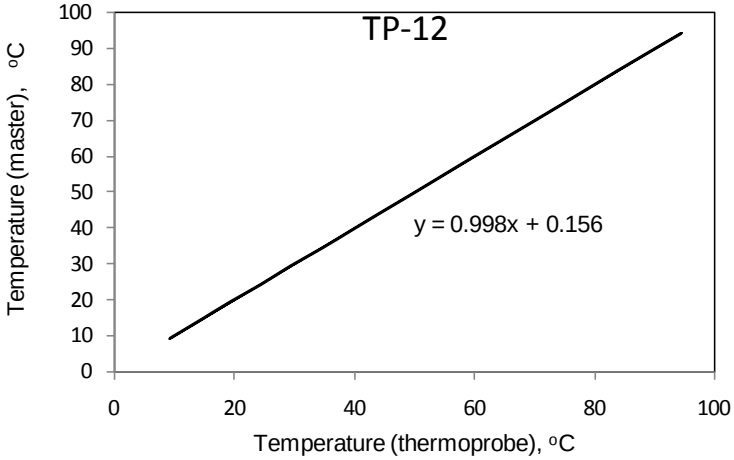
TP-12
y = 0.998x + 0.156
Temperature (master), °C
Temperature (thermoprobe), °C
0
10
20
30
40
50
60
70
80
90
100
0
20
40
60
80
100

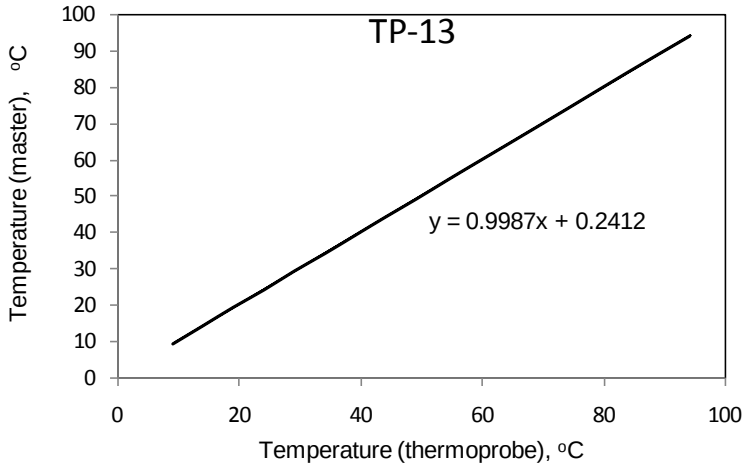

Where, X and Y are the temperature in degree Celsius

D2. Humidity Transmitter

$RH = 25.0.X - 25.0$

$T = 25.0.X - 45.0$

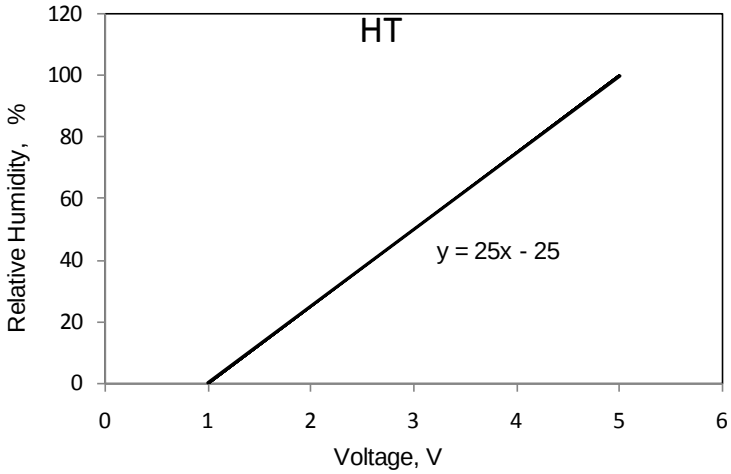

Figure A.4 Humidity transmitter calibration chart (Relative Humidity)

Where RH is the relative humidity (%) and X the voltage in V.

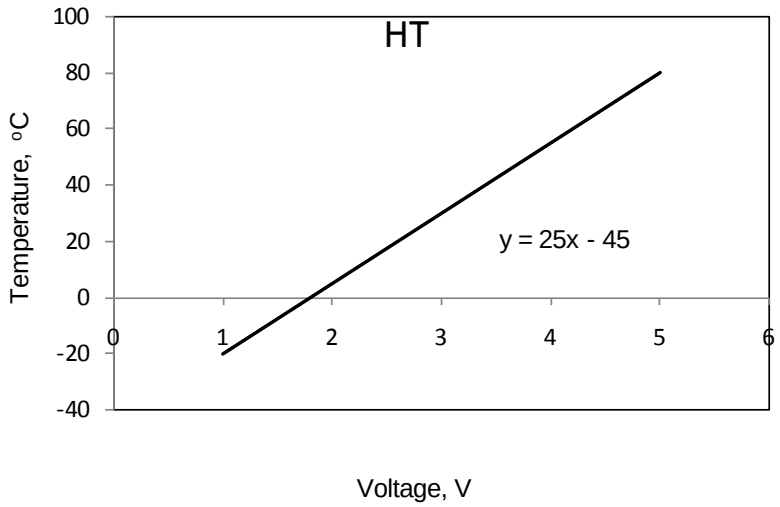

Figure A.5 Humidity transmitter calibration chart (Temperature)

Where, Y is the temperature ^{o}C and X the voltage in V.

D3. Pressure Transducer

$$P = 5.8521.Y - 6.25$$

Where P is the pressure in bar and Y the voltage in V.

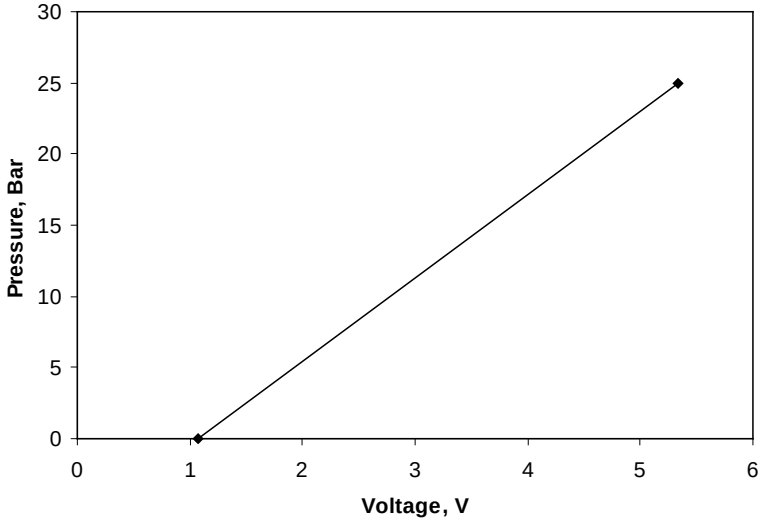

Figure A.6 Pressure transducer calibration chart.

Appendix E
UNCERTAINTY ANALYSIS FOR DERIVED PARAMETERS

E.1 Uncertainty Analysis for the Coefficient of Performance (COP) and mass flux of water evaporated from the condenser tube surface

Error analysis is the process of estimating the uncertainty level in calculated results from the measurements with known uncertainties. For the estimation of the error or uncertainty of the calculated result, one uses the equations by which the result was calculated to estimate the effects of measurement uncertainties on the value of the result. Generally, uncertainty or error analysis is performed and presented while reporting the results, to demonstrate the audience the range within which the true values are believed to contain.

The standard mathematical form for expressing a measurement is: $x = x \pm \delta x$.

When the result is a function of only one variable, the uncertainty in the result is: $\delta R = \frac{\partial R}{\partial x}.\delta x = R_{x+\delta x} - R_x$. The numerical approximation to the uncertainty of the result R is determined by calculating the value of R twice: once with x augmented by δx and the other with the value of x at its recorded value and finally, subtracting the values.

In this study, the mass flux of water evaporated (m_{ev}) from the condenser tube surface and the Coefficient of Performance (COP) are determined from the measured values from the experiments. The equations for the determination of m_{ev} and the COP presented in the theoretical models are function of a number of independent parameters. Each of the above independent parameter is with its own uncertainty level and contributes to the overall uncertainty of m_{ev} and the COP. The development of an

uncertainty analysis for the overall uncertainty of the mass flux of water evaporated (m_{ev}) and the coefficient of performance (COP) following the method of Moffat [10] are described below:

E.1.1 Mass of water evaporated from the condenser tube surface

The evaporated mass flux is a function of the saturated air humidity ratio at the air-water interface, humidity ratio of the air as well as the convective heat transfer coefficient of the air. The saturated humidity ratio is a function of the air-water interface temperature, T_{if} , and the humidity ratio of air is a function of air temperature and relative humidity (RH).

The related expressions for the determination of the mass of water evaporated from the condenser surface are listed as follow:

The saturation pressure of moist air is determined as follows [8]:

$$P_s = \exp\left(23.19 - \frac{3830}{(T_a - 44.83)}\right) \qquad \text{(E .1)}$$

The relative humidity and humidity ratio of the air are determined as follows [9]:

$$RH = \frac{p_v}{p_s} \qquad \text{(E.2)}$$

$$\omega = 0.622.\frac{p_v}{P - p_v} \qquad \text{(E.3)}$$

The mass of water evaporated at the water film-air interface can be determined from the expression:

$$m_v = \frac{h_a}{c_{pm}}.(\omega_{w,if} - \omega_a),. \quad \text{(E.4)}$$

where, ω is a function of the vapour pressure P_v. The vapour pressure at the water film-air interface and the interfacial temperature are related as follows:

$$P_{v,if} = \exp\left(23.19 - \frac{3830}{(T_{w,if} - 44.83)}\right) \quad \text{(E.5)}$$

From the equations E.1 to E.5, the following functional dependency of the related variables can be established.

$$m_{ev} = m_{ev}(\omega_{s,}\, \omega_{a,}\, h_a) \quad \text{(E.6)}$$

$$\omega_s = \omega_s(T_{if}) \quad \text{(E.7)}$$

$$\omega_a = \omega_s(T_a, RH) \quad \text{(E.8)}$$

$$h_a = h_a(V_a, A) \quad \text{(E.9)}$$

Therefore, functional dependency of the mass flux of the water evaporated from the condenser surface on the independent variables can be expressed as:

$$m_{ev} = m_{ev}(T_{if,}T_{a,}\, RH, A, V_a) \quad \text{(E.10)}$$

These uncertainties are estimated using the procedures given by Moffat (1988) as follows:

Writing equation E.10 in differential form we get,

$$dm_{ev} = \frac{\partial m_{ev}}{\partial T_{if}}\ \mathrm{d}T_{if} + \frac{\partial m_{ev}}{\partial T_a}\ \mathrm{d}T_a + \frac{\partial m_{ev}}{\partial RH}\ \mathrm{d}RH + \frac{\partial m_{ev}}{\partial A}\ \mathrm{d}A + \frac{\partial m_{ev}}{\partial V_a}\ \mathrm{d}V_a \tag{E.11}$$

If the quantities dm_{ev}, $\mathrm{d}T_{if}$, $\mathrm{d}T_a$, $\mathrm{d}RH$, $\mathrm{d}A$, $\mathrm{d}V_a$ are considered to be the uncertainties $U_{m_{ev}}, U_{T_{if}}, U_{T_a}, U_{RH}, U_A,\ U_{V_a}$ in the measured quantities $m_{ev},\ T_{if}, T_a, RH,\ A,\ V_a$, respectively, then from equation E.11 we get,

$$Um_{ev} = \frac{\partial m_{ev}}{\partial T_{if}}\ U_{T_{if}} + \frac{\partial m_{ev}}{\partial T_a}\ U_{T_a} + \frac{\partial m_{ev}}{\partial RH}\ U_{RH} + \frac{\partial m_{ev}}{\partial A}\ U_A + \frac{\partial m_{ev}}{\partial V_a}\ U_{V_a} \tag{E.12}$$

Now the maximum value of uncertainty in $m_{ev},\ Um_{ev\,max}$ would be obtained when all the uncertainties happen to have the same sign and this would be a worst possible case, that is:

$$Um_{ev\,max} = \left|\frac{\partial m_{ev}}{\partial T_{if}}\ U_{T_{if}}\right| + \left|\frac{\partial m_{ev}}{\partial T_a}\ U_{T_a}\right| + \left|\frac{\partial m_{ev}}{\partial RH}\ U_{RH}\right| + \left|\frac{\partial m_{ev}}{\partial A}\ U_A\right| + \left|\frac{\partial m_{ev}}{\partial V_a}\ U_{V_a}\right| \tag{E.13}$$

However, the probability of such an occurrence is very small. Therefore, the more realistic way is to square both sides of equation E.12 to ensure equal weightage to positive as well as negative values of uncertainties.

Therefore, squaring equation E.12 and neglecting the terms involving products of the derivatives we get,

$$U^2 m_{ev} = \left(\frac{\partial m_{ev}}{\partial T_{if}}\right)^2 \left(U_{T_{if}}\right)^2 + \left(\frac{\partial m_{ev}}{\partial T_a}\right)^2 \left(U_{T_a}\right)^2 + \left(\frac{\partial m_{ev}}{\partial RH}\right)^2 (U_{RH})^2 + \left(\frac{\partial m_{ev}}{\partial A}\right)^2 (U_A)^2 + \left(\frac{\partial m_{ev}}{\partial V_a}\right)^2 \left(U_{V_a}\right)^2 \quad \text{(E.14)}$$

The uncertainties in the various measured parameters result in an overall uncertainty in m_{ev}. The uncertainty in m_{ev} can be expressed as:

$$Um_{ev} = \pm\left[\left(\frac{\partial m_{ev}}{\partial T_{if}}\, U_{T_{if}}\right)^2 + \left(\frac{\partial m_{ev}}{\partial T_a}\, U_{T_a}\right)^2 + \left(\frac{\partial m_{ev}}{\partial RH}\, U_{RH}\right)^2 + \left(\frac{\partial m_{ev}}{\partial A}\, U_A\right)^2 + \left(\frac{\partial m_{ev}}{\partial V_a}\, U_{V_a}\right)^2\right]^{0.5} \quad \text{(E.15)}$$

Equation E.15 is equivalent to:

$$Um_{ev} = \pm\left[\begin{array}{c}\left\{m_{ev\left(T_{if}+U_{T_{if}}\right)} - m_{ev_{T_{if}}}\right\}^2 + \left\{m_{ev(T_a+U_{T_a})} - m_{ev_{T_a}}\right\}^2 + \left\{m_{ev(RH+U_{RH})} - m_{ev_{RH}}\right\}^2 \\ + \\ \left\{m_{ev(A+U_A)} - U_A\right\}^2 + \left\{m_{ev(V_a+U_{V_a})} - m_{ev_{V_a}}\right\}^2\end{array}\right]^{0.5}$$

(E.16)

A generalised form of equation (E.15) can be expressed as:

$$U_y = \pm\left[\sum_{i=1}^{n}\left(\frac{\partial y}{\partial x_i}\, U_{x_i}\right)^2\right]^{0.5} \quad \text{(E.17)}$$

E.1.2 Coefficient of Performance

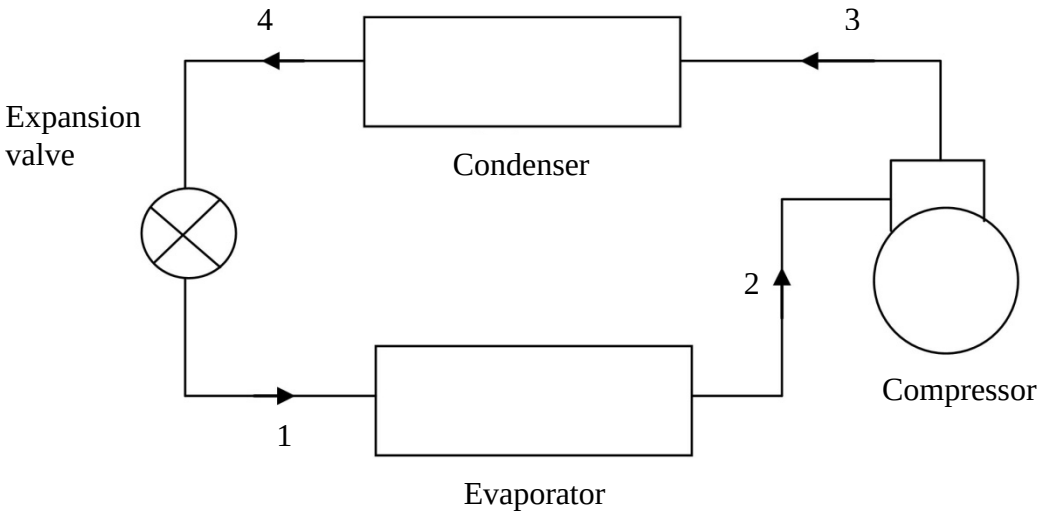

Figure E.1 Schematic diagram of a vapour compression refrigeration cycle

Coefficient of Performance (COP) of air-conditioners is defined as the ratio of the refrigerating effect to the compressor work input.

COP = Cooling Capacity / Compressor Power, P_{comp} (E.18)

The COP is a function of the refrigerant enthalpies at the various points of the vapour compression refrigeration system shown in Fig.E.1.

The refrigerating effect (referring to Fig. 1) can be expressed as:

$Q_{ev} = m_r (h_2 - h_1)$ (E.19)

The compressor work input can be expressed as:

The functional dependency of COP on the variables can be expressed as follows:

$$COP = COP\left(h_{1,}\, h_{2,}\, P_{comp}\right) \quad \text{(E.21)}$$

$$h_2 \;= h_2\;(\,P_{2,}\;T_2)$$

Assuming isenthalpic expansion process,

$$h_1 \;= h_4 \;= h_4\;(\,T_4)$$

$$COP = COP\left(m_{r,} P_{2,}\, T_{2,}\, T_{4,}\, P_{comp}\right) \quad \text{(E.22)}$$

Using equation E.17, the uncertainty COP can be expressed as:

$$U(COP) = \left[\left(\frac{\partial COP}{\partial m_r}U_{m_r}\right)^2 + \left(\frac{\partial COP}{\partial P_2}U_{P_2}\right)^2 + \left(\frac{\partial COP}{\partial T_2}U_{T_2}\right)^2 + \left(\frac{\partial COP}{\partial T_4}U_{T_4}\right)^2 + \left(\frac{\partial COP}{\partial P_{comp}}U_{P_{comp}}\right)^2\right]^{0.5} \quad \text{(E.23)}$$

Equivalently equations (E.23) can be expressed as:

$$U(COP) = \left[\begin{array}{c}\left\{COP_{(m_{r+}U_{m_r})} - COP_{m_r}\right\}^2 + \left\{COP_{(P_{2+}U_{P_2})} - COP_{P_2}\right\}^2 + \\ + \\ + \left\{COP_{(T_{2+}U_{T_2})} - COP_{T_2}\right\}^2 + \left\{COP_{(T_{4+}U_{T_4})} - COP_{T_4}\right\}^2 + \left\{COP_{\left(P_{comp}+U_{P_{comp}}\right)} - COP_{P_{comp}}\right\}^2\end{array}\right]^{0.5} \quad \text{(E.24)}$$

The uncertainty δT involved in the measurement of temperatures can be determined as:

$$\delta T = \left(\,\delta T_{fixed}{}^2 + \delta T_{random}{}^2\right)^{0.5} \quad \text{(E.25)}$$

The fixed error, δT_{fixed} in the measurement of temperature which is ± 0.05 ^{o}C and δT_{random} is the random error which can be determined from the standard deviation of the population of measured data as:

$$\delta T_{random} = \left[\sum_1^N \frac{(T_i - \overline{T})^2}{N-1}\right]^{0.5} \quad \text{(E.26)}$$

where $\overline{T}$ is the mean of the population of measured data and N is the population size.

The uncertainties of other instruments used in the measurements are given in Table E.1.

Table E.1 Uncertainties of various instruments

Instrument	**Uncertainty %**
Humidity transmitter	2.0
Pressure transducer	1.0
Hotwire Anemometer	4.0
Refrigerant flowmeter	2.0
Power meter	2.0

The uncertainty analysis of the mass flux of water evaporated from the condenser surface, m_{ev} and the coefficient of performance (COP) is accomplished by sequentially perturbing the independent variables with their individual uncertainties:

1. Calculate the nominal m_{ev} and COP for the measured data
2. Increase the value of the first independent variable by its uncertainty level and calculate the value of m_{ev1+} and COP_{1+} keeping all other variables at their measured value. Find the difference m_{ev1+} - m_{ev} and COP_{1+}-COP which represent the contribution to the uncertainty of m_{ev} and COP caused by the perturbation of the first independent variable by its individual uncertainty level. The above differences in values of m_{ev} and COP, C_{m1+} and C_{cop1+} are stored.

3. Repeat step 2 for all the other independent variables in the functional relationships of equations E.10 and E.22 to get the absolute values of C_{m2+} to C_{m5+} and C_{cop2+} to C_{cop6+} for the m_{ev} and COP, respectively.
4. The uncertainty in the value of m_{ev} and COP are the root-sum-square of the C_{m1+} to C_{m5+} and C_{cop1+} to C_{cop6+}, respectively.

Table E.2 Uncertainties in the measured parameters (Unfinned Condenser)

Run	δT_2	δT_4	δP_2	δm_r	δT_{if}	δT_a	δRH_{in}	δRH_{out}	δV
1	0.147694	0.068033	0.034	0.000706	0.11453	0.098656	0.0084	0.01384	0.16
2	0.082193	0.064825	0.035	0.000706	0.09866	0.089656	0.00664	0.01182	0.16
3	0.075811	0.059671	0.0351	0.000706	0.11552	0.132325	0.00592	0.01042	0.16
4	0.080844	0.063837	0.0355	0.000706	0.09856	0.045865	0.00546	0.00964	0.16
5	0.080631	0.064825	0.033	0.000706	0.3259	0.298568	0.0083	0.01404	0.16
6	0.072405	0.065535	0.034	0.000706	0.11453	0.098656	0.00842	0.01384	0.16
7	0.077309	0.073317	0.034	0.000706	0.19866	0.202563	0.00836	0.01462	0.16
8	0.067871	0.065680	0.0358	0.000706	0.10526	0.098969	0.00852	0.01262	0.16
9	0.075714	0.077102	0.035	0.000706	0.09866	0.085025	0.00584	0.00994	0.16
10	0.067448	0.064996	0.037	0.000706	0.09856	0.045865	0.00604	0.00902	0.16
11	0.058240	0.061436	0.036	0.000706	0.05896	0.085698	0.00596	0.0086	0.16
12	0.060796	0.067440	0.038	0.000706	0.14526	0.278585	0.00602	0.00864	0.16
13	0.065164	0.064810	0.039	0.000668					
14	0.067462	0.063164	0.038	0.000668					
15	0.064825	0.058240	0.039	0.000668					
16	0.063835	0.059672	0.04	0.000668					

Table E.3 Uncertainties in the derived parameters (Unfinned Condenser)

Run	m_{ev} kg/m^2 h	δm_{ev} kg/m^2 h	$(\delta m_{ev}/m_{ev})100$ %	Q_{ev} kW	δQ_{ev} kW	$(\delta Q_{ev}/Q_{ev})100$ %	P_{comp} kW	δP_{comp} kW	$(\delta P_{comp}/P_{comp})100$ %	COP	δCOP	$(\delta COP/COP)100$ %
1	14.35	0.517	3.6	5.56	0.211	3.8	1.97	0.0394	2.0	2.82	0.120	4.27
2	13.625	0.461	3.38	5.51	0.212	3.84	2.01	0.0402	2.0	2.74	0.118	4.31
3	12.865	0.440	3.42	5.48	0.209	3.82	2.02	0.0404	2.0	2.71	0.117	4.3
4	12.025	0.366	3.04	5.42	0.212	3.92	2.04	0.0408	2.0	2.65	0.116	4.38
5	14.602	0.946	6.48	5.62	0.210	3.73	1.94	0.0388	2.0	2.9	0.122	4.22
6	14.35	0.517	3.6	5.56	0.211	3.79	1.97	0.0394	2.0	2.82	0.120	4.27
7	12.845	0.565	4.4	5.5	0.212	3.86	2.00	0.04	2.0	2.75	0.119	4.33
8	11.646	0.380	3.26	5.48	0.212	3.87	2.03	0.0406	2.0	2.69	0.117	4.34
9	12.263	0.397	3.24	5.52	0.211	3.83	1.99	0.0398	2.0	2.77	0.119	4.31
10	12.025	0.366	3.04	5.49	0.210	3.82	2.03	0.0406	2.0	2.71	0.116	4.29
11	10.856	0.321	2.96	5.44	0.212	3.9	2.07	0.0414	2.0	2.63	0.115	4.36
12	9.865	0.391	3.96	5.36	0.213	3.98	2.16	0.0432	2.0	2.48	0.110	4.44
13				4.86	0.206	4.23	2.21	0.0442	2.0	2.2	0.103	4.66
14				4.64	0.204	4.4	2.23	0.0446	2.0	2.08	0.100	4.82
15				4.55	0.206	4.52	2.26	0.0452	2.0	2.01	0.099	4.93
16				4.52	0.206	4.56	2.31	0.0462	2.0	1.96	0.097	4.95

Table E.4 Uncertainties in the measured parameters (Finned Condenser)

Run	δT_2	δT_4	δP_2	δm_r	δT_{if}	δT_a	δRH_{in}	δRH_{out}	δV
17	0.059311	0.065104	0.03	0.000812	0.12536	0.098659	0.0084	0.01442	0.16
18	0.060785	0.059286	0.033	0.000812	0.21357	0.1278965	0.00664	0.01204	0.16
19	0.057695	0.066648	0.032	0.000812	0.1257	0.0968965	0.00592	0.01186	0.16
20	0.060786	0.063398	0.037	0.000812	0.45899	0.4589653	0.00546	0.01142	0.16
21	0.061424	0.067724	0.031	0.000812	0.48524	0.478523	0.0083	0.01504	0.16
22	0.062612	0.071510	0.033	0.000812	0.12536	0.098659	0.00842	0.01442	0.16
23	0.064109	0.063956	0.034	0.000812	0.35699	0.2589635	0.00836	0.01422	0.16
24	0.060786	0.065529	0.031	0.000812	0.18965	0.1963568	0.00852	0.01344	0.16
25	0.060786	0.066304	0.035	0.000812	0.25699	0.1986532	0.00584	0.01226	0.16
26	0.060786	0.058247	0.038	0.000812	0.45899	0.4589653	0.00604	0.0114	0.16
27	0.066245	0.062612	0.034	0.000812	0.09856	0.4286356	0.00596	0.01124	0.16
28	0.061424	0.075661	0.038	0.000812	0.17897	0.2589658	0.00602	0.01102	0.16
29	0.060786	0.066391	0.036	0.000804					
30	0.066333	0.060788	0.038	0.000804					
31	0.067724	0.055228	0.037	0.000804					
32	0.059610	0.065665	0.036	0.000804					

Table E.5 Uncertainties in the derived parameters (Finned Condenser)

Run	m_{ev} kg/m^2 h	δm_{ev} kg/m^2 h	$(\delta m_{ev}/m_{ev})100$ %	Q_{ev} kW	δQ_{ev} kW	$(\delta Q_{ev}/Q_{ev})100$ %	P_{comp} kW	δP_{comp} kW	$(\delta P_{comp}/P_{comp})100$ %	COP	δCOP	$(\delta COP/COP)100$ %
17	16.52	0.502	3.04	6.98	0.238	3.41	1.732	0.0346	2.0	4.03	0.158	3.92
18	15.36	0.574	3.74	6.95	0.239	3.44	1.755	0.0351	2.0	3.96	0.157	3.96
19	15.01	0.435	2.9	6.90	0.241	3.49	1.756	0.0351	2.0	3.93	0.158	4.01
20	14.326	0.920	6.42	6.88	0.242	3.52	1.792	0.0358	2.0	3.84	0.155	4.03
21	17.823	1.034	5.8	7.01	0.239	3.41	1.701	0.0340	2.0	4.12	0.162	3.93
22	16.52	0.502	3.04	6.98	0.238	3.41	1.732	0.0346	2.0	4.03	0.158	3.92
23	14.78	0.816	5.52	6.91	0.239	3.46	1.767	0.0353	2.0	3.91	0.155	3.97
24	13.43	0.459	3.42	6.75	0.240	3.56	1.78	0.0356	2.0	3.79	0.154	4.07
25	15.875	0.654	4.12	6.94	0.237	3.42	1.718	0.0344	2.0	4.04	0.160	3.95
26	14.326	0.920	6.42	6.87	0.241	3.51	1.771	0.0354	2.0	3.88	0.156	4.02
27	12.589	0.350	2.78	6.80	0.241	3.55	1.789	0.0358	2.0	3.80	0.154	4.05
28	10.985	0.367	3.34	6.74	0.241	3.58	1.817	0.0363	2.0	3.71	0.152	4.09
29				6.50	0.239	3.67	2.321	0.0464	2.0	2.80	0.116	4.16
30				6.47	0.238	3.68	2.352	0.0470	2.0	2.73	0.114	4.17
31				6.44	0.240	3.73	2.421	0.0484	2.0	2.66	0.112	4.22
32				6.36	0.225	3.53	2.446	0.0489	2.0	2.60	0.105	4.05

Appendix F

Steady State Experimental Data

Table F1: Experimental Data Legend

Item	Definition
T_1	refrigerant temperature at condenser inlet ^oC
T_2	refrigerant temperature 2 in condenser tube, ^oC
T_3	refrigerant temperature 3 in condenser tube , ^oC
T_4	refrigerant temperature 3 in condenser tube , ^oC
T_5	refrigerant temperature 3 in condenser tube , ^oC
T_6	refrigerant temperature 3 in condenser tube , ^oC
T_7	refrigerant temperature 3 in condenser tube , ^oC
T_8	refrigerant temperature 3 in condenser tube , ^oC
$T_{ev,in}$	refrigerant temperature at evaporator inlet, ^oC
$T_{ev,out}$	refrigerant temperature at evaporator outlet, ^oC
$P_{comp.}$	compressor pressure, bar
$P_{cond.}$	condenser pressure, bar
$P_{evp,in}$	evaporator inlet pressure, bar
$P_{evp,out}$	evaporator exit pressure, bar
Rh_{in}	relative humidity of inlet air, %
Rh_{out}	relative humidity of exit air, %
$T_{a,in}$	air inlet temperature, ^oC
$T_{a,out}$	air exit temperature, ^oC
M_r	refrigerant flow rate, kg/s
EC	evaprative cooling
CM	conventional mode (without EC)

Table F2: Experimental Details (bare-tube condenser)

Run	Air inlet	Film Reynolds	Air	Mode of
1	30	9	4	EC
2	35	9	4	EC
3	38	9	4	EC
4	40	9	4	EC
5	30	5	4	EC
6	30	9	4	EC
7	30	15	4	EC
8	30	24	4	EC
9	40	5	4	EC
10	40	9	4	EC
11	40	15	4	EC
12	40	24	4	EC
13	30	5	4	CM
14	35	9	4	CM
15	38	15	4	CM
16	40	24	4	CM

Table F3: Experimental Details (finned-tube condenser)

Run no.	Air inlet temperature, ^{o}C	Film Reynolds number, Re_f	Air velocity m/s	Mode of operation
17	30	9	4	EC
18	35	9	4	EC
19	38	9	4	EC
20	40	9	4	EC
21	30	5	4	EC
22	30	9	4	EC
23	30	15	4	EC
24	30	24	4	EC
25	40	5	4	EC
26	40	9	4	EC
27	40	15	4	EC
28	40	24	4	EC
29	30	5	4	CM
30	35	9	4	CM
31	38	15	4	CM
32	40	24	4	CM

Table F4: Steady state experimental data for the bare-tube condenser

Run	$T_{1,}$ °C	T_2 °C	$T_{3,}$ °C	$T_{4,}$ °C	$T_{5,}$ °C	$T_{6,}$ °C	$T_{7,}$ °C	$T_{8,}$ °C	$T_{ev,in}$ °C	$T_{ev,out}$ °C	$P_{comp,\ bar}$	$P_{cond,\ bar}$	$P_{e,in,\ bar}$	$P_{e,out,\ bar}$	Rhin %	Rhout %	$T_{a,in}$ °C	$T_{a,out}$ °C	Mr kg/s
1	76.195	68.49	61.464	54.451	54.47	54.031	45.155	38.099	6.1132	15.392	14.506	14.4655	3.808	3.708	41.8872	69.1192	30.1131	27.9658	0.0353
2	78.16	69.384	61.959	55.247	55.116	55.067	46.121	38.831	7.0247	16.042	14.821	14.8041	3.6974	3.6877	33.2559	59.0435	35.0926	31.1722	0.0353
3	78.649	69.384	61.738	55.288	55.246	55.127	47.224	39.102	7.0047	16.534	14.936	14.9004	3.7074	3.6978	29.6488	52.0525	38.0989	34.0278	0.0353
4	80.352	72.48	64.644	55.889	55.897	55.91	48.125	39.172	7.4957	15.632	15.222	15.075	3.8096	3.806	27.3442	48.0861	40.1631	36.0018	0.0353
5	75.994	67.47	60.636	53.354	53.403	53.349	46.222	37.849	6.0928	15.29	14.32	14.2345	3.505	3.4192	41.5725	70.221	30.0722	28.066	0.0353
6	76.158	67.67	61.137	54.11	54.09	54.08	45.32	37.949	5.9926	15	14.59	14.434	3.5992	3.3991	42.1736	69.1994	30.1724	27.9858	0.0353
7	77.128	68.572	60.135	54.451	54.124	54.08	46.923	38.551	6.694	15.381	14.691	14.5343	3.5892	3.4903	41.6726	73.0056	30.1424	27.034	0.0353
8	78.26	70.426	62.941	55.187	55.166	55.082	47.574	38.25	6.7142	15.581	15.032	15.0358	3.489	3.4883	42.4641	63.0097	30.0602	28.8676	0.0353
9	79.933	72.458	65.143	55.185	55.124	55.116	46.467	38.279	6.8737	14.879	14.74	14.6924	3.7673	3.6876	30.1694	49.7087	40.1626	36.092	0.0353
10	80.352	72.48	64.644	55.889	55.897	55.91	48.125	39.172	7.4957	15.632	15.222	15.075	3.8096	3.806	27.3442	48.0861	40.1631	36.0018	0.0353
11	80.324	73.44	65.103	55.796	55.966	55.597	46.938	38.8	7.024	15.21	15.191	15.1336	3.8876	3.8279	29.8088	43.0482	40.0725	38.0058	0.0353
12	81.356	74.592	65.954	56.858	56.848	56.799	47.439	39.422	7.3547	15.871	15.612	15.4947	3.7974	3.7778	30.1394	43.1885	40.0875	37.2042	0.0353
13	93.159	83.819	75.973	60.095	60.124	60.145	54.392	48.059	9.028	18.957	16.795	16.7282	4.0178	3.9883	42.2031	32.1406	30.1721	35.053	0.0334
14	94.531	85.282	77.396	60.235	60.244	60.206	55.434	49.753	8.6673	16.462	16.865	16.8185	3.8876	3.7879	34.1874	29.4964	35.1623	39.5423	0.0334
15	95.343	86.324	77.997	61.036	61.136	61.127	56.256	48.52	8.8075	16.142	17.025	16.999	3.6571	3.5975	30.1995	27.5935	38.2186	43.1999	0.0334
16	96.305	88.388	80.772	61.678	61.767	61.608	58.26	50.985	8.7073	14.318	17.416	17.1695	3.5269	3.4973	27.1635	21.584	40.1626	44.8934	0.0334

Table F5: Steady state experimental data for the finned-tube condenser

Run	$T_{1,}$ °C	T_{2} °C	$T_{3,}$ °C	$T_{4,}$ °C	$T_{5,}$ °C	$T_{6,}$ °C	$T_{7,}$ °C	$T_{8,}$ °C	$T_{ev,in}$ °C	$T_{ev,out}$ °C	$P_{comp,\ bar}$	$P_{cond,\ bar}$	$P_{e,in,\ bar}$	$P_{e,out,\ bar}$	Rhin %	Rhout %	$T_{a,in}$ °C	$T_{a,out}$ °C	M_r kg/s
17	62.232	54.532	49.944	36.519	36.578	36.454	30.778	28.308	6.1624	16.142	9.4996	9.3063	3.1962	3.0964	42.2372	72.044	30.2923	28.577	0.0406
18	63.621	57.598	50.475	38.693	38.492	38.583	32.381	29.22	5.4309	16.237	9.8253	9.74753	3.2964	3.1165	33.3057	60.3255	35.1824	30.8416	0.0406
19	64.301	58.129	51.477	39.054	39.093	39.124	33.473	29.641	5.4911	16.352	9.9245	9.80771	3.3565	3.2467	29.6484	59.2538	38.3889	32.8857	0.0406
20	63.308	56.304	48.952	38.613	38.229	38.748	32.401	28.709	7.1043	15.278	9.8103	9.68535	3.6821	3.5894	30.2446	57.2005	40.5413	34.2082	0.0406
21	61.921	54.502	49.253	36.188	36.418	36.489	30.618	27.667	6.0221	16.112	9.2291	9.20602	3.086	3.0113	41.5819	74.8486	30.147	27.9758	0.0406
22	62.232	54.532	49.944	36.519	36.578	36.454	30.778	28.308	6.1624	16.142	9.4996	9.3063	3.1962	3.0964	42.2372	72.044	30.2923	28.577	0.0406
23	62.598	54.703	45.135	37.891	38.081	38.092	31.209	29.826	6.2626	15.891	9.5878	9.34742	3.2463	3.0864	41.9025	71.0724	30.4827	28.2764	0.0406
24	63.269	56.726	49.443	38.523	38.462	38.884	31.038	29.511	5.7616	15.07	9.7702	9.53293	3.3965	3.1766	42.6039	67.126	30.147	29.2183	0.0406
25	61.536	54.192	47.269	36.163	36.224	36.333	32.04	28.45	5.8618	15.891	9.199	9.05057	3.2022	3.0022	29.3078	60.9865	40.7488	34.4989	0.0406
26	63.308	56.304	48.952	38.613	38.229	38.748	32.401	28.709	7.1043	15.278	9.8103	9.68535	3.6821	3.5894	30.2446	57.2005	40.5413	34.2082	0.0406
27	63.876	57.381	49.328	40.039	40.062	40.081	33.213	30.228	6.8838	15.681	10.081	10.0133	3.63	3.5063	29.7787	56.229	40.0915	35.1202	0.0406
28	65.693	58.409	51.459	41.473	41.062	41.11	34.196	31.651	7.1704	16.097	10.611	10.4144	3.6661	3.5193	30.7556	55.2575	40.2949	33.9878	0.0406
29	79.248	70.468	63.151	52.995	53.125	53.133	39.359	35.095	8.253	17.132	14.015	13.824	3.8314	3.6395	42.4035	29.2814	30.4877	36.599	0.0402
30	82.475	74.71	67.723	54.214	54.113	54.088	40.401	36.31	7.5351	16.753	14.425	14.168	3.9125	3.8159	34.2274	28.365	35.2025	40.3105	0.0402
31	84.299	76.544	69.551	54.583	54.522	54.513	41.238	37.367	7.3247	17.174	14.791	14.6814	3.8674	3.6977	30.2596	25.0597	38.0984	44.2683	0.0402
32	87.044	77.275	70.693	55.585	55.424	55.265	43.291	38.86	8.3267	17.324	15.107	14.892	4.0578	3.858	27.2337	25.4604	40.0625	43.4266	0.0402